Many-body entanglement in gapped quantum systems: representation, classification, and application

by

Xie Chen

B.Sc., Tsinghua University (2006)

Submitted to the Department of Physics
in partial fulfillment of the requirements for the degree of

Doctor of Philosophy in Physics

at the

MASSACHUSETTS INSTITUTE OF TECHNOLOGY

June 2012
[SEPTEMBER 2012]

Author .....
Department of Physics
June 2012

Certified by .....
Isaac L. Chuang
Professor of Physics
Professor of Electrical Engineering and Computer Science
Thesis Supervisor

Certified by .....
Xiao-Gang Wen
Professor of Physics
Thesis Co-Supervisor

Accepted by .....
John Belcher
Associate Department Head for Education, Professor of Physics

Many-Body Entanglement in Gapped Quantum Systems: Representation, Classification, and Application

by

Xie Chen

Submitted to the Department of Physics
on June 2012, in partial fulfillment of the
requirements for the degree of
Doctor of Philosophy in Physics

Abstract

Entanglement is a special form of quantum correlation that exists among quantum particles and it has been realized that surprising things can happen when a large number of particles are entangled together. For example, topological orders emerge in condensed matter systems where the constituent 10^{23} particles are entangled in a nontrivial way; moreover, quantum computers, which can perform certain tasks significantly faster than classical computers, are made possible by the existence of entanglement among a large number of particles. However, a systematic understanding of entanglement in many-body systems is missing, leaving open the questions of what kinds of many-body entanglement exist, where to find them and what they can be used for.

In this thesis, I present my work towards a more systematic understanding of many-body entanglement in systems where the particles interact with each other locally and the ground state of the system is separated from the excited states by a finite energy gap. Under such physically realistic locality and gap constraints, I am able to obtain more understanding concerning the efficient representation of many-body entangled states, the classification of such states according to their universal properties and the application of such states in quantum computation.

More specifically, this thesis is focused on the tensor network representation of many-body entangled states and studies how the tensors in the representation reflect the universal properties of the states. An algorithm is presented to extract the universal properties from the tensors and certain symmetry constraints are found necessary for the tensors to represent states with nontrivial topological order. Classification of gapped quantum states is then carried out based on this representation. An operational procedure relating states with the same universal properties is established which is then applied to systems in one and higher dimensions. This leads not only to the discovery of new quantum phases but also to a more systematic understanding of them. A more complete understanding of possible many-body entanglement structures enables us to design an experimentally more feasible many-body entangled state for application in measurement-based quantum computation. Moreover, the framework of measurement-based quantum computation is generalized from spin to fermion systems leading to new possibilities for experimental realization.

Thesis Supervisor: Isaac L. Chuang
Title: Professor of Physics
Professor of Electrical Engineering and Computer Science

Thesis Co-Supervisor: Xiao-Gang Wen
Title: Professor of Physics

Acknowledgments

I am indebted to my teachers, collegues, friends and family for all their help and support during my years of graduate study.

First, I would like to express my sincere gratitude to my thesis advisor Prof. Isaac L. Chuang for teaching me the most important things in research and for his continuous support and guidance during my Ph.D. study. Also I must thank my co-adviosr Prof. Xiao-Gang Wen for inspiring me with his deep insight and great enthusiasm in science and for taking me into the exciting area of quantum many-body physics. Besides that, I would like to thank my academic advisor Prof. David Pritchard for his patience and encouragement and for all the helpful advice. Moreover, I am grateful to my other thesis committe members, Prof. Senthil Todadri and Prof. Allan Adams for carefully reading my thesis and giving their valuable suggestions.

My thanks also go to all my collaborators, collegues and friends: Sergey Bravyi, Jianxin Chen, Yu-Ju Chiu, Hyeyoun Chung, Andrew Cross, Luming Duan, Runyao Duan, Liang Fu, Daniel Gottesman, Zheng-Cheng Gu, Ching-Yu Huang, Zhengfeng Ji, Feng-li Lin, Zheng-Xin Liu, Fangzhou Liu, Ling Lu, Sam Ocko, Ying Ran, Mary Beth Ruskai, Brian Swingle, Evelyn Tang, Juwen Wang, Zhenghan Wang, Beni Yoshida, Bei Zeng ... and many others. I have learned so much from each one of you.

Last but not least, my deepest gratitute to my family: my parents, who have been a constant source of support and love and my husband Jie Bao, whose support and encouragement made all this possible.

Contents

I Background 11

1 Introduction 13
- 1.1 Extreme quantumness in many-body systems . . . 13
- 1.2 What is many-body entanglement . . . 14
  - 1.2.1 Entanglement . . . 14
  - 1.2.2 Many-body entanglement . . . 16
- 1.3 Why do we care about many-body entanglement . . . 17
  - 1.3.1 Condensed matter motivation . . . 17
  - 1.3.2 Quantum information motivation . . . 18
- 1.4 Important questions about many-body entanglement . . . 18
  - 1.4.1 How to characterize many-body entanglement . . . 18
  - 1.4.2 How is it related to physical properties of the system . . . 19
- 1.5 What is known about many-body entanglement . . . 20
  - 1.5.1 Efficient representation of many-body entangled states . . . 20
  - 1.5.2 Many-body entanglement and quantum phase and phase transition . 20
  - 1.5.3 Many-body entanglement and quantum computation . . . 23
  - 1.5.4 Many-body entanglement in experiment . . . 24
- 1.6 Summary of thesis . . . 25
  - 1.6.1 Central topic and general structure . . . 25
  - 1.6.2 Summary of results on representation . . . 26
  - 1.6.3 Summary of results on classification . . . 27
  - 1.6.4 Summary of results on applications . . . 27
  - 1.6.5 Organization of content . . . 28
  - 1.6.6 List of publications . . . 28

II Tensor Network Representation 31

2 Matrix product states 33
- 2.1 Definition and basic properties . . . 34
  - 2.1.1 Definition . . . 34
  - 2.1.2 Area Law . . . 34
  - 2.1.3 Gauge degree of freedom . . . 35
  - 2.1.4 Projected Entangled Pair picture . . . 35
  - 2.1.5 Double tensor . . . 36
- 2.2 Canonical form . . . 37
- 2.3 Renormalization . . . 38

3 Tensor product states **41**
3.1 Definition and basic properties 42
3.1.1 Definition 42
3.1.2 Other properties 42
3.2 Renormalization 43
3.2.1 Algorithm 44
3.2.2 Complication: corner double line 46
3.2.3 Examples 47
3.2.4 $\mathbb{Z}_2$ topological ordered phase 49

4 Symmetry constraint on tensor network representation of topological order **53**
4.1 Models and results 55
4.1.1 Spin model with $\mathbb{Z}_2$ topological order 55
4.1.2 $\mathbb{Z}_2$ model with string tension 58
4.1.3 $\mathbb{Z}_2$ model with end of strings 60
4.1.4 Necessary symmetry condition 62
4.2 Conclusion and discussion 63
4.3 Supplementary material for S_{tp} calculation 65
4.3.1 Calculating S_{tp} for $\mathbb{Z}_2$ model with string tension 65
4.3.2 Calculating S_{tp} for $\mathbb{Z}_2$ model with end of strings 66
4.3.3 Calculating S_{tpr} for random tensors in the neighborhood of $\mathbb{Z}_2$ . . . 67
4.3.4 Gauge symmetry of tensor product states and topological order . . . 67

III Classification of Topological Order **69**

5 Topological order and long/short range entanglement **71**
5.1 Background: quantum phase and topological order 72
5.1.1 Quantum phase and phase transition 72
5.1.2 What is missing in symmetry breaking theory 73
5.2 Quantum phases and local unitary quantum circuits 74
5.2.1 Quantum phases and local unitary evolutions in ground states . . . 75
5.2.2 Local unitary evolutions and local unitary quantum circuits 76
5.2.3 Local unitary quantum circuits and wave-function renormalization . 77
5.3 Topological order as pattern of many-body entanglement 79
5.3.1 Long-range entanglement and intrinsic topological order 79
5.3.2 Short-range entanglement and symmetry protected topological order 80
5.3.3 Quantum phase diagram 81

6 Symmetry protected topological phases in one dimension **83**
6.1 No intrinsic topological order in 1D spin systems 84
6.2 Symmetry protected topological order in 1D spin systems 85
6.2.1 On-site Symmetry 85
6.2.2 Translation invariance and parity 90
6.3 Summary of results for spin systems 95
6.4 1D symmetry protected topological phases in fermion systems 96
6.4.1 Fermion Parity Symmetry Only 96

6.4.2 Fermion Parity and $T^2 = 1$ Time Reversal 97
6.4.3 Fermion Parity and $T^2 \neq I$ Time Reversal 98
6.4.4 Fermion Number Conservation 98
6.5 Details of 1D classification 98
6.5.1 Projective Representation 98
6.5.2 Solving symmetry condition for fixed point 99
6.5.3 Equivalence Between Symmetric Fixed Point States 101
6.5.4 Deformation of TI states with on-site symmetry or parity symmetry 103
6.5.5 A proof of Eq. (6.11) 104

7 Symmetry protected topological phases in two and higher dimensions 107
7.1 Model with Z_2 symmetry protected topological order in 2D bosonic system 108
7.1.1 Summary of CZX model 108
7.1.2 CZX model in the bulk 108
7.1.3 CZX model on the boundary 110
7.1.4 Matrix Product Unitary Operators and its relation to 3 cocycle . . . 112
7.1.5 Nontrivial 3-cocycle of MPUO and nonexistence of SRE symmetric state 114
7.2 Systematic construction of SPT phases in two and higher dimensions 116
7.2.1 Construction of SPT phases in Hamiltonian formulation 117
7.2.2 Construction of SPT phases in Lagrangian formulation 122
7.3 Summary of result 131
7.4 Supplementary materials for the systematic construction 133
7.4.1 Group cohomology 133
7.4.2 Review: obtaining canonical form of MPS 137
7.4.3 Matrix Product Unitary Operators 140
7.4.4 (1+1)D solutions of Eq. (7.25) 143
7.4.5 (2+1)D solutions of Eq. (7.25) 146
7.4.6 $(2+1)D$ SPT states constructed from 3-cocycles and matrix product unitary operator 150

IV Application to Quantum Computation 153

8 Measurement-based quantum computation and tensor product states 155
8.1 Measurement-based quantum computation 155
8.2 MBQC in tensor product states 157
8.2.1 Teleportation 157
8.2.2 Measurement-based quantum computation as teleportation in projected entangled pair state 159

9 Measurement-based quantum computation in gapped ground states of two-body Hamiltonian 163
9.1 Construction of model 164
9.1.1 Building on PEPS 164
9.1.2 The tri-Cluster State 165
9.2 Uniqueness & Gap of parent Hamiltonian 166
9.3 Universality for measurement-based quantum computation 168

9.4 More recent developments 169

10 Fermionic measurement-based quantum computation **171**
10.1 Fermionic teleportation 172
10.1.1 Fermionic teleportation as a generalization of spin teleportation . . . 173
10.1.2 $n \to 2n$ encoding scheme 174
10.1.3 Fermionic teleportation for a universal set of gates 175
10.2 Fermionic Projected Entangled Pair States for MBQC 176
10.2.1 A simple example of fermionic resource state 176
10.2.2 Dealing with measurement randomness in the simple model 178
10.2.3 General fPEPS construction for fMBQC 179
10.3 Conclusion 182

V Conclusion **184**

11 Summary and outlook **185**
11.1 What we have learned about many-body entanglement 185
11.2 Future directions 186

Part I

Background

Chapter 1

Introduction

1.1 Extreme quantumness in many-body systems

It was realized more than 100 years ago that the world is quantum. Yet up until now, we are still exploring the the extent of the realm of quantum mechanics. As lower temperature and better control of systems are achieved in experiments, the quantumness of the world at different levels is being exposed, which has kept surprising us all these years.

The first sign of quantum mechanics emerged from the finding that the energy of microscopic objects, like atoms and light, is quantized. It was then realized that quantum mechanics rules over classical mechanics for microscopic objects and many other strange phenomena were also discovered, like the wave-particle duality and the uncertainty principle. Such quantum properties were subsequently observed in particles as large as C_{60}. These observations, all together, firmly establish quantum mechanics as the basic working principle for individual microscopic objects.

When a large number of microscopic objects are put together into a macroscopic ensemble, new interesting quantum mechanical behaviors appear. For example, the idea of identical particles divides microscopic objects into two classes: bosons and fermions. Therefore, macroscopic ensembles of microscopic objects also fall under the rules of quantum mechanics, through the appearance of quantum statistics. The most striking manifestation of quantum statistics comes in the experimental realization of a Bose-Einstein condensate, which contains millions of atoms.

In a Bose-Einstein condensate or a Fermi gas, each particle knows about the existence of other particles only through statistics and apart from that they live lives of their own. But the particles in an ensemble can interact with each other and their interaction can lead to perhaps the most exotic quantum phenomenon of all – entanglement. The existence of entanglement perplexed the greatest minds like Einstein and its experimental verification establishes a fundamental difference between the quantum and the classical world. Since the first experimental observation of entanglement, the limits of quantum mechanics have been extended by the creation of entanglement between four, six, or eight microscopic quantum particles or even between objects of macroscopic size.

And now, we are ready to push the quantumness of the world to its extreme. We are interested in macroscopic ensembles of microscopic particles each obeying the laws of quantum mechanics and at the same time interacting strongly with each other and hence being entangled with all the other particles. This is the subject of many-body entanglement. We ask what the world looks like at this level of quantumness and what happens if we can

take control. We do not have a complete answer, but we know that there are new surprises in store. And this is the subject that I focus on in this thesis.

I begin my exploration of the subject of many-body entanglement by discussing what it is (section 1.2), why it is interesting (section 1.3), what we expect to learn about it (section 1.4) and what we already know (section 1.5). In section 1.6, I summarize the results presented in this thesis towards the general goal of understanding many-body entanglement in quantum systems.

1.2 What is many-body entanglement

1.2.1 Entanglement

First we need to take a step back and review the notion of entanglement in quantum mechanics.

Quantum mechanical systems exhibit many interesting properties compared to classical systems and entanglement is definitely one of the most exotic. Entanglement is a special form of correlation between quantum mechanical objects, which exists beyond the ways classical objects can be correlated. Imagine a classical system composed of several objects, where each object can be in one of several possible states and the state total state of the system has some random distribution. The component objects of the system are said to be correlated if the states they take have certain inter-dependence among each other. One property of such classically correlated system is that, once the total state of the system is fixed, the states of the component objects are fixed too and randomness is completely suppressed. However, this is not necessarily true in quantum correlated systems. In a quantum ensemble of correlated objects where the quantum state of each component depends on the quantum states of others, it is possible that even when the total state of the system is determined, the state of each component object can still be random and mutually correlated. Entanglement hence describes such quantum correlation that exists among components without requiring global randomness.

This feature is best illustrated by the simplest entangled state, the Einstein-Podolsky-Rosen (EPR) pair[EPR35]. The EPR pair is composed of two spin 1/2 particles, each pointing either up or down. Denote the two states as $|\uparrow\rangle$ and $|\downarrow\rangle$. The pair is in the singlet state

$$|\psi\rangle = \frac{1}{\sqrt{2}}(|\uparrow\rangle|\downarrow\rangle - |\downarrow\rangle|\uparrow\rangle) \tag{1.1}$$

With fixed total angular momentum, $|\psi\rangle$ provides a definite description of the two spin system. However, the state of the two individual spins are random and correlated with each other. Actually, if we measure the spins of the two particles separately, we will find that the first one can point in any direction in space and the second one will always take the opposite direction. This provides the simplest example of entangled states in quantum systems without global randomness.

In general, for quantum systems in such pure states (with no global randomness), unentangled states are tensor products of pure states of each component objects, for example $|\psi\rangle = |\uparrow\rangle|\uparrow\rangle$, and entangled states can be written as a linear superposition of such states.

Quantum systems can have global randomness also and the notion of entanglement applies to this general case as well. For such mixed states, entanglement describes the quantum correlation that exist beyond possibilities of classical global randomness. More

specifically, we say that a quantum mixed state is entangled, if it cannot be thought of as a random distribution over unentangled pure states.

Entanglement is not only an interesting property of quantum systems, it also turns out to be a hugely useful resource for quantum information processing. The existence of quantum correlations between different parties enables us to process information in a more reliable, efficient and secure way. In fact, entanglement has become an indispensable resource for quantum information processing, which determines how well we can do not only qualitatively but also quantitatively. Therefore, this subject has been extensively studied in quantum information theory. For review, see [NC00] and [HHHH09]. Here we only briefly mention some major results about entanglement between a few quantum objects, to set the stage for our discussion of many-body entanglement in later sections.

For a quantitative description of entangled states, different entanglement measures have been defined to characterize 'how much' entanglement is contained in a particular state. The most used one is the entanglement entropy defined for pure states. In a bipartite system with two components A and B, the entanglement entropy for a pure state $|\psi_{AB}\rangle$ is equal to

$$S(|\psi_{AB}\rangle) = -\mathrm{Tr}(\rho_A \ln \rho_A), \text{ where } \rho_A = \mathrm{Tr}_B |\psi_{AB}\rangle \langle\psi_{AB}| \tag{1.2}$$

where Tr_B is the partial trace operation over basis states only in subsystem B. We can exchange A with B in the above formula and the resulting entanglement entropy would be the same. Entanglement entropy provides a simple description of entanglement in bipartite pure states. However, in order to describe the more complicated structure of entanglement in tripartite or multi-partite system and in mixed quantum states, more sophisticated entanglement measures are necessary. These include Renyi entropy, negativity, three tangle, and geometric entanglement, to name but a few. For a more complete review, see [PV06].

The nature of quantum correlation in an entangled state and its usefulness in quantum communication does not depend on how we label the states of each party. Therefore, different entangled states can be equivalent in this sense if they can be mapped to each other by local change of basis for each party separately. This defines the Local Unitary (LU) equivalence between entangled states. The measures of entanglement should be invariant under such equivalence transformations, as is indeed the case for all the entanglement measures discussed above. In some cases, more general local operations and classical communications are allowed in quantum communication protocols, which leads to the Local Operation and Classical Communication (LOCC) equivalence relation between entangled states. If entangled states can be classified according to such equivalence relations, then a complete understanding of their quantum communication capacities can be obtained. This program has been successfully carried out for bipartite pure states, three qubit pure states[DVC00], and four qubit pure states[VDDMV02]. However, generalization of this program to larger multi-partite systems becomes extremely hard.

Note that in the context of bipartite or multi-partite entanglement, 'local' operations are strictly restricted to within each party. This notion of locality will be different in the context of many-body systems and hence for the rest of this thesis. 'Local operations' in the many-body context refers to those that act on two, three or any finite number of parties in a system of infinite size. If the system under consideration lives in a finite dimensional space, then 'locality' also means that the parties involved in an operation are within a finite distance from each other.

1.2.2 Many-body entanglement

The topic we are interested in in this thesis, is what happens when many quantum objects are entangled together. Here by 'many', we are not referring to five or ten quantum objects as compared to two or three discussed above. Instead, we are interested in entanglement in atomic ensembles of thousands or millions of particles, in macroscopic condensed matter systems of 10^{23} spins or electrons, and more or less equivalently systems with an infinite number of particles. We call entanglement in such systems the 'many-body entanglement' and correspondingly that in systems of two or three objects the 'few-body entanglement'.

The basic definition of entanglement remains the same as we move from few-body systems to many-body systems. As we are be mostly focused on pure states, many-body entanglement will be manifested as a superposition of different many-body product states, which is totally analogous to the few-body case. Given all the similarities, the first question we need to clarify here is how many-body entanglement is different from its few-body counterpart and why it is a separate area of study and worth special treatment.

First of all, this is because for many-body systems we are interested in different kinds of behavior than the few-body systems. While with two entangled spins we are interested in what state each spin is in and how information can be encoded and carried around by each of them, in a many-body system it is in most cases impossible and unnecessary to keep track of the dynamics of every individual particle. Instead, we are interested in the emergent collective behavior of all the particles in the system. A classical situation which clearly illustrate this point is a sound wave through a medium. Instead of watching how individual particles in the medium vibrate, we are interested in how sound wave propagates through the medium, involving the motion of all particles in it and at a much larger length scale. Similarly, in quantum many-body systems we are be interested in the collective behavior of the system at low energies, which provides a different background motivation for the study of entanglement.

Because of the change in motivation, we are asking different questions about entanglement in many-body systems. Instead of asking, for example, how two particular particles are entangled, we look for global entanglement patterns among all particles. Usually it is important to understand how such entanglement patterns changes as systems size grows larger, which reflects the collective physical property of the system.

Finally, there is one more important change in the study of entanglement when moving from few-body to many-body systems – the notion of locality. As few-body entangled states are usually applied to quantum communications protocols where the component quantum objects are distributed to widely separated parties, local operations refer to those limited strictly within each component. Many-body entangled states are often considered in different context. Many-body systems usually occupy certain spatial region, in many cases a lattice in certain spatial dimension. Each particle in the system will have neighbors with which it can interact. In this situation, local operations can act on a few particles in the same neighborhood at the same time, but the size of the neighborhood and the number of particles within the neighborhood is usually limited. In most cases, locality in many-body systems means a finite limit on such neighborhoods which does not grow with system size. As the meaning of locality changes, many of the previous notions for few-body entanglement break down, for example the local unitary equivalence relation between entangled states. New ideas and approaches are necessary to establish a new theory for many-body entanglement.

1.3 Why do we care about many-body entanglement

But why should we care about many-body entanglement? In most many-body systems we see everyday, like gases, liquids or solids, thermal noise is always strong enough to suppress quantum effects and classical correlation dominates over the quantum ones. However, as temperature goes down, noise is reduced, quantum coherence is enhanced, and quantum effects in many-body systems begin to show up. In fact, nowadays we have such effective cooling methods that not only can we observe strong quantum effects in condensed matter systems at effectively zero temperature, but we are also able to generate and manipulate quantum many-body systems as designed to implement controlled quantum information and quantum computation protocols in these systems. Many-body entanglement, as a special manifestation of the quantumness of the system, hence emerges as important subject of study in both condensed matter physics and quantum information theory. We discuss motivations for studying many-body entanglement in these two areas respectively.

1.3.1 Condensed matter motivation

A central issue in condensed matter theory is to understand what phases exist in many-body systems and how a phase transition happens. For classical many-body systems, the Landau-Ginzberg theory provides an almost complete answer to this question, which says that different phases exist because the symmetry of the system is spontaneously broken in different ways and phase transition happens through thermal fluctuation[Lan37]. A simple example of a classical symmetry breaking phase is a ferromagnet whose spins all choose to point in a particular direction in space and hence breaks the rotational symmetry of the system. Because of this symmetry breaking, the direction of the spins are all strongly correlated with each other. Note that the correlation generated by symmetry breaking is purely classical. In fact, such long range classical correlation is the tell-tale sign of symmetry breaking phases. As the ferromagnet is heated, near the phase transition point, thermal fluctuations destroy such long range correlations and bring the system into a symmetric paramagnetic phase.

Symmetry is a generic feature of systems and applies to quantum many-body systems as well. Many quantum phases and phase transitions can also be well described by the symmetry breaking theory[Sac01]. These include the quantum ferromagnetic phase and the highly nonclassical superfluid phase. A common feature of such quantum symmetry breaking phases is again the existence of long range classical correlation. One difference of quantum symmetry breaking phases from classical ones is that in quantum systems phase transitions can happen at zero temperature. It is therefore not thermal fluctuations in the form of random mixtures but quantum fluctuations in the form of linear superpositions that destroys the classical correlation and brings the system to a symmetric phase. The effects of the different forms of fluctuations are similar at the transition from symmetry breaking phases to symmetric phases, hence such quantum phase transitions are also well captured by Landau's theory.

But this is not the end of the story. In recent decades, starting with the discovery of chiral spin liquids[KL87, WWZ89, Wen89], it has been realized that quantum phases and phase transitions exist beyond the possibilities of symmetry breaking. In particular, nontrivial quantum phases exist even when no long range classical correlation can be detected. These quantum phases are in general said to be 'topological'. It turns out that entanglement, the quantum correlation, plays a major role in such topological phases and is essential

for their understanding. Phase transitions outside the Landau paradigm are said to be unconventional[Sac01, Xu12]. Without the classical thermal analog, we need to in general deal with quantum fluctuations directly, which in many cases indicate the existence of many-body entanglement. Therefore, understanding many-body entanglement is the key to a more complete theory of quantum phases and phase transitions.

1.3.2 Quantum information motivation

While the idea of entanglement is introduced to condensed matter theory relatively recently, Quantum information theory, on the other hand, starts dealing with entangled quantum systems, but of very small size. The first quantum information protocols, like teleportation [BBC+93], employed mostly bipartite entangled states for the efficient and secure communication of quantum information. Much has been understood and achieved with such few-body entangled states. However, in order to achieve the full glory of quantum information theory, it is necessary to involve many-body entangled systems.

One of the most exciting promises of quantum information is a quantum computer. A quantum computer computes according to the quantum mechanical principles of the world, like superposition and entanglement. By maintaining quantum coherence of the computational device throughout the computational process, it solves certain problems, like factoring big integers[Sho97], in an exponentially faster way than known algorithms on classical computers. In order to realize such a speedup, a quantum computer with thousands or millions of quantum mechanical bits (qubits) and a large amount of entanglement is necessary. While experimental progress is being made towards such scalable quantum computation architectures, theoretical challenges remain as to understand not only how much entanglement this many-body system must have in order to support quantum computation but also the details of the necessary many-body entanglement structures.

Therefore, many-body entanglement has also become a central subject of study in quantum information theory. This is especially true in certain 'top-down' approaches to building a quantum computer, like the Measurement-based Quantum Computation model[RB01] and the Topological Quantum Computation model[Kit03]. Unlike the 'bottom-up' approach in the circuit model of quantum computation where many-body entanglement is built up from few-body ones and exists as an intermediate step in the computational process, the 'top-down' approaches start with a many-body entangled state and use it as a resource for the whole computation. If the many-body entangled state naturally exists in real materials or can be easily generated in lab, the computational effort can be greatly reduced. Therefore, it is very important to understand what many-body entanglement structure is necessary for quantum computation and what is available in nature. If a match can be found, it will lead to a big step forward towards the experimental realization of quantum computation.

1.4 Important questions about many-body entanglement

So what are the important question to be answered and important issues to be solved to understand many-body entanglement?

1.4.1 How to characterize many-body entanglement

First of all, we need to find a way to efficiently describe many-body entangled states. This is not a trivial question.

For few-body entangled states like the EPR pair, it is easy to give a complete description of it by writing down its wave-function as in Eq. (1.1). In fact, the wave-function of such two qubit systems can be written as a superposition of at most four product states and hence only four complex numbers are necessary to completely characterize the system. However, the number of parameters necessary to write down a general entangled wave-function of N qubit system grows exponentially as 2^N. Such exponential growth quickly exceeds the memory capacity of classical computers available today for a moderate $N \sim 50$, before any many-body collective behavior becomes evident or any large integer can be factorized. Therefore, a brute force approach to describe many-body entanglement in the same way as few-body entanglement is doomed to fail and we need to refine the question before we can get a useful answer.

In fact, we are not interested in the whole set of many-body entangled states, but only those that we have access to. More specifically, we are only interested in the set of many-body entangled states which can be generated in nature or in lab in a finite or polynomial amount of time. States which require an exponential amount of time to generate will not appear at very large size. It turns out that such 'accessible' states occupy only a very tiny proportion in the total Hilbert space of many-body systems and by adding this reasonable condition we reduce our question to a much smaller one.

So the question is now, how can we efficiently characterize many-body entangled states that are 'accessible'? In particular, how can we benefit from the fact that we are restricting ourselves to a specific subset of all states and extract the important parameters out of the exponentially many to provide a succinct and useful description?

1.4.2 How is it related to physical properties of the system

Understanding how to describe many-body entangled states efficiently is necessary but not sufficient to make the study of many-body entanglement useful. A connection needs to be established between the understanding of many-body entanglement and physical properties of the system, just like in the few-body entanglement case where connections are made between various entanglement measures and the quantum communication capacities of the states. Otherwise, many-body entanglement will remain merely a theoretical concept without physical relevance.

More specifically, we need to understand

1. How is many-body entanglement related to experimentally observable phenomena of quantum many-body systems? For example, what many-body entanglement structure is responsible for the existence of magnetism and what structure is responsible for quantum Hall effect? Can we find a relation between many-body entanglement measures and physical measurable quantities like specific heat and compressibility of the system? More generally, what is the relation between many-body entanglement and the universal features of quantum phase and phase transitions?

2. How does many-body entanglement reflect the quantum computation capacities of the system? That is, what kind of many-body entangled state is useful for quantum computation and how. The answer to this question would depend on the quantum computation model under consideration. Many-body entangled states useful in, for example, the measurement based quantum computation might be useless for topological quantum computation. It is then important to understand the different many-body entanglement requirement in different quantum computation models.

On the other hand, the relation of many-body entanglement to physical properties of the systems also guides our study of the characterization of many-body entanglement. After all there are so many aspects of many-body entanglement to be explored and it can be hard to determine which one is important. Physical relevance hence provides one guiding principle as to which many-body entanglement features are worth studying and which are not.

1.5 What is known about many-body entanglement

Much progress has been made towards answering the previous questions. In this section we briefly review what is known about the efficient characterization of physically 'accessible' many-body entangled states, the relation between many-body entanglement and quantum phase and phase transition, and the relation between many-body entanglement and quantum computation. Also we discuss experimental detection and realization of many-body entangled states.

1.5.1 Efficient representation of many-body entangled states

Important progress has been made in providing an efficient characterization of 'accessible' many-body entangled states using the so called 'Tensor Network Representation' [VMC08, FNW92b, PGVWC07, Vid03, Vid07]. Starting from the one-dimensional version of matrix product states, the tensor network representation incorporates just the right amount of entanglement into the description such that it captures the essential features of physically 'accessible' quantum states and at the same time avoids exponential complexity. As our work builds extensively on the tensor network representation, we will give a detailed review of the formalism in part II.

While the formalism is very promising in providing an efficient tool to study many-body entangled states both analytically and numerically, many questions remain open, mostly in two and higher dimensions. Some important questions include: 1. What is the best way to efficiently and accurately find a tensor network description of a many-body entangled quantum state and calculate physical observables from it, especially in two and higher dimensions? 2. How to determine which phase the system belongs to from the representation, especially for topological phases where local order parameters do not exist? 3. Are there degrees of freedom in the representation that are unphysical and hence should be removed when we study the physical properties of the system? We address some of the questions in part II.

1.5.2 Many-body entanglement and quantum phase and phase transition

It has been realized that the many-body entanglement structure of a state carries universal features of the underlying quantum phase and phase transitions, as has been demonstrated in various condensed matter systems by applying few-body entanglement measures to the many-body systems. We review prior results below.

Condensed matter many-body systems usually reside on a regular lattice in certain spatial dimensions and each lattice site holds a local quantum degree of freedom, which can be bosons, fermions, or spins. The local degrees of freedom can interact with its neighbors but the interaction range usually has a finite limit. This locality condition puts a strong constraint on the amount and form of entanglement that can be present in the many-body system.

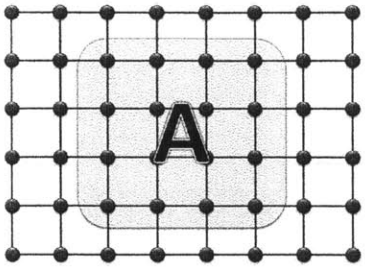

Figure 1-1: 2D square lattice with subregion A

Consider, for example, a two dimensional square lattice as shown in Fig. 1-1 with local interactions. Suppose that the energy difference–the gap–between the ground state of the system and all the excited states is Δ. If Δ is lower bounded by a finite number as the system size goes to infinity, then the system is said to be gapped. Its ground state is called a gapped ground state. Sometimes we say a state is a gapped quantum state without explicitly identifying the interactions in the Hamiltonian of the system. In such cases we are implying that a Hamiltonian with local interactions can be constructed which has the state as a gapped ground state. If on the other hand Δ goes to zero as system size grows, then the system and its ground state are said to be gapless. Many-body entanglement behaves in very different ways in gapped and gapless systems.

If the system is gapped, then the entanglement in the ground state satisfies a surprising property called the 'area law'. More specifically, suppose we take a subregion A (as shown in Fig. 1-1) of size L^2 from the whole system and calculate the entanglement entropy for this region. The number of degrees of freedom in this region is proportional to L^2, so the maximum entanglement entropy we can get (and actually will get for a generic man-body entangled state) scales as L^2. However, the calculation for a gapped ground state always gives entanglement entropy S which is proportional to the length of the boundary of the region, which grows as L,

$$S \sim \alpha L \tag{1.3}$$

Therefore, a gapped ground state in a locally interacting system always contains much less entanglement than a generic many-body entangled state. Such understanding is crucial towards an efficient description of many-body entangled states in gapped quantum systems.

The term 'area law' is better suited to a three dimensional system where the entanglement entropy of a subregion in a gapped ground state scales as the surface area of the region rather than the volume of the region. The basic idea applies to systems in any dimension though, which says that the entanglement entropy of a subregion scales as the size of the boundary rather than the size the bulk of the system. An easy way to understand why this is true is to realize that quantum correlation is generated by interactions. Between subregion A and the rest of the system, only degrees of freedom close to the boundary can be interacting with each other. Moreover, in a gapped system, propagation of correlation is suppressed by the existence of a gap. Therefore, the entanglement entropy satisfies the 'area law'. Of course, if the locality condition is removed, the area law no longer holds.

In one dimensional systems, the existence of an area law has been established as a rigorous mathematical theorem[Has07]. In two or higher dimensions, a full proof of the theorem does not exist yet but it has been supported by a large amount of numerical

evidence. For a more detailed review of the subject, see [ECP10].

In a critical or gapless system, the area law can be violated, but usually only mildly by a term that scales as the logarithm of L. For example, at one dimensional critical points described by conformal field theory, the entanglement entropy of a segment of the chain of length L scales as[HLW94, CC09, VLRK03]

$$S \sim \frac{c+\bar{c}}{6} \log L \tag{1.4}$$

where c and $\bar{c}$ are the central charges of the conformal field theory. Also for gapless free fermion system in D dimensions with a Fermi surface, the entanglement entropy of a region of linear size L scales as[ECP10]

$$S \sim L^{D-1} \log L \tag{1.5}$$

The violation of area law comes from the existence of low energy excitations which carries correlations as it propagates. However, the locality constraint still exists and and keeps the entanglement content in the state far from maximum.

The change in entanglement content from an 'area law' to beyond as one moves from gapped phases to phase transitions has become a useful tool in detecting phase transitions. In fact, not only entanglement entropy, but also many other different entanglement measures have been found to exhibit diverging behavior as a phase transition point is approached and therefore can be used as a probe for detecting phase transitions. While numerical and experimental challenges remain to calculate or measure entanglement in a system, one special advantage of such a probe is that it works for both symmetry breaking and topological phases. Some conventional probes of phase transitions, like order parameter, apply only to symmetry breaking phases and fail for topological phases. Entanglement measures, however, are generic probes independent of the nature of the phase transition. For summary of these results, see [AFOV08].

Other than revealing the gapped/gapless nature of the system, entanglement entropy can provide more detailed information about the order in the quantum phase if we look at it more carefully. In particular for a gapped quantum system, if the system has nontrivial topological order, then the entanglement entropy of a region has a sub-leading constant term apart from the leading area law term[KP06, LW06]

$$S \sim \alpha L - \gamma \tag{1.6}$$

with $\gamma > 0$. Such a term indicates the existence of certain long range entanglement structure that originates from the topological nature of the system. Different methods have been proposed to extract such a constant term from the ground state and hence determine the nature of the topological order of the system[KP06, LW06].

Recently, it has been realized that more detailed information about topological order can be extracted from the entanglement structure of the system than just a single number of entanglement entropy. It has been proposed in [LH08, PTBO10] that, the entanglement spectrum, i.e. the eigenvalue spectrum of the reduced density matrix, has meaning of its own. In fact for a gapped topologically ordered system, the 'low energy' sector of the entanglement spectrum should reflect the nature of the low energy excitations on the edge of the system. Such a correspondence established a connection between the more theoretical notion of entanglement and the directly measurable physical response of the system, and has hence received a great deal of attention.

By identifying universal features of many-body entanglement for states in different quantum phases, these works have shown that many-body entanglement can be a useful tool in the detection and characterization of quantum phase and phase transitions. Actually, many-body entanglement is more powerful than just being another characterization tool of known phases. It has been realized that many-body entanglement carries so much information about the universal properties of the phase that it could provide more complete knowledge of the whole quantum phase diagram, answering questions like what new quantum phases exist and what is the global structure of the phase diagram. In particular, if many-body entangled states can be classified according to their universal properties, then we can have a classification of all quantum phases. Some classification results have been obtained for one dimensional states in [VCL+05]. Moreover, for two dimensional topological orders it has been realized that all abelian topological orders can be systematically described by K-matrices[BW90, Rea90, WZ92, FK91]. Also the string-net picture provides a general construction of time reversal symmetric topological orders and may even classify them[LW05]. We carry out this classification scheme in broader settings (especially in systems with short range entanglement and symmetry) in part III, where we find new topological phases and obtain a more complete understanding of the structure of the quantum phase diagram.

1.5.3 Many-body entanglement and quantum computation

From the earliest proposals of quantum communication to the ultimate goal of building a quantum computer, entanglement has always been a central theme in quantum information theory. A general consensus is that entanglement is a necessary and essential resource for the power of quantum information protocols. Without entanglement, most quantum protocols become equivalent to classical ones. The question is, exactly how much entanglement is necessary to realize such protocols?

Quantum communication protocols are usually based upon few-body entangled states distributed among several parties for the exchange of quantum information. In order to transmit a large mount of information, a large number of few-body entangled states are necessary. How many few-body entangled states need to be consumed for the transmission of certain amount of information is extensively studied in the subject of quantum communication complexity.

Quantum computation, on the other hand, has been found to require many-body entanglement in a much stronger sense. In fact, it has been shown that for pure state quantum computation algorithms, many-body entangled states with a number of parties that increases unboundedly with input size is necessary if the quantum algorithm is to offer an exponential speed-up over classical computation[JL03]. Actually, it was shown that if a quantum algorithm only involves a large number of few-body entangled states rather than a many-body entangled state of many parties, then the algorithm can be efficiently simulated with classical computers. This result clearly establishes the necessity of big many-body entangled states for quantum computation.

Moreover, it has been realized that there exists a lower bound on the amount of many-body entanglement that must appear during the process of useful quantum computation. Actually it has been shown that in a one dimensional system, if the entanglement of a segment of the chain always remains finite during the computational process, then the whole computation can be simulated classically[Vid03, Has09]. This provides a tighter necessary condition for the many-body entanglement needed in quantum computation.

On the other hand, with the general notion that entanglement is crucial and indispens-

able for quantum computation, it is a bit surprising to learn that sometimes too much entanglement can also kill the power of quantum computer. This result is obtained for the model of measurement-based quantum computation, where the computation starts with a many-body entangled state and performs purely single particle measurement to implement the algorithm. It has been realized that for this purpose some states could contain so much many-body entanglement that the measurement process could be efficiently simulated classically[GFE09, BMW09]. In fact, it turns out that most of the many-body states in the total Hilbert space belong to this set and hence are useless for measurement-based quantum computation. The lesson is that entanglement, like any other resources, must be consumed moderately. Of course the upper bound on entanglement is much higher than the 'accessible' amount in real physical systems.

The upper and lower bound on many-body entanglement necessary for quantum computation provides a starting point for the study of the role of many-body entanglement in quantum computation. However, this seems to be a hard question in general and the details of the answer would depend on the specific quantum computation model under consideration.

A more practical issue is to find many-body entangled states that are useful for quantum computation and also experimentally accessible. For example, in the topological quantum computation model, the $\nu = 5/2$ fractional quantum Hall state has been identified to be capable of supporting arbitrary quantum computation[Bra06].

In the measurement-based quantum computation model, finding a proper many-body entangled resource state is also a major theoretical challenge in the realization of this model. In this model, quantum computation is performed by doing only single particle measurement on a many-body entangled states. Without the need of coherent unitary operations, measurement-based quantum computation reduces the experimental effort greatly compared to the circuit model of quantum computation, on the condition that a proper many-body entangled resource state exists. It is then important to find such a state which is useful for measurement-based quantum computation and at the same time easy to realize in the lab. Many efforts have been made towards this goal. We give a detailed review of previous works and present our own contributions in part IV.

1.5.4 Many-body entanglement in experiment

One major problem with abstract notions like many-body entanglement is whether it has any experimental relevance. The answer is yes and here we review recent progress on two aspects of this problem: the experimental measurement of entanglement entropy in real condensed matter systems and the realization of many-body entangled states in atomic systems.

Many-body entanglement as a nonlocal quantity is in general very hard to measure. In a two or three body entangled state, entanglement can be extracted from a full measurement of the reduced density matrix of a subsystem, but this may require hundreds or thousands of measurement operations even for a state of very small size. In many-body system, a brute-force determination of the whole density matrix is not possible and clever schemes are needed to relate entanglement measures to suitable physically measurable quantities.

One approach is to relate entanglement entropy in a non-interacting many-body system to the distribution of certain conserved quantities, like charge or spin[KRS06, SFR+11]. A key observation made in [KL09] is that a universal relation exists between entanglement entropy and the fluctuations of the current flowing through a quantum point contact,

which made direct experimental measurement of entanglement entropy possible. However, this relation is system specific and was found to be invalid for system with strong interaction[HGF09]. A different approach proposed in [Car11] is to measure entanglement (Renyi) entropy with a local quantum quench. It was shown that near some quantum critical points, entanglement entropy can be related to the low energy distribution of the system after the quench and hence can be measured.

While measuring entanglement may be hard in general, one may argue that after all we are interested in the physical properties induced by strong entanglement instead of particular values of entanglement measures. Therefore, it would suffice if we can create strongly entangled many-body states and use them for our purposes. There has been exciting progress in this respect in photonic, atomic and solid state experiments, where our ability to accurately control and manipulate microscopic quantum mechanical objects has expanded greatly. There has been many theoretical proposals about how to create strong interaction and generate entanglement, usually in a parallel fashion, in a system of a large number of photons[BD06], trapped ions[JVW09], cavities[HBP08, TF10], and cold atoms[BDZ08, JZ05]. The motivation is two fold. First, to build a quantum simulator[Fey82] to simulate strongly correlated condensed matter systems and probe regimes which are hard to reach in real materials. Second, to generate many-body entangled state useful for quantum computation, for example in the measurement-based quantum computation model.

There has been much progress for the first objective in recent years, especially in cold atom systems. By cooling boson or fermion gases to extremely low temperatures and loading them into a optical lattice, many interesting condensed matter phenomena have been reproduced in atomic systems, including the Mott-insulator to superfluid transition in Bose-Hubbard model[GME$^+$02], one dimensional bosonic Luttinger liquid[PWM$^+$04, KWW04], Kosterlitz-Thouless transition in two dimension[HKC$^+$06] etc. For a more comprehensive review see [BDZ08].

While the Mott-insulator and superfluid phases are more conventional with regard to many-body entanglement, recent theoretical and experimental advances have made much progress towards realizing highly entangled topological phases in cold atom systems. Such efforts include small scale demonstrations of resonating valence bonds and topological matter[PB08, NCA$^+$12] and the realization of synthetic gauge fields in neutral atomic systems[DGJO11]. These provide the necessary elements to realize highly nontrivial topological phases with highly entangled ground states in cold atom systems, from spin liquids, string-net states, to fractional quantum Hall systems.

1.6 Summary of thesis

1.6.1 Central topic and general structure

In this thesis, we focus on the theoretical understanding of the many-body entanglement properties of gapped quantum systems. More specifically, we are interested in quantum many-body systems residing on a lattice, interacting locally, and having a finite energy gap between its ground state and all the excited states. Gapped quantum systems have attracted a great deal of attention in recent years. Our interest in gapped quantum systems is due to two reasons. On the one hand, the discovery of topological order has revealed new fundamental physics in gapped many-body systems and many new quantum phases are waiting to be explored which could provide the crucial step towards our understanding of some of the most puzzling condensed matter phenomena, like high temperature super-

conductivity. On the other hand, the existence of a gap could provide protection against thermal noise to the ground state of the system where quantum computation can be carried out in a more reliable way. Therefore, we are interested in exploring possibilities of using gapped quantum states for quantum computation. Both topics are closely related to the study of many-body entanglement as we have discussed in previous sections, therefore many-body entanglement in gapped quantum systems is our central topic in this thesis. We also hope that our understanding of the (possibly) simpler many-body entanglement structure in gapped quantum systems could give us some hint about what to expect in gapless systems.

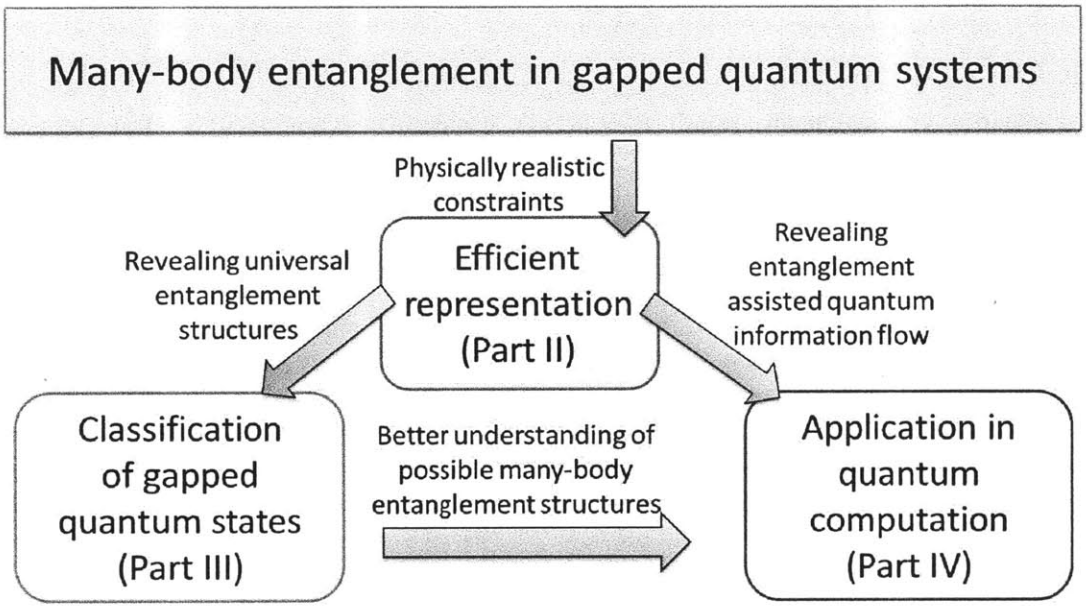

Figure 1-2: Structure of the thesis

The thesis work presented here concerns the representation, classification and application of many-body entanglement in gapped quantum systems. The general structure of the thesis is summarized in Fig. 1-2. With the realistic physical constraints on the many-body systems (including locality and gap), an efficient representation–the tensor network representation–of many-body entangled states exists. We review the representation and present our studies of open questions in part II. The representation reveals the universal entanglement structure of gapped many-body states which enables us to classify these states in part III. The representation also provides a clear picture of how many-body entanglement assists quantum information flow in a quantum state, based on which we design applications of many-body entangled states for quantum computation in part IV. A detailed summary of the results is given below.

1.6.2 Summary of results on representation

Our study of the tensor network representation of many-body entangled states focuses on two questions: 1. How to determine which phase the system belongs to from the representation? 2. Are there degrees of freedom in the representation that are unphysical and hence

should be removed when we study the physical properties of the system? We study the first problem in [CGW10] where we propose an efficient algorithm for the two dimensional tensor product states to extract the universal phase information of the state from the tensors. We demonstrate that the algorithm works not only for conventional symmetry breaking phases but for topological phases also. For the second problem, we find in [CZG+10] that the answer to the question is yes and we provide an explicit example of how illegal variations of the representing tensors lead to unphysical changes in the universal properties of the represented state. Moreover, we point out that for some topologically ordered systems, such illegal variations can be avoided if we impose certain symmetry constraints on the tensors. Imposing such constraints is important for a successful numerical study of topologically ordered systems using the tensor network representation.

1.6.3 Summary of results on classification

Based on the tensor network representation of gapped quantum states, we try to classify the states according to their universal properties and and hence classify all gapped quantum phases as we discussed in section 1.5.2. First, we establish in [CGW10] the general framework for this classification by giving an operational definition of the equivalence relation between gapped quantum states with the same universal properties. We find that gapped quantum states are in the same phase, hence having the same universal properties, if they are related by local unitary time evolution or equivalently a local unitary quantum circuit. Based on such an equivalence relation, we find that many-body entangled gapped ground states can be divided into two classes, those with long range entanglement and those with short range entanglement. The first class of states have different intrinsic topological orders. While the second class does not have intrinsic topological order, by adding symmetry requirement to the system we can have different symmetry protected topological orders. With this, we obtain the general structure of the quantum phase diagram in gapped systems. We then try to identify all the entries in the diagram for systems of different spatial dimensions. In [CGW11a] we classify all gapped ground states and hence all gapped quantum phases in one dimensional systems based on the entanglement structure of matrix product states. We find that there is no intrinsic topological order in one dimension but many symmetry protected topological orders exist. Then we move on to higher dimensions but restricting ourselves to only symmetry protected topological orders, whose ground states have simpler entanglement structure. We present an explicit example (in [CLW11]) and also a systematic construction (in [CGLW11]) of symmetry protected topological phases in interacting bosonic systems, which provides a substantial extension of the existing knowledge about such phases in free fermion systems.

1.6.4 Summary of results on applications

With our better understanding of many-body entanglement structure in gapped quantum states obtained from the tensor network representation and our classification results, we study the application of such states in quantum computation. In particular, we focus on the model of Measurement-based Quantum Computation and address the issue of finding an experimentally more feasible resource state as discussed in section 1.5.3. We find in [CZG+09] a many-body entangled state useful for measurement-based quantum computation which exists as the gapped ground state of a system with only nearest neighbor two-body interactions. With two-body interactions which can be engineered in cold atom

systems and a gap which protects the ground state from thermal noise and perturbations, this model presents a step forward towards the experimental realization of measurement-based quantum computation. Moreover, we generalize the framework of measurement-based quantum computation from spin to fermion systems, in the hope of finding simpler and more realistic resource state for measurement-based quantum computation by utilizing the unique entanglement structure of many-body fermion systems.

1.6.5 Organization of content

The thesis is organized as follows.

In Part II, we give a detailed review of matrix product states and tensor product states including their basic definition and important properties in Chapter 2 and Chapter 3 respectively. Our work builds extensively on these representations of many-body entangled states. We present our renormalization algorithm for tensor product states in Chapter 3 section 3.2 which extracts the universal properties of a many-body entangled state from its tensor network representation. In Chapter 4, we present our study of how illegal variations in the tensors lead to unphysical changes in the topological order of the represented state and how this can be avoided with proper symmetry constraints on the tensors.

Based on the tensor network representation discussed in Part II, we try to classify gapped quantum phases based on the many-body entanglement structure of their gapped ground states in Part III. In Chapter 5, we establish local unitary time evolution or local unitary quantum circuits as the equivalence relation between gapped quantum states in the same phase. Chapter 6 and Chapter 7 are then devoted to applying this equivalence relation to systems in one and higher dimensions respectively and classifying gapped quantum phases. In particular, in Chapter 6 we show how we are able to classify all gapped quantum phases in one dimensional systems using the matrix product formalism. Our understanding of one dimensional systems are then carried over to higher dimensions in Chapter 7, where we present first an example and then a systematic construction of symmetry protected topological phases in interacting bosonic systems.

In Part IV, we discuss the application of gapped quantum states in quantum computation. First, in Chapter 8, we review the measurement-based quantum computation model and its relation to the tensor network representation of quantum states. This relation forms the basis of our construction in later chapters. In Chapter 9, we present our construction of a resource state for measurement-based quantum computation which is also the gapped ground state of a system with nearest neighbor two-body interactions. Then in Chapter 10, we generalize the framework of measurement-based quantum computation to many-body fermion systems based on the fermionic tensor network representation.

Finally in Part V, we conclude the thesis by summarizing what we have learned about many-body entanglement and future directions to go.

1.6.6 List of publications

In this section, I list all my publications for this thesis work, including both the ones that are presented in this thesis document and the ones that are not.

1. Local unitary transformation, long-range quantum entanglement, wave function renormalization, and topological order, Xie Chen, Zheng-Cheng Gu, and Xiao-Gang Wen, *Phys. Rev. B* **82**, 155138 (2010).

Section XI and section XII of this paper are presented in Chapter 3 section 3.2 of this thesis where I propose an algorithm to implement the renormalization transformation on tensor product states. Section II to VII of this paper is presented in Chapter 5 where I use the 'quasi-adiabatic continuation' proposed in [HW05] to show the equivalence between local unitary time evolution and local unitary quantum circuit.

2. Tensor product representation of topological ordered phase: necessary symmetry conditions, Xie Chen, Bei Zeng, Zheng-Cheng Gu, Isaac L. Chuang, Xiao-Gang Wen, *Phys. Rev. B* **82**, 165119 (2010).

   This paper is presented in Chapter 4 where I demonstrate the necessity of symmetry constraints on tensor variations by calculating the topological entanglement entropy for the Z_2 topological model.

3. Classification of gapped symmetric phases in one-dimensional spin systems, Xie Chen, Zheng-Cheng Gu, and Xiao-Gang Wen, *Phys. Rev. B* **83**, 035107 (2011).

   This paper is presented in Chapter 6 where I use the matrix product state formalism to classify gapped one dimensional quantum phases.

4. Two-dimensional symmetry-protected topological orders and their protected gapless edge excitations, Xie Chen, Zheng-Xin Liu, Xiao-Gang Wen, *Phys. Rev. B* **84**, 235141 (2011).

   This paper is presented in Chapter 7 section 7.1 where I propose the CZX model and prove its nontrivial symmetry protected topological order.

5. Symmetry protected topological orders and the cohomology class of their symmetry group, Xie Chen, Zheng-Cheng Gu, Zheng-Xin Liu, Xiao-Gang Wen, arXiv:1106.4772 (2011).

   This paper is presented in Chapter 7 section 7.2 where I propose the form of the symmetry transformation in the Hamiltonian formalism of the construction.

6. Gapped two-body Hamiltonian whose unique ground state is universal for one-way quantum computation, Xie Chen, Bei Zeng, Zhengcheng Gu, Beni Yoshida, Isaac L. Chuang, *Phys. Rev. Lett.* **102**, 220501 (2009).

   This paper is presented in Chapter 9 where I propose the tri-Cluster model and show that it is both universal for measurement-based quantum computation and a unique gapped ground state of two-body interactions.

Chapter 10 is based on paper 'Fermionic measurement-based quantum computation' by Yu-Ju Chiu, Xie Chen, and Isaac L. Chuang, where I propose to generalize measurement-based quantum computation to fermion system based on the fermionic PEPS formalism. The paper is in preparation.

My other publications related to many-body entanglement and measurement-based quantum computation include

1. Quantum state reduction for universal measurement based computation, Xie Chen, Runyao Duan, Zhengfeng Ji, Bei Zeng, *Phys. Rev. Lett.* **105**(2), 020502 (2010).

2. No-go theorem for one-way quantum computing on naturally occurring two-level systems, Jianxin Chen, Xie Chen, Runyao Duan, Zhengfeng Ji, and Bei Zeng, *Phys. Rev. A* **83**, 050301 (2011).

My other publications related to many-body entanglement and topological phases include

1. Symmetry-protected topological orders of one-dimensional spin systems with $D_2 + T$ symmetry, Zheng-Xin Liu, Xie Chen, and Xiao-Gang Wen, *Phys. Rev. B* **84**, 195145 (2011)

2. Complete classification of one-dimensional gapped quantum phases in interacting spin systems, Xie Chen, Zheng-Cheng Gu, and Xiao-Gang Wen, *Phys. Rev. B* **84**, 235128 (2011)

I also work on quantum error correction and fault-tolerant quantum computation, with publications

1. Semi-Clifford operations, structure of C_k hierarchy, and gate complexity for fault-tolerant quantum computation, Bei Zeng, Xie Chen, and Isaac L. Chuang, *Phys. Rev. A* **77**, 042313 (2008).

2. Subsystem stabilizer codes cannot have a universal set of transversal gates for even one encoded qudit, Xie Chen, Hyeyoun Chung, Andrew W. Cross, Bei Zeng, Isaac L. Chuang, *Phys. Rev. A* **78**, 012353 (2008).

3. Nonbinary codeword stabilized quantum codes, Xie Chen, Bei Zeng, Isaac L. Chuang, *Phys. Rev. A* **78**, 062315 (2008).

I am also involved in the study of N-representability problem of quantum states with publication 'Quantum codes give counterexamples to the unique preimage conjecture of the N-representability problem', Samuel A. Ocko, Xie Chen, Bei Zeng, Beni Yoshida, Zhengfeng Ji, Mary Beth Ruskai, and Isaac L. Chuang, *Phys. Rev. Lett.* **106**, 110501 (2011).

Part II

Tensor Network Representation

Is there a way to write down many-body entangled states such that it is sophisticated enough to describe possible many-body entanglement in real physical systems but is not so complicated as to require an exponential amount of space and time? The answer is yes! As reviewed in [VMC08], the tensor network representation provides an efficient description of many-body entangled states satisfying an area law (or slight violation of it). These are exactly the states that appear in local quantum systems. Thus, the tensor network representation has become a powerful tool in the study of many-body entanglement and forms the basis for discussions in the next two parts. In part I, we review two basic forms of tensor network representations–the matrix product states in one dimension and the tensor product states in two and higher dimensions. Chapter 2 is devoted to the review of the matrix product state formalism and Chapter 3 focuses on its higher dimensional generalization–the tensor product states.

One important open question about the tensor network representation is how the tensors in the representation reflect the universal properties of the represented states. To address this question, we present a new renormalization algorithm in Chapter 3 section 3.2 which extracts universal properties of a state from its representing tensors. We also point out in Chapter 4 that caution must be taken when representation topological phases with tensors as we find that smooth variations in the tensors can lead to unphysical abrupt changes in the universal properties of the represented states. We present an example of this kind and show that for some topological phases, certain symmetry constraints on the tensors are necessary for them to provide a stable representation of the many-body entangled states.

We focus on the representations which satisfy an exact area law as we are studying gapped quantum systems in this thesis. Important developments in tensor network representation generalizes the framework to also deal with gapless systems[Vid07], continuous systems[VC10], fermionic systems[KSVC10, GVW10], and the path integral/partition function of local systems[LN07].

Chapter 2

Matrix product states

Quantum many-body systems in one dimension host a variety of interesting physical phenomena, like symmetry breaking, phase transition, and topological order. Many of the exactly solvable or approximately solvable one dimensional systems provide us with our basic intuition to think about and formulate theories for higher dimensional more complicated systems. Due to their geometrical simplicity, it also turns out that one dimensional quantum systems are the most amenable to numerical attacks. Indeed, the Density Matrix Renormalization Group (DMRG) algorithm developed in recent decades[Whi92] has proved to be a very powerful and also efficient tool for the numerical study of one dimensional quantum systems. It has been realized from the start that the success of this algorithm is due to the preservation of entanglement in the density matrix. Recently, such an intuition is made more rigorous and it is shown that the DMRG algorithm can be thought of as a variational method based on matrix product states. Using the matrix product formalism, we can see more clearly and even prove in some cases that the DMRG algorithm is able to give the right answer in an efficient way. Moreover, the matrix product representation also reveals certain analytical structure of one dimensional quantum states and enables us to have a more complete understanding of them beyond numerical results.

In this chapter, we review the matrix product formalism. We focus mainly on gapped quantum systems. For one dimensional gapped quantum states, it has been realized that they can be described efficiently using the matrix product states representation. That is, to represent the wave function of a system of size N, the number of parameters used in the representation grows only polynomially with N. We discuss its basic definition and important properties in section 2.1, the canonical form of the matrices in the representation in section 2.2 and how to implement an renormalization procedure on the state based on the representing matrices in section 2.3. This chapter is based on results in [FNW92b, PGVWC07, VCL$^+$05].

Note that by talking about dimensionality of a system, we are always assuming implicitly certain degree of locality. For example, in one dimensional systems where quantum degrees of freedom are aligned along a chain, only degrees of freedom within certain distance can interact. Otherwise it is not meaningful to arrange them into a chain. Such a locality constraint lies at the heart of all our understanding of one dimensional systems.

2.1 Definition and basic properties

2.1.1 Definition

Matrix product states describe many-body entangled states of spins living on a one dimensional chain.

A matrix product state (MPS) is expressed as

$$|\phi\rangle = \sum_{i_1,i_2,...,i_N} \mathrm{Tr}(A^{[1]}_{i_1} A^{[2]}_{i_2} ... A^{[N]}_{i_N}) |i_1 i_2 ... i_N\rangle \tag{2.1}$$

where $i_k = 1...d$ with d being the dimension of a spin at each site, $A^{[k]}_{i_k}$'s are $D \times D$ matrices on site k with D being the dimension of the MPS. d is the dimension of the physical Hilbert space at each site and is called the physical dimension. D is the dimension of the matrices used in the matrix product representation which does not correspond to physical Hilbert spaces. D is called the inner dimension of the MPS.[1] The representation is efficient as with fixed D for a state of N spins, the number of parameters involved is at most ND^2 as compared to d^N in the generic case.

If $D = 1$, i.e. if A are numbers, then $|\phi\rangle$ is a product state. However, if $D \geq 2$, then $|\phi\rangle$ would in general be an entangled state of many spins. As the simplest example, consider matrices

$$A_0 = \begin{pmatrix} 1 & 0 \\ 0 & 0 \end{pmatrix}, A_1 = \begin{pmatrix} 0 & 0 \\ 0 & 1 \end{pmatrix} \tag{2.2}$$

which are independent of site. Then the matrix product state they produce is the many-body entangled GHZ state,

$$|\phi\rangle = |00...0\rangle + |11...1\rangle \tag{2.3}$$

2.1.2 Area Law

Entanglement in a matrix product state satisfies an exact area law. Actually, it is easy to show that if we take a continuous segment out of the chain, the reduced density matrix has rank at most D^2. Therefore, the entanglement entropy is upper bounded by $2 \ln D$.

$$S \leq 2 \ln(D) \tag{2.4}$$

On the other hand, it is not true that every one-dimensional state satisfying an exact area law can be written exactly as a matrix product state with finite inner dimension. For example, consider a 1D chain composed of nearest-neighbor dimers of the form

$$|\psi\rangle = \sum_i \alpha_i |ii\rangle \tag{2.5}$$

This state satisfies area law as long as $\sum_i \alpha_i \ln \alpha_i$ is finite. But this does not necessarily mean that there is a finite number of i's. As long as α_i decays fast enough with i, the entanglement of a segment will be bounded. However, if i is unbounded, the reduced density matrix of a segment will have an infinite rank and therefore not possible to represent with a finite dimensional MPS.

[1] We suppress the normalization of wave functions in this thesis, unless it is important and explicitly written out.

The situation is not too bad though. As shown in [SWVC08], for any 1D state satisfying an area law, the necessary inner dimension to approximately describe the state scales only polynomially with system size. Therefore the matrix product state representation is still efficient. As has been proven by Hastings [Has07] that all gapped ground states of 1D local Hamiltonians satisfy an area law, the matrix product representation for such states is always efficient. The power of matrix product states is limited to one spatial dimension though. To represent a gapped two-dimensional quantum state satisfying an area law using matrix product formalism would require in general matrices of exponential size. Therefore, we need more general constructions – the tensor product states – to deal with higher dimensional systems.

2.1.3 Gauge degree of freedom

The matrix product state representation is not unique. Actually, any MPS represented by a set of matrices $\{A_i\}$ is equally well represented by $\{B_i = MA_iM^{-1}\}$, for any invertible matrix M. As

$$\mathrm{Tr}(B_{i_1}B_{i_2}...B_{i_N}) = \mathrm{Tr}(MA_{i_1}M^{-1}MA_{i_2}M^{-1}...MA_{i_N}M^{-1}) = \mathrm{Tr}(A_{i_1}A_{i_2}...A_{i_N}) \tag{2.6}$$

This is what we call the gauge degree of freedom in MPS representation. This can be generalized to site-dependent A's as well.

This gauge degree of freedom will play an important role in our understanding of symmetry protected topological orders in one dimension.

2.1.4 Projected Entangled Pair picture

Matrix product states have another name – the Projected Entangled Pair State (PEPS) [FNW92b, PGVWC07, VWPGC06]. It comes from the following construction. (The construction applies to higher dimensional tensor product states as well.)

Consider a chain of maximally entangled pairs as shown in Fig. 2-1. Suppose that they connect into a ring, Each pair of connected dots represents a maximally entangled pair of

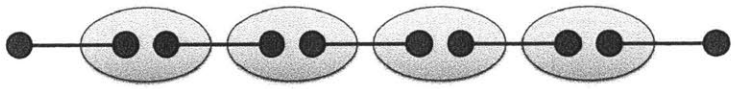

Figure 2-1: Projected Entangled Pair State(PEPS)

spins in state

$$|\psi\rangle = \frac{1}{\sqrt{D}}\sum_{\alpha=1}^{D}|\alpha\alpha\rangle \tag{2.7}$$

where D is the dimension of each spin. Each shaded big circle represents a projection P (a mapping) from two spins of dimension D to a physical degree of freedom of dimension d (a physical spin)

$$P = \sum_{i,\alpha,\beta} A_{i,\alpha,\beta}\,|i\rangle\,\langle\alpha\beta| \tag{2.8}$$

where the summation is over $i = 1...d$, and $\alpha, \beta = 1..D$. Direct calculation shows that after the projection, we obtain a many-body entangled state of physical spins which can be written as

$$|\phi\rangle = \sum_{i_1, i_2 ... i_N} \mathrm{Tr}(A_{i_1} A_{i_2} ... A_{i_N}) \, |i_1 i_2 ... i_N\rangle \tag{2.9}$$

which is exactly the matrix product states given in Eq. (2.1). Here A_i is treated as a matrix with row index α and column index β. In this projected entangled pair construction of matrix product states, the spins in maximally entangled pairs are said to be virtual and the spins obtained after projection are physical.

The PEPS and MPS (or more generally tensor product states (TPS)) formalisms are totally equivalent. But sometimes, one picture is more convenient and intuitive than the other as we see in Part IV when we use the PEPS picture to understand measurement-based quantum computation in many-body entangled states.

2.1.5 Double tensor

An important mathematical construction in the MPS description is the double tensor defined as

$$\mathbb{E}_{\alpha\gamma, \beta\chi} = \sum_i A_{i,\alpha\beta} \times (A_{i,\gamma\chi})^* \tag{2.10}$$

If we combine α with γ and β with χ and treat $\mathbb{E}$ as a matrix, then we can write

$$\mathbb{E} = \sum_i A_i \otimes A_i^* \tag{2.11}$$

The double tensor is important because, first, it is involved in the computation of norm and any physical observable of the states. The norm of an MPS is given by

$$\langle\phi|\phi\rangle = \mathrm{Tr}(\mathbb{E} \times \mathbb{E} ... \times \mathbb{E}) = \mathrm{Tr}(\mathbb{E}^N) \tag{2.12}$$

The expectation value of measuring any local observable O (on the kth spin for example) on the state is equal to

$$\langle O\rangle = \frac{\mathrm{Tr}(\mathbb{E}^{k-1} \mathbb{E}[O] \mathbb{E}^{N-k})}{\langle\phi|\phi\rangle}, \text{ where } \mathbb{E}[O] = \sum_{i,j} O_{i,j} A_i \otimes A_j^* \tag{2.13}$$

Note that as matrix multiplication takes time $\sim D^3$, the calculation of any physical observable is efficient (polynomial in inner dimension D and linear in system size N) for MPS.

Moreover, double tensor is directly related to an important quantity for many-body systems, the correlation length. In fact, an MPS has a finite correlation length if the largest eigenvalue of $\mathbb{E}$ is nondegenerate. This is shown as follows:

WLOG, we can set the largest eigenvalue of $\mathbb{E}$ to be 1 and hence the norm goes to a finite value (dimension of the eigenspace) as N goes to infinity. The correlation between two operators O_1 and O_2 becomes

$$\langle O_1 O_2\rangle - \langle O_1\rangle\langle O_2\rangle = \frac{\mathrm{Tr}(\mathbb{E}^{N-L-2} \mathbb{E}[O_1] \mathbb{E}^L \mathbb{E}[O_2])}{\mathrm{Tr}(\mathbb{E}^N)} - \frac{\mathrm{Tr}(\mathbb{E}^{N-1} \mathbb{E}[O_1]) \mathrm{Tr}(\mathbb{E}^{N-1} \mathbb{E}[O_2])}{\mathrm{Tr}^2(\mathbb{E}^N)} \tag{2.14}$$

It is easy to see that degeneracy of the largest eigenvalue of the double tensor implies non-decaying correlation. To describe quantum states with finite correlation length, the double

tensor must have a largest eigenvalue which is non-degenerate and the correlation length ξ is given by

$$\xi = -1/\ln \lambda_2 \tag{2.15}$$

where λ_2 is the second largest eigenvalue and $\lambda_2 < 1$. Here ξ is measured in units of lattice spacing.

Double tensor is important in studying not only the correlation length but also the many-body entanglement structure of an MPS. In fact, $\mathbb{E}^{[k]}$ uniquely determines the state up to a local change of basis on each site[PGVWC07] and hence contains all the entanglement information of the state. That is, if

$$\mathbb{E}^{[k]}_{\alpha\gamma,\beta\chi} = \sum_i A^{[k]}_{i,\alpha\beta} \times (A^{[k]}_{i,\gamma\chi})^* = \sum_i B^{[k]}_{i,\alpha\beta} \times (B^{[k]}_{i,\gamma\chi})^* \tag{2.16}$$

then $A^{[k]}_{i,\alpha\beta}$ and $B^{[k]}_{i,\alpha\beta}$ are related by a unitary transformation $U^{[k]}$:

$$B^{[k]}_{i,\alpha\beta} = \sum_j U^{[k]}_{ij} A^{[k]}_{j,\alpha\beta}. \tag{2.17}$$

Therefore, states described by $A^{[k]}_i$ and $B^{[k]}_i$ have exactly the same entanglement structure, which is faithfully captured in $\mathbb{E}^{[k]}$. A proof of this fact can be found in [NC00] in the form of the unitary degree of freedom in the operator sum representation of quantum channels $\mathcal{E}$ which is defined in terms the matrices as

$$\mathcal{E}(X) = \sum_i A_i X A_i^\dagger \tag{2.18}$$

This property is useful for applying renormalization transformation on the state, as discussed in Section 2.3.

2.2 Canonical form

In [PGVWC07], a canonical form is given for the matrices in an MPS representation, which provides much insight into the structure of the many-body state. We summarize the result in this section. We focus on the case where the matrices are not site dependent and hence the state is translational invariant.

The matrices A_i's in an MPS representation can be put into a 'canonical' form which is block diagonal[PGVWC07]

$$A_i = \begin{bmatrix} A_i^{(0)} & & \\ & A_i^{(1)} & \\ & & \ddots \end{bmatrix} \tag{2.19}$$

where the double tensor for each block $\mathbb{E}^{(k)} = \sum_i A_i^{(k)} \otimes (A_i^{(k)})^*$ has a positive non-degenerate largest eigenvalue $\lambda_i > 0$. Note that $\mathbb{E}^{(k)}$ can have eigenvalues with the same magnitude as λ_i, in the form $\lambda_i e^{i2\pi/p}$, $p \in \mathbb{Z}_q$.

There are several implications that can be directly read from this 'canonical form'. First the matrix product state $|\phi\rangle$ represented by A_i can be written as a superposition of $|\phi^{(k)}\rangle$'s, represented by matrices $A_i^{(k)}$. If $\mathbb{E}^{(k)}$ has only one eigenvalue with magnitude λ_i, then $|\phi^{(k)}\rangle$

is short range correlated (with finite correlation length). If $\mathbb{E}^{(k)}$ has other eigenvalues with the same magnitude as λ_i, then $|\phi^{(k)}\rangle$ can be further decomposed into states with block translation symmetry of block size q and finite correlation length. Therefore, the canonical form directly yields a decomposition of the MPS into a finite (and minimum) number of short range correlated states.

We set out to study MPS because it describes gapped ground states of 1D local Hamiltonians. However, up to now, it is unclear what the Hamiltonian is for a given MPS and what kind of gapped ground state is the MPS. From the decomposition obtained from the 'canonical form', a 'parent Hamiltonian' can be constructed which has the MPS as a gapped ground state, thus making contact with usual condensed matter studies.

In particular, if there is only one component in the decomposition of $|\phi\rangle$, then the parent Hamiltonian has $|\phi\rangle$ as a unique gapped ground state, which implies that if the Hamiltonian has a certain symmetry, then the ground state also has it. On the other hand, if $|\phi\rangle$ can be decomposed into a bunch of short range correlated $|\phi^{(k)}\rangle$'s, then the parent Hamiltonian has a degenerate ground space spanned by all $|\phi^{(k)}\rangle$'s. $|\phi\rangle$ is then one of the ground states. This is the result of spontaneous symmetry breaking in the system, where the Hamiltonian has a certain symmetry, but the $|\phi^{(k)}\rangle$'s do not. They are related to each other by the symmetry transformation.

A useful property of MPS is called 'injectivity', which says that there exists a finite number M such that the set of matrices

$$\tilde{A}_{I_M} = A_{i_1} ... A_{i_M} \tag{2.20}$$

spans the the whole space of $D \times D$ matrices. This is equivalent to the condition that $|\phi\rangle$ has only one component in the canonical decomposition and hence the unique gapped ground state of a local Hamiltonian. The 'injectivity' property is generically true for random MPS, but breaks down in special cases like the GHZ state.

2.3 Renormalization

Renormalization is a procedure in many-body systems where structures at smaller scales are removed and an effective description of the system at larger scales are obtained, keeping the long range and low energy dynamics of the system invariant. Applying renormalization procedure to a system allows us to extract universal properties of the system at low energy and large scale. For quantum systems, the small scale structures that need to be removed are short range entanglement and the MPS formalism provides a simple way to realize renormalization in 1D gapped systems. Discussion in this section is based on methods presented by Verstraete et. al. in [VCL+05].

Renormalization transformation on quantum states are realized with local unitary operations and local unitary operations on MPS can be applied through manipulation of $\mathbb{E}^{[k]}$. Here we have explicitly labeled the double tensor by their site number k. Treat $\mathbb{E}^{[k]}$ in Eqn. (2.10) as a $D^2 \times D^2$ matrix with row index $\alpha\gamma$ and column index $\beta\chi$. To apply a unitary operation on n consecutive sites, we combine the double tensor of the n sites together into

$$\tilde{\mathbb{E}} = \mathbb{E}^{[1]}\mathbb{E}^{[2]} ... \mathbb{E}^{[n]} \tag{2.21}$$

and then decompose $\tilde{\mathbb{E}}$ into a set of matrices $\tilde{A}_{\tilde{i}}$'s

$$\tilde{\mathbb{E}}_{\alpha\gamma,\beta\chi} = \sum_{\tilde{i}} \tilde{A}_{\tilde{i},\alpha\beta} \times \tilde{A}^*_{\tilde{i},\gamma\chi}. \tag{2.22}$$

Note $\tilde{A}_{\tilde{i},\alpha\beta}$ is determined up to a unitary transformation on $\tilde{i}$. The index $\tilde{i}$ of $\tilde{A}_{\tilde{i},\alpha\beta}$, up to an unitary transformation, can be viewed as the combination of $i_1, i_2, ..., i_n$, the indices of $A^{[1]}_{i_1,\alpha\beta}$, $A^{[2]}_{i_2,\alpha\beta}$, ... $A^{[n]}_{i_n,\alpha\beta}$. Going from original indices $i_1, i_2, ..., i_n$ to the effective index $\tilde{i}$ corresponds to applying a unitary operation on the n-block and $\tilde{A}_{\tilde{i}}$ describes the new state after operation.

The unitary operation can be chosen so that local entanglement is maximally removed. $\tilde{\mathbb{E}}$ contains all the information about the entanglement of the block with the rest of the system but not any detail of entanglement structure within the block. Hence we can determine from $\tilde{\mathbb{E}}$ the optimal way of decomposition into $\tilde{A}$ which corresponds to the unitary operation that maximally removes local entanglement while preserving the global structure. To do so, think of $\tilde{\mathbb{E}}_{\alpha\gamma,\beta\chi}$ as a matrix with row index $\alpha\beta$ and column index $\gamma\chi$. It is easy to see that with such a recombination, $\tilde{\mathbb{E}}$ is a positive matrix and can be diagonalized

$$\tilde{\mathbb{E}}_{\alpha\gamma,\beta\chi} = \sum_{\tilde{i}} \lambda_{\tilde{i}} V_{\tilde{i},\alpha\beta} V^*_{\tilde{i},\gamma\delta}, \tag{2.23}$$

where we have kept only the non-zero eigenvalues $\lambda_{\tilde{i}} > 0$ and the corresponding eigenvectors $V_{\tilde{i},\alpha\beta}$. $\tilde{A}$ is then given by

$$\tilde{A}_{\tilde{i},\alpha\beta} = \sqrt{\lambda_{\tilde{i}}} V_{\tilde{i},\alpha\beta}, \tag{2.24}$$

which are the matrices representing the new state. In retaining only the non-zero eigenvalues, we have reduced the physical dimension within the block to only those necessary for describing the entanglement between this block and the rest of the system. Local entanglement within the block has been optimally removed.

Each renormalization step in the renormalization procedure hence works by grouping every n consecutive sites together and then applying the above transformation to map $A^{[1]}$, $A^{[2]}$,..., $A^{[n]}$ to $\tilde{A}$. So one renormalization step maps the original matrices $(A^{[k]}_{i_k})^{(0)}$ on each site to renormalized matrices $(A^{[k]}_{i_k})^{(1)}$ on each block. Repeating this procedure for a finite number of times corresponds to applying a finite depth quantum circuit to the original state. If the matrices reaches a simple fixed point form $(A^{[k]}_{i_k})^{(\infty)}$ (up to local unitaries), we can determine from it the universal properties of the phase which the original state belongs to. In Chapter 6, we apply this procedure to classify gapped quantum phases in one dimensional systems.

Chapter 3

Tensor product states

The study of one dimensional systems serves as a starting point for the exploration of quantum many-body physics in higher dimensions. It has been discovered that, in higher (two or three) dimensional systems, more exotic quantum phenomena can appear. For example, in two dimensional electron systems put under huge magnetic fields and at very low temperatures, the Hall conductance can be quantized to exact integer or fractional multiples of the constant $\frac{e^2}{h}$, irrespective of the shape, composition, or other dynamical details of the specimen under investigation. Besides such quantum Hall effects[TSG82], two and three dimensional systems have been shown to be able to sustain special phases like quantum spin liquids[KL87, WWZ89, RS91, Wen91, MS01], topological insulators and topological superconductors[KM05a, BZ06, KM05b, MB07, FKM07, QHZ08], and string-net condensation[LW05].

A key feature common to all these exotic phases is the existence of many-body entanglement in the ground states of the systems. Therefore, it is of high interest to be able to find a proper description of many-body entanglement patterns in two and three dimensions which reveals the underlying mechanism of these quantum many-body phenomena. As we have discussed in the previous chapter, matrix product states provide an efficient description of one dimensional gapped quantum states, but it fails to do so in higher dimensions. To represent, for example, a gapped two-dimensional quantum state satisfying an area law using matrix product formalism would require in general matrices of exponential size. Therefore, we need more general constructions to deal with higher dimensional systems. The idea of introducing virtual Hilbert space in the form of inner dimensions of matrices to describe many-body entanglement can be generalized to higher dimensions, which leads to the Tensor Product State (TPS) representation. In this chapter, we review basic definition and simple properties of TPS studied in previous works in section 3.1. We also address the question of how to determine which phase the system belongs to from the representation by presenting in section 3.2 a new renormalization procedure for TPS which extracts the universal properties of the represented states from the tensors. This section is based on our work [CGW10].

3.1 Definition and basic properties

3.1.1 Definition

A tensor product state is given as

$$|\phi\rangle = \sum_{i_1,i_2,...i_m...} \mathrm{tTr}(T^{i_1}T^{i_2}...T^{i_m}...)|i_1 i_2...i_m...\rangle \tag{3.1}$$

Here $i = 1...d$, with d being the physical dimension of each spin in the system. T_i's are tensors living on each site with three or more inner indices.[1] The tensors are usually connected according to the underlying lattice structure of the system and tTr represents tensor contraction.

For example, consider a two-dimensional spin model on a hexagonal lattice with one spin (or one qudit) living at each vertex. The state can be represented by assigning to every vertex a set of tensors $T^i_{\alpha\beta\gamma}$, where i labels the local physical dimension and takes value from 1 to d. α, β, γ are inner indices along the three directions in the hexagonal lattice respectively. The dimension of the inner indices is D. Note that Fig. 3-1, Fig. 3-2, Fig. 3-3, Fig. 3-5, Fig. 3-6 in this section are all side views with inner indices in the horizontal plane and the physical indices pointing in the vertical direction, if not specified otherwise.

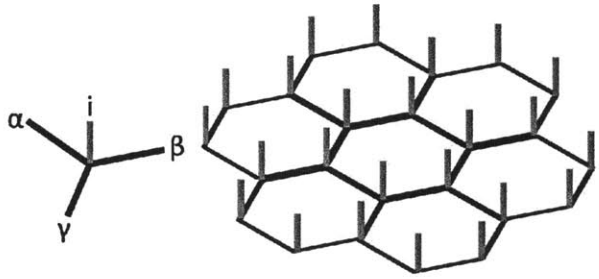

Figure 3-1: Left: tensor T representing a 2D quantum state on hexagonal lattice. i is the physical index, α, β, γ are inner indices. Right: a tensor product state where each vertex is associated with a tensor. The inner indices of the neighboring tensors connect according to the underlying hexagonal lattice.

3.1.2 Other properties

Tensor product states are similar to matrix product states in terms of area law, gauge degree of freedom, PEPS description and the formulation of double tensor.

Tensor product states enjoy the nice property of having an entanglement area law [VWPGC06]. In fact, for a TPS with inner dimension D, the rank of the reduced density matrix of a subregion is bounded by D^n, where n is the number of indices connecting the subregion with the rest of the system. As n scales linearly with the boundary L of the subregion

$$S \sim \alpha L \tag{3.2}$$

[1] A tensor in general is a set of numbers labeled by indices. A vector is a tensor with one index and a matrix is a tensor with two indices. In this thesis, we use the word 'tensor' to refer to those with three or more indices. Two tensors can be contracted if we match their corresponding indices, multiply their values and sum over the matched indices.

Therefore, TPS could provide a nice description of gapped quantum systems in two and higher dimensions.

Similar to MPS, TPS representation also has a gauge degree of freedom. In particular,

$$T'_{\alpha'\beta'\gamma'} = \sum_{\alpha,\beta,\gamma} M_{\alpha'\alpha} N_{\beta'\beta} O_{\gamma'\gamma} T_{\alpha\beta\gamma} \tag{3.3}$$

represents the same state as T if the invertible matrices M,N,O cancel out for each pair of connected indices.

The projected entangled pair representation of TPS can be constructed analogously as for MPS, starting from a two or higher dimensional lattice with maximally entangled pairs between nearest neighbor sites. The definition of double tensor is similar to MPS also. We will not repeat the constructions here.

However, besides these, much less is known about TPS than MPS. In particular, there is no easy way to extract correlation length of the state from the tensors, hence not easy to identify TPS which are gapped ground states of local Hamiltonians. A parent Hamiltonian having the state as ground state can always be constructed[PGVCW08]. However, there is no guarantee that the Hamiltonian is gapped. Finally, one major difficulty with using TPS for numerical simulation is that the contraction of tensor networks in two and higher dimensions is in general not efficient. Usually an approximate renormalization algorithm is used[LN07], but the error is not always well bounded.

While the structure of TPS is not as clear as MPS, it does cover more interesting many-body entangled systems. For example, the ground states of the topologically ordered string-net models in two dimension can be easily represented with tensors of small inner dimension, even though the states are entangled in a very nontrivial way.[BAV09, GLSW09]

3.2 Renormalization

The renormalization algorithm presented in [LN07] allows efficient (approximate) contraction of a two dimensional tensor network which can be used to calculate the expectation value of local physical observables in a quantum state. In particular, order parameters of symmetry breaking phases can be calculated using this renormalization method to determine the symmetry breaking phase the state belongs to. However, not all phases can be detected with local measurements. In particular, no local order parameter exists for topological phases. To detect topological orders in the states, more information needs to be preserved along the renormalization flow.

In this section, we describe such a renormalization algorithm for TPS which carefully preserves the physical degrees of freedom of the state as renormalization transformations are implemented. The algorithm removes short range entanglement from the state and extracts universal properties, including possible topological orders, of the system at large length scale. This section is based on our work [CGW10].

The renormalization procedure of quantum states is composed of local unitary transformations and isometry maps such that the state flows along the path $|\psi^{(0)}\rangle$, $|\psi^{(1)}\rangle$, $|\psi^{(2)}\rangle$,...and finally towards a fixed point $|\psi^{\infty}\rangle$. With the tensor network representation, flow of states corresponds to a flow of tensors $T^{(0)}$, $T^{(1)}$, $T^{(2)}$... We give the detailed procedure of how the tensors are mapped from one step to the next.

3.2.1 Algorithm

On a hexagonal lattice, the mapping can be broken into two parts: the F-move and the P move.

Step 1: F-move

In the F-move, we take a  configuration in the tensor network and map it to a  configuration by doing a local unitary operation. We will see that the tensor product representation of a state leads to a natural way of choosing an appropriate unitary operation for the renormalization of the state.

In order to do so, first we define the double tensor $\mathbb{T}$ of tensor T as

$$\mathbb{T}_{\alpha'\beta'\gamma',\alpha\beta\gamma} = \sum_i (T^i_{\alpha'\beta'\gamma'})^* \times T^i_{\alpha\beta\gamma} \tag{3.4}$$

Graphically the double tensor $\mathbb{T}$ is represented by two layers of tensor T with the physical indices connected.

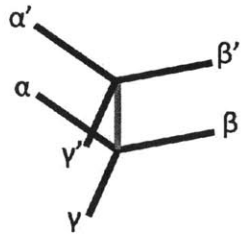

Figure 3-2: Double tensor $\mathbb{T}$ represented as two layers of tensor T with the physical indices contracted. The gray layer is the lower layer.

The tensor T giving rise to the same double tensor $\mathbb{T}$ is not unique. Any tensor T' which differs from T by an unitary transformation U on physical index i gives the same $\mathbb{T}$ as U and $U^\dagger$ cancels out in the contraction of i. On the other hand, an unitary transformation on i is the only degree of freedom possible, i.e. any T' which gives rise to the same $\mathbb{T}$ as T differs from T by a unitary on i. Therefore, in the process of turning a tensor T into a double tensor $\mathbb{T}$ and then split it again into a different tensor T', we apply a non-trivial local unitary operation on the corresponding state. A well designed way of splitting the double tensor will give us the appropriate unitary transformation we need, as we show below.

F-move has the following steps. First, construct double tensors for two neighboring sites on the lattice and combine them into a single double tensor with 8 inner indices.

$$\mathbb{T}_{\alpha'\beta'\delta'\epsilon',\alpha\beta\delta\epsilon} = \sum_{\gamma',\gamma} \mathbb{T}_{1,\alpha'\beta'\gamma',\alpha\beta\gamma} \times \mathbb{T}_{2,\delta'\epsilon'\gamma',\delta\epsilon\gamma} \tag{3.5}$$

Note that with respect to the bipartition of indices $\alpha'\beta'\delta'\epsilon'$ and $\alpha\beta\delta\epsilon$, $\mathbb{T}$ is Hermitian

$$\mathbb{T}_{\alpha'\beta'\delta'\epsilon',\alpha\beta\delta\epsilon} = \left(\mathbb{T}_{\alpha\beta\delta\epsilon,\alpha'\beta'\delta'\epsilon'}\right)^* \tag{3.6}$$

and positive semidefinite. Therefore it has a spectral decomposition with positive eigenval-

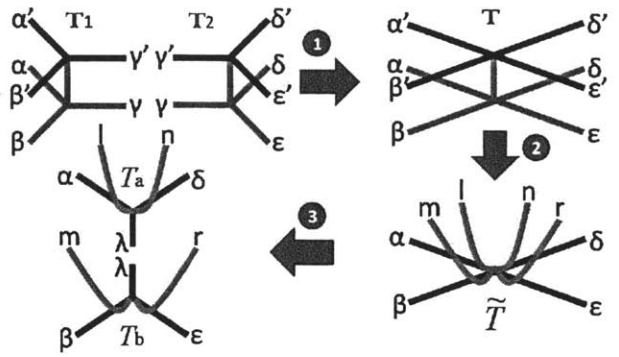

Figure 3-3: F-move in the renormalization procedure: (1) combining double tensors $\mathbb{T}_1$ and $\mathbb{T}_2$ on neighboring sites into a single double tensor $\mathbb{T}$ (2)Splitting double tensor $\mathbb{T}$ into tensor $\tilde{T}$ (3) SVD decomposition of tensor $\tilde{T}$ into tensors T_a and T_b.

ues $\{\lambda_j \geq 0\}$. The corresponding eigenvectors are $\{\hat{T}^j\}$

$$\mathbb{T}_{\alpha'\beta'\delta'\epsilon',\alpha\beta\delta\epsilon} = \sum_j \lambda_j \left(\hat{T}^j_{\alpha'\beta'\delta'\epsilon'}\right)^* \times \hat{T}^j_{\alpha\beta\delta\epsilon} \tag{3.7}$$

This spectral decomposition lead to a special way of decomposing double tensor $\mathbb{T}$ into tensors. Define a rank 8 tensor $\tilde{T}$(as shown in Fig. 3-3 after step 2) as follows:

$$\tilde{T}^{lmnr}_{\alpha\beta\delta\epsilon} = \sum_j \sqrt{\lambda_j} \left(\hat{T}^j_{lmnr}\right)^* \times \hat{T}^j_{\alpha\beta\delta\epsilon} \tag{3.8}$$

$\tilde{T}$ has four inner indices $\alpha, \beta, \delta, \epsilon$ of dimension d and four physical indices l, m, n, r also of dimension d which are in the direction of $\alpha, \beta, \delta, \epsilon$ respectively. As $\{\hat{T}^j\}$ form an orthonormal set, it is easy to check that $\tilde{T}$ gives rise to double tensor $\mathbb{T}$. Going from T_1 and T_2 to $\tilde{T}$, we have implemented a local unitary transformation on the physical degrees of freedom on the two sites, so that in $\tilde{T}$ the physical indices and the inner indices represent the same configuration. In some sense, we are keeping only the physical degrees of freedom necessary for entanglement with the rest of the system while getting rid of those that are only entangled within this local region. Now we do a singular value decomposition of tensor $\tilde{T}$ in the direction orthogonal to the link between T_1 and T_2 and $\tilde{T}$ is decomposed into tensors T_a and T_b.

$$\tilde{T}^{lmnr}_{\alpha\beta\delta\epsilon} = \sum_\lambda T^{ln}_{a,\alpha\delta\lambda} \times T^{mr}_{b,\beta\epsilon\lambda} \tag{3.9}$$

This step completes the F-move. Ideally, this step should be done exactly so we are only applying local unitary operations to the state. Numerically, we keep some large but finite cutoff dimension for the SVD step, so this step is approximate.

On a hexagonal lattice, we do F-move on the chosen neighboring pairs of sites (dash-circled in Fig. 3-4), so that the tensor network is changed into a configuration shown by thick dark lines in Fig. 3-4. Physical indices are omitted from this figure. Now by grouping together the three tensors that meet at a triangle, we can map the tensor network back into a hexagonal lattice, with 1/3 the number of sites in the original lattice. This is achieved by the P-move introduced in the next section.

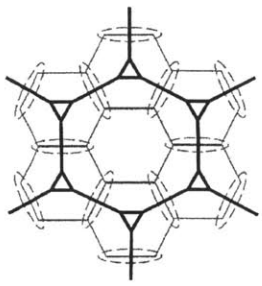

Figure 3-4: Original hexagonal lattice (gray line) and renormalized lattice (black line) after F-move has been applied to the neighboring pairs of sites circled by dash line.

Step 2: P-move

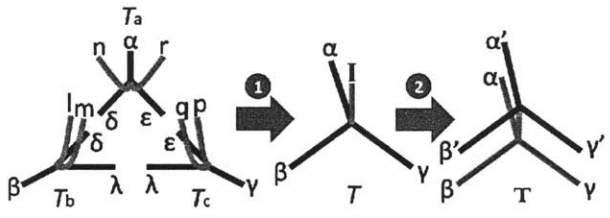

Figure 3-5: P-move in the renormalization procedure: (1) contracting three tensors that meet at a triangle T_a, T_b, T_c to form a new tensor $T^{(1)}$ on one site of the renormalized hexagonal lattice. (2)constructing the double tensor $\mathbb{T}^{(1)}$ from $T^{(1)}$ so that we can start to do F-moves again.

Now we contract the three tensors that meet at a triangle together to form a new tensor in the renormalized lattice as shown in the first step in Fig. 3-5

$$T^{I}_{\alpha\beta\gamma} = \sum_{\delta\epsilon\lambda} T^{nr}_{a,\alpha\delta\epsilon} \times T^{lm}_{b,\beta\lambda\delta} \times T^{pq}_{c,\gamma\epsilon\lambda} \tag{3.10}$$

where I is the physical index of the new tensor which includes all the physical indices of T_a, T_b, T_c: l, m, n, r, p, q. Note that in the contraction, only inner indices are contracted and the physical indices are simply group together.

Constructing the double tensor $\mathbb{T}$ from T, we get the renormalized double tensor on the new hexagonal lattice which is in the same form as $\mathbb{T}_1$,$\mathbb{T}_2$ and we can go back again and do the F-move.

3.2.2 Complication: corner double line

One problem with the above renormalization algorithm is that, instead of having one isolated fixed-point tensor for each phase, the algorithm has a continuous family of fixed points which all correspond to the same phase. Consider a tensor with structure shown in Fig. 3-6. The tensor is a tensor product of three parts which include indices $\{\alpha, \beta, i_1\}, \{\gamma, \delta, i_2\}, \{\epsilon, \lambda, i_3\}$ respectively. It can be shown that this structure remains invariant under the renormalization flow. Therefore, any tensor of this structure is a fixed point of our renormalization flow.

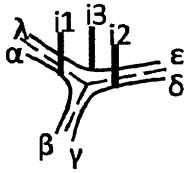

Figure 3-6: The corner double line tensor which is a fixed point of the renormalization algorithm. The three groups of indices $\{\alpha, \beta, i_1\}, \{\gamma, \delta, i_2\}, \{\epsilon, \lambda, i_3\}$, are entangled within each group but not between the groups.

However, it is easy to see that the state it represents is a tensor product of loops around each plaquette, which can be disentangled locally into a trivial product state. Therefore, the states all have only short-range entanglement and correspond to the topologically trivial phase. The trivial phase has then a continuous family of fixed-point tensors. This situation is very similar to that discussed in [GW09, LN07]. We will keep the terminology and call such a tensor a corner double line tensor. Not only does corner double line tensor complicate the situation in the trivial phase, it leads to a continuous family of fixed points in every phase. It can be checked that the tensor product of a corner double line with any other fixed-point tensor is still a fixed-point tensor. The states they correspond to differ only by small loops around each plaquette and represent the same topological order. Therefore any single fixed-point tensor gets complicated into a continuous class of fixed-point tensors. In practical application of the renormalization algorithm, in order to identify the topological order of the fixed-point tensor, we need to get rid of such corner double line structures. Due to their simple structure, this can always be done, as discussed in the next section.

3.2.3 Examples

Now we discuss two particular examples, the Ising symmetry breaking phase and the $\mathbb{Z}_2$ topological ordered phase, to demonstrate how our algorithm can be used to determine the phase of a tensor product state. These two examples are defined on square lattice. A small modification of the previous algorithm is needed[CGW10], which we will not detail here.

Ising symmetry breaking phase

A typical example for symmetry breaking phase transition is the transverse field Ising model. Consider a square lattice with one spin $1/2$ on each site. The transverse field Ising model is

$$H_{Ising} = \sum_{ij} Z_i Z_j + \epsilon \sum_k X_k \tag{3.11}$$

where $\{ij\}$ are nearest neighbor sites and X, Y and Z are pauli matrices on spin $1/2$'s. The Hamiltonian is invariant under spin flip transformation $\prod_k X_k$ for any ϵ.

When $\epsilon = 0$, the ground state spontaneously breaks this symmetry into either the all spin up state $|00...0\rangle$ or the all spin down state $|11...1\rangle$. In this case any global superposition $\alpha|00...0\rangle + \beta|11...1\rangle$ represents a degenerate ground state. When $\epsilon = \infty$, the ground state has all spin polarized in the X direction ($|++...+\rangle$) and does not break this symmetry.

In the variational study of this system, we can require that the variational ground state always have this symmetry, regardless if the system is in the symmetry breaking phase or

not. Then we will find for $\epsilon = 0$ the ground state to be $|00...0\rangle + |11...1\rangle$. Such a global superposition represents the spontaneous symmetry breaking. For $\epsilon = \infty$, we will find the ground state to be $|++...+\rangle$ and does not break the symmetry. For $0 < \epsilon < \infty$, we will need to decide which of the previous two cases it belongs to. We can first find a tensor network representation of an approximate ground state which is symmetric under the spin flip transformation, then apply the renormalization algorithm to find the fixed point and decide which phase the state belongs to. Below we will assume a simple form of tensor and demonstrate how the algorithm works.

Suppose that the tensors obtained from the variational study $T^i_{\alpha\beta\gamma\delta}$, where i,α,β,γ,δ can be 0 or 1, takes the following form

$$\begin{aligned} T^0_{\alpha\beta\gamma\delta} &= \lambda^{\alpha+\beta+\gamma+\delta} \\ T^1_{\alpha\beta\gamma\delta} &= \lambda^{4-(\alpha+\beta+\gamma+\delta)} \end{aligned} \tag{3.12}$$

λ is a parameter between 0 and 1. Under an X operation to the physical index, the tensor is changed to $\tilde{T}$

$$\begin{aligned} \tilde{T}^0_{\alpha\beta\gamma\delta} &= \lambda^{4-(\alpha+\beta+\gamma+\delta)} \\ \tilde{T}^1_{\alpha\beta\gamma\delta} &= \lambda^{\alpha+\beta+\gamma+\delta} \end{aligned}$$

$\tilde{T}$ can be mapped back to T by switching the 0,1 label for the four inner indices $\alpha\beta\gamma\delta$. Such a change of basis for the inner indices does not change the contraction result of the tensor and hence the state that is represented. Therefore, the state is invariant under the spin flip transformation $\prod_k X_k$ and we will say that the tensor has this symmetry also.

When $\lambda = 0$, the tensor represents state $|00...0\rangle + |11...1\rangle$, which corresponds to the spontaneous symmetry breaking phase. We note that the $\lambda = 0$ tensor is a direct sum of dimension-1 tensors. Such a direct-sum structure corresponds to spontaneous symmetry breaking, as discussed in detail in [GW09]. When $\lambda = 1$, the tensor represents state $|++...+\rangle$ which corresponds to the symmetric phase. When $0 < \lambda < 1$, there must be a phase transition between the two phases. However, as λ goes from 0 to 1, the tensor varies smoothly with well defined symmetry. It is hard to identify the phase transition point. Now we can apply our algorithm to the tensor. First, we notice that at $\lambda = 0$ or 1, the tensor is a fixed point for our algorithm. Next, we find that for $\lambda < 0.358$, the tensor flows to the form with $\lambda = 0$, while for $\lambda > 0.359$, it flows to the form with $\lambda = 1$. Therefore, we can clearly identify the phase a state belongs to using this algorithm and find the phase transition point.

Note that in our algorithm, we explicitly keep the spin flip symmetry in the tensor. That is, after each renormalization step, we make sure that the renormalized tensor is invariant under spin flip operations up to change of basis for the inner indices. If the symmetry is not carefully preserved, we will not be able to tell the two phases apart.

We also need to mention that for arbitrary λ, the fixed point that the tensor flows to can be different from the tensor at $\lambda = 0$ or 1 by a corner double line structure. We need to get rid of the corner double line structure in the result to identify the real fixed point. This is possible by carefully examining the fixed point structure. Another way to distinguish the different fixed points without worrying about corner double lines is to calculate some quantities from the fixed-point tensors that are invariant with the addition of corner double lines. We also want the quantity to be invariant under some trivial changes to the fixed point, such as a change in scale $T \to \eta T$ or the change of basis for physical and inner indices. One such quantity is given by the ratio of X_2 and X_1 defined as $X_1 =$

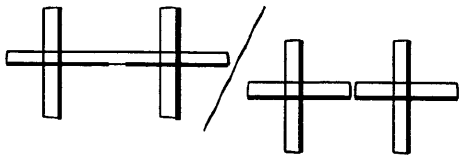

Figure 3-7: Quantity X_2/X_1 obtained by taking the ratio of the contraction value of the double tensor in two different ways. X_2/X_1 is invariant under change of scale, basis transformation and corner double line structures of the double tensor and can be used to distinguish different fixed point tensors. For clarity, only one layer of the double tensor is shown. The other layer connects in exactly the same way.

$\left(\sum_{\alpha'\gamma',\alpha\gamma} \mathbb{T}_{\alpha'\alpha'\gamma'\gamma',\alpha\alpha\gamma\gamma}\right)^2$, and $X_2 = \sum_{\alpha'\beta'\gamma'\delta',\alpha\beta\gamma\delta} \mathbb{T}_{\alpha'\alpha'\gamma'\delta',\alpha\alpha\gamma\delta} \times \mathbb{T}_{\beta'\beta'\delta'\gamma',\beta\beta\delta\gamma}$. Fig. 3-7 gives a graphical representation of these two quantities. In this figure, only one layer of the double tensor is shown. The other layer connects in the exactly the same way. It is easy to verify that X_2/X_1 is invariant under the change of scale, basis transformation and corner double lines.

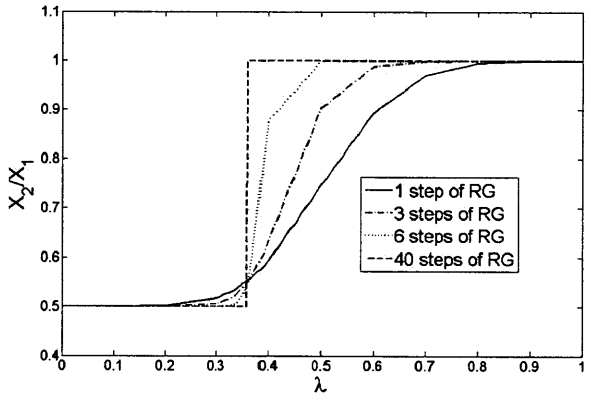

Figure 3-8: (Color online) X_2/X_1 for tensors Eq. (3.12) under the renormalization flow. As the number of RG steps increases, the transition in X_2/X_1 becomes sharper and finally approaches a step function at fixed point. The critical point is at $\lambda_c = 0.358$.

We calculate X_2/X_1 along the renormalization flow. The result is shown in Fig. 3-8. At the $\lambda = 0$ fixed point, $X_2/X_1 = 0.5$ while at $\lambda = 1$, $X_2/X_1 = 1$. As we increase the number of renormalization steps, the transition between the two fixed points becomes sharper and finally approaches a step function with critical point at $\lambda_c = 0.358$. Tensors with $\lambda < \lambda_c$ belongs to the symmetry breaking phase while tensors with $\lambda > \lambda_c$ belongs to the symmetric phase.

3.2.4 $\mathbb{Z}_2$ topological ordered phase

The algorithm can also be used to study topological order of quantum states. In this section, we demonstrate how the algorithm works with $\mathbb{Z}_2$ topological order.

Consider again a square lattice but now with one spin 1/2 per each link. A simple

Hamiltonian on this lattice with $\mathbb{Z}_2$ topological order can be defined as

$$H_{\mathbb{Z}_2} = \sum_p \prod_{i \in p} X_i + \sum_v \prod_{j \in v} Z_j \tag{3.13}$$

where p means plaquettes and $i \in p$ is all the spin 1/2s around the plaquette and v means vertices and $j \in v$ is all the spin 1/2s connected to the vertex. The ground state wave function of this Hamiltonian is a fixed-point wave function and corresponds to the $N = 1$ loop state with $\eta = 1$ as discussed in the previous section.

The ground state wave function has a simple tensor product representation. For simplicity of discussion we split every spin 1/2 into two and associate every vertex with four spins. The tensor $T^{ijkl}_{\alpha\beta\gamma\delta,\mathbb{Z}_2}$ has four physical indices $i, j, k, l = 0, 1$ and three inner indices $\alpha, \beta, \gamma, \delta = 0, 1$.

$$\begin{aligned} &T^{ijkl}_{ijkl,\mathbb{Z}_2} = \mathbf{1}, \text{ if } \mathrm{mod}(i+j+k+l, 2) = 0 \\ &\text{all other terms being } 0 \end{aligned} \tag{3.14}$$

It can be checked that $T_{\mathbb{Z}_2}$ is a fixed-point tensor of our algorithm. This tensor has a $\mathbb{Z}_2$ gauge symmetry. If we apply Z operation to all the inner indices, where Z maps 0 to 0 and 1 to -1, the tensor remains invariant as only even configurations of the inner indices are nonzero in the tensor.

Consider then the following set of tensor parameterized by g

$$\begin{aligned} &T^{ijkl}_{ijkl} = g^{i+j+k+l}, \text{ if } \mathrm{mod}(i+j+k+l, 2) = 0 \\ &\text{all other terms being } 0 \end{aligned} \tag{3.15}$$

At $g = 1$, this is exactly $T_{\mathbb{Z}_2}$ and the corresponding state has topological order. At $g = 0$, the tensor represents a product state of all 0 and we denote the tensor as T_0. At some critical point in g, the state must go through a phase transition. This set of tensors are all invariant under gauge transformation $ZZZZ$ on their inner indices and the tensor seems to vary smoothly with g. One way to detect the phase transition is to apply our algorithm. We find that, at $g > g_c$, the tensors flow to $T_{\mathbb{Z}_2}$, while at $g < g_c$, the tensors flow to T_0. We determine g_c to be between $0.804 \sim 0.805$. As this model is mathematically equivalent to two dimensional classical Ising model where the transition point is known to great accuracy, we compare our result to that result and find our result to be within 1% accuracy ($g_c = 0.8022$). Again in the renormalization algorithm, we need to carefully preserve the $\mathbb{Z}_2$ gauge symmetry of the tensor so that we can correctly determine the phase of the states.

The fixed-point tensor structure might also be complicated by corner double line structures, but it is always possible to identify and get rid of them. Similarly, we can calculate the invariance quantity X_2/X_1 to distinguish the two fixed points. $X_2/X_1 = 1$ for $T_{\mathbb{Z}_2}$ while $X_2/X_1 = 0.5$ for T_0. The result is plotted in Fig. 3-9 and we can see that the transition in X_2/X_1 approaches a step function after a large number of steps of RG, i.e. at the fixed point. The critical point is at $g_c = 0.804$. For $g < g_c$, the tensor belongs to the trivial phase, while for $g > g_c$, the tensor belongs to the $\mathbb{Z}_2$ topological ordered phase.

Our algorithm can also be used to demonstrate the stability of topological order against local perturbation. As is shown in Ref.[CZG+10], local perturbations to the $\mathbb{Z}_2$ Hamiltonian correspond to variations in tensor that do not break the $\mathbb{Z}_2$ gauge symmetry. We picked tensors in the neighborhood of $T_{\mathbb{Z}_2}$ which preserve this gauge symmetry randomly and applied our renormalization algorithm (gauge symmetry is kept throughout the renor-

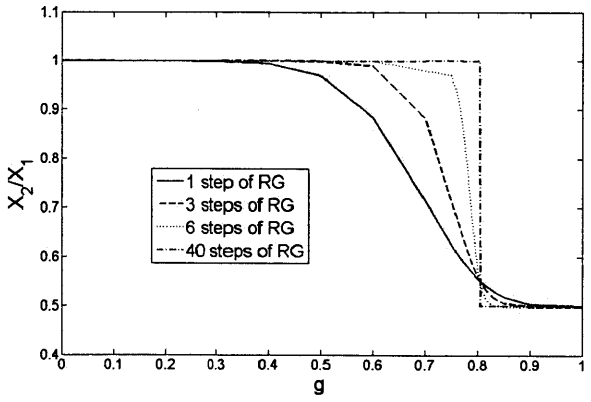

Figure 3-9: (Color online) X_2/X_1 for tensors Eq. (3.15) under the renormalization flow. As the number of RG steps increases, the transition in X_2/X_1 becomes sharper and finally approaches a step function at fixed point. The critical point is at $g_c = 0.804$.

malization process). We find that as long as the variation is small enough, the tensor flows back to $T_{\mathbb{Z}_2}$, up to a corner double line structure. This result shows that the $\mathbb{Z}_2$ topological ordered phase is stable against local perturbations.

Chapter 4

Symmetry constraint on tensor network representation of topological order

As matrix product state and tensor product state representations provide an efficient description of gapped many-body entangled states and also an efficient way to (approximately) calculate local physical observables from them, they have become a powerful numerical tool in the study of quantum many-body systems [VMC08]. These methods deal with the complex numbers of quantum systems directly and do not have a sign problem, as compared to quantum Monte Carlo. However, as with any numerical method, we must study the numerical stability of the program before we can trust any of the calculation result. If small numerical errors in the process lead to small and smooth changes in the output, then the result can give useful information. If, on the other hand, small numerical errors can lead to qualitatively different output, then the program is doomed to fail. In this chapter we study the numerical stability of using tensor product states as variational ground states for gapped quantum systems. As we show in the following, numerical stability is not always guaranteed, but can be enforced with proper constraints.

In the variational approach based on TPS, we try to find a TPS which minimizes the average energy of a local Hamiltonian. As we change the Hamiltonian by adding perturbation, the tensors in the TPS are also changed in order to minimize the average energy for the new Hamiltonian. While local physical perturbations can always be reflected by variations in the tensors, the other direction of this problem remains unclear: can an arbitrary variation of the tensor be induced by a local perturbation of the Hamiltonian?

This is a very important question if we want to discuss phase based on states. Because phase is defined as a region in Hamiltonian space, where any two points H_1, H_2 within the region can be connected by a smooth path without encounter singularities (*i.e.* phase transitions). So the question about tensor and phase becomes, which set of states in Hilbert space correspond to such a region in Hamiltonian space and which set of tensors in the tensor space represent these states. Starting from one point in the phase region, we would like to know what kind of variations in the tensors correspond to local perturbations to the Hamiltonian.

We can discuss this important question in more concrete setting. Assume a TPS Ψ_T minimizing the average energy of a Hamiltonian H has a property. We would like to ask if the property is a universal property of a phase, or just a special property of H. If

the property is a universal property of a phase, then the ground state $\Psi_T + \Delta\Psi_T$ for the perturbed Hamiltonian $H + \Delta H$ still has the same property. If the property is a special property of H, the ground state for the perturbed Hamiltonian will lose this property. It is the collection of universal properties that defines a phase. So a study of universal properties is a study of phases. If all the variations of the tensors can be induced by local perturbations of the Hamiltonian, then we can study the stability of a property against local perturbation ΔH of the Hamiltonian by studying the stability of a property against variations of the tensors. This will give us a powerful tool to study phases using TPS.

Unfortunately, it turns out that not all variations of the tensors can be induced by local perturbations of the Hamiltonian, as we show in this chapter. For a generic TPS, which satisfies a condition called injectivity [PGVCW08], tensor variations indeed correspond to Hamiltonian perturbations. However, this is not true in the general case, as we show in this chapter with a special system with topological order. So it is not easy to study universal properties and phases using TPS. In order to use TPS to study phases and phases transitions, we need to find the subset of variations in tensors that are physical, *i.e.* corresponding to local perturbations of the Hamiltonian.

For clarity, we will always refer to small changes in the Hamiltonian as 'perturbation' and to those in the tensors as 'variation'. Without any efficient method to solve for exact TPS representation of ground states of quantum many-body systems, finding the subset of the variations of the tensors that can be induced by local perturbation of Hamiltonian is in general very difficult.

We want to, in particular, study this problem for topologically ordered phases. As TPS can give a simple description of a large class of topological ordered states, we expect that it might provide a powerful tool for studying topological phases in general. As we know, topologically ordered phases are proven to be stable against any local perturbations of the Hamiltonian[WN90, HW05, BHM10]. That is, the topological properties, such as ground state degeneracy[WN90] and quasi-particle statistics[ASW84, Kit06], are robust under any local perturbation to the Hamiltonian. So in the TPS approach to topologically ordered phase, it is natural to ask: are those topological properties robust against any variation of tensors, that is, for any tensor which represents a topologically ordered state, is the topological order robust against arbitrary variation in the tensors? Surprisingly, we find that this is not true.

We focus on the $\mathbb{Z}_2$ topological order represented by an ideal TPS in this chapter and study how the topological order of the state changes as we vary certain parameters in the representing tensors. We characterize topological order by calculating the topological entanglement entropy S_{tp} [KP06, LW06] for the state and observe that topological order (*i.e.* the topological entanglement entropy S_{tp}) is stable only against variations of the tensors that preserve certain $\mathbb{Z}_2$ symmetry of the tensors. Since the topological order is robust against any local perturbations of Hamiltonian, this result shows that not all variations of the tensors correspond to local perturbations of Hamiltonian. For this $\mathbb{Z}_2$ model, we show that in the generic case $\mathbb{Z}_2$ symmetry is a necessary condition for the variations in tensors to correspond to physical perturbations of the Hamiltonian. This claim is further supported by checking stability of the topological Renyi entropy of TPS with $\mathbb{Z}_2$ symmetry preserving variations and $\mathbb{Z}_2$ symmetry breaking variations of the tensors respectively.

While calculating S_{tp} for a general state is exponentially hard[HZHL08], we find efficient ways to do so for two sets of TPS near the ideal TPS with $\mathbb{Z}_2$ topological order. For a general TPS, we calculate the topological Renyi entropy by mapping it to the contraction of a 2D tensor network, which is accomplished by using the Tensor Entanglement Renormalization

Algorithm[LN07]. Hence we are able to calculate topological entropy for regions much larger than was possible previously and determine the topological order of the state more accurately.

Our result on the stability of topological order will help us in the TPS based variational approach to $\mathbb{Z}_2$ topological phase: we should only consider the variations of the tensors within the subspace of tensors with $\mathbb{Z}_2$ symmetry. The $\mathbb{Z}_2$ symmetry condition and possibly other conditions will help us to understand the physical variations of tensors in TPS. This is crucial in using TPS to study quantum phases and quantum phase transitions. It may even lead to a classification of topological order.

This chapter is based on our work [CZG+10] and is organized as follows. We start by introducing an 'ideal' lattice spin model with $\mathbb{Z}_2$ topological order in section 4.1.1 and show how the presence of topological order in the ground state wave function can be understood nicely with a physical mechanism called 'string-net condensation'. Such a physical picture naturally gives rise to a simple tensor product representation of the wave function, to which we then add two kinds of local variations, 'string tension' and 'end of strings'. By calculating topological entanglement entropy numerically for the first case and analytically for the second case, we show in section 4.1.2 and 4.1.3 how topological order is stable against $\mathbb{Z}_2$ preserving variations ('string tension'), but breaks down immediately when $\mathbb{Z}_2$ symmetry is broken (by 'end of strings'). We then randomly pick 200 tensors in the neighborhood of the ideal $\mathbb{Z}_2$ TPS in section 4.1.4 and calculate the topological Renyi entropy of the corresponding states. Tensors with and without $\mathbb{Z}_2$ symmetry demonstrate totally different behavior as system size scales up. We discuss in the last section 4.2 the implications of our findings in variational studies of topological phase and phase transitions. The details of the calculations are given in section 4.3.

4.1 Models and results

4.1.1 Spin model with $\mathbb{Z}_2$ topological order

We start from an exactly solvable model which has $\mathbb{Z}_2$ topological order[RS91, Wen91, Kit03]. In this section, we give the system Hamiltonian, find the ground state wave function and explain its structure and how that leads to a nontrivial topological order which can be detected with topological entanglement entropy. With these insights about the state we then present a simple tensor product representation of this wave function.

The model is defined on a two-dimensional hexagonal lattice where each link is occupied by a qubit (spin-1/2). The Hamiltonian is a sum of commuting projection operators

$$H^0_{\mathbb{Z}_2} = -\sum_p \prod_{i\in p} X_i - \sum_v \prod_{j\in v} Z_j \tag{4.1}$$

X and Z are qubit Pauli operators defined as $X = \begin{pmatrix} 0 & 1 \\ 1 & 0 \end{pmatrix}, Z = \begin{pmatrix} 1 & 0 \\ 0 & -1 \end{pmatrix}$. p stands for each hexagon plaquette in the lattice and $\prod_{i\in p} X_i$ is the tensor product of six X operators around the plaquette. v stands for each vertex and $\prod_{j\in v} Z_j$ is the tensor product of three Z operators connected to the vertex. The ground state wave function has a nice interpretation using the 'string-net' picture where state $|0\rangle$ corresponds to no string on a link and state $|1\rangle$ corresponds to the presence of a string. The vertex term $\prod_{j\in v} Z_j$ enforces that there are even number of strings connected to each vertex and hence the strings form closed loop

while the plaquette term $\prod_{i\in p} X_i$ gives dynamics to the closed loops. The ground state wave function is an equal weight superposition of all closed loop configurations on the lattice.

$$|\Phi_{\mathbb{Z}_2}\rangle = \sum_{cl} |\phi_{cl}\rangle \tag{4.2}$$

The normalization factor is omitted. If we refer to each closed loop configuration as a string-net, the appearance of $\mathbb{Z}_2$ topological order in this system has then a natural interpretation as being due to the condensation of string-nets. We will refer to this model as the ideal $\mathbb{Z}_2$ model.

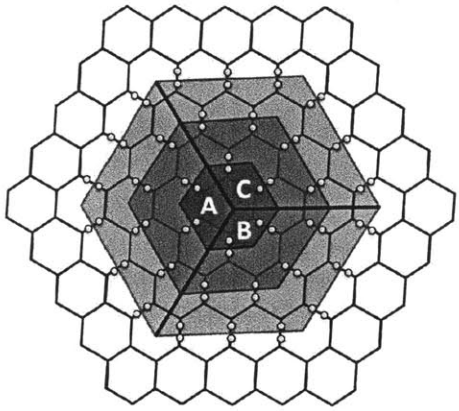

Figure 4-1: Hexagonal lattice where each link is occupied by two qubits. The three gray regions are configurations used for calculating topological entanglement entropy. Qubits on the boundaries are drawn explicitly while others are omitted for clarity. Notice that regions are always separated by breaking links in half. For $\mathbb{Z}_2$ model with string tension, numerical calculation for S_{tp} is done for the three gray regions, while for $\mathbb{Z}_2$ model with end of strings, analytically calculation is possible for any region.

For simplicity of discussion, we split each qubit on a link into two qubits as illustrated in Fig. 4-1. The string-net condensed $\mathbb{Z}_2$ wave function on the original lattice can be naturally extended to a state on the new lattice by replacing a 0 link with 00 and a 1 link with 11. This new state is still an equal weight superposition of all string-nets and hence maintains the $\mathbb{Z}_2$ topological order. The new system Hamiltonian can be obtained from the old one by adding a $-ZZ$ term to each link and expand the plaquette term into a product of X operators on all twelve qubits around the plaquette

$$H_{\mathbb{Z}_2} = -\sum_p \prod_{i\in p} X_i - \sum_v \prod_{j\in v} Z_j - \sum_l Z_{l_1} Z_{l_2} \tag{4.3}$$

where l denotes all the links and l_1, l_2 are the two qubits on the link. It is easy to see that the new Hamiltonian indeed has the new string-net condensed state as its ground state. The topological order of the system can be detected from the ground state wave function by calculating the topological entanglement entropy of the state. The mapping to the new lattice allows this calculation to be carried out exactly in a few steps, as illustrated below.

According to the definition of topological entanglement entropy in Ref. [KP06](or equivalently defined in Ref. [LW06]), we take out a simply connected region from the whole lattice

and divide it into three parts A, B, C as shown in Fig. 4-1. By calculating the entanglement entropy for regions A, B, C, AB, AC, BC, ABC and combining them according to

$$S_{tp} = S_A + S_B + S_C - S_{AB} - S_{BC} - S_{AC} + S_{ABC} \tag{4.4}$$

we arrive at the topological entanglement entropy S_{tp} of the state, where the entanglement entropy for region A for example is denoted as S_A. The above definition needs to be applied to regions much larger than the correlation length of the state. For the state in consideration, the correlation length is zero and the calculation gives the right result for whatever regions we take. We divide the regions by cutting through the pair of qubits on boundary links as illustrated in Fig. 4-1. For a region with n outgoing links on the boundary, there are 2^{n-1} orthogonal boundary configurations due to the closed loop constraint of the wave function. Tracing out each boundary configuration contributes equally and independently to the entropy of the region and hence $S = n - 1$, which includes one term proportional to the length of the boundary n and one constant term -1. The combination in the definition of S_{tp} makes sure that the boundary terms of different regions cancel out with each other, so topological entanglement entropy for the state is then $S_{tp} = -1$.

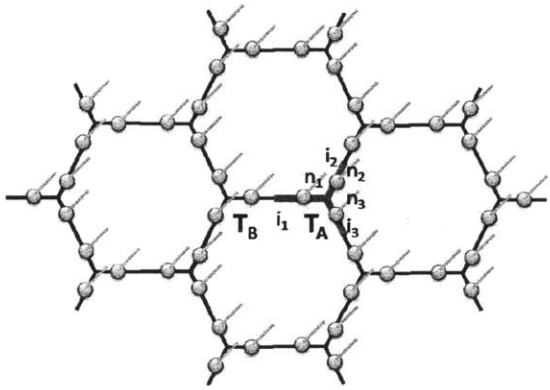

Figure 4-2: Tensor product representation of $\mathbb{Z}_2$ ground state. One tensor is assigned to every three qubits connected to the same vertex. Tensors T_A are on vertices in sublattice A and T_B are in sublattice B. The out-of-plane gray links represent the physical indices of the qubits. The tensors connect according to the underlying hexagonal lattice.

This globally entangled state has yet a surprisingly simple local representation using the tensor product language. A tensor product state of two dimensional lattice model is represented by associating with each lattice site m a set of s tensors $T^m_{[k]}(\alpha\beta\gamma...)$, $k = 1, 2, ..., s$, where s is the dimension of local Hilbert space at site m. k is called the physical index of the tensor. $\alpha\beta\gamma$, the inner indices of the tensors, connect to each other and form a graph. The wave function (unnormalized) is then given by

$$|\psi\rangle = \sum_{k_1,k_2,...k_m...} \mathcal{C}(T^1_{[k_1]}T^2_{[k_2]}...T^m_{[k_m]}...)|k_1k_2...k_m...\rangle \tag{4.5}$$

where $\mathcal{C}$ denotes tensor contraction of the inner indices according to the connection graph. We omit the inner indices here. (We will in most cases ignore normalization of wave function in the following discussion and mention specifically when normalization is needed.) The tensors representing the ground state of the ideal $\mathbb{Z}_2$ model can be given as follows. We

group every three qubits connected to the same vertex together and assign a rank three tensor to each of the eight physical basis states of the three qubits. Now every physical index k in Eqn.4.5 is represented with three bits $n_1n_2n_3$. The eight tensors are:

$$\begin{array}{ll} T_{[000]}(000)=1 & T_{[011]}(011)=1 \\ T_{[101]}(101)=1 & T_{[110]}(110)=1 \\ \text{all other terms are zero} & \end{array} \tag{4.6}$$

The physical indices $[n_1n_2n_3]$ correspond to the out-of-plane gray links in Fig. 4-2. The inner indices $(i_1i_2i_3)$ correspond to the in-plane links in Fig. 4-2. The inner and physical indices all have dimension two and are given in the same order as shown in Fig. 4-2. Hence the inner indices truthfully reflect the configuration of the physical space and only configurations with even number of strings at each vertex are allowed. It can then be checked that only string-net configurations have non-zero amplitude in this representation and the amplitude are actually all equal. Therefore, the tensors given in 4.6 indeed represent a string-net condensed state–the ideal $\mathbb{Z}_2$ ground state.

This set of tensors serves as a starting point for our variational study of topological phase transitions and we wish to know what kind of variations of the tensors correspond to physical perturbations of the Hamiltonian. We will study first two specific cases in the following two sections.

4.1.2 $\mathbb{Z}_2$ model with string tension

Suppose that we want to know how magnetic field in the Z direction might affect topological order. The perturbed Hamiltonian reads:

$$\begin{aligned} H &= H_{\mathbb{Z}_2} + \lambda \sum_k Z_k \\ &= -\sum_p \prod_{i\in p} X_i - \sum_v \prod_{j\in v} Z_j - \sum_l Z_{l_1} Z_{l_2} + \lambda \sum_k Z_k \end{aligned} \tag{4.7}$$

The Z_k term commute with the vertex and link term $\prod_{j\in v} Z_j$, $Z_{l_1}Z_{l_2}$ in the unperturbed Hamiltonian, so the closed loop constraint is maintained. The ground state wave function is still a superposition of string-net configurations, but with different weight. The magnetic field adds energy to each string segment, therefore one reasonable guess about the ground state is that each string-net configuration has weight exponential in its total length of string.

$$|\Phi^g_{\mathbb{Z}_2}\rangle = \sum_{cl} g^{-L(\phi_{cl})/2} |\phi_{cl}\rangle \tag{4.8}$$

where the summation is over all string-net configurations and $L(\phi_{cl})$ is the total string length of a configuration. When g is positive, this variational wave function has been extensively studied in Ref.[PRF07, CC08] by mapping to an Ising model where the corresponding Hamiltonian perturbation from the $\mathbb{Z}_2$ model is obtained and topological entropy of the state is calculated. It is found that topological order of the state is stable as g deviates from 1 and the perturbation in Hamiltonian can indeed be local. Here, we study this wave function from the tensor point of view and reach similar conclusions. The parameter g in our TPS can be complex in general.

This weighted superposition can still have a simple tensor product representation by

locally modifying the tensors in Eq.4.6 to

$$\begin{array}{ll} T_{[000]}(000) = g & T_{[011]}(011) = 1 \\ T_{[101]}(101) = 1 & T_{[110]}(110) = 1 \\ \text{all other terms are zero} & \end{array} \tag{4.9}$$

For $|g| > 1$, the weight of each string segment is smaller by a factor of $|g|^{-1/2}$ than that of no string, lowering the weight of string-net configurations exponentially. Physically, we can imagine this is due to some kind of tension in the strings. Therefore, we refer to this wave function as $\mathbb{Z}_2$ state with string tension (g). This state cannot be the exact ground state of the Hamiltonian given in Eq.4.7, but it is possible that it gives a qualitatively right and quantitatively close approximation to the ground state and hence might be a good guess for variational study. One necessary condition for this conjecture to be true is that the topological order of the state remains stable with g close to 1, and this is indeed the case as we will show below by calculating topological entanglement entropy of the state. Our calculation can be done for any g and when g is positive, our result is consistent with Ref.[PRF07, CC08].

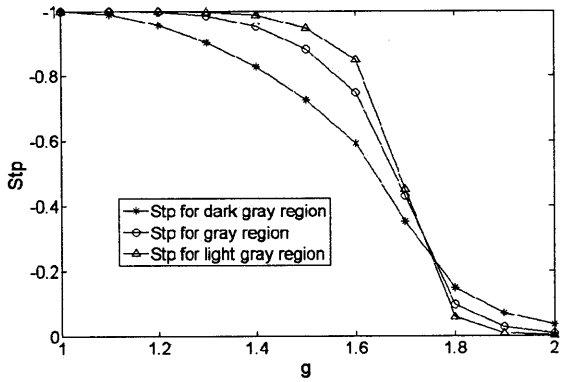

Figure 4-3: Topological entanglement entropy S_{tp} of the $\mathbb{Z}_2$ model with string tension calculated for the three gray regions as shown in Fig. 4-1. $1/g$ is the weight of each string segment relative to vacuum. S_{tp} remains stable for a finite region away from the ideal $\mathbb{Z}_2$ model and goes sharply to zero at $g \sim 1.75$.

In general, this computation is intractable. The equality in Eq.4.4 holds only in the limit of infinitely large regions A, B, C. Therefore the computation involves diagonalization of exponentially large matrices, each element of which takes exponential time to calculate. For $\mathbb{Z}_2$ state with string tension, we circumvent this difficulty by appealing to the special structure of the tensors in Eq.4.9. In order to find the entanglement entropy of a region, we map the computation of the eigenvalues of the reduced density matrix to the contraction of a two dimensional tensor network. While contracting general two-dimensional tensor networks is $\#P$-complete[SWVC07][1], the tensor networks we are dealing with turn out to be of a special type, called the 'matchgate' tensor [Val02]. 'Matchgate' tensors can be contracted efficiently, which leads to an efficient algorithm for determining the topological

[1]A problem is in the computational complexity class $\#P$ if it is of the form "compute f(x)," where f is the number of accepting paths of an NP machine. A $\#P$-complete problem is the hardest in this class.

entanglement entropy of this state. The details of the procedure will be explained in section 4.3.1.

In the computation, we take the total system size to be large enough such that it does not affect the result of the computation. Taking the size of regions A, B and C to infinity is hard. We manage to carry out the computation for progressively larger regions as shown in Fig. 4-1, with 18, 72 and 162 qubits inside respectively. The resulting topological entanglement entropy for $g \in [1,2]$ is plotted in Fig. 4-3. We do see a trend of sharper transition of S_{tp} from -1 to 0 as the size of the region is increased. At g close to zero or g very large when the correlation length is small compared to the size of the region, the calculated value for S_{tp} is reliable and we find that it remains stable within a finite range of the ideal $\mathbb{Z}_2$ TPS and goes to zero beyond certain critical string tension g_c. We can decide from the plot the critical point g_c to be around 1.75. We would like to comment that the tensor network representing the norm of the $\mathbb{Z}_2$ state with string tension g is the same as that representing the partition function of classical Ising model on triangular lattice with coupling constant J at inverse temperature $\beta = \ln g/(2J)$[PRF07, CC08]. A phase transition at $g = \sqrt{3}$ is known for this classical model. Our calculation for the quantum model confirms this observation and shows that the quantum phase transition is in fact topological.

The stability of topological order at $g \geq 1$ is a necessary condition for string tension to correspond to local Hamiltonian perturbations. In this particular case, we can actually find the corresponding perturbations explicitly. The relation we mentioned above between the $\mathbb{Z}_2$ state with string tension and 2D classical Ising model at finite temperature allows the construction of a continuous family of parent Hamiltonian $H(g)$ for the quantum states[VWPGC06, Hen04, AFF04, CCMP05]. The Hamiltonian $H(g)$ is local, has the state $|\Phi^g_{\mathbb{Z}_2}\rangle$ as its exact ground state and remains gapped for $g < g_c$. The Hamiltonian for this variational wave function is also given in Ref.[PRF07, CC08]. Therefore we can conclude that string tension can be induced by local perturbations of the Hamiltonian and hence is an allowed variation of the $\mathbb{Z}_2$ tensors.

4.1.3 $\mathbb{Z}_2$ model with end of strings

Another simple model one might want to study is the $\mathbb{Z}_2$ model with magnetic field perturbation in the X direction.

$$\begin{aligned} H &= H_{\mathbb{Z}_2} + \lambda \sum_k X_k \\ &= -\sum_p \prod_{i \in p} X_i - \sum_v \prod_{j \in v} Z_j - \sum_l Z_{l_1} Z_{l_2} + \lambda \sum_k X_k \end{aligned} \tag{4.10}$$

The action of the perturbation operator X_k on $\mathbb{Z}_2$ ground state will flip a link from no string to having a string (or back) and hence break one or more closed loops. The perturbed ground state would contain configurations with end of strings. In tensor language, this seems to allow some odd configurations to be non-zero. However, as we will see, this is actually not true. Even though the physical configuration contains end of strings, the tensor variation could never have odd terms. As shown by the following example, the appearance of odd terms in the tensor destroys topological order immediately and hence cannot be induced by any local Hamiltonian perturbation.

Taking the translational and rotational symmetries of the Hamiltonian into considera-

tion, one might expect that the following tensors which assign a small and equal weight ϵ to all odd configurations might represent a good trial wave function for the ground state.

$$\begin{array}{llll} T_{[000]}(000)=1 & T_{[011]}(011)=1 & T_{[101]}(101)=1 & T_{[110]}(110)=1 \\ T_{[001]}(001)=\epsilon & T_{[010]}(010)=\epsilon & T_{[100]}(100)=\epsilon & T_{[111]}(111)=\epsilon \\ \text{all others are zero} & & & \end{array} \tag{4.11}$$

Again the inner indices $(i_1 i_2 i_3)$ truthfully reflect the configurations of the physical indices $[n_1 n_2 n_3]$. When $\epsilon = 0$, this is reduced to the tensors in the ideal $\mathbb{Z}_2$ TPS. When ϵ is non-zero, the wave function contains all possible string configurations, closed loop or open string. The weight of each string configuration is exponentially small in the number of end of strings contained.

$$|\Phi^{\epsilon}_{\mathbb{Z}_2}\rangle = \sum_{sc} \epsilon^{q(\phi_{sc})} |\phi_{sc}\rangle \tag{4.12}$$

where the summation is over all possible string configurations and $q(\phi_{sc})$ is the number of end of strings in a particular configuration.

To see how topological order of the state changes as ϵ varies from 0, we again calculate the topological entanglement entropy of the state. In this case, it turned out that analytical calculation is possible. The detailed procedure is given in section 4.3.2. The entanglement entropy and topological entropy of this variational wave function has been computed in Ref.[PRF07] and our calculation in terms of the tensors agrees with this result. We find that for any finite value of ϵ, when system size goes to infinity, S_{tp} goes to zero. Hence topological order is unstable under this kind of variation. At first sight this may be a surprising result, as we are only changing the tensors locally and we are not expected to change the global entanglement pattern of the state. However, when we write out the wave function explicitly we will see that we have actually induced global changes to the state. The wave function in Eq. 4.12 can be expanded in powers of ϵ as

$$|\Phi^{\epsilon}_{\mathbb{Z}_2}\rangle = |\Phi_{\mathbb{Z}_2}\rangle + \epsilon^2 \sum_{v_i, v_j} |\Phi^{v_i, v_j}_{\mathbb{Z}_2}\rangle + ... \tag{4.13}$$

where the v's are any vertices in the lattice. $|\Phi^{v_i,v_j}_{\mathbb{Z}_2}\rangle$ is an excited eigenstate of the $\mathbb{Z}_2$ Hamiltonian (Eq. 4.3) which minimizes energy of all local terms except the vertex terms at v_i, v_j and is hence an equal weight superposition of all configurations with end of strings at v_i and v_j. Note that end of strings always appear in pairs. We will call such a pair a defect in the string-net condensate. v_i, v_j can be separated by any distance and the number of local operations needed to take $|\Phi_{\mathbb{Z}_2}\rangle$ to $|\Phi^{v_i,v_j}_{\mathbb{Z}_2}\rangle$ scale with this distance.

On the other hand, with arbitrary local perturbation to the dynamics, the Hamiltonian reads

$$H' = H_{\mathbb{Z}_2} + \eta \sum_u h_u \tag{4.14}$$

where h_u's are any local operator and η is small. The perturbed ground state wave function will contain terms like $|\Phi^{v_i,v_j}_{\mathbb{Z}_2}\rangle$ but only with weight $\eta^{distance(v_i,v_j)}$. When v_i, v_j are separated by a global distance, the weight will be exponentially small. Hence a constant, finite weight ϵ^2 for all $|\Phi^{v_i,v_j}_{\mathbb{Z}_2}\rangle$ as required in Eq. 4.13 is not possible. Therefore, while we are only modifying the tensors locally, we introduce global 'defects' to the state, which cannot be the result of any local perturbation to the Hamiltonian. We can, of course, design a Hamiltonian H_ϵ which has $|\Phi^{\epsilon}_{\mathbb{Z}_2}\rangle$ as its exact ground state using the method introduced in

Ref. [PGVCW08] or [Hen04, AFF04, CCMP05]. However, H_ϵ will not be able to smoothly connect to $H_{\mathbb{Z}_2}$ as $\epsilon \to 0$.

4.1.4 Necessary symmetry condition

The two kinds of tensor variations we have studied have drastically different effects on the topological order of the state. While the first type corresponds to local perturbations of the Hamiltonian and keeps topological order intact, the second type does not have a physical correspondence and destroys the topological order completely. What leads to such a difference? Given a general variation of $\mathbb{Z}_2$ tensor, how can we tell if it is allowed?

We observe that the tensor representing the ideal $\mathbb{Z}_2$ state (Eq.4.6) has certain inner symmetry, that is, the tensor is invariant under some non-trivial operations on the inner indices, as shown in Fig. 4-4.

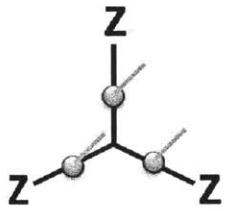

Figure 4-4: Symmetry of the $\mathbb{Z}_2$ tensor. The tensor representing the ideal $\mathbb{Z}_2$ state is invariant under the action of $Z \otimes Z \otimes Z$ to its inner indices. The variation in string tension (Eq.4.9) does not break this symmetry and topological order is stable. The variation with end of strings (Eq.4.11) breaks this symmetry and destroys topological order

Z does nothing to the tensor when the index is 0 and changes the sign of the tensor when the index is 1. In the ideal $\mathbb{Z}_2$ tensor, only even configurations of the inner indices are non-zero. Hence applying Z at the same time to all three inner indices does not change the tensor. That is, $Z \otimes Z \otimes Z$ is a symmetry of the tensor. As $Z \otimes Z \otimes Z$ squares to identity, we will say that the tensor has $\mathbb{Z}_2$ symmetry. Note that we can insert a set of unitary operators $U, U^\dagger$ between any connected links in a tensor network without affecting the result of tensor contraction and hence the quantity represented by the tensor network. Therefore, the $\mathbb{Z}_2$ symmetry could take any form which is local unitary equivalent to $Z \otimes Z \otimes Z$. This $\mathbb{Z}_2$ symmetry is closely related to the closed loop constraint of the state. Due to this symmetry, the tensor network cannot be 'injective' as defined in Ref. [PGVCW08].

Adding string tension to the $\mathbb{Z}_2$ tensor (Eq.4.9) does not violate this symmetry, as all the odd terms of inner indices are still zero. We found that topological order of the state is stable with small string tension. On the other hand, adding end of strings (Eq.4.11) breaks this symmetry for any finite ϵ. In general, assume the variation of the tensor T contains a $\mathbb{Z}_2$ symmetry breaking term dT of magnitude δ. Such a term would represent an end of string in the tensor network. To the leading order in δ, the wave function would contain terms on the order $O(\delta^2)$ with dT on two of the sites and T on the others. In the physical space, this would correspond to an open string configuration(up to local unitaries at the ends). The weight of such a term is $O(\delta^2)$ even though the two sites with dT may be globally apart, hence introducing global defects to the wave function and breaking topological order. Such defect terms cannot be created by local perturbation to the Hamiltonian. Therefore, $\mathbb{Z}_2$

symmetry breaking variations to the tensors are not allowed and preserving $\mathbb{Z}_2$ symmetry of the tensor is shown to be a necessary condition for any variation of the ideal $\mathbb{Z}_2$ tensor to be physical. This argument is valid for a generic $\mathbb{Z}_2$ breaking variation. There can be specially designed cases where $\mathbb{Z}_2$ breaking variations does not lead to breakdown of topological order, e.g. when such variations only occur within a finite region of the system or different contributions to the global defects exactly cancel each other. However, for a random $\mathbb{Z}_2$ breaking variation, topological order will be lost and it cannot correspond to local perturbation of Hamiltonian.

The necessity of $\mathbb{Z}_2$ symmetry in the generic case is clearly reflected in the following calculation. We randomly pick tensors in the neighborhood of the ideal $\mathbb{Z}_2$ tensor and find the topological order of the corresponding state numerically. To do this, we make use of a generalization of topological entanglement entropy, the Topological Entanglement Renyi Entropy[FHHW09]. Renyi entropy for a reduced density matrix ρ of order α, where $\alpha \geq 0$

$$S_\alpha(\rho) = \frac{1}{1-\alpha} log[Tr(\rho^\alpha)] \tag{4.15}$$

is a valid measure of entanglement. In the limit of $\alpha \to 1$, it reduces to the usual von Neumann entropy. It was shown in Ref. [FHHW09] that we can replace von Neumann entropy with Renyi entropy in the definition of topological entanglement entropy (Eq.4.4) and still have a valid characterization of topological order. The resulting quantity, topological entanglement Renyi entropy S_{tpr}, does not depend on α. We are hence free to choose α for the ease of computation and we take it to be 2. The calculation of Renyi entropy is mapped to the contraction of a two-dimensional tensor network which can be computed approximately using the tensor entanglement renormalization algorithm[LN07]. We take the same geometry of regions as in Fig.4-1 and the Renyi entropies of different regions are then combined in the same way as in Eq.4.4 to yield S_{tpr}. The details of the computation will be described in section 4.3.3. Here we present our result. We restrict ourselves to a small neighborhood near the $\mathbb{Z}_2$ tensor

$$\left|T_{[n_1n_2n_3]}(i_1i_2i_3) - T_{\mathbb{Z}_2[n_1n_2n_3]}(i_1i_2i_3)\right| < 0.1 \tag{4.16}$$

We pick 100 tensors with $\mathbb{Z}_2$ symmetry and plot how their topological entanglement Renyi entropy scales with reduced region size in the left half of Fig.4-5 and do the same for 100 tensors without $\mathbb{Z}_2$ symmetry in the right half of Fig.4-5. We see that for tensors with $\mathbb{Z}_2$ symmetry, S_{tpr} approach -1 very quickly as we include more and more qubits in the reduced region, while for tensors without $\mathbb{Z}_2$ symmetry, S_{tpr} goes towards 0 as the region gets larger. This confirms our statement that $\mathbb{Z}_2$ symmetry is a necessary condition for any generic variation of $\mathbb{Z}_2$ tensor to correspond to physical perturbations of the Hamiltonian and hence characterize variations within the topological ordered phase. The plot also suggests that $\mathbb{Z}_2$ symmetry might be a sufficient condition.

4.2 Conclusion and discussion

Our result on $\mathbb{Z}_2$ topological order provides useful perspective on the general relation between tensor variation and Hamiltonian perturbation. First, it is shown that not all variations in tensor correspond to perturbations to the Hamiltonian. For the $\mathbb{Z}_2$ model in particular, based on our calculation of topological entanglement (Renyi) entropy for tensors

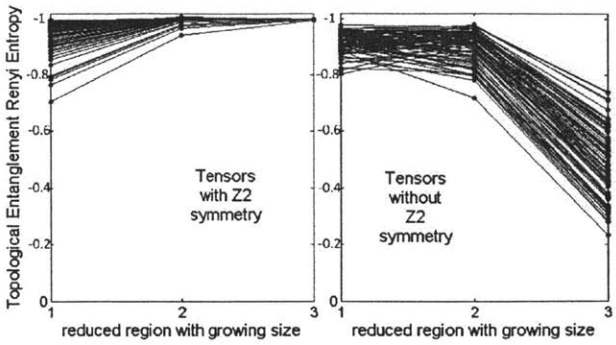

Figure 4-5: Topological entanglement Renyi entropy (S_{tpr}) calculated for the three gray regions as shown in Fig.4-1. Size of regions grow from region 1 to 3. The calculation is done for 200 random tensors in the neighborhood of $\mathbb{Z}_2$ tensor. 100 of them have $\mathbb{Z}_2$ symmetry (plotted on the left hand side), while the other 100 have not (plotted on the right hand side). For tensors with $\mathbb{Z}_2$ symmetry, S_{tpr} approach -1 very quickly as we include more and more qubits in the reduced region, while for tensors without $\mathbb{Z}_2$ symmetry, S_{tpr} goes towards 0 as the region gets larger.

in the neighborhood of the ideal $\mathbb{Z}_2$ tensor [see eq. (4.6)], we show that, one necessary condition is that the tensor is invariant under $\mathbb{Z}_2$ symmetry operation $Z \otimes Z \otimes Z$ (or any local unitary equivalent operator) on its inner indices. A generic variation which breaks this symmetry cannot be induced by local perturbation of the Hamiltonian and the tensors no longer represent state with $\mathbb{Z}_2$ topological order. This gives partial answer to the question of what kind of variations in the $\mathbb{Z}_2$ tensor correspond to physical perturbations to the Hamiltonian and hence represent states within the same topological ordered phase. Note that we start with a particular Hamiltonian in order to better explain the property of the state. Our result does not depend on this particular form of this Hamiltonian and remains valid for any local Hamiltonian of the $\mathbb{Z}_2$ topological ordered state. (Certain uniformity condition of the Hamiltonian must be satisfied, as pointed out in Ref. [BHM10]) Moreover for simplicity of calculation, we restricted ourselves to hexagonal lattice in the above discussion. However, the $\mathbb{Z}_2$ symmetry requirement is generally true for any lattice structure and the symmetry operation would take the form $Z \otimes Z \otimes ... \otimes Z$ on all inner indices(or any local unitary equivalent operator). We expect that similar necessary symmetry condition also holds for other quantum double model with gauge symmetry [Kit03]. The generalization to other gauge symmetries are discussed in more detail in section 4.3.4.

This understanding will provide important guidance for variational studies of topological order using tensor product states. Suppose that, for example, we want to find a tensor product state which is the approximate ground state of a Hamiltonian with $\mathbb{Z}_2$ topological order. It is then very important to search within the set of variational tensors that have $\mathbb{Z}_2$ symmetry. If the numerical calculation does not carefully preserve this symmetry, we might result in a tensor without $\mathbb{Z}_2$ invariance. As the $\mathbb{Z}_2$ breaking term can be arbitrarily small, the corresponding tensor product state might still give good approximation to local properties such as energy, but will have totally wrong global properties such as topological order. Then any attempt to decide the phase diagram based on the state would be misleading.

We would like to comment that, the tensor product approach allows us to study wave function variation in a general setting. While the models we studied, $\mathbb{Z}_2$ model with string

tension or end of string, are well understood in the 'wave function deformation'[CCMP05, PRF07] formalism where the wave function amplitudes have to be positive, the wave function variations that can be studied using tensors can be negative and complex in general. In section II D, the random variations we tested are complex and can be studied with the Tensor Entanglement Renormalization Algorithm with no extra complexity.

Finally we would like to note that the symmetry conditions might not be sufficient. A complete understanding of the correspondence between Hamiltonian perturbation and tensor variation would be very much desired as it might lead to full classification of quantum states and quantum phases using the tensor language.

4.3 Supplementary material for S_{tp} calculation

4.3.1 Calculating S_{tp} for $\mathbb{Z}_2$ model with string tension

In this section, we give detailed procedure of how topological entanglement entropy S_{tp} of $\mathbb{Z}_2$ model with string tension can be calculated using the matchgate tensor technique. Following the definition in [KP06], we take out a region (as in Fig. 4-1) from the hexagonal lattice by breaking the m out-going links in half. Due to the closed loop constraint on the wave function, the boundary qubits have only 2^{m-1} possible configurations c_i. Regrouping terms in the wave function according to different boundary configurations, we have (up to normalization)

$$|\Phi^g_{\mathbb{Z}_2}\rangle = \sum_{c_i} \alpha_i |\phi^{out}_{c_i}\rangle |\phi^{in}_{c_i}\rangle \tag{4.17}$$

This wave function is automatically in Schmidt-decomposition form because for different boundary configurations c_i, $|\phi^{out}_{c_i}\rangle$'s are orthogonal to each other, and so are $|\phi^{in}_{c_i}\rangle$'s. Knowing the norm and all the α_i's would enable us to calculate entropy of the reduced density matrix of the the region.

Define rank three tensors $\mathbb{T}$, $\mathbb{T}_0$, $\mathbb{T}_1$ with inner dimension two as

$$\begin{array}{llll} \mathbb{T}(000) = g^2 & \mathbb{T}(011) = 1 & \mathbb{T}(101) = 1 & \mathbb{T}(110) = 1 \\ \mathbb{T}_0(000) = g^2 & \mathbb{T}_0(011) = 1 & & \\ \mathbb{T}_1(101) = 1 & \mathbb{T}_1(110) = 1 & & \\ \text{all others are 0} & & & \end{array} \tag{4.18}$$

It can be verified that the contraction of $\mathbb{T}$ on all vertices of the hexagonal lattice gives the norm of $|\Phi^g_{\mathbb{Z}_2}\rangle$. To calculate α_i for a particular boundary condition c_i, replace tensors at the boundary with $\mathbb{T}_0$ if the boundary qubit is 0 and with $\mathbb{T}_1$ if the qubit is 1 and make sure the first inner index is on the boundary link. Contraction of the new tensor network will give $|\alpha_i|^2$. These three tensors satisfy the conditions as defined in Ref. [Val02] and are called 'matchgate' tensors. The contraction of a tensor network of N 'matchgate' tensors can be done efficiently (in time N^3). Therefore, for a fixed reduced region with boundary length m in a system of total size N, the computation of entanglement entropy takes time polynomial in N but exponential in m.

We start from a small reduced region (dark gray region in Fig. 4-1) with a small m, calculate S_{tp} and increase the total system size N until the change in S_{tp} is negligible (< 0.01). We repeat this process for different values of g and for progressively larger reduced regions (lighter gray in Fig. 4-1). The result is plotted in Fig. 4-3.

4.3.2 Calculating S_{tp} for $\mathbb{Z}_2$ model with end of strings

Now we show how the calculation of S_{tp} can be carried out for $\mathbb{Z}_2$ model with end of strings, analytically. We start again with the division of the lattice into sections A, B, C as in Fig. 4-1. Without the closed loop constraint, a region with m boundary links has 2^m different boundary configurations. Rewriting the wave function according to different boundary configurations c_i as

$$|\Phi^{\epsilon}_{\mathbb{Z}_2}\rangle = \sum_{c_i} \beta_i |\phi^{out}_{c_i}\rangle |\phi^{in}_{c_i}\rangle \tag{4.19}$$

we have obtained the Schmidt-decomposed form of the wave function and all we need to know to calculate entropy are the β_i's and the norm.

Define rank three tensors $\mathbb{S}$, $\mathbb{S}_0$, $\mathbb{S}_1$ with inner dimension two as

$$\begin{array}{llll} \mathbb{S}(000)=1 & \mathbb{S}(011)=1 & \mathbb{S}(101)=1 & \mathbb{S}(110)=1 \\ \mathbb{S}(001)=\epsilon^2 & \mathbb{S}(010)=\epsilon^2 & \mathbb{S}(100)=\epsilon^2 & \mathbb{S}(111)=\epsilon^2 \\ \mathbb{S}_0(000)=1 & \mathbb{S}_0(011)=1 & \mathbb{S}_0(001)=\epsilon^2 & \mathbb{S}_0(010)=\epsilon^2 \\ \mathbb{S}_1(101)=1 & \mathbb{S}_1(110)=1 & \mathbb{S}_1(100)=\epsilon^2 & \mathbb{S}_1(111)=\epsilon^2 \\ \text{all others are 0} & & & \end{array} \tag{4.20}$$

Contraction of tensor $\mathbb{S}$ on every vertex of the lattice gives the norm of $|\Phi^{\epsilon}_{\mathbb{Z}_2}\rangle$. To calculate β_i for a particular boundary condition c_i, replace tensors at the boundary with $\mathbb{S}_0$ if the boundary qubit is 0 and with $\mathbb{S}_1$ if the qubit is 1 and make sure the first inner index is on the boundary link. Contraction of the new tensor network will give $|\beta_i|^2$. The contraction of these two-dimensional tensor networks can be made efficient by applying a Hadamard transformation ($|0\rangle \to (|0\rangle + |1\rangle)/\sqrt{2}$, $|1\rangle \to (|0\rangle - |1\rangle)/\sqrt{2}$)to each of the three inner indices of the tensors and transforming them into

$$\begin{array}{llll} \mathbb{S}'(000)=\sqrt{2}(1+\epsilon^2) & \mathbb{S}'(111)=\sqrt{2}(1-\epsilon^2) & & \\ \mathbb{S}'_0(000)=1+\epsilon^2 & \mathbb{S}'_0(100)=1+\epsilon^2 & \mathbb{S}'_0(011)=1-\epsilon^2 & \mathbb{S}'_0(111)=1-\epsilon^2 \\ \mathbb{S}'_1(000)=1+\epsilon^2 & \mathbb{S}'_1(100)=-1-\epsilon^2 & \mathbb{S}'_1(011)=-1+\epsilon^2 & \mathbb{S}'_1(111)=1-\epsilon^2 \\ \text{all others are 0} & & & \end{array} \tag{4.21}$$

It is easy to see that the contraction value of this tensor network can be computed analytically, from which we know that the entropy of any region with m outgoing links is

$$\begin{aligned} S = m &- \frac{1}{2}\frac{(1+b^{N_i})(1+b^{N_o})}{1+b^N} * \ln \frac{(1+b^{N_i})(1+b^{N_o})}{1+b^N} \\ &- \frac{1}{2}\frac{(1-b^{N_i})(1-b^{N_o})}{1+b^N} * \ln \frac{(1-b^{N_i})(1-b^{N_o})}{1+b^N} \end{aligned} \tag{4.22}$$

where $b = (1-\epsilon^2)/(1+\epsilon^2)$ and $N_i(N_o)$ is the number of vertices inside (outside) the region. $N = N_i + N_o$ is the total system size.

Combining the entropy of different regions according to Eq. 4.4 and taking the limit $N_i \to \infty$, $N \to \infty$, we get $S^{\epsilon}_{tp} = 0$ whenever $\epsilon \neq 0$ for $\mathbb{Z}_2$ model with end of strings.

4.3.3 Calculating S_{tpr} for random tensors in the neighborhood of $\mathbb{Z}_2$

Redefining topological entanglement entropy in terms of Renyi entropy might simplify the calculation. Specifically, the calculation of Renyi entropy at $\alpha = 2$ for a tensor product state can be mapped to the contraction of a single tensor network, which can be computed efficiently in one dimension and approximated in two or higher dimension. For example,

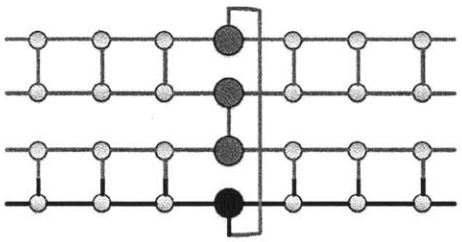

Figure 4-6: Tensor network for calculating Renyi entropy ($\alpha = 2$) of the big site in a one-dimensional tensor product state. The contraction of the tensor network gives $Tr(\rho^2) = exp(-S_2(\rho))$, where ρ is the reduced density matrix . The lowest level represents the state, where horizontal links represent inner indices along the one-dimensional chain and vertical links represent physical indices. Four copies of the state are stacked together and corresponding physical indices are connected between the levels. For physical indices outside the reduced region, the connection is between levels 1&2 and levels 3&4. For those in the reduced region, the connection is between levels 1&4 and levels 2&3.

consider a one dimensional tensor product state (also called a matrix product state). The lowest dark level in Fig.4-6 gives a side view of the state, where horizontal links represent inner indices along the one-dimensional chain and vertical links represent physical indices. Renyi entropy at $\alpha = 2$ is defined as $S_2(\rho) = -log[Tr(\rho^2)]$. To find out $Tr(\rho^2)$, we stack four copies of the states together as in Fig.4-6, connect corresponding physical indices outside the reduced region between levels 1&2, 3&4 and connect those within the reduced region between levels 1&4, 2&3. Contraction of this four-layer one-dimensional tensor network gives $Tr(\rho^2)$. For two dimensional tensor product states, the generalization is straightforward. The only difference is that now we have to contract a four-layer two-dimensional tensor network. To this end, we apply the Tensor Entanglement Renormalization Algorithm [LN07]. Having obtained the Renyi entropy for different regions, we then combine them to get S_{tpr}.

4.3.4 Gauge symmetry of tensor product states and topological order

This section discusses in general the relation between gauge symmetries of tensor product states and topological order, and the implication of our result on other topological ordered models with gauge symmetry.

For a tensor product state, the network of tensors which represents the same state is not unique. In particular, if we change a pair of connected tensors by rotating the basis of one of the connected inner index with an invertible operator A and rotating the other connected inner index with operator A^{-1}, any tensor trace would remain unchanged and hence the tensor product state remains the same. This corresponds to inserting a pair of invertible operators A, A^{-1} onto any link in the graphical representation of the state. Following the definition in Ref. [SW10], this is called a gauge transformations of the tensor product state, which form a very large group. Hence the correspondence between the tensor network

and the physical state is many-to-one. As a result, the variation energy as a function of tensors has a very large symmetry: the variation energy is invariant under the gauge transformations.

On the other hand, when we try to find the best description of ground state for a model Hamiltonian by minimizing energy with respect to the variations of the tensors, the tensors that minimize the average energy may not be invariant under all the gauge transformations and in general have much less symmetry. For example, in the ideal $\mathbb{Z}_2$ case, the tensors are only invariant if we insert Z, Z^{-1} to all the links in the 2-dimensional graph. Generalizing this to any symmetry group and to any dimension d, we define the d-dimensional Invariant Gauge Group(d-IGG). The d-IGG is nothing but the invariant group of the tensors under gauge transformations. Thus the minimization of the average energy leads to a spontaneous symmetry breaking. The d-IGG's are the unbroken symmetry of the tensors that describe the ground state. As we change the Hamiltonian, the tensors that minimize the average energy may have some different symmetry structures described by different d-IGG's. As is shown in Ref. [SW10], when d equals the dimension of system space d_{space}, d_{space}-IGG (such as the $\mathbb{Z}_2$ symmetry discussed in this chapter) can be used to determine the topological orders of a tensor product state. A closely related concept is discussed in Ref. [SCPG10]. Therefore, a change in d_{space}-IGG will in general represent a change in topological order. Apart from d_{space}-IGG, the tensors might also have lower dimensional IGG's. For example, if we trivially map every inner index i to $ii(i = 0, 1)$ in the $\mathbb{Z}_2$ tensor, the tensors still represent the same state but have a 0-IGG ZZ in additional to its 2-IGG. However, we believe that such 0-IGG's are not related to the topological order in two dimension and changing them may not lead to a change in topological order.

Note that in order to use d_{space}-IGG of a tensor network to decide topological order, we only require that the network is composed of patches of tensors which are invariant under certain gauge transformations. It is not necessary that every single tensor is d_{space}-IGG invariant. However, in the generic case, if the single tensors do not have special symmetry structure, it is not possible to have d_{space}-IGG invariance on a bigger patch. As discussed in Ref. [PGVCW08], such a tensor network will generically satisfy a condition called 'injectivity', i.e. for a large enough region in the network, when the single tensors are contracted together to form a new tensor, the set of tensor vectors labeled by their physical indices will span the full tensor space of the n outgoing inner indices of the region. Therefore, the tensor network cannot have nontrivial d_{space}-IGG. In order for a bigger patch in the network to have d_{space}-IGG invariance, it is in general necessary for every tensor to be d_{space}-IGG invariant.

Hence, we believe that the invariance of every tensor under d_{space}-IGG is a more general necessary conditions for generic variations of the tensor to correspond to physical perturbations of the Hamiltonian. Breaking of the d_{space}-IGG invariance of the tensors will in general correspond to a change in topological order. Therefore in a numerical variational calculation it is very important to preserve the d_{space}-IGG invariance. Otherwise we would not be able to correctly determine the topological order of the resulting state from the tensors.

Part III

Classification of Topological Order

With an efficient method to describe many-body entangled ground states of locally interacting gapped quantum systems, we now want to know what universal properties, in particular what universal entanglement patterns, exist in such states at macroscopic length scale. As the ground state contains the full dynamics of gapped systems at temperature well below the gap, universal properties of the ground state will fully characterize the quantum phase of the system at zero temperature. Therefore, if we set the stage right, we can obtain a complete understanding of zero temperature quantum phases from the classification of gapped many-body quantum states. As symmetry breaking phases are already well understood using Landau's symmetry breaking theory, we are interested in what topological phases exist. This is what we try to achieve in this part. In Chapter 5, we review the notion of quantum phases with emphasis on topological order and set up the necessary equivalence condition for the classification of gapped many-body quantum states and hence the corresponding quantum phases. In Chapter 6 and Chapter 7, we apply this classification procedure to one dimensional and two and higher dimensional systems respectively. As many-body entanglement is naturally included in the formalism, this approach turns out to be powerful enough to reveal new topological phases and even classify them in some cases.

Chapter 5

Topological order and long/short range entanglement

Many-body entanglement provides a unique point of view and a powerful tool to the study of quantum phases and phase transitions, especially for zero temperature gapped quantum phases whose ground state contains much of the universal properties of the phase. Before we try to classify gapped quantum phases from our understanding of many-body entanglement patterns, we need to think carefully about what is a quantum phase and what is the criteria for their classification. By defining carefully the meaning of quantum phase and phase transition, we can also see immediately their close connection to many-body entanglement. This is the goal of this chapter and the chapter is based partly on our work [CGW10].

This chapter is structured as follows: In the first section 5.1, we review what is the general definition of a quantum phase. We start from an intuitive picture of systems with very different physical properties being in different phases and arrive at a mathematically rigorous definition of phase based on phase transitions. In particular, we are interested in quantum phases that are beyond the classical understanding of symmetry breaking. These phases are said to contain topological order. The key ingredient which distinguishes topologically ordered phases from symmetry breaking phases is the existence of nontrivial entanglement patterns in the ground states of the system, which becomes more clear through our discussion in section 5.2. We demonstrate in this section that quantum states are in the same phase if and only if they are connected through local unitary transformations. We present two equivalent forms of local unitary transformation: the local unitary time evolution and the local unitary quantum circuit, which are useful in different circumstances. As local unitary transformations can only modify the entanglement structure of a state locally, we see that topological order corresponds to the existence of long-range entanglement in the state while topologically trivial states contain only short-range entanglement. The notion of long/short range entanglement is discussed in more detail in section 5.3. This formalism also allows us to discuss the situations where the system has certain symmetries and we obtain a generic structure of the possible phase diagram at the end of this chapter in section 5.3.3.

5.1 Background: quantum phase and topological order

5.1.1 Quantum phase and phase transition

Different quantum many-body systems have different properties. Some are liquids, some are solids; some are magnetic, some are not; some are insulators, some are conductors, some are superconductors... Of course one magnet can still be very different from another magnet, for example in terms of their magnetization, however there is a sense of equivalence among all different magnets and we say that they belong to the same phase. Generally speaking, a phase is composed of systems with qualitatively the same but quantitatively different properties. Therefore, as a system evolves within a phase, for example by changing temperature or exterior magnetic field, its property changes smoothly. However, when we reach a critical temperature or magnetic field, something dramatic could happen in the system and its property changes qualitatively as the system transits into a different phase. This is the point of phase transition. Different phases are hence separated by singular phase transition points where some physical observables of the system diverges.

Therefore, a more rigorous way to define phase is to say that two systems are in the same phase if and only if they can evolve into each other smoothly without inducing singularity in any local physical observable. Note that such evolution is allowed to take any path. In this sense, liquid water and water vapor belong to the same phase as above critical temperature the two can change into each other smoothly without crossing a phase boundary.

One special aspect of quantum many-body systems is that even at zero temperature, there can be different phases and phase transitions can happen without adding heat to the system. For gapped quantum systems, quantum phase transition at zero temperature is closely related to gap closing in the system. Consider a local Hamiltonian $H(0)$, with ground state $|\psi(0)\rangle$ and a finite gap $\Delta(0)$ above the ground state. Expectation value of any physical observable O is given by $\langle O\rangle(0) = \langle\psi(0)|\, O\, |\psi(0)\rangle$. Suppose that we smoothly change certain parameter g in the Hamiltonian so that the system follows a path $H(g)$. The ground state $|\psi(g)\rangle$ and the expectation value of the physical observable $\langle O\rangle(g) = \langle\psi(g)|\, O\, |\psi(g)\rangle$ will change accordingly. As long as the gap of the system $\Delta(g)$ remains finite, $\langle O\rangle(g)$ will change smoothly [HW05]. Only when the gap $\Delta(g)$ closes, can there be singularity in any physical quantity. The possible and impossible situations are depicted in Fig. 5-1. Therefore, for gapped quantum systems at zero temperature, two systems $H(0)$ and $H(1)$ are within the same phase if and only if there exists a smooth path $H(g), 0 \leq g \leq 1$ connecting the two and has a finite gap for all g.

The question which is of general interest in condensed matter physics and which we will try to answer in this part is: what quantum phases could possibly exist at zero temperature in local gapped quantum systems? That is, for a class of local gapped quantum systems, how many sets can we group them into such that systems within a set can be smoothly connected and systems in different sets can not? Here we are considering quantum systems with arbitrary local degrees of freedom: bosons, fermions, spins... We also allow arbitrary form of local interaction between them, as long as the interaction involves a finite number of parties and affects a finite region in the lattice.

First, we want to emphasize that quantum phase is a property of a class of Hamiltonians, not of a single Hamiltonian. We call such a class of Hamiltonian an H-class. For an H-class, of a certain dimension and with possible symmetry constraints, we ask whether the Hamiltonians in it are separated into different groups by phase transition and hence form different phases. Two Hamiltonians in an H-class are in the same/different phase if

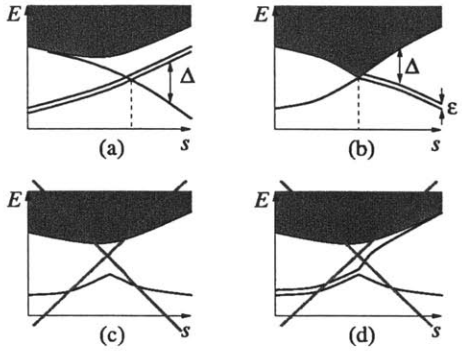

Figure 5-1: Energy spectrum of a gapped system as a function of a parameter s in the Hamiltonian. (a,b) For gapped system, a quantum phase transition can happen only when energy gap closes. (a) describes a first order quantum phase transition (caused by level crossing). (b) describes a continuous quantum phase transition which has a continuum of gapless excitations at the transition point. (c) and (d) cannot happen for generic states. A gapped system may have ground state degeneracy, where the energy splitting ϵ between the ground states vanishes when system size $L \to \infty$: $\lim_{L\to\infty} \epsilon = 0$. The energy gap Δ between ground and excited states on the other hand remains finite as $L \to \infty$.

they can/cannot be connected *within the H-class* without going through phase transition. We see that without identifying the class of Hamiltonians under consideration, it is not meaningful to ask which phase a Hamiltonian belongs to. Two Hamiltonians can belong to the same/different phases if we embed them in different H-classes.

For an H-class with certain symmetry constraints, one mechanism leading to distinct phases is symmetry breaking.[Lan37, GL50] Starting from Hamiltonians with the same symmetry, the ground states of them can have different symmetries, hence resulting in different phases. This symmetry breaking mechanism for phases and phase transitions is well understood.[Lan37, LL58]

However, it has been realized that quantum systems at zero temperature can be in different phases even without breaking any symmetry. Such phases are often said to be 'topological'. Fractional quantum Hall is one of the first and most important systems found to have topological order[TSG82]. It was realized that, different fractional quantum Hall systems at different filling fractions all have the same symmetry in the ground state, yet there must be a phase transition if the system is to go from one to another[WN90]. In one dimensional spin chains, the Haldane chain is another example of gapped topological phase, which does not break any symmetry of the system and is separate from a trivial phase[Hal83b]. More recently, the exciting discovery of topological insulators and superconductors offers another class of topological phases with interesting topological features[KM05a, BZ06, KM05b, MB07, FKM07, QHZ08].

So we would like to have a theory beyond Landau's symmetry breaking theory for a more complete understanding of the quantum phase diagram at zero temperature.

5.1.2 What is missing in symmetry breaking theory

In order to formulate a theory for topological orders, first we need to understand what is missing in the symmetry breaking theory. And the answer turns out to be – entanglement.

Consider the simplest quantum system which can be described by the symmetry breaking theory – the transverse field Ising model in two dimensions: $H = -B\sum X_i - J\sum Z_iZ_j$, where X_i, Y_i, and Z_i are the Pauli matrices on site i. In $B \gg J$ limit, the ground state of the system is an equal-weight superposition of all possible spin-up and spin-down states: $|\Phi^+\rangle = \sum_{\{\sigma_i\}} |\{\sigma_i\}\rangle$, where $\{\sigma_i\}$ labels a particular spin-up ($Z_i = 1$) and spin-down ($Z_i = -1$) configuration. In the $J \gg B$ limit, the system has two degenerate ground states $|\Phi^\uparrow\rangle = |\uparrow\uparrow\cdots\uparrow\rangle$ and $|\Phi^\downarrow\rangle = |\downarrow\downarrow\cdots\downarrow\rangle$.

The transverse field Ising model has a symmetry given by $\prod_i X_i$. The ground state $|\Phi^+\rangle$ respects such a symmetry while the ground state $|\Phi^\uparrow\rangle$ (or $|\Phi^\downarrow\rangle$) breaks the symmetry. Thus the small J ground state $|\Phi^+\rangle$ and the small B ground state $|\Phi^\uparrow\rangle$ (or $|\Phi^\downarrow\rangle$) describe different phases since they have different symmetries. $|\Phi^+\rangle$ describes a symmetric phase, while $|\Phi^\uparrow\rangle$ (or $|\Phi^\downarrow\rangle$) describes a symmetry breaking phase.

We note that $|\Phi^\uparrow\rangle$ is the exact ground state of the transverse field Ising model with $B = 0$. The state has no quantum entanglement since $|\Phi^\uparrow\rangle$ is a direct product of local states: $|\Phi^\uparrow\rangle = \otimes_i|\uparrow\rangle_i$ where $|\uparrow\rangle_i$ is an up-spin state at site i. The state $|\Phi^+\rangle$ is the exact ground state of the transverse field Ising model with $J = 0$. It is also a state with no quantum entanglement: $|\Phi^+\rangle = \otimes_i(|\uparrow\rangle_i + |\downarrow\rangle_i) \propto \otimes_i|+\rangle_i$ where $|+\rangle_i \equiv |\uparrow\rangle_i + |\downarrow\rangle_i$ is a state with spin in x-direction at site i.

For generic values of J and B, the ground state is entangled. However, such entanglement is not essential for either the symmetry breaking phase or the symmetric phase. In fact, for J/B below the critical point, the system remains gapped and is in the symmetric phase. By slowly turning down J and turning up B, we can smoothly connect the ground state to $|\Phi^+\rangle$, hence remove all entanglement in the state. On the other hand, for J/B above the critical point, the system is also gapped with symmetry breaking ground states. By slowly turning up J and turning down B, we can smoothly connect the ground state either to $|\Phi^\uparrow\rangle$ or to $|\Phi^\downarrow\rangle$, hence again removing all entanglement in the state. Therefore, entanglement in both phases is always removable.

This is true for general symmetry breaking phases described by Landau's theory. There exists at least one point in the symmetry breaking phase where the ground state is totally unentangled. Therefore, we see that Landau's theory fails to describe more exotic topological orders because the ground state contains only removable entanglement. It is the unremovable entanglement that makes topological orders possible. We will see later that there are two reasons why entanglement in the ground state might be unremovable: 1. the entanglement is 'long-ranged' and hence cannot be removed by local deformations 2. symmetry constrain in the system requires the presence of entanglement in the ground state. In order to better explain these two situations and understand what topological phases they give rise to, we first need to discuss more carefully the relation between quantum phases and ground state entanglement.

5.2 Quantum phases and local unitary quantum circuits

Quantum phase and phase transitions are usually discussed in terms of the Hamiltonian of the system[Sac01]. For example for gapped quantum systems at zero temperature, two systems are in the same phase if and only if their Hamiltonians can be connected smoothly without closing gap. In fact, gapped quantum phases at zero temperature can be equally well studied in terms of its ground state. In this section, we describe carefully how to determine the phase relation between two systems from their ground states. Such a relation

has also been used in [VCL+05, Vid07, Yos11] to study universal properties of quantum states.

Note that when we say a gapped ground state $|\psi\rangle$, we are always assuming that there exists a gapped Hamiltonian which has the state as its ground state. There can be multiple Hamiltonians satisfying this requirement, but their difference is not important, as their zero temperature property is completely determined by $|\psi\rangle$.

5.2.1 Quantum phases and local unitary evolutions in ground states

Suppose that we have two gapped quantum systems with Hamiltonians $H(0)$ and $H(1)$ and ground states $|\Phi(0)\rangle$ and $|\Phi(1)\rangle$ respectively. We want to determine from the ground states when the two systems are in the same phase.

For Hamiltonians we know that they are in the same phase iff there exists a gapped smooth path $H(g), 0 \leq g \leq 1$ connecting them in the class of local quantum systems of the same dimension. [1] Such a smooth connection in Hamiltonians induces an adiabatic evolution connecting the ground states. Actually, if we change the Hamiltonian $H(g)$ very slowly (compared to the inverse gap of the system), then the ground state follows an adiabatic evolution which begins with $|\Phi(0)\rangle$ and ends with $|\Phi(1)\rangle$. Therefore, we see that: two gapped quantum states are in the same phase $|\Phi(0)\rangle \sim |\Phi(1)\rangle$ if and only if they can be connected by an adiabatic evolution that does not close the energy gap.

Given two states, $|\Phi(0)\rangle$ and $|\Phi(1)\rangle$, determining the existence of such a gapped adiabatic connection can be hard. We would like to have a more operationally practical equivalence relation between states in the same phase. Here we would like to show that *two gapped states $|\Phi(0)\rangle$ and $|\Phi(1)\rangle$ are in the same phase, if and only if they are related by a local unitary (LU) evolution.* We define a local unitary(LU) evolution as an unitary operation generated by time evolution of a local Hamiltonian for a finite time. That is,

$$|\Phi(1)\rangle \sim |\Phi(0)\rangle \text{ iff } |\Phi(1)\rangle = \mathcal{T}[e^{-i\int_0^1 dg\, \tilde{H}(g)}]|\Phi(0)\rangle \tag{5.1}$$

where $\mathcal{T}$ is the path-ordering operator and $\tilde{H}(g) = \sum_i O_i(g)$ is a sum of local Hermitian operators. Note that $\tilde{H}(g)$ is in general different from the adiabatic path $H(g)$ that connects the two states.

First, assume that two states $|\Phi(0)\rangle$ and $|\Phi(1)\rangle$ are in the same phase, therefore we can find a gapped adiabatic path $H(g)$ between the states. The existence of a gap prevents the system to be excited to higher energy levels and leads to a local unitary evolution, the Quasi-adiabatic Continuation as defined in [HW05], that maps from one state to the other. That is,

$$|\Phi(1)\rangle = U|\Phi(0)\rangle, \qquad U = \mathcal{T}[e^{-i\int_0^1 dg\, \tilde{H}(g)}] \tag{5.2}$$

The exact form of $\tilde{H}(g)$ is given in [HW05, BHM10].

On the other hand, the reverse is also true: *if two gapped states $|\Phi(0)\rangle$ and $|\Phi(1)\rangle$ are related by a local unitary evolution, then they are in the same phase.* Since $|\Phi(0)\rangle$ and $|\Phi(1)\rangle$ are related by a local unitary evolution, we have $|\Phi(1)\rangle = \mathcal{T}[e^{-i\int_0^1 dg\, \tilde{H}(g)}]|\Phi(0)\rangle$. Let us introduce

$$|\Phi(s)\rangle = U(s)|\Phi(0)\rangle, \qquad U(s) = \mathcal{T}[e^{-i\int_0^s dg\, \tilde{H}(g)}]. \tag{5.3}$$

[1] We do not impose symmetry constraint on the class of systems for now. The symmetry constrained case is considered later.

Assume that $|\Phi(0)\rangle$ is a ground state of $H(0)$, then $|\Phi(s)\rangle$ is a ground state of $H(s) = U(s)HU^\dagger(s)$. If $H(s)$ remains local and gapped for all $s \in [0,1]$, then we have found an adiabatic connection between $|\Phi(0)\rangle$ and $|\Phi(1)\rangle$.

First, let us show that $H(s)$ is a local Hamiltonian. Since H is a local Hamiltonian, it has a form $H = \sum_i O_i$ where O_i only acts on a cluster whose size is ξ. ξ is called the range of interaction of H. We see that $H(s)$ has a form $H(s) = \sum_i O_i(s)$, where $O_i(s) = U(s)O_iU^\dagger(s)$. To show that $O_i(s)$ only acts on a cluster of a finite size, we note that for a local system described by $\tilde{H}(g)$, the propagation velocities of its excitations have a maximum value v_{max}. Since $O_i(s)$ can be viewed as the time evolution of O_i by $\tilde{H}(t)$ from $t = 0$ to $t = s$, we find that $O_i(s)$ only acts on a cluster of size $\xi + \tilde{\xi} + sv_{max}$,[LR72, HW05] where $\tilde{\xi}$ is the range of interaction of $\tilde{H}$. Thus $H(s)$ is indeed a local Hamiltonian.

If H has a finite energy gap, then $H(s)$ also have a finite energy gap for any s. As s goes for 0 to 1, the ground state of the local Hamiltonians, $H(s)$, goes from $|\Phi(0)\rangle$ to $|\Phi(1)\rangle$. Thus the two states $|\Phi(0)\rangle$ and $|\Phi(1)\rangle$ belong to the same phase. This completes our argument that states related by a local unitary evolution belong to the same phase.

The finiteness of the evolution time is very important in the above discussion. Here 'finite' means the evolution time does not grow with system size and in the thermodynamic limit, phases remain separate under such evolutions, as proven in [BHV06]. On the other hand, if the system size under consideration is finite, there is a critical time limit above which phase separation could be destroyed. The time limit depends on the propagation speed of interactions in the Hamiltonian. This is the case in [THZ+09], where topological order as measured by topological entropy and fidelity was found to decay under certain local Hamiltonian evolution(a quantum quench). However this result does not contradict our statement. As the calculation is done for a particular system size, the critical time limit could be below or above the time period they studied. If the calculation could be done for larger and larger system sizes for a fixed amount of time, we expect that topological order should emerge as stable against local quenches.

Thus through the above discussion, we show that

Two gapped ground states, $|\Phi(0)\rangle$ and $|\Phi(1)\rangle$, belong to the same phase if and only if they are related by a local unitary evolution Eq. (5.1).

The relation Eq. (5.1) defines an equivalence relation between $|\Phi(0)\rangle$ and $|\Phi(1)\rangle$. The equivalence classes of such an equivalence relation represent different quantum phases. So the above result implies that the equivalence classes of the LU evolutions are the universality classes of quantum phases for gapped states.

5.2.2 Local unitary evolutions and local unitary quantum circuits

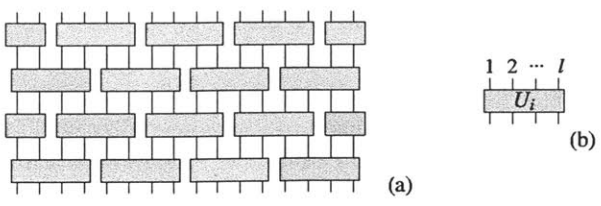

Figure 5-2: (a) A graphic representation of a quantum circuit, which is formed by (b) unitary operations on patches of finite size l. The green shading represents a causal structure.

The LU evolutions introduced here is closely related to *quantum circuits with finite depth*. To define quantum circuits, let us introduce piece-wise local unitary operators. A piece-wise local unitary operator has a form $U_{pwl} = \prod_i U_i$ where $\{U_i\}$ is a set of unitary operators that act on non overlapping regions. The size of each region is less than some finite number l. The unitary operator U_{pwl} defined in this way is called a piece-wise local unitary operator with range l. A quantum circuit with depth M is given by the product of M piece-wise local unitary operators (see Fig. 5-2): $U^M_{circ} = U^{(1)}_{pwl} U^{(2)}_{pwl} \cdots U^{(M)}_{pwl}$. In quantum information theory, it is known that finite time unitary evolution with local Hamiltonian (LU evolution defined before) can be simulated with constant depth quantum circuit and vice-verse. Therefore, the equivalence relation Eq. (5.1) can be equivalently stated in terms of constant depth quantum circuits:

$$|\Phi(1)\rangle \sim |\Phi(0)\rangle \text{ iff } |\Phi(1)\rangle = U^M_{circ}|\Phi(0)\rangle \tag{5.4}$$

where M is a constant independent of system size. Because of their equivalence, we will use the term "Local Unitary Transformation" to refer to both local unitary evolution and constant depth quantum circuit in general.

The LU transformation defined through LU evolution Eq. (5.1) is more general. It can be easily generalized to study topological orders and quantum phases with symmetries (see section 5.3.2).[Wen02, GW09] The quantum circuit has a more clear and simple causal structure. However, the quantum circuit approach breaks the translation symmetry. So it is more suitable for studying quantum phases that do not have translation symmetry.

Such a relation has also been used in [VCL+05, Vid07, Yos11] to study universal properties of quantum states. In [VCL+05], the local unitary transformations described by quantum circuits was used to define a renormalization group transformations for states and establish an equivalence relation in which states are equivalent if they are connected by a local unitary transformation. Such an approach was used to classify 1D matrix product states. In [Vid07], the local unitary transformations with disentanglers was used to perform a renormalization group transformations for states, which give rise to the multi-scale entanglement renormalization ansatz (MERA) in one and higher dimensions. The disentanglers and the isometries in MERA can be used to study quantum phases and quantum phase transitions in one and higher dimensions. For a class of exactly solvable Hamiltonians which come from the stabilizer codes in quantum computation, topological order has also been classified using local unitary circuits[2][Yos11].

5.2.3 Local unitary quantum circuits and wave-function renormalization

As an application of the notion of LU transformation, we would like to describe a wave function renormalization group flow introduced in [LW05],[Vid07]. The wave function renormalization can remove entanglement structure at small length scale and simplify the wave function. In [LW05], the wave function renormalization for string-net states is generated by

[2]Private communication with Sergey Bravyi.

the following two basic moves

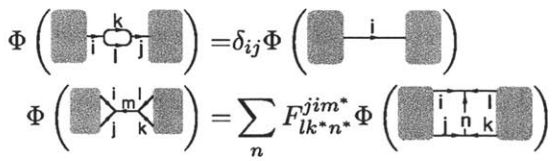

(Note that the definition of the F-tensor in [LW05] is slightly different from the definition here.) The two basic moves can generate a generic wave function renormalization which can reduce the string-net wave functions to very simple forms.[LW05, LW06] Later in [Vid07], the wave function renormalization for generic states was discussed in a more general setting, and was called MERA. The two basic string-net moves Eq. (5.5) and Eq. (5.6) correspond to the isometry and the disentangler in MERA respectively. In the MERA approach, the isometries and the disentanglers are applied in a layered fashion, while in the string-net approach, the two basic moves can be applied arbitrarily. In this section, we will follow the MERA setup to describe the wave function renormalization.

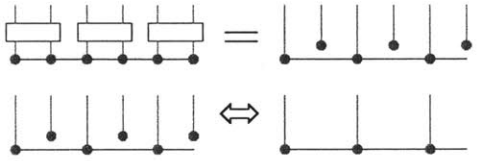

Figure 5-3: A piece-wise local unitary transformation can transform some degrees of freedom in a state $|\Phi\rangle$ into a direct product. Removing/adding the degrees of freedom in the form of direct product defines an additional equivalence relation between quantum states.

First we can use a LU transformation U to transform some degrees of freedom in a state into direct product (see Fig. 5-3). We then remove those degrees of freedom in the form of direct product. Such a procedure does not change the phase the state belongs to. The reverse process of adding degrees of freedom in the form of direct product also does not change the phase. We call the local transformation in Fig. 5-3 that changes the degrees of freedom a generalized local unitary (gLU) transformation. It is clear that a generalized local unitary transformation inside a region A does not change the reduced density matrix ρ_A for the region A. This is the reason why we say that (generalized) local unitary transformations cannot change entanglement structure at large length scale and the quantum phase of the system. Similarly, the addition or removal of decoupled degrees of freedom to or from the Hamiltonian, $H \leftrightarrow H \otimes H_{dp}$, will not change the phase of the Hamiltonian (i.e. the ground states of H and $H \otimes H_{dp}$ are in the same phase), if those degrees of freedom form a direct product state (i.e. the ground state of H_{dp} is a direct product state).

Let us define the gLU transformation U more carefully and in a more general setting. Consider a state $|\Phi\rangle$. Let ρ_A be the reduced density matrix of $|\Phi\rangle$ in region A. ρ_A may act in a subspace of the total Hilbert space V_A in region A, which is called the support space V_A^{sp} of region A. The dimension D_A^{sp} of V_A^{sp} is called support dimension of region A. Now the Hilbert space V_A in region A can be written as $V_A = V_A^{sp} \oplus \bar{V}_A^{sp}$. Let $|\tilde{\psi}_i\rangle$, $i = 1, ..., D_A^{sp}$ be a basis of this support space V_A^{sp}, $|\tilde{\psi}_i\rangle$, $i = D_A^{sp} + 1, ..., D_A$ be a basis of $\bar{V}_A^{sp}$, where D_A is the dimension of V_A, and $|\psi_i\rangle$, $i = 1, ..., D_A$ be a basis of V_A. We can

introduce a LU transformation U^{full} which rotates the basis $|\psi_i\rangle$ to $|\tilde{\psi}_i\rangle$. We note that in the new basis, the wave function only has non-zero amplitudes on the first D_A^{sp} basis vectors. Thus, in the new basis $|\tilde{\psi}_i\rangle$, we can reduce the range of the label i from $[1, D_A]$ to $[1, D_A^{sp}]$ without losing any information. This motivates us to introduce the gLU transformation as a rotation from $|\psi_i\rangle$, $i = 1, ..., D_A$ to $|\tilde{\psi}_i\rangle$, $i = 1, ..., D_A^{sp}$. The rectangular matrix U is given by $U_{ij} = \langle\tilde{\psi}_i|\psi_j\rangle$. We also regard the inverse of U, $U^\dagger$, as a gLU transformation. A LU transformation is viewed as a special case of gLU transformation where the degrees of freedom are not changed. Clearly $U^\dagger U = P$ and $UU^\dagger = P'$ are two projectors. The action of P does not change the state $|\Phi\rangle$ (see Fig. 5-4(b)).

We note that despite the reduction of the degrees of freedom, a gLU transformation defines an equivalent relation. Two states related by a gLU transformation belong to the same phase. The renormalization flow induced by the gLU transformations always flows within the same phase. The renormalization algorithm described in Chapter 2 and 3 are (approximate) implementations of such a gLU transformation on matrix product states and tensor product states. The discussion in this chapter hence provides more rigorous meaning to the renormalization procedure described.

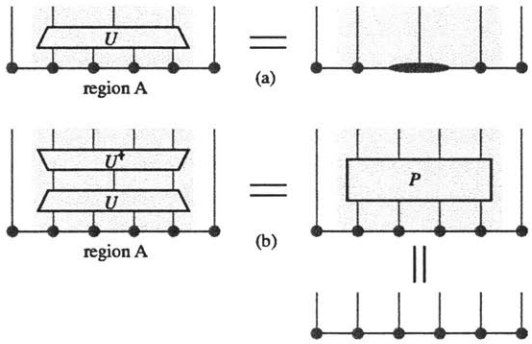

Figure 5-4: (a) A gLU transformation U acts in region A of a state $|\Phi\rangle$, which reduces the degree freedom in region A to those contained only in the support space of $|\Phi\rangle$ in region A. (b) $U^\dagger U = P$ is a projector that does not change the state $|\Phi\rangle$.

5.3 Topological order as pattern of many-body entanglement

5.3.1 Long-range entanglement and intrinsic topological order

Using the (generalize) local unitary transformation, we can define the notion of short-range entanglement and long-range entanglement in gapped quantum states and relate them to topological order.

A state has only short-range entanglement if and only if it can be transformed into an unentangled state (i.e. a direct-product state) through a local unitary transformation.

If a state cannot be transformed into an unentangled state through a LU transformation, then the state has long-range entanglement. We also see that *All states with short-range entanglement can transform into each other through local unitary transformations.* Thus all states with short-range entanglement belong to the same phase. The local unitary transformations we consider here do not have any symmetry. If we require certain symmetry

of the local unitary transformations, states with short-range entanglement may belong to different phases, which will be discussed in section 5.3.2.

Since a direct-product state is a state with trivial topological order, we see that a state with a short-range entanglement also has a trivial topological order. This leads us to conclude that a non-trivial topological order is related to long-range entanglement. Since two gapped states related by a LU transformation belong to the same phase, thus two gapped states related by a local unitary transformation have the same topological order. In other words, *Topological order describes the equivalent classes defined by local unitary transformations.* Or more pictorially, topological order is a pattern of long-range entanglement. In [BHV06], it was shown that the 'topologically non-trivial' ground states, such as the toric code,[Kit03] cannot be changed into a 'topologically trivial' state such as a product state by any unitary locality-preserving operator. In other words, those 'topologically non-trivial' ground states have long-range entanglement.

In section 5.3.2, we will discuss a different kind of topological order which exists only under the protection of certain symmetry. To distinguish these two, we will call the topological order related to long-range entanglement the 'intrinsic' topological order. This type of order is defined for the class of systems without any symmetry constraint, which corresponds to the original definition of 'topological order'.[Wen89, Wen90] That is, it refers to quantum phases in an H-class which includes all local Hamiltonians (of a certain dimension). If we believed that Landau symmetry breaking theory describes all possibles phases, this whole H-class would belong to the same phase as there is no symmetry to break. However, in two and three dimensions, there are actually distinct phases even in the H-class that has no symmetries. These phases have universal properties stable against any small local perturbation to the Hamiltonian. To change these universal properties, the system has to go through a phase transition. Systems with nontrivial 'intrinsic' topological order include quantum Hall systems[WN90], chiral spin liquids,[KL87, WWZ89] Z_2 spin liquids,[RS91, Wen91, MS01] quantum double model[Kit03] and string-net model[LW05]. Such systems can have ground state degeneracy which depends on topology of the system and fractional charge and fractional statistics[Wen89, Wen90]. Ground states with 'intrinsic' topological order can also have non-zero topological entanglement entropy[LW06, KP06].

5.3.2 Short-range entanglement and symmetry protected topological order

In the above discussions, we have defined phases without any symmetry consideration. The $\tilde{H}(g)$ or U_{pwl} in the LU transformation does not need to have any symmetry and can be sum/product of any local operators. In this case, two Hamiltonians with an adiabatic connection are in the same phase even if they may have different symmetries. Also, all states with short-range entanglement belong to the same phase (under the LU transformations that do not have any symmetry).

On the other hand, we can consider only Hamiltonians H with certain symmetries and define phases as the equivalent classes of symmetric local unitary transformations:

$$|\Psi\rangle \sim \mathcal{T}\left(e^{-i\int_0^1 dg\, \tilde{H}(g)}\right)|\Psi\rangle \quad \text{or} \quad |\Psi\rangle \sim U_{circ}^M|\Psi\rangle \tag{5.7}$$

where $\tilde{H}(g)$ or U_{circ}^M has the same symmetries as H. [3]

[3]We note that the symmetric local unitary transformation in the form $\mathcal{T}\left(e^{-i\int_0^1 dg\, \tilde{H}(g)}\right)$ always connect

The equivalent classes of the symmetric LU transformations have very different structures compared to those of LU transformations without symmetry. Each equivalent class of the symmetric LU transformations is smaller and there are more kinds of classes, in general.

In particular, states with short range entanglement can belong to different equivalent classes of the symmetric LU transformations even if they do not break any symmetry of the system. (In this case, they have the same symmetry.) We say those states have Symmetry Protected Topological orders. Haldane phase[Hal83a] and $S_z = 0$ phase of spin-1 chain are examples of states with the same symmetry which belong to two different equivalent classes of symmetric LU transformations (with parity symmetry).[GW09, PBTO12] Band and topological insulators[KM05a, BZ06, KM05b, MB07, FKM07, QHZ08] are other examples of states that have the same symmetry and at the same time belong to two different equivalent classes of symmetric LU transformations (with time reversal symmetry). Systems with symmetry protected topological order cannot have ground state degeneracy, fractional charge and statistics, nor nonzero topological entanglement entropy. They can, however, have gapless edge excitations which are protected by symmetry.

5.3.3 Quantum phase diagram

We are now ready to summarize what we have learned and obtain a general structure of the quantum phase diagram at zero temperature.

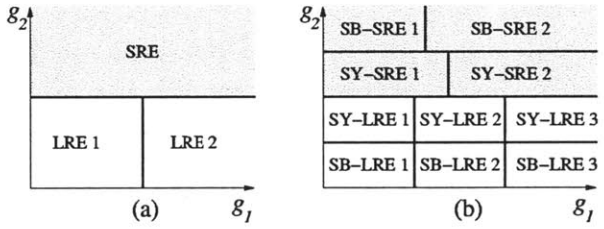

Figure 5-5: (a) The possible phases for a Hamiltonian $H(g_1, g_2)$ without any symmetry. (b) The possible phases for a Hamiltonian $H_{\text{symm}}(g_1, g_2)$ with some symmetries. The shaded regions in (a) and (b) represent the phases with short range entanglement (i.e. those ground states can be transformed into a direct product state via a generic LU transformations that do not have any symmetry.)

Fig. 5-5 compares the structure of phases for systems without any symmetry and systems with some symmetry in more detail.

For a system without any symmetry, all the short-range-entangled (SRE) states (i.e. those ground states can be transformed into a direct product state via a generic LU transformations that do not have any symmetry) are in the same phase (SRE in Fig. 5-5(a)). On the other hand, long range entanglement (LRE) can have many different patterns that give rise to different 'intrinsic' topological phases (LRE 1 and LRE 2 in Fig. 5-5(a)). The different 'intrinsic' topological orders usually give rise to quasi particles with different fractional statistics and fractional charges.

to the identity transformation continuously. This may not be the case for the transformation in the form U_{circ}^{M}. To rule out that possibility, we define symmetric local unitary transformations as those that connect to the identity transformation continuously.

For a system with some symmetries, the phase structure can be much more complicated. The short-range-entangled states no longer belong to the same phase, since the equivalence relation is described by more special symmetric LU transformations:
(A) States with short range entanglement belong to different equivalent classes of the symmetric LU transformations if they have different broken symmetries. They correspond to the symmetry-breaking (SB) short-range-entangled phases SB-SRE 1 and SB-SRE 2 in Fig. 5-5(b). They are Landau's symmetry breaking states.
(B) States with short range entanglement can belong to different symmetry protected topological phases if they do not break any symmetry of the system. They correspond to the symmetric (SY) short-range-entangled phases SY-SRE 1 and SY-SRE 2 in Fig. 5-5(b).

Also, for a system with some symmetries, the long-range-entangled states are divided into more classes (more phases):
(C) Symmetry breaking and long range entanglement can appear together in a state, such as SB-LRE 1, SB-LRE 2, etc. in Fig. 5-5(b). The topological superconducting states are examples of such phases.[RG00, KLW09]
(D) Long-range-entangled states that do not break any symmetry can also belong to different phases such as the symmetric long-range-entangled phases SY-LRE 1, SY-LRE 2, etc. in Fig. 5-5(b). The many different $\mathbb{Z}_2$ symmetric spin liquids with spin rotation, translation, and time-reversal symmetries are examples of those phases.[Wen02, KLW08, KW09] Some time-reversal symmetric topological orders, called topological Mott-insulators or fractionalized topological insulators[RQHZ08, ZRV09, PB10, YK10, MQKZ10, SBMS11], also belong to this case.

Now we want to find out what the entries are in this phase diagram, or in other words, to classify all possible phases in strongly correlated systems, especially the topological ones. Some partial classifications of have been discussed for strongly correlated systems through string-net states,[LW05] and for free fermion systems with certain symmetries through K-theory.[Kit09, RSFL10] In the next two chapters, we will try to classify symmetry protected topological phases (SY-SRE in Fig. 5-5(b)) in one and higher dimensions.

Chapter 6

Symmetry protected topological phases in one dimension

Having established the criteria for the classification of gapped quantum states and hence gapped quantum phases, we would like to apply it to many-body systems of interest. In this chapter, we consider one dimensional gapped strongly correlated spin systems both with and without symmetry, and try to classify all such systems whose ground state does not break any symmetry. (In other words, the ground state has the same symmetry as the Hamiltonian.)[1]

Completely classifying strongly correlated spin systems seems to be a hard task as in general strongly interacting quantum many-body systems are very hard to solve. However, as reviewed in Chapter 2, the insight about describing 1D gapped ground states of spin systems with the matrix product state formalism[FNW92b, PGVWC07] provides us with a handle to deal with this problem.

It has been shown that matrix product states capture the essential features of 1D gapped ground states, for example an entanglement area law[Has07] and finite correlation length[Has04, HK05], and provide an efficient description of such states[SWVC08]. On the other hand, generic matrix product states satisfying a condition called 'injectivity' are all gapped ground states of local Hamiltonians[FNW92b, PGVWC07]. Therefore, studying this class of MPS will enable us to give a full classification of 1D gapped spin systems.

Now the question of what phases exist in 1D gapped spin systems can be restated as what equivalence classes of matrix product states exist under LU transformations. As reviewed in Chapter 2, [VCL+05] gave a specific way to apply such LU transformations, which realizes a renormalization group transformation on MPS that removes local entanglement and takes the states to a simple fixed point form. A partial classification of MPS is also given in [VCL+05]. In the following we will use this procedure to classify gapped phases of 1D spin system, in particular the 1D systems with various symmetries. We see that the possible phases in 1D strongly correlated systems depend on the symmetry of the class of systems. This chapter is based on our work [CGW11a].

[1] Symmetry breaking phases are classified by Landau's symmetry breaking theory and are not our focus here.

6.1 No intrinsic topological order in 1D spin systems

When no symmetry is required for the class of system, we want to know what kind of long range entanglement exists and thereby classify topological orders in 1D gapped spin systems. We will show that: *All gapped 1D spin systems belong to the same phase if there is no symmetry.* In other words, there is no intrinsic topological order in 1D. This is similar to the generic case discussed in [VCL+05].

To obtain such a result, we use the fact that gapped 1D spin states[2] are described by short-range correlated (SRC) matrix product states. Then one can show that all SRC matrix product states can be mapped to product states with LU transformations and hence there is no topological order in 1D.

Consider a generic system without any symmetry (including translation symmetry) whose gapped ground state is described as an MPS with matrices $A_i^{[k]}$ that vary from site to site. [PGVWC07] gives a 'canonical form' for the matrices so that the double tensor $\mathbb{E}^{[k]}_{\alpha\gamma,\beta\chi}$, when treated as a matrix with row index $\alpha\gamma$ and column index $\beta\chi$, has a left eigenvector $\Lambda^{[k]}_{\alpha\gamma} = \lambda^{[k]}_\alpha \delta_{\alpha\gamma}$ and corresponding right eigenvector $\Lambda^{[k+1]}_{\beta\chi} = \lambda^{[k+1]}_\beta \delta_{\beta\chi}$. Here λ's are positive numbers and $\sum_\alpha \lambda_\alpha^2 = 1$. $\delta_{\alpha\gamma} = 1$ when $\alpha = \gamma$ and $\delta_{\alpha\gamma} = 0$ otherwise.[3] This eigenspace has the largest eigenvalue in $\mathbb{E}^{[k]}$ [EHK78] and is usually set to be 1. Note that the right eigenvector on site k is the same as the left eigenvector on site $k+1$ and has norm 1, therefore when multiplying the double tensors together, this one dimensional eigenspace will always be of eigenvalue 1.

There could be other eigenvectors of eigenvalue 1 in $\mathbb{E}^{[k]}$. However, this will lead to an infinite correlation length[FNW92b, PGVWC07, FNW94] and hence not possible in 1D gapped state. Therefore, for short-range correlated MPS, $\mathbb{E}^{[k]}$ must have a non-degenerate largest eigenvalue 1. When multiplying the double tensors together, the remaining block of $\mathbb{E}^{[k]}$ will decay exponentially with the number of sites. This consideration is essential for determining the fixed point of the renormalization procedure when applied to the MPS, as shown below.

Now we apply the renormalization procedure as discussed in Chapter 2 to remove local entanglement from a general SRC MPS. Take block size n. The double tensor on the renormalized sites are given by $(\mathbb{E}^{[K]})^{(1)} = \prod_{k\in K} (\mathbb{E}^{[k]})^{(0)}$, where k's are the n sites in block K. ($\mathbb{E}$, again, is treated as a $D^2 \times D^2$ matrix with row index $\alpha\gamma$ and column index $\beta\chi$.)

After repeating the renormalization process a finite number of times, $(\mathbb{E}^{[k]})^{(R)}$ will be arbitrarily close to a fixed point form $(\mathbb{E}^{[k]})^{(\infty)}$ with non-degenerate eigenvalue 1 and $(\mathbb{E}^{[k]})^{(\infty)}_{\alpha\gamma,\beta\chi} = \tilde{\Lambda}^{[k]}_{\alpha\gamma}\tilde{\Lambda}^{[k+1]}_{\beta\chi}$, where $\tilde{\Lambda}^{[K]}_{\alpha\gamma} = \tilde{\lambda}^{[k]}_\alpha \delta_{\alpha\gamma}$ and $\tilde{\Lambda}^{[k+1]}_{\beta\chi} = \tilde{\lambda}^{[k+1]}_\beta \delta_{\beta\chi}$.

Now we can decompose $(\mathbb{E}^{[k]})^{(\infty)}$ into matrices to find the fixed point state. One set of matrices giving rise to this double tensor is given by

$$(A^{[k]}_{i^l i^r,\alpha\beta})^{(\infty)} = \sqrt{\tilde{\lambda}^{[k]}_{i^l}}\delta_{i^l\alpha} \cdot \sqrt{\tilde{\lambda}^{[k+1]}_{i^r}}\delta_{i^r\beta} \tag{6.1}$$

$i^l, i^r = 1...D$. Here we use a pair of indices (i^l, i^r) to label the effective physical degrees of freedom on the renormalized site k, and $(A^{[k]}_{i^l,i^r})^{(\infty)}$ is a set of matrices that defines the

[2] A state is a gapped state if there exist a Hamiltonian H such that the state is the non-degenerate gapped ground state of H.

[3] The convention chosen here is different from [PGVWC07], but equivalent up to an invertible transformation on the matrices $A_i^{[k]}$.

fixed-point MPS. It is clear from the form of the matrices that at fixed point every site is composed of two virtual spins of dimension D. Every virtual spin is in an entangled pair with another virtual spin on the neighboring site $|EP_{k,k+1}\rangle = \sum_{i=1}^{D} \tilde{\lambda}_i^{[k+1]} |i,i\rangle$ and the full many-body state is a product of these pairs. An illustration of this state is given in Fig. 6-1(upper layer).

Obviously we can further disentangle these pairs by applying one layer of local unitary transformations between every neighboring sites and map the state to a product state (Fig. 6-1, lower layer).

Therefore, through these steps we have shown that all SRC matrix product states can be mapped to product states with LU transformations and hence there is no topological order in 1D non-translation invariant system.

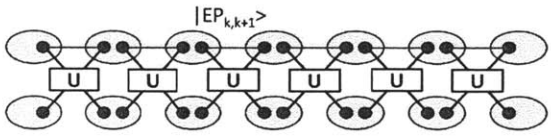

Figure 6-1: Disentangling fixed point state (upper layer, product of entangled pairs) into direct product state (lower layer) with LU transformations.

6.2 Symmetry protected topological order in 1D spin systems

If the class of systems under consideration has certain symmetry, the equivalence classes of states are defined in terms of LU transformations that do not break the symmetry. Therefore, when applying the renormalization procedure, we should carefully keep track of the symmetry and make sure that the resulting state has the same symmetry at each step. Due to such a constrain on local unitary equivalence, we will see that gapped ground states which do not break the symmetry of the system divide into different universality classes corresponding to different symmetry protected topological orders. We will first discuss the case of on-site symmetries in detail for non-translational invariant (NTI) systems, i.e., the system has only an on-site symmetry and no translation symmetry. We consider both unitary and anti-unitary symmetries (time reversal). Then we shall study translational invariant (TI) systems, with the possibility of having on-site symmetry or parity symmetry.

6.2.1 On-site Symmetry

A large class of systems are invariant under on-site symmetry transformations. For example, the Ising model is symmetric under the Z_2 spin flip transformation and the Heisenberg model is symmetric under $SO(3)$ spin rotation transformations. In this section, we will consider the general case where the system is symmetric under $u^{(0)}(g) \otimes ... \otimes u^{(0)}(g)$ with $u^{(0)}(g)$ being a unitary or anti-unitary representation of a symmetry group G on each site. The representation can be linear or projective. That is, for any $g_1, g_2 \in G$,

$$u(g_1)u(g_2) = e^{i\theta(g_1,g_2)}u(g_1g_2) \tag{6.2}$$

where $\theta(g_1, g_2) = 0$ in a linear representation and $\theta(g_1, g_2)$ could take non-trivial value in a projective representation. A projective representation of a symmetry group is generally allowed in a quantum description of system because the factor $e^{i\theta(g_1,g_2)}$ only changes the global phase of a quantum state but not any physically measurable quantity. Therefore, in our classification, we will consider not only the case of linear representation, but also in general projective representations.

The on-site symmetry is the only symmetry required for the class of system. In particular, we do not require translational symmetry for the systems. However, for a simple definition of phase, we will assume certain uniformness in the state, which we will define explicitly in the following. We will classify possible phases for different G when the ground state is invariant (up to a total phase) under such on-site symmetry operations and is gapped (i.e. short-range correlated). Specifically, the ground state $|\phi_L\rangle$ on L sites satisfies

$$u^{(0)}(g) \otimes ... \otimes u^{(0)}(g)|\phi_L\rangle = \alpha_L(g)|\phi_L\rangle \tag{6.3}$$

where $|\alpha_L(g)| = 1$ are g and L dependent phase factors.

On-site Linear Unitary Symmetry

First, let us consider the simpler case where $u^{(0)}(g)$ forms a linear unitary representation of G. $\alpha_L(g)$ is then a one-dimensional linear representation of G. Now we will try to classify these symmetric ground states using symmetric LU transformations and we find that: *For 1D spin systems with ONLY an on-site symmetry G which is realized linearly, all the gapped phases that do not break the symmetry are classified by $H^2(G, U(1))$, the second cohomology group of G, if $H^2(G, U(1))$ is finite and G has a finite number of 1D representations.* We will also discuss the case of $U(1)$ group which has an infinite number of 1D representations.

We will again assume that all gapped states can be represented as short range correlated matrix product states. We will use the renormalization flow used before[VCL+05] to simplify the matrix product states and use the fixed-point matrix product states to characterize different equivalent classes of LU transformations, as two symmetric states belong to the same class if and only if their corresponding fixed-point states can be mapped to each other with symmetric LU transformations.

In order to compare different equivalent classes under *symmetric* LU transformations, it is important to keep track of the symmetry while doing renormalization.

First, in the renormalization procedure we group n sites together into a new site. The on-site symmetry transformation becomes $\tilde{u}^{(0)}(g) = (\otimes u^{(0)}(g))^n$, which is again a linear representation of G. The next step in RG transformation applies a unitary transformation $w_1^{[k]}$ to the support space of new site k. This is actually itself composed of two steps. First we project onto the support space of the new site, which is the combination of n sites in the original chain. This is an allowed operation compatible with symmetry G as the reduced density matrix ρ_n is invariant under $\tilde{u}^{(0)}(g)$, so the support space form a linear representation for G. The projection of $\tilde{u}^{(0)}(g)$ onto the support space $P_n\tilde{u}^{(0)}(g)P_n$ hence remains a linear representation of G. In the next step, we do some unitary transformation $w_1^{[k]}$ within this support space which relabels different states in the space. The symmetry property of the state should not change under this relabeling. In order to keep track of the symmetry of the state, the symmetry operation needs to be redefined as $(u^{[k]})^{(1)}(g) = w_1^{[k]}P_n\tilde{u}^{(0)}(g)P_n(w_1^{[k]})^\dagger$. After this redefinition, the symmetry operations $(u^{[k]})^{(1)}(g)$ on each new site k form a new linear representation of G.

By redefining $(u^{[k]})^{(i)}(g)$ at each step of RG transformation, we keep track of the symmetry of the system. Finally at the fixed point (i.e. at a large RG step $i = R$), we obtain a state described by $(A^{[k]}_{i^l i^r})^{(R)}$ which is again given by the fixed point form Eq. (6.1). To describe a state that does not break the on-site symmetry, here $(A^{[k]}_{i^l i^r})^{(R)}$ is invariant (up to a phase) under $(u^{[k]})^{(R)}(g)$ on each site k. Therefore[PGWS+08],

$$\sum_{j^l j^r} u^{[k]}_{i^l i^r, j^l j^r}(g) A^{[k]}_{j^l j^r} = \alpha^{(R)}_{[k]}(g) N^{-1}_{[k]}(g) A^{[k]}_{i^l i^r} M_{[k]}(g)$$
$$N_{[k]}(g) = M_{[k-1]}(g) \tag{6.4}$$

must be satisfied with some invertible matrix $N_{[k]}(g)$ and $M_{[k]}(g)$. Here k labels the coarse grained sites and we have dropped the RG step label R (except in $\alpha^{(R)}_{[k]}(g)$). Each coarse grained site is a combination of n^R original lattice sites and $\alpha^{(R)}_{[k]}(g)$ form a 1D (linear) representation of G.

Solving this equation we find the following results (see section 6.5.2):
(a) $N_{[k]}(g)$ and $M_{[k]}(g)$ are projective representations of G (see Eq. (6.24)). Projective representations of G belong to different classes which form the second cohomology group $H^2(G, U(1))$ of G. (For a brief introduction on projective representation, see section 6.5.1). $M_{[k]}(g)$ and $N_{[k]}(g)$ corresponds to the same element ω in $H^2(G, U(1))$.
(b) The linear symmetry operation $u^{[k]}(g)$ must be of the form $\alpha^{(R)}_{[k]}(g) u^{[k],l}(g) \otimes u^{[k],r}(g)$ where $u^{[k],l}$ and $u^{[k],r}$ are projective representations of G and correspond to inverse elements ω and $-\omega$ in $H^2(G, U(1))$ respectively. $\alpha^{(R)}_{[k]}(g)$ is a 1D (linear) representation of G. $u^{[k],l}$ and $u^{[k],r}$ act on the two virtual spins separately (see Eq. (6.30)).

Therefore, the fixed point state is formed by entangled pairs $|EP_{k,k+1}\rangle$ of virtual spins which are invariant, up to a phase (due to the non-trivial $\alpha^{(R)}_{[k]}(g)$), under linear transformation $u^{[k],r}(g) \otimes u^{[k+1],l}(g)$.

Now we use the uniformness of the state and simplify our discussions. Specifically, we assume that $\alpha^{(R)}_{[k]}(g)$ does not depend on the site index k. Certainly, $\alpha^{(R)}_{[k]}(g)$ does not depend on k if the state has the translation symmetry. If the 1D representations of G are discrete, then for weak randomness that slightly break the translation symmetry, $\alpha^{(R)}_{[k]}(g)$ still does not depend on k. So we can drop the k index and consider $\alpha^{(R)}(g)$.

Does different $\alpha^{(R)}(g)$ label different symmetric phases? First, the answer is no if the number of 1D representations of G is finite (as is the case for Z_n, $SO(3)$, etc). Because for two different 1D representations $\alpha^{(R)}(g)$ and $\tilde{\alpha}^{(R)}(g)$, we can always choose the same blocking scheme (for example of size n) such that $(\alpha^{(R)}(g))^n = 1$ and $(\tilde{\alpha}^{(R)}(g))^n = 1$. The difference between symmetric states due to $\alpha^{(R)}(g)$ hence disappears. In the case of $U(1)$ group, there are infinitely many different 1D representations $e^{im\theta}$, labeled by integer m. There is not a consistent blocking scheme to make two 1D representations equivalent. Therefore, different 1D representations label different phases, even in the absence of translation symmetry. After these considerations, we will ignore the 1D representations $\alpha^{(R)}(g)$ in the following discussion.

We find that the entangled pairs $|EP_{k,k+1}\rangle$ of virtual spins in the fixed point state are exactly invariant under linear transformation $u^{[k],r}(g) \otimes u^{[k+1],l}(g)$. The left virtual spin of each site forms a projective representation of G corresponding to element ω in $H^2(G, U(1))$, while the right virtual spin corresponds to element $-\omega$ as shown in Fig. 6-2. In section

6.5.3, we will show that fixed point states with the same ω can be related by a symmetric LU transformation, while those with different ω cannot. Therefore, the phases of SRC MPS that are invariant under linear on-site symmetry of group G are classified by the second cohomology group $H^2(G, U(1))$. (When $G = U(1)$, further division of classes due to different 1D representations of G exist. The equivalence classes are labeled by $m \in \mathbb{Z}$ and $\omega \in H^2(U(1), U(1))$.)

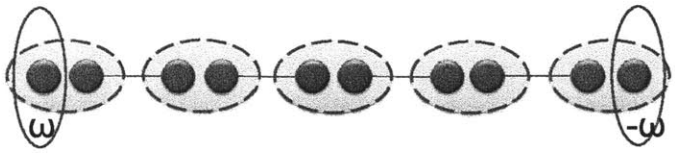

Figure 6-2: 1D gapped ground state at fixed point. If the system has a linear on-site symmetry of group G, then the left edge degree of freedom forms a projective representation ω of group G while the right edge forms $-\omega$.

On-site Projective Unitary Symmetry

Due to the basic assumption of quantum mechanics that the global phase of a quantum state will not have any effect on the physical properties of the system, it is necessary to consider not only the linear representation of symmetry operations on the system, but also the projective representations. For example, on a half-integer spin, rotation by 2π is represented as $-I$, minus the identity operator instead of I. Hence, the rotation symmetry $SO(3)$ is represented projectively on half integer spins. In order to cover situations like this, we discuss in this section systems with on-site projective symmetry of group G.

Again, we consider the case when the ground state does not break the symmetry, i.e. $u^{(0)}(g) \otimes ... \otimes u^{(0)}(g)|\phi_L\rangle = \alpha_L(g)|\phi_L\rangle$, where $u^{(0)}(g)$ form a projective representation of group G corresponding to class ω. Assuming uniformness of the state, we require that ω does not vary from site to site.

But this can be reduced to the previous linear case. As long as $H^2(G, U(1))$ is finite and ω has a finite order n, we can take block size n so that after blocking, the symmetry operation on the renormalized site $\tilde{u}^{(0)}(g) = (\otimes u^{(0)}(g))^n$ corresponds to $n\omega = \omega_0$ in $H^2(G, U(1))$. Therefore, the state after one blocking step is symmetric under an on-site linear representation of group G and all the reasoning in the previous section applies. We find that the classification with projective on-site symmetry is the same as linear on-site symmetry. That is: *Consider 1D spin systems with ONLY an on-site symmetry G which is realized projectively, all the gapped phases that do not break the symmetry are classified by $H^2(G, U(1))$, the second cohomology group of G, if $H^2(G, U(1))$ is finite and G has a finite number of 1D representations.* The $U(1)$ group does not have a non-trivial projective representation and will not introduce any complication here.

Examples

Since $G = \mathbb{Z}_n$ has no non-trivial projective representations, we find that: *All 1D gapped systems with only on-site $\mathbb{Z}_n$ symmetry belong to the same phase.*

For spin systems with only spin rotation symmetry, $G = SO(3)$. $SO(3)$ has two types of projective representations described by $H^2(SO(3), U(1)) = \{0, 1\}$, corresponding to integer

and half-integer spin representations. We find that: *For integer-spin systems, all 1D gapped systems with only on-site $SO(3)$ spin rotation symmetry have two different phases.* Such a result has some relation to a well known result[HY97] for NTI spin-1 Heisenberg chain

$$H = \sum_i J_i \boldsymbol{S}_i \cdot \boldsymbol{S}_{i+1}. \tag{6.5}$$

The model undergoes an impurity driven second order phase transition from the Haldane phase[Hal83a] to the random singlet phase[MDH79, Fis94] as the randomness in J_i increases.

For half-integer-spin systems, $SO(3)$ is represented projectively on each site, yet the classification is the same as the integer case. we find that: *For half-integer-spin systems, all 1D gapped states with only on-site $SO(3)$ spin rotation symmetry have two different phases.* Representative states of the two phases are nearest-neighbor dimer states, but with dimer between sites $2i$ and $2i+1$ in the first phase and between sites $2i-1$ and $2i$ in the second phase.

The projective representation of $SO(3)$ on half-integer-spins form a linear representation of $SU(2)$. If we think of the linear representation of $SO(3)$ on integer-spins as a (unfaithful) linear representation of $SU(2)$ and allow the mixture of integer and half-integer spins on one site, then the two phases of $SO(3)$ merge into one[AR07]. Therefore, systems with only on-site $SU(2)$ symmetry (which implies the mixture of integer and half-integer spins on each site) belong to one phase as we can map integer-spin singlets into half-integer-spin singlets without breaking the $SU(2)$ symmetry (see section 6.5.3). Such a procedure breaks down if $SO(3)$ symmetry is required for each site as the direct sum of a linear representation (on integer-spin) and a projective representation (on half-integer-spin) is no longer a projective representation for $SO(3)$.

In this way, we have obtained a full classification of the phases of gapped NTI 1D spin systems with various on-site unitary symmetries.

Time Reversal Symmetry

Time reversal, unlike other symmetries, is represented by anti-unitary operator T, which is equivalent to the complex conjugate operator K followed by a unitary operator U. T has two projective representations: one on integer spins with $T^2 = I$ and the other on half-integer spins with $T^2 = -I$. The classification of gapped 1D time reversal invariant phases follows closely the cases discusses before. In this section, we will highlight the differences and give our conclusion.

First, a state $|\phi\rangle$ is called time reversal invariant if $T \otimes T ... \otimes T |\phi\rangle = \beta |\phi\rangle$, where $|\beta| = 1$. But for anti-unitary T, the global phase β is arbitrary and in particular we can redefine $|\phi'\rangle = \sqrt{\beta}|\phi\rangle$, such that $T \otimes T ... \otimes T |\phi'\rangle = |\phi'\rangle$. Therefore, in the following discussion, we will assume WLOG that $\beta = 1$.

Now let us consider system without translational invariance. $T^2 = I$ or $-I$ does not make a difference here as we can take block size 2 so that on the renormalized site, T^2 is always equal to I. Using argument similar to the case of on-site unitary symmetry, we can keep track and redefine symmetry operations as we do renormalization. Finally, at the fixed point we have a state described by matrices $(A^{[k]}_{i l_i r})^{(\infty)}$ which is invariant under time

reversal operation $(T^{[k]})^{(\infty)} = (u^{[k]})^{(\infty)}K$, that is,

$$\sum_{j^l j^r} u^{[k]}_{i^l i^r, j^l j^r} (A^{[k]}_{j^l j^r})^* = N^{-1}_{[k]} A^{[k]}_{i^l i^r} M_{[k]}$$
$$N_{[k]} = M_{[k-1]} \tag{6.6}$$

where the fixed-point label ∞ has been omitted. Solving this equation we find,
(a)$M_{[k]} M^*_{[k]} = e^{i\theta} I$. As $M_{[k]}$ is invertible, $e^{i\theta} = \pm 1$.
(b)$u^{[k]} = u^{[k],l} \otimes u^{[k],r}$. where $u^{[k],l}(u^{[k],l})^* = \pm I$ and $u^{[k],r}(u^{[k],r})^* = \pm I$. Therefore, each entangled pair is time reversal invariant

$$(u^{[k],r} \otimes u^{[k+1],l}) K |EP_{k,k+1}\rangle = |EP_{k,k+1}\rangle \tag{6.7}$$

Similar to previous sections, we can show that $uu^* = I$ and $uu^* = -I$ correspond to two equivalence classes and two time reversal invariant fixed point states can be mapped into each other if and only if they belong to the same class. Therefore, our classification result for time reversal symmetry is: *For 1D gapped spin systems with ONLY time reversal symmetry, there are two phases that do not break the symmetry.*

6.2.2 Translation invariance and parity

In this section, we would like to discuss translational invariant systems whose ground states are gapped and also translational invariant. The renormalization procedure breaks translation symmetry and hence can not be used to study topological phases with translation symmetry. In this section, we will use the time evolution formulation of LU transformation Eq. (5.1) and find a smooth path of gapped TI Hamiltonian whose adiabatic evolution connects two states within the same TI phase.

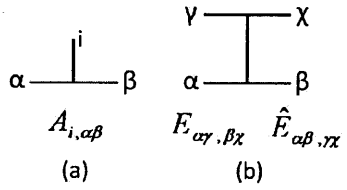

Figure 6-3: Graphical representation of (a) matrices labeled by physical index i (b) double tensor denoted by $\mathbb{E}$ or $\hat{\mathbb{E}}$. $\mathbb{E}$ is a matrix with $\alpha\gamma$ as row index and $\beta\chi$ as column index. $\hat{\mathbb{E}}$ is a matrix with $\alpha\beta$ as row index and $\gamma\chi$ as column index.

Translation invariance only

First, as an example, we consider the case of TI only and show that there is only one gapped TI phase. Each translational invariant MPS is described(up to local change of basis) by a double tensor $\mathbb{E}$(see Fig.6-3)

$$\mathbb{E}_{\alpha\gamma,\beta\chi} = \sum_i A_{i,\alpha\beta} \otimes A^*_{i,\gamma\chi} \tag{6.8}$$

The MPS is short-range correlated if $\mathbb{E}$ has a non-degenerate largest eigenvalue 1. $\mathbb{E}$ can be written as

$$\mathbb{E}_{\alpha\gamma,\beta\chi} = \mathbb{E}^0_{\alpha\gamma,\beta\chi} + \mathbb{E}'_{\alpha\gamma,\beta\chi} = \Lambda_{\alpha\gamma}\Lambda_{\beta\chi} + \mathbb{E}'_{\alpha\gamma,\beta\chi} \tag{6.9}$$

where Λ is the eigenvector of eigenvalue 1 and $\mathbb{E}'$ is of eigenvalue less than 1. In the 'canonical form'[PGVWC07], $\Lambda_{\alpha\gamma} = \lambda_\alpha \delta_{\alpha\gamma}$, $\lambda_\alpha > 0$. Obviously, $\mathbb{E}^0$ is a valid double tensor and represents a state in fixed point form. We can smoothly change $\mathbb{E}$ to $\mathbb{E}^0$ by turning down the $\mathbb{E}'$ term to 0 from $t = 0$ to $t = T$ as

$$\mathbb{E}(t) = \mathbb{E}^0 + (1 - \frac{t}{T})\mathbb{E}' \tag{6.10}$$

Every $\mathbb{E}(t)$ represents a TI SRC MPS state. To see this, note that if we recombine the indices $\alpha\beta$ as row index and $\gamma\chi$ as column index and denote the new matrix as $\hat{\mathbb{E}}$(see Fig.6-3), then both $\hat{\mathbb{E}}$ and $\hat{\mathbb{E}}^0$ are positive semidefinite matrices. But then every $\hat{\mathbb{E}}(t)$ is also positive semidefinite, as for any vector $|v\rangle$

$$\begin{aligned} \langle v|\hat{\mathbb{E}}(t)|v\rangle &= \langle v|\hat{\mathbb{E}}^0|v\rangle + (1 - \tfrac{t}{T})\langle v|\hat{\mathbb{E}}'|v\rangle \\ &= (1 - \tfrac{t}{T})\langle v|\hat{\mathbb{E}}|v\rangle + \tfrac{t}{T}\langle v|\hat{\mathbb{E}}^0|v\rangle > 0 \end{aligned}$$

$\mathbb{E}(t)$ is hence a valid double tensor and the state represented can be determined by decomposing $\mathbb{E}(t)$ back into matrices $A_i(t)$. Such a decomposition is not unique. $A_i(t)$ at different time is determined only up to a local unitary on the physical index i. But WLOG, we can choose the local unitary to be continuous in time, so that $A_i(t)$ vary continuously with time and reach the fixed point form at $t = T$(up to local change of basis). The state represented $|\phi(t)\rangle$ hence also changes smoothly with t and is a pure state with a finite correlation length as all eigenvalues of $\mathbb{E}(t)$ expect for 1 are diminishing with t[FNW92b, FNW92a]. Therefore, $\mathbb{E}(t)$ represents a smooth path in TI SRC MPS that connects any state to a fixed point state(up to local change of basis).

How do we know that no phase transition happens along the path? This is because for every state $|\phi(t)\rangle$, we can find a parent Hamiltonian which changes smoothly with t and has the state as a unique gapped ground state.[SPGC11] Following the construction in [FNW92b, PGVWC07], we choose a sufficiently large but finite l and set the parent Hamiltonian to be $H(t) = -\sum_k h(t)_{k,k+l}$, where $h(t)_{k,k+l}$ is the projection onto the support space of the reduced density matrix on site k to $k + l$ at time t. Note that this Hamiltonian is translation invariant. For large enough l, $h(t)_{k,k+l}$ will always be $D \times D$ dimensional. As the state changes continuously, its reduced density matrices of site k to $k + l$ changes smoothly. Because the dimension of the space does not change, $h(t)_{k,k+l}$ also changes smoothly with time. Moreover, it can be shown that $H(t)$ is always gapped as the second largest eigenvalue of $\mathbb{E}(t)$ never approaches 1 [FNW92b, PGVWC07]. Therefore, by evolving the Hamiltonian adiabatically from $t = 0$ to $t = T$, we obtain a local unitary transformation[HW05] connecting any state to the fixed point form, and in particular without breaking the translation symmetry.

Because any TI fixed point state can be disentangled into product state in a TI way, we find that *all TI 1D gapped ground states are in the same phase, if no other symmetries are required.*

Translation invariance and on-site symmetry

If the system is TI and has on-site symmetry, we need to maintain the on-site symmetry while doing the smooth deformation. Details of the procedure is presented in section 6.5.4. Here we summarize what we have learned.

First we can show that: *For a 1D spin system with translation and an on-site projective symmetry $u(g)$, the symmetric ground state cannot be short-range correlated, if the projective symmetry $u(g)$ corresponds to a non-trivial element in $H^2(G, U(1))$.*

The reason is as follows. If a 1D state with translation symmetry is short-range correlated, it can be represented by a TI MPS. Its fixed-point MPS also has an on-site projective unitary symmetry $\tilde{u}(g)$. For a proper choice of block size n, we can make $u(g)$ and $\tilde{u}(g)$ to be the same type of projective representation described by $\omega_{sym} \in H^2(G, U(1))$. For TI fixed-point MPS, we have $\omega_{[k]} = \omega_{[k-1]}$ since $M_{[k]}(g) = M_{[k-1]}(g)$(cf. section 6.5.2). Thus $\omega_{sym} = 0$, that is, the trivial element in $H^2(G, U(1))$. So, if $\omega_{sym} \neq 0$, the 1D TI state cannot be short-range correlated. In other words: *1D spin systems with translation and an on-site projective symmetry are always gapless or have degenerate ground states that break the symmetries.*

If the ground state of the 1D spin system does not break the on-site symmetry and the translation symmetry, then ground state is not short-range correlated and is gapless. If the ground state of the 1D spin system breaks the on-site symmetry or the translation symmetry, then the ground state is degenerate.

As an application of the above result, we find that: *1D half-integer-spin systems with translation and the $SO(3)$ spin rotation symmetry are always gapless or have degenerate ground states.* which agrees with the well known result of [LSM61] and its generalizations [Mat01].

To have a gapped TI 1D state with an on-site symmetry, the symmetry must act linearly (i.e. not projectively). In this case, we can show that the total phase factor of the state $\alpha_L(g)$ breaks up into L 1D representations $\alpha(g)$: (see section 6.5.5) *For 1D spin systems of L sites with translation and an on-site symmetry G, a gapped state that does not break the two symmetries must transform as*

$$u^{(0)}(g) \otimes ... \otimes u^{(0)}(g)|\phi_L\rangle = [\alpha(g)]^L|\phi_L\rangle \tag{6.11}$$

for all values of L that is large enough. Here $u^{(0)}(g)$ is the linear representation of G acting on the physical states in each site and $\alpha(g)$ is a one-dimensional linear representation of G.

Let us apply the above result to a boson system with p/q bosons per site. Here the bosons number is conserved and there is an $U(1)$ symmetry. Certainly, the system is well defined only when the number of sites L has a form $L = Jq$ (assuming p and q have no common factors). For such an L, we find that $\alpha_L(g) = \alpha_0(g)^J = \alpha_0(g)^{L/q}$, where $\alpha_0(g)$ is the generating 1D representation of the $U(1)$ symmetry group. So Eq. (6.11) is *not* satisfied for some large L. Therefore *a 1D state of conserved bosons with fractional bosons per site must be gapless, if the state does not break the $U(1)$ and the translation symmetry.*

In higher dimensions, the situation is very different. A 2D state of conserved bosons with fractional bosons per site can be gapped, and, at same time, does not break the $U(1)$ and the translation symmetry. 2D fractional quantum Hall states of bosons on lattice provide examples for such kind of states.

Also, we can show that: *For 1D spin systems with only translation and an on-site linear symmetry G, all the phases of gapped states that do not break the two symmetries*

are classified by a pair (ω, α) *where* $\omega \in H^2(G, U(1))$ *label different types of projective representations of* G *and* α *label different 1D representations of* G. Here $\alpha(g)$ is an 1D representation of G that appear in Eq. (6.11). The symmetric LU transformations cannot change 1D representation $\alpha(g)$. So the different phases are also distinguished by the 1D representations α of G.

Here are a few concrete examples: If we choose the symmetry group to be $G = \mathbb{Z}_n$, we find: *For 1D spin systems with only translation and on-site* $\mathbb{Z}_n$ *symmetry, there are* n *phases for gapped states that do not break the two symmetries.*

This is because $\mathbb{Z}_n$ has no projective representations and has n different 1D representations. As an example, consider the following model

$$H = \sum_i [-h\sigma_i^z - \sigma_{i-1}^x \sigma_i^y \sigma_{i+1}^z], \tag{6.12}$$

where $\sigma^{x,y,z}$ are the Pauli matrices. The model has a Z_2 symmetry generated by σ^z. The two different Z_2 symmetric phases correspond the $h \to \infty$ phase and the $h \to -\infty$ phase of the model.

If we choose the symmetry group to be $G = SO(3)$, we find: *For 1D integer-spin systems with only translation and* $SO(3)$ *spin rotation symmetry, there are two phases for gapped states that do not break the two symmetries.*

This is because $SO(3)$ has only one 1D representation and $H^2(SO(3), U(1)) = \mathbb{Z}_2$. Such a result agrees with the well known result that the AKLT state[AKLT87] of spin-1 chain and the direct product state with spin-0 on each site represent two different $SO(3)$ symmetric TI phases. The AKLT state (and the related Haldane phase[Hal83a]) has gapless boundary spin-1/2 states[HKA+90, GGL+91, Ng94] and non-trivial string orders,[dNR89, KT92] which indicate that the AKLT state is really different from the spin-0 product state. Actually, the full symmetry of $SO(3)$ can be relaxed to only the dihedral group $D_2(\mathbb{Z}_2 \times \mathbb{Z}_2)$ of rotation by π around x, y and z axis. As explained in section 6.5.1, D_2 has one non-trivial projective representation, to which the AKLT state corresponds. AKLT is different from the spin-0 product state as long as on-site D_2 symmetry is preserved. This is consistent with the result in [KT92, PBTO12].

Translation invariance and parity

1D systems with translation and parity symmetries

In this section, we will consider the case of parity symmetry for translational invariant system. We define the parity operation P for a spin chain to be in general composed of two parts: P_1, exchange of sites n and $-n$; P_2, on-site unitary operation $u^{(0)}$ where $(u^{(0)})^2 = I$. [4] From section 6.5.4 we know that the matrices describing the state can be deformed to a fixed point form, which satisfies:

$$\sum_{j^l j^r} u_{i^l i^r, j^l j^r} A^T_{j^l j^r} = \pm M^{-1} A_{i^l i^r} M \tag{6.13}$$

[4] The Z_2 operation $u^{(0)}$ is necessary in the definition of parity if we want to consider for example, fixed point state with $|EP\rangle = |00\rangle + |11\rangle$ be to parity symmetric. The state is not invariant after exchange of sites, and only maps back to itself if in addition the two virtual spins on each site are also exchanged.

for some invertible matrix M and $u^2 = I$, where we have used that the 1D representation of parity is either $(1,1)$ or $(1,-1)$. We label the two 1D representations with $\alpha(P) = \pm 1$. Here M satisfies $M^{-1}M^T = e^{i\theta}$. But $M = (M^T)^T = e^{2i\theta}M$, therefore, $e^{i\theta} = \pm 1$ and correspondingly M is either symmetric $M = M^T$ or antisymmetric $M = -M^T$. We will label this sign factor as $\beta(P) = \pm 1$.

Solving this equation gives that $u = \alpha(P)v(u^l \otimes u^r)$, where v is the exchange operation of two virtual spins i^l and i^r and u^l,u^r act on i^l,i^r respectively. $(u^l)^T = \beta(P)u^l$ and $(u^r)^T = \beta(P)u^r$. It can then be shown that each entangled pair $|EP_{k,k+1}\rangle$ must be symmetric under parity operations and satisfies $u_k^r \otimes u_{k+1}^l |EP_{k+1,k}\rangle = \alpha(P)|EP_{k,k+1}\rangle$. There are hence four different symmetric phases corresponding to $\alpha(P) = \pm 1$ and $\beta(P) = \pm 1$. We can show similarly as before that fixed points within each class can be mapped from one to the other with TI LU transformation preserving the parity symmetry. On the other hand, fixed points in different classes can not be connected without breaking the symmetries. Therefore, there are four parity symmetric TI phases: *For 1D spin systems with only translation and parity symmetry, there are four phases for gapped states that do not break the two symmetries.*

As an example, consider the following model

$$H = \sum_i [-BS_i^z + \boldsymbol{S}_i \cdot \boldsymbol{S}_{i+1}], \tag{6.14}$$

where $\boldsymbol{S}_i$ are the spin-1 operators. The model has a parity symmetry. The $B = 0$ phase and the $B \to +\infty$ phase of the model correspond to two of the four phases discussed above. The $B = 0$ state[Hal83a] is in the same phase as the AKLT state. In the fixed-point state for such a phase, $|EP_{k,k+1}\rangle = |\uparrow\downarrow\rangle - |\downarrow\uparrow\rangle$. The parity transformation exchange the first and the second spin, and induces a minus sign: $P : |EP_{k,k+1}\rangle \to -|EP_{k,k+1}\rangle$. The $B \to +\infty$ state is the $S^z = 1$ state. Its entangled pairs are $|EP_{k,k+1}\rangle = |\uparrow\uparrow\rangle$ which do not change sign under the parity transformation. Thus the stability of the Haldane/AKLT state is also protected by the parity symmetry.[BDTGA08, GW09, PBTO12]

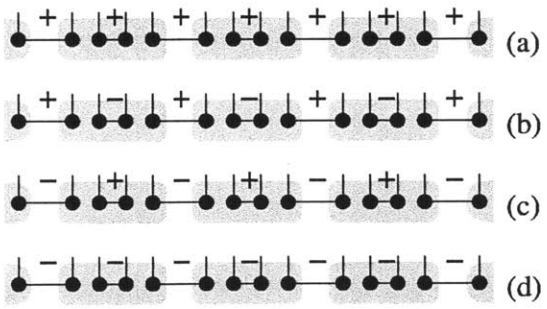

Figure 6-4: Representative states of the four parity symmetric phases, each corresponding to (a) $\alpha(P) = 1$, $\beta(P) = 1$ (b) $\alpha(P) = -1$, $\beta(P) = 1$ (c) $\alpha(P) = -1$, $\beta(P) = -1$ (d) $\alpha(P) = 1$, $\beta(P) = -1$. $+$ stands for a parity even entangled pair (e.g. $|00\rangle + |11\rangle$), $-$ stands for a parity odd entangled pair (e.g. $|01\rangle - |10\rangle$). Each site contains four virtual spins.

To understand why there are four parity symmetric phases instead of two (parity even/parity odd), we give four representative states in Fig. 6-4, one for each phase. Connected pair of black dots denotes an entangled pair. $+$ stands for a parity even pair, for example $|00\rangle + |11\rangle$, and $-$ stands for a parity odd pair, for example $|01\rangle - |10\rangle$. Each

Symmetry	No. or Label of Different Phases	Example System
None	1	
On-site Linear Symmetry of Group G	$\omega \in H^2(G, U(1))$ (*)	On-site Z_n or $SU(2)$: 1 phase On-site $SO(3)/D_2$ on integer spin: 2 phases
On-site Projective Symmetry of Group G	$\omega \in H^2(G, U(1))$	On-site $SO(3)$ or D_2 on half-integer spin: 2 phases
Time Reversal(TR)	2	
Translational Invariance(TI)	1	
TI+On-site Linear Symmetry of Group G	$\omega \in H^2(G, U(1))$ and $\alpha(G)$	TI+On-site Z_n: n phases TI+On-site $SO(3)$ on integer spin: 2 phases
TI+ On-site Projective Symmetry of Group G	0	TI+On-site $SO(3)$ or D_2 on half-integer spin: no gapped phase
TI+Parity	4	
TI+TR	2 if $T^2 = I$ 0 if $T^2 = -I$	TI+TR on integer spin: 2 phases on half-integer spin: no gapped phase

Table 6.1: Summary of classification result for 1D gapped spin system with symmetric ground states. TI stands for translational invariance. TR stands for time reversal symmetry. $H^2(G, U(1))$ is the second cohomology group of group G over complex number $U(1)$. $\alpha(G)$ is a 1D representation of G. (*): this result applies when $\alpha(G)$ form a finite group, when $G = U(1)$, further classification according to different $\alpha(U(1))$ exist.

rectangle corresponds to one site, with four virtual spins on each site. The four states are all translational invariant. If the parity operation is defined to be exchange of sites together with exchange of virtual spins 1 and 4, 2 and 3 on each site, then states (a) and (d) are parity even while (b) and (c) are parity odd. But (a) and (d) (or (b) and (c)) are different parity even (odd) states and cannot be mapped to each other through local unitary transformations without breaking parity symmetry. Written in the matrix product representation, the matrices of the four states will transform with $\alpha(P) = \pm 1$ and $\beta(P) = \pm 1$ respectively. Therefore, the parity even/odd phase breaks into two smaller phases and there are in all four phases for parity symmetric systems.

6.3 Summary of results for spin systems

Here we summarize our classification of topological phases in 1D spin systems with different symmetries in Table 6.1.

Moreover, we want to mention that the possibility of symmetry breaking can be easily incorporated into this classification. We find that 1D gapped spin phases with on-site symmetry of group G are basically labeled by (1) the unbroken symmetry subgroup G', (2) projective representations of G'. This result was derived in [CGW11b, SPGC11]. We will not repeat the details here. While this result is straightforward for spin systems, it can be applied to classify topological phases in 1D fermions systems, as we will show in the next section.

6.4 1D symmetry protected topological phases in fermion systems

Although our previous discussions have been focused on spin systems, it actually also applies to fermion systems. Because in 1D, fermion systems and spin systems can be mapped to each other through Jordan Wigner transformation, we can classify fermionic phases by classifying corresponding spin phases. Specifically, for a class of fermion systems with certain symmetry we are going to 1. identify the corresponding class of spin systems by mapping the symmetry to spin 2. classify possible spin phases with this symmetry, including symmetry breaking and symmetry protected topological order 3. map the spin phases back to fermions and identify the fermionic order. In the following we are going to apply this strategy to 1D fermion systems in the following four cases respectively: no symmetry(other than fermion parity), time reversal symmetry for spinless fermions, time reversal symmetry for spin half integer fermions, and $U(1)$ symmetry for fermion number conservation. Our classification result is consistent with previous studies in [FK11, TPB11]. One special property of fermionic system is that it always has a fermionic parity symmetry. That is, the Hamiltonian is a sum of terms composed of even number of creation and annihilation operators. Therefore, the corresponding spin systems we classify always have an on-site Z_2 symmetry. Note that this approach can only be applied to systems defined on an open chain. For system with translation symmetry and periodic boundary condition, Jordan Wigner transformation could lead to non-local interactions in the spin system.

6.4.1 Fermion Parity Symmetry Only

For a 1D fermion system with only fermion parity symmetry, how many gapped phases exist?

To answer this question, first we do a Jordan-Wigner transformation and map the fermion system to a spin chain. The fermion parity operator $P_f = \prod(1 - 2a_i^\dagger a_i)$ is mapped to an on-site Z_2 operation. On the other hand, any 1D spin system with an on-site Z_2 symmetry can always be mapped back to a fermion system with fermion parity symmetry(expansion of local Hilbert space maybe necessary). As the spin Hamiltonian commute with the Z_2 symmetry, it can be mapped back to a proper physical fermion Hamiltonian. Therefore, the problem of classifying fermion chains with fermion parity is equivalent to the problem of classifying spin chains with Z_2 symmetry.

There are two possibilities in spin chains with Z_2 symmetry: (1) the ground state is symmetric under Z_2. As Z_2 does not have non-trivial projective representation, there is one symmetric phase. (If translational symmetry is required, systems with even number of fermions per site are in a different phase from those with odd number of fermions per site. This difference is somewhat trivial and we will ignore it.) (2) the ground state breaks the Z_2 symmetry. The ground state will be two-fold degenerate. Each short-range correlated ground state has no particular symmetry($G' = I$) and they are mapped to each other by the Z_2 operation. There is one such symmetry breaking phases. These are the two different phases in spin chains with Z_2 symmetry.

This tells us that there are two different phases in fermion chains with only fermion parity symmetry. But what are they? First of all, fermion states cannot break the fermion parity symmetry. All fermion states must have a well-defined parity. Does the spin symmetry breaking phase correspond to a real fermion phase?

The answer is yes and actually the spin symmetry breaking phase corresponds to a Z_2

symmetric fermion phase. Suppose that the spin system has two short-range correlated ground states $|\psi_0\rangle$ and $|\psi_1\rangle$. All connected correlations between spin operators decay exponentially on these two states. Mapped to fermion systems, $|\psi_0^f\rangle$ and $|\psi_1^f\rangle$ are not legitimate states but $|\tilde{\psi}_0^f\rangle = |\psi_0^f\rangle + |\psi_1^f\rangle$ and $|\tilde{\psi}_1^f\rangle = |\psi_0^f\rangle - |\psi_1^f\rangle$ are. They have even/odd parity respectively. In spin system, $|\psi_0\rangle$ and $|\psi_1\rangle$ are not short range correlated states but mapped to fermion system they are. To see this, note that any correlator between bosonic operators on the $|\tilde{\psi}_0^f\rangle$ and $|\tilde{\psi}_1^f\rangle$are the same as that on $|\psi_0\rangle$ and $|\psi_1\rangle$ and hence decay exponentially. Any correlator between fermionic operators on the $|\tilde{\psi}_0^f\rangle$ and $|\tilde{\psi}_1^f\rangle$ gets mapped to a string operator on the spin state, for example $a_i^\dagger a_j$ is mapped to $(X-iY))_i Z_{i+1}...Z_{j-1}(X-iY)_j$, which also decays with separation between i and j. Therefore, the symmetry breaking phase in spin chain corresponds to a fermionic phase with symmetric short range correlated ground states. The degeneracy can be understood as isolated Majorana modes at the two ends of the chain[Kit01, Kit09].

On the other hand, the short-range correlated ground state in spin symmetric phase still correspond to short-range correlated fermion state after JW transformation. Therefore, the symmetric and symmetry breaking phases in spin system both correspond to symmetric phases in fermion system. The two fermion phases cannot be connected under any physical fermion perturbation.

6.4.2 Fermion Parity and $T^2 = 1$ Time Reversal

Now consider the more complicated situation where aside from fermion parity, there is also a time reversal symmetry $\mathcal{T}$. $\mathcal{T}$ acts as an anti-unitary $T = UK$ on each site. In this section we consider the case where $T^2 = 1$(spinless fermion).

So now the total symmetry for the fermion system is the Z_2 fermion parity symmetry P_f and $T^2 = 1$ time reversal symmetry. T commutes with P_f. The on-site symmetry group is a $Z_2 \times Z_2$ group and has four elements $G = \{I, T, P_f, TP_f\}$. Mapped to spin system, the symmetry group structure is kept.

The possible gapped phases for a spin system with on-site symmetry $G = \{I, T, P_f, TP_f\}$ include: (1) $G' = G$. Following discussion in previous sections we find that it has four different projective representations. Examples of the four representations are a.$\{I, K, Z, KZ\}$, b. $\{I, iYK, Z, iYKZ\}$, c. $\{I, iYKZ \otimes I, I \otimes Z, iYKZ \otimes Z\}$ d. $\{I, K, Y, KY\}$. There are hence four different symmetric phases. (If translational symmetry is required, the number is multiplied by 2 due to $\alpha(Z_2)$) (2) $G' = \{I, P_f\}$ with no non-trivial projective representation, the time reversal symmetry is broken. There is one such phase. (If translational symmetry is required, there are two phases) (3) $G' = \{I, T\}$, with two different projective representations(time reversal squares to $\pm I$ on boundary spin). The Z_2 fermion parity is broken. There are two phases in this case. (4) $G' = \{I, TP_f\}$, with two different projective representations. The fermion parity symmetry is again broken. Two different phases. (5) $G' = I$, no projective representation, all symmetries are broken.

Mapped back to fermion systems, fermion parity symmetry is never broken. Instead, the P_f symmetry breaking spin phases are mapped to fermion phases with Majorana boundary mode on the edge as discussed in the previous section. Therefore the above spin phases correspond in the fermion system to: (1) Four different symmetric phases (2) One time reversal symmetry breaking phase. (3) Two symmetric phases with Majorana boundary mode (4) Another two symmetric phases with Majorana boundary mode. (5) One time reversal symmetry breaking phase. (1)(3)(4) contains the eight symmetric phases for time

reversal invariant fermion chain with $T^2 = 1$. This is consistent with previous studies in [FK10, TPB11].

6.4.3 Fermion Parity and $T^2 \neq I$ Time Reversal

When $T^2 \neq I$, the situation is different. This happens when we take the fermion spin into consideration and for a single particle, time reversal is defined as $e^{i\pi\sigma_y}K$. With half integer spin, $\left(e^{i\pi\sigma_y}K\right)^2 = -I$. Note that for every particle the square of time reversal is $-I$, however when we write the system in second quantization as creation and annihilation operator on each site, the time reversal operation defined on each site satisfies $T^2 = P_f$. Therefore, the symmetry group on each site is a Z_4 group $G = \{I, T, P_f, TP_f\}$. To classify possible phases, we first map everything to spin.

The corresponding spin system has on-site symmetry $G = \{I, T, P_f, TP_f\}$. $T^2 = P_f$, $P_f^2 = I$. The possible phases are: (1) $G' = G$, with two possible projective representations, one with $T^4 = I$, the other with $T^4 = -I$. Example for the latter includes $T = (1/\sqrt{2})(X + Y)K$. Therefore, there are two possible symmetric phases. (If translational symmetry is required, there are four phases.) (2) $G' = \{I, P_f\}$, the time reversal symmetry is broken. One phase. (If translational symmetry is required, there are two phases.) (3) $G' = I$, all symmetries are broken. One phase.

Therefore, the fermion system has the following phases: (1) Two symmetric phases (2) One time reversal symmetry breaking phase. (3) One time reversal symmetry breaking phase with Majorana boundary mode. (1) contains the time reversal symmetry protected topological phase. Models in this phase can be constructed by first writing out the spin model in the corresponding spin phase and then mapping it to fermion system with Jordan-Wigner transformation.

6.4.4 Fermion Number Conservation

Consider the case of a gapped fermion system with fixed fermion number. This corresponds to an on-site $U(1)$ symmetry, $e^{i\theta N}$. Mapped to spins, the spin chain will have an on-site $U(1)$ symmetry. This symmetry cannot be broken and $U(1)$ does not have a non-trivial projective representation. One thing special about $U(1)$ symmetry though, is that it has an infinite family of 1D representations. If translational symmetry is required, fermion number per site is a good quantum number and labels different phases. Therefore, mapped back to fermions, there is an infinite number of phases with different average number of fermions per site.

6.5 Details of 1D classification

6.5.1 Projective Representation

Operators $u(g)$ form a projective representation of symmetry group G if

$$u(g_1)u(g_2) = \omega(g_1, g_2)u(g_1g_2), \qquad g_1, g_2 \in G. \tag{6.15}$$

Here $\omega(g_1, g_2) \in U(1)$, the factor system of the projective representation, satisfies

$$\omega(g_2, g_3)\omega(g_1, g_2g_3) = \omega(g_1, g_2)\omega(g_1g_2, g_3), \tag{6.16}$$

for all $g_1, g_2, g_3 \in G$. If $\omega(g_1, g_2) = 1$, this reduces to the usual linear representation of G.

A different choice of pre-factor for the representation matrices $u'(g) = \beta(g)u(g)$ will lead to a different factor system $\omega'(g_1, g_2)$:

$$\omega'(g_1, g_2) = \frac{\beta(g_1 g_2)}{\beta(g_1)\beta(g_2)}\omega(g_1, g_2). \tag{6.17}$$

We regard $u'(g)$ and $u(g)$ that differ only by a pre-factor as equivalent projective representations and the corresponding factor systems $\omega'(g_1, g_2)$ and $\omega(g_1, g_2)$ as belonging to the same class ω.

Suppose that we have one projective representation $u_1(g)$ with factor system $\omega_1(g_1, g_2)$ of class ω_1 and another $u_2(g)$ with factor system $\omega_2(g_1, g_2)$ of class ω_2, obviously $u_1(g) \otimes u_2(g)$ is a projective presentation with factor group $\omega_1(g_1, g_2)\omega_2(g_1, g_2)$. The corresponding class ω can be written as a sum $\omega_1 + \omega_2$. Under such an addition rule, the equivalence classes of factor systems form an Abelian group, which is called the second cohomology group of G and denoted as $H^2(G, U(1))$. The identity element ω_0 of the group is the class that contains the linear representation of the group.

Here are some simple examples:
(a) cyclic groups Z_n do not have non-trivial projective representation. Hence for $G = Z_n$, $H^2(G, U(1))$ contains only the identity element.
(b) a simple group with non-trivial projective representation is the Abelian dihedral group $D_2 = Z_2 \times Z_2$. For the four elements of the group $(0/1, 0/1)$, consider representation with Pauli matrices $g(0,0) = \begin{bmatrix} 1 & 0 \\ 0 & 1 \end{bmatrix}$, $g(0,1) = \begin{bmatrix} 0 & 1 \\ 1 & 0 \end{bmatrix}$, $g(1,0) = \begin{bmatrix} 1 & 0 \\ 0 & -1 \end{bmatrix}$, $g(1,1) = \begin{bmatrix} 0 & -i \\ i & 0 \end{bmatrix}$. It can be check that this gives a non-trivial projective representation of D_2.
(c) when $G = SO(3)$, $H^2(G, U(1)) = Z_2$. The two elements correspond to integer and half-integer representations of $SO(3)$ respectively.
(d) when $G = U(1)$, $H^2(G, U(1))$ is trivial: $H^2(U(1), U(1)) = Z_1$. We note that $\{e^{im\theta}\}$ form a representation of $U(1) = \{e^{i\theta}\}$ when m is an integer. But $\{e^{im\theta}\}$ will form a projective representation of $U(1)$ when m is not an integer. But under the equivalence relation Eq. (6.17), $\{e^{im\theta}\}$ correspond to the trivial projective representation, if we choose $\beta(g) = e^{-im\theta}$. Note that $\beta(g)$ can be a discontinuous function over the group manifold.

6.5.2 Solving symmetry condition for fixed point

In this section, we explicitly solve the symmetry condition Eq. (6.4). The goal is to 1. classify possible symmetry operations at fixed point and 2. find the corresponding symmetric fixed point state. For simplicity, we drop the site index $[k]$ and rewrite Eq. (6.4) as

$$\sum_{j^l j^r} \frac{u_{i^l i^r, j^l j^r}(g)}{\alpha^{(R)}(g)} A_{j^l j^r} = N^{-1}(g) A_{i^l i^r} M(g) \tag{6.18}$$

where $u(g)$ is a projective or linear unitary representation of G, the matrix $A_{i^l i^r}$ is given by its matrix elements $A_{i^l i^r, \alpha\beta} = \sqrt{\lambda^l_{i^l}}\delta_{i^l \alpha} \cdot \sqrt{\lambda^r_{i^r}}\delta_{i^r \beta}$ with $i^l, \alpha = 1, ..., D_l$, $i^r, \beta = 1, ..., D_r$, and $M(g)$, $N(g)$ are sets of invertible matrices labeled by g. Since $\frac{u(g)}{\alpha^{(R)}(g)}$ is also a projective or linear unitary representation of G, we can absorb $\alpha^{(R)}(g)$ into $u(g)$ and rewrite Eq. (6.18)

as

$$\sum_{j^l j^r} u_{i^l i^r, j^l j^r}(g) A_{j^l j^r} = N^{-1}(g) A_{i^l i^r} M(g) \tag{6.19}$$

We note that matrix elements $A_{i^l i^r, \alpha\beta}$ is non-zero only when $\alpha = i^l$, $\beta = i^r$ and the full set of $\{A_{i^l i^r}\}$ form a complete basis in the space of $D_l \times D_r$ dimensional matrices.

$M(g)$, $N(g)$ do not necessarily form a representation of G. But the fixed point form of the matrices requires that $M(g)$, $N(g)$ be a projective representation, as on the one hand

$$\begin{aligned} &\sum_{j^l j^r} u_{i^l i^r, j^l j^r}(g_1 g_2) A_{j^l j^r} \\ =&\sum_{j^l j^r k^l k^r} \omega_{sym}(g_1, g_2) u_{i^l i^r, k^l k^r}(g_1) u_{k^l k^r, j^l j^r}(g_2) A_{j^l j^r} \\ =&\sum_{k^l k^r} \omega_{sym}(g_1, g_2) u_{i^l i^r, k^l k^r}(g_1) N^{-1}(g_2) A_{k^l k^r} M(g_2) \\ =&\omega_{sym}(g_1, g_2) N^{-1}(g_2) N^{-1}(g_1) A_{i^l i^r} M(g_1) M(g_2) \end{aligned} \tag{6.20}$$

and on the other hand

$$\sum_{j^l j^r} u_{i^l i^r, j^l j^r}(g_1 g_2) A_{j^l j^r} = N^{-1}(g_1 g_2) A_{i^l i^r} M(g_1 g_2) \tag{6.21}$$

Therefore

$$\omega_{sym}(g_1, g_2) N^{-1}(g_2) N^{-1}(g_1) A_{i^l i^r} M(g_1) M(g_2) = N^{-1}(g_1 g_2) A_{i^l i^r} M(g_1 g_2) \tag{6.22}$$

for all $i^l i^r$. However, the set of matrices $\{A_{i^l i^r}\}$ form a complete basis in the space of $D_l \times D_r$ dimensional matrices. Therefore,

$$\omega_{sym}(g_1, g_2) N^{-1}(g_2) N^{-1}(g_1) \otimes M(g_1) M(g_2) = N^{-1}(g_1 g_2) \otimes M(g_1 g_2), \tag{6.23}$$

and $N(g)$ and $M(g)$ form two projective representations

$$\begin{aligned} N(gh) &= \omega_N(g, h) N(g) N(h), \\ M(gh) &= \omega_M(g, h) M(g) M(h), \end{aligned} \tag{6.24}$$

with $|\omega_N(g_1, g_2)| = |\omega_M(g_1, g_2)| = 1$ and

$$\omega_{sym}(g_1, g_2) = \frac{\omega_M(g_1, g_2)}{\omega_N(g_1, g_2)} \tag{6.25}$$

Let us rewrite Eq. (6.19) as

$$N(g)(\sum_{j^l j^r} u_{i^l i^r, j^l j^r}(g) A_{j^l j^r}) M^{-1}(g) = A_{i^l i^r} \tag{6.26}$$

We note that

$$N(g)(\sum_{j^l j^r} (\tilde{N}^{-1})_{j^l, i^l} \tilde{M}_{i^r, j^r} A_{j^l j^r}) M^{-1}(g) = A_{i^l i^r} \tag{6.27}$$

where the matrices $\tilde{M}$ and $\tilde{N}$ are given by

$$\tilde{M}_{\alpha\beta} = M_{\alpha\beta}\frac{\sqrt{\lambda^r_\alpha}}{\sqrt{\lambda^r_\beta}}, \quad \tilde{N}_{\alpha\beta} = N_{\alpha\beta}\frac{\sqrt{\lambda^l_\beta}}{\sqrt{\lambda^l_\alpha}}. \tag{6.28}$$

Since the set of matrices $\{A_{i^l i^r}\}$ form a complete basis in the space of $D_l \times D_r$ dimensional matrices, we find

$$u_{i^l i^r, j^l j^r}(g) = (\tilde{N}^{-1})_{j^l, i^l}(g)\tilde{M}_{i^r, j^r}(g). \tag{6.29}$$

Putting back the factor of $\alpha^{(R)}(g)$, we find that

$$u_{i^l i^r, j^l j^r}(g) = \alpha^{(R)}(g)(\tilde{N}^{-1})_{j^l, i^l}(g)\tilde{M}_{i^r, j^r}(g). \tag{6.30}$$

6.5.3 Equivalence Between Symmetric Fixed Point States

From the solution in section 6.5.2, we know that the fixed point state symmetric under linear on-site symmetry of group G takes the form

$$|\phi\rangle^{(\infty)} = |EP_{1,2}\rangle|EP_{2,3}\rangle...|EP_{k,k+1}\rangle... \tag{6.31}$$

where $|EP_{k,k+1}\rangle$ is an entangled pair between the right virtual qubit on site k and the left virtual qubit on site $k+1$(see Fig. 6-1 upper layer). Each entangled pair is invariant under a linear symmetry transformation of the form $u^{[k],r}(g) \otimes u^{[k+1],l}(g)$

$$u^{[k],r}(g) \otimes u^{[k+1],l}(g)|EP_{k,k+1}\rangle = |EP_{k,k+1}\rangle \tag{6.32}$$

But $u^{[k],r}(g)$ or $u^{[k+1],l}(g)$ alone might not form a linear representation of G. They could in general be a projective representation of G. If $u^{[k],r}(g)$ is a projective representation corresponding to class ω in $H^2(G, U(1))$, then $u^{[k+1],l}$ must correspond to class $-\omega$. ω does not vary from site to site and labels a particular symmetric fixed point state.

Now we will show that symmetric fixed point states with the same ω can be connected through symmetric LU transformations and hence belong to the same phase while those with different ω cannot and belong to different phases.

First, suppose that two symmetric fixed point states $|\phi_1\rangle$ and $|\phi_2\rangle$ are related with the same ω, i.e.

$$\begin{aligned} u_1^{[k],r}(g) \otimes u_1^{[k+1],l}(g)|EP_{k,k+1}\rangle_1 &= |EP_{k,k+1}\rangle_1 \\ u_2^{[k],r}(g) \otimes u_2^{[k+1],l}(g)|EP_{k,k+1}\rangle_2 &= |EP_{k,k+1}\rangle_2 \end{aligned} \tag{6.33}$$

where $|EP_{k,k+1}\rangle_{1(2)}$ is an entangled pair of virtual spins on Hilbert space $\mathcal{H}^{[k],r}_{1(2)} \otimes \mathcal{H}^{[k+1],l}_{1(2)}$. $u^{[k],r}_{1(2)}(g)$ is a projective representation of G corresponding to ω on $\mathcal{H}^{[k],r}_{1(2)}$ and $u^{[k+1],l}_{1(2)}(g)$ a projective representation corresponding to $-\omega$ on $\mathcal{H}^{[k+1],l}_{1(2)}$.

We can think of $|EP_{k,k+1}\rangle_1$ and $|EP_{k,k+1}\rangle_2$ as living together in a joint Hilbert space $(\mathcal{H}_1^{[k],r} \oplus \mathcal{H}_2^{[k],r}) \otimes (\mathcal{H}_1^{[k+1],l} \oplus \mathcal{H}_2^{[k+1],l})$. The symmetry representation on this joint Hilbert

space can be defined as

$$u^{[k],r}(g) \otimes u^{[k+1],l}(g) = (u_1^{[k],r}(g) \oplus u_2^{[k],r}(g)) \otimes (u_1^{[k+1],l}(g) \oplus u_2^{[k+1],l}(g)) \tag{6.34}$$

As $u_1^{[k],r}(g)$ and $u_2^{[k],r}(g)$ (also $u_1^{[k+1],l}(g)$ and $u_2^{[k+1],l}(g)$) both correspond to ω ($-\omega$), their direct sum $u^{[k],r}(g)(u^{[k+1],l}(g))$ is also a projective representation corresponding to $\omega(-\omega)$. Therefore, we have a linear representation of G on each site k, $u^{[k],l}(g) \otimes u^{[k],r}(g)$ and both $|EP_{k,k+1}\rangle_1$ and $|EP_{k,k+1}\rangle_2$ are symmetric under $u^{[k],r}(g) \otimes u^{[k+1],l}(g)$.

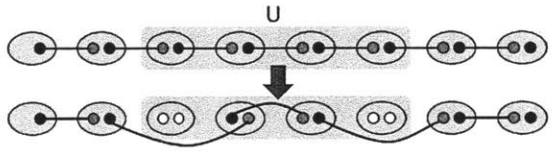

Figure 6-5: (Color online) Fixed point state related to projective representation of class ω before (upper) and after (lower) a local unitary operation on the shaded region that does not break the symmetry. White dots correspond to ω_0, the identity element in $H^2(G, U(1))$, black dots correspond to ω and gray dots correspond to $-\omega$.

Now we can perform a LU transformation on the joint Hilbert space and rotate continuously between $|EP_{k,k+1}\rangle_1$ and $|EP_{k,k+1}\rangle_2$. That is,

$$U(\theta) = \cos(\frac{\theta}{2})I - i\sin(\frac{\theta}{2})(|a\rangle\langle b| + |b\rangle\langle a|) \tag{6.35}$$

where $|a\rangle = |EP_{k,k+1}\rangle_1$, $|b\rangle = |EP_{k,k+1}\rangle_2$ and θ goes from 0 to π. By doing this locally to each pair, we can map $|\phi_1\rangle$ to $|\phi_2\rangle$ (and vice verse) with LU transformations without breaking the on-site symmetry of group G. Therefore, $|\phi_1\rangle$ and $|\phi_2\rangle$ belong to the same phase if they are related with the same ω.

On the other hand, if $|\phi_1\rangle$ and $|\phi_2\rangle$ are related to ω_1 and ω_2 respectively, we will show that they cannot be connected by any LU transformation that does not break the symmetry.

Suppose that ω_1 is non-trivial, we start with $|\phi_1\rangle$ and apply a local unitary operation U to a finite region (shaded in Fig. 6-5). $|\phi_1\rangle$ is composed of invariant singlets of symmetry group G. If U does not break the symmetry, the resulting state should still be composed of singlets. The singlet pairs outside of the shaded region are not changed while those overlapping with the shaded region can take any possible structure after the operation U.

No matter what the change is, the right virtual spin on the site to the left of the region corresponding to ω_1 should form a singlet with some degrees of freedom in the region. As the singlet is invariant under a linear representation of G, these degrees of freedom in the region must form a projective representation of G corresponding to $-\omega_1$. These degrees of freedom could live on one site or distribute over several sites. However, the sites only support linear representations. Therefore, there must be some remaining degrees of freedom on the same sites that correspond to ω_1. These remaining degrees of freedom must form singlets again with other degrees of freedoms in the region that correspond to $-\omega_1$. We can continue this argument until finally some degree of freedom in the region corresponding to $-\omega_1$ connect with the left virtual spin on the site to the right of the region corresponding to ω_1 and form a singlet.

In Fig. 6-5, we illustrate one possible structure of singlets after operation U. White dots correspond to ω_0, the identity element in $H^2(G,U(1))$, black dots correspond to ω_1 and gray dots correspond to $-\omega_1$.

Therefore, we can see that no matter what the symmetric LU operation might be on $|\phi_1\rangle$, singlet entangled pairs related to ω_1 must connect head to tail and cover the whole length of the chain. In other words, we can not shrink a chain of singlet entangled pairs related to non-trivial ω_1 continuously to a point or change it to ω_2 by acting on it locally and without breaking the symmetry. Hence fixed point states with different ω cannot be related to each other with symmetric LU transformation and hence belong to different classes.

6.5.4 Deformation of TI states with on-site symmetry or parity symmetry

A TI SRC MPS which is symmetric under on-site symmetry of group G is described by matrices which satisfy

$$\sum_j u_{ij}(g)A_j = \alpha(g)M^{-1}(g)A_iM(g) \tag{6.36}$$

for some invertible projective representation $M(g)$. The double tensor $\mathbb{E}$ hence satisfies

$$\mathbb{E}_{\alpha\gamma,\beta\chi} = \sum_{\alpha'\beta'\gamma'\chi'} M^{-1}_{\alpha\alpha'}M_{\beta\beta'}(M^*)^{-1}_{\gamma\gamma'}M^*_{\chi\chi'}\mathbb{E}_{\alpha'\gamma',\beta'\chi'} \tag{6.37}$$

where the group element label g has been omitted. Being the non-degenerate one dimensional eigenspace of $\mathbb{E}$, $\mathbb{E}^0$ must be invariant under the same transformation, and so does $\mathbb{E}'$. Therefore we have

$$\begin{aligned}\mathbb{E}^0_{\alpha\gamma,\beta\chi} &= \sum_{\alpha'\beta'\gamma'\chi'} M^{-1}_{\alpha\alpha'}M_{\beta\beta'}(M^*)^{-1}_{\gamma\gamma'}M^*_{\chi\chi'}\mathbb{E}^0_{\alpha'\gamma',\beta'\chi'} \\ \mathbb{E}'_{\alpha\gamma,\beta\chi} &= \sum_{\alpha'\beta'\gamma'\chi'} M^{-1}_{\alpha\alpha'}M_{\beta\beta'}(M^*)^{-1}_{\gamma\gamma'}M^*_{\chi\chi'}\mathbb{E}'_{\alpha'\gamma',\beta'\chi'}\end{aligned} \tag{6.38}$$

Now we smoothly change the double tensor as in Eqn.6.10. Evidently, the symmetry condition Eqn.6.37 is satisfied for all t.

Decompose $\mathbb{E}(t)$ back to matrices $A_i(t)$ so that the represented state $|\phi(t)\rangle$ changes smoothly with time. Denote the symmetry transformed double tensor as $\mathbb{E}_{M(g)}$. As $\mathbb{E}_{M(g)}(t) = \mathbb{E}(t)$, there must exist a unitary operator $\tilde{u}(g)(t)$, such that

$$\sum_j \tilde{u}_{ij}(g)(t)A_j(t) = M^{-1}(g)A_i(t)M(g) \tag{6.39}$$

where $\tilde{u}(g)(t)$ is a linear representation of G. Redefine $u(g)(t) = \tilde{u}(g)(t) \times \alpha(g)$, then

$$\sum_j u_{ij}(g)(t)A_j(t) = \alpha(g)M^{-1}(g)A_i(t)M(g) \tag{6.40}$$

As $A_i(t)$ is chosen to be continuous with time, from the above equation we can see that $u(g)(t)$ is also continuous in time. On the other hand, $u(g)(t)$ form a linear representation of G. For all the cases we are interested in, the linear representations of G are discrete. Therefore, as $u(g)(t)$ evolves smoothly with time, it cannot change from one representation to another but only from one equivalent form to another which differ by a unitary conjugation.

That is, $u(g)(t) = V(t)u(g)V^\dagger(t)$, with a continuous $V(t)$. We can incorporate $V(t)$ into the matrices $A_i(t)$ and define $\tilde{A}_i(t) = \sum_j V^\dagger_{ij}(t)A_j(t)$, so that $\tilde{A}_i(t)$ is symmetric under $u(g)$ for all t. In the following discussion, we will assume that such a redefinition is made and the symmetry operation of the system will always be $u(g)\otimes...\otimes u(g)$. Therefore, the continuous evolution of $\mathbb{E}(t)$ from $t = 0$ to $t = T$ corresponds to a continuous evolution of short range correlated states $|\phi(t)\rangle$ which is always symmetric under the same on-site symmetry $u(g)$, with the same phase factor $(\alpha(g))^L$ and related to the same projective representation ω.

Such a smooth path in symmetric state space corresponds to a smooth path in symmetric Hamiltonian space. Construct parent Hamiltonian as discussed previously. Because the state is symmetric under on-site $u(g)$, the support space on site k to $k+l$ must then form a representation space for $(\otimes u(g))^l$. Therefore, it is easy to see that the parent Hamiltonian, being a summation of projections onto such spaces, is also symmetry under on-site $u(g)$. Moreover, the Hamiltonian remains gapped and TI. In this way, we have found a smooth path of symmetric, in particular TI, Hamiltonian whose adiabatic evolution connects any symmetric state labeled by $\alpha(g)$ and ω to the corresponding fixed point state(up to a local change of basis) and hence establishing the symmetric TI LU equivalence between them.

As we show in section 6.5.3 that fixed point states with the same $\alpha(g)$ and ω can be related by symmetric local unitary transformations to each other, we now complete the proof that *for 1D spin systems with only translation and an on-site linear symmetry G, all gapped phases that do not break the two symmetries are classified by a pair (ω, α) where $\omega \in H^2(G, U(1))$ label different types of projective representations of G and α label different 1D representations of G.*

Similarly, if the system has translation and parity symmetry, we can establish the equivalence between states labeled by the same $\alpha(P)$ and $\beta(P)$ in a translational invariant way (see the discussion below Eq. (6.13)). The procedure is totally analogous to the on-site symmetry case, with the only difference that the symmetry condition for the matrices and double tensors become

$$\begin{aligned}&\textstyle\sum_j u_{ij}A_j^T = \pm M^{-1}A_iM\\ &\mathbb{E}_{\beta\chi,\alpha\gamma} = \textstyle\sum_{\alpha'\beta'\gamma'\chi'} M^{-1}_{\alpha\alpha'}M_{\beta\beta'}(M^*)^{-1}_{\gamma\gamma'}M^*_{\chi\chi'}\mathbb{E}_{\alpha'\gamma',\beta'\chi'}\end{aligned}$$

6.5.5 A proof of Eq. (6.11)

A gapped TI state can be represented by a uniform MPS. Suppose that we perform R steps of RG transformation on the state, each with block size n_i. Then we obtain a MPS described by matrices $(A_{i^l i^r})^{(R)}$. To describe a state that does not break the on-site linear symmetry, here $(A_{i^l i^r})^{(R)}$ is invariant (up to a phase) under $u^{(R)}(g)$ on each site. Therefore[PGWS+08],

$$\sum_{j^l j^r} u_{i^l i^r, j^l j^r}(g)A_{j^l j^r} = \alpha^{(R)}(g)M^{-1}(g)A_{i^l i^r}M(g) \tag{6.41}$$

must be satisfied with some invertible matrix $M(g)$. Here we have dropped the RG step label R (except in $\alpha^{(R)}(g)$). Each coarse grained site is a combination of $\prod_{i=1}^R n_i$ original lattice sites and $\alpha^{(R)}(g)$ form a 1D representation of G.

So if the number of sites has a form $L = Q\prod_{i=1}^R n_i$, then $\alpha_L(g)$ in Eq. (6.3) will have a form

$$\alpha_L(g) = [\alpha^{(R)}(g)]^Q \tag{6.42}$$

for any value of Q. Now let us choose $Q = \prod_{i=1}^{R'} n_i'$ where $\prod_{i=1}^{R} n_i$ and $\prod_{i=1}^{R'} n_i'$ have no common factors. The total system size becomes $L = \prod_{i=1}^{R} n_i \prod_{i=1}^{R'} n_i'$. We can perform, instead, a R' step of $\{n_i'\}$-block RG transformation, which leads to a 1D representation $\alpha^{(R')}(g)$. We find that $\alpha_L(g)$ in Eq. (6.3) will have a form

$$\alpha_L(g) = [\alpha^{(R')}(g)]^{Q'} \tag{6.43}$$

where $Q' = L/\prod_{i=1}^{R'} n_i' = \prod_{i=1}^{R} n_i$. Thus

$$\alpha_L(g) = [\alpha^{(R)}(g)]^{\prod_{i=1}^{R'} n_i'} = [\alpha^{(R')}(g)]^{\prod_{i=1}^{R} n_i}. \tag{6.44}$$

Since $\prod_{i=1}^{R} n_i$ and $\prod_{i=1}^{R'} n_i'$ have no common factors, there must exist a 1D representation $\alpha(g)$ of G, such that

$$\alpha^{(R)}(g) = [\alpha(g)]^{\prod_{i=1}^{R} n_i}, \quad \alpha^{(R')}(g) = [\alpha(g)]^{\prod_{i=1}^{R'} n_i'}. \tag{6.45}$$

Now Eq. (6.42) becomes

$$\alpha_L(g) = [\alpha(g)]^{Q \prod_{i=1}^{R} n_i} = [\alpha(g)]^L \tag{6.46}$$

which gives us Eq. (6.11).

Chapter 7

Symmetry protected topological phases in two and higher dimensions

With a complete understanding of one-dimensional gapped quantum phases, we now want to move on to the more interesting case of two and higher dimensions. The phase diagram changes dramatically in higher dimensions. First of all, nontrivial intrinsic topological order does exist in two or higher dimensions. Much has been learned about possible intrinsic topological orders[WZ92, Kit03, LW05, CGW10, GWW10] although a complete understanding is still missing. In this chapter, we focus only on the symmetry protected topological (SPT) phases. Most SPT phases in two and higher dimensions have been identified in free fermion systems due to the simplicity and versatility of the formalism. A classification of possible SPT phases in non-interacting fermion systems has been obtained.[SRFL08, RSFL10, Kit09] The major open question about SPT phases is which of these free fermion phases remain and what new SPT phases are possible when the system is strongly interacting. In boson systems, even less is known as non-interacting bosons are necessarily topologically trivial. [1]

A pattern has emerged from the study of lower dimensional symmetric states[SPGC11]. In zero dimensional systems, a symmetric ground state forms a 1D representation of the symmetry. Different 1D representations cannot be smoothly connected without breaking the symmetry. There must be a level crossing to go from one to another. The 1D representations, which form the first cohomology group of the symmetry group $\mathcal{H}^1[G, U(1)]$, hence label different zero dimensional symmetric 'phases'. In one dimensional systems, as we have seen, a symmetric ground state is labeled by a projective representation of the symmetry group. Different projective representations, which form the second cohomology group of the symmetry group $\mathcal{H}^2[G, U(1)]$, hence label different one dimensional symmetric phases. The conjecture is then, SPT phases in d dimension are labeled by $d+1$th order cohomology group $\mathcal{H}^{d+1}[G, U(1)]$. And we will show that this is indeed true.

In section 7.1, we present the explicit construction of a two dimensional interacting bosonic model with Z_2 symmetry protected topological order that is stable even under

[1] Recently, there are several proposals for 'fractional topological insulators',[LS09, SBMS11, MQKZ10, LBKJS11] which incorporate interaction effect into topological insulators and find topologically ordered phases. However, these phases all have intrinsic topological order and does not belong to SPT phases discussed here.

strong interactions. The construction is generalized to arbitrary symmetry and arbitrary spatial dimensions in section 7.2 through the connection between bosonic SPT order and group cohomology of the symmetry group. In this way, we have a systematic construction of SPT orders in strongly interacting bosonic systems. While the tensor product formalism is less powerful than the matrix product formalism and falls short of providing a rigorous full classification of topological orders in two and higher dimensions, we will argue that our construction is based on a generic picture of short range entangled states and could potentially lead to a complete classification of SPT orders in these systems using group cohomology. Section 7.1 is based on our work [CLW11]. Section 7.2 is based on our work [CGLW11].

7.1 Model with Z_2 symmetry protected topological order in 2D bosonic system

7.1.1 Summary of CZX model

We will present the construction of an exactly solvable model, which we call the CZX model for reasons that will become clear later, in a two dimensional interacting bosonic system. On a closed surface the CZX model looks simple. Its Hamiltonian is composed of commuting projectors. Its symmetric gapped ground state is a product of local loops and hence short range entangled. However, the model becomes highly nontrivial if it has a boundary. The boundary must have gapless excitation as long as symmetry is not broken, a signature of nontrivial SPT order. We prove this fact by relating the effective symmetry transformation on the boundary with a nontrivial 3-cocycle of the Z_2 group.

The effective theory on the boundary can be seen as a generalization of the Wess-Zumino-Witten (WZW) model.[WZ71, Wit83] The WZW model describes conformally invariant 1D systems with an internal symmetry of a compact Lie group. The WZW model obtained by adding a topological term (the WZW term) to the usual dynamical term in the Lagrangian of the nonlinear sigma model, is exactly solvable in semi-classical limit. It explains the physics of 1D gapless systems with a global Lie group symmetry. However, the construction of the model depends crucially on the fact that the symmetry group is continuous and does not apply to, for example, the Z_2 group. Our proof of the gapless-ness of the 1D effective theory on the boundary of the CZX model hence generalizes the understanding of the WZW model to discrete groups. Our method based on the nontrivial 3-cocycles applies to both continuous and discrete symmetry groups, although it does not give the conformal field theory of the system directly. Also our proof is non-perturbative, not relying on semi-classical approximation. The connection between the CZX model and the WZW model is not particularly clear in the formulation of this section, as the WZW model is usually given in the Lagrangian form. In the next section, we reformulate our models (including the CZX model and those for all other symmetries and in all dimensions) in the Lagrangian language where the connection with the WZW model would become obvious.

7.1.2 CZX model in the bulk

In this section, we construct the CZX model explicitly which turns out to have nontrivial SPT order protected only by on-site Z_2 symmetry. We will give the Hamiltonian, the ground state and the symmetry action of the system in the bulk (on surfaces without boundary).

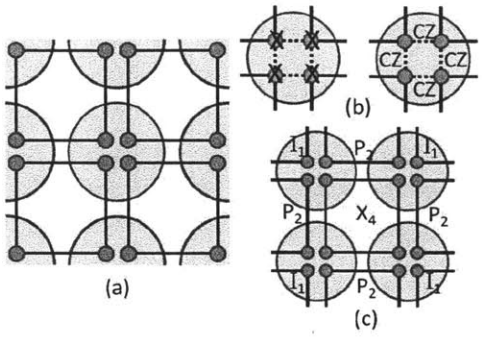

Figure 7-1: CZX model (a) each site (circle) contains four spins (dots) and the spins in the same plaquette (square) are entangled. (b) on-site Z_2 symmetry is generated by $U_{CZX} = X_1X_2X_3X_4CZ_{12}CZ_{23}CZ_{34}CZ_{41}$ (c) a local term in the Hamiltonian, which is a tensor product of one X_4 term and four P_2 terms as defined in the main text.

Consider a square lattice with four two-level spins per site, as shown in Fig. 7-1(a) where sites are represented by circles and spins are represented by dots. We denote the two levels as $|0\rangle$ and $|1\rangle$. The system has an on-site Z_2 symmetry as given in Fig. 7-1(b). It is generated by

$$U_{CZX} = U_X U_{CZ} \tag{7.1}$$

where

$$U_X = X_1 \otimes X_2 \otimes X_3 \otimes X_4 \tag{7.2}$$

X_i is Pauli X operator on the ith spin and

$$U_{CZ} = CZ_{12}CZ_{23}CZ_{34}CZ_{41} \tag{7.3}$$

where CZ is the controlled-Z operator on two spins defined as

$$CZ = |00\rangle\langle 00| + |01\rangle\langle 01| + |10\rangle\langle 10| - |11\rangle\langle 11| \tag{7.4}$$

As defined, CZ does nothing if at least one of the spins is in state $|0\rangle$ and it adds a minus sign if both spins are in state $|1\rangle$. Different CZ operators overlap with each other. But because they commute, U_{CZ} is well defined. Note that U_{CZ} cannot be decomposed into separate operations on the four spins and the same is true for U_{CZX}. U_X and U_{CZ} both square to I and they commute with each other. Therefore, U_{CZX} generates a Z_2 group.

The Hamiltonian of the system is defined as a sum of local terms around each plaquette. Plaquettes are represented by squares in Fig. 7-1. $H = \sum H_{p_i}$, where the term around the ith plaquette H_{p_i} acts not only on the four spins in the plaquette but also on the eight spins in the four neighboring half plaquettes as shown in Fig. 7-1(c)

$$H_{p_i} = -X_4 \otimes P_2^u \otimes P_2^d \otimes P_2^l \otimes P_2^r \tag{7.5}$$

where X_4 acts on the four spins in the middle plaquette as

$$X_4 = |0000\rangle\langle 1111| + |1111\rangle\langle 0000| \tag{7.6}$$

and P_2 acts on the two spins in every neighboring half plaquette as

$$P_2 = |00\rangle\langle 00| + |11\rangle\langle 11| \tag{7.7}$$

P_2^u, P_2^d, P_2^l, P_2^r acts on the up, down, left and right neighboring half plaquettes respectively. For the remaining four spins at the corner, H_{p_i} acts as identity on them. The P_2 factors ensure that each term in the Hamiltonian satisfies the on-site Z_2 symmetry defined before.

All the local terms in the Hamiltonian commute with each other, therefore it is easy to solve for the ground state. If the system is defined on a closed surface, it has a unique ground state which is gapped. In the ground state, every four spins around a plaquette are entangled in the state

$$|\psi_{p_i}\rangle = |0000\rangle + |1111\rangle \tag{7.8}$$

and the total wave function is a product of all plaquette wave function. If we allow any local unitary transformation, it is easy to see that the ground state can be disentangled into a product state, just by disentangling each plaquette separately into individual spin states. Therefore, the ground state is short range entangled. However, no matter what local unitary transformations we apply to disentangle the plaquettes, they necessarily violate the on-site symmetry and in fact, the plaquettes cannot be disentangled if the Z_2 symmetry is preserved, due to the nontrivial SPT order of this model which we will show in the next sections.

It can be checked that this ground state is indeed invariant under the on-site Z_2 symmetry. Obviously this state is invariant under U_X applied to every site. It is also invariant under U_{CZ} applied to every site. To see this note that between every two neighboring plaquettes, CZ is applied twice, at the two ends of the link along which they meet. Because the spins within each plaquette are perfectly correlated (they are all $|0\rangle$ or all $|1\rangle$), the effect of the two CZ's cancel each other, leaving the total state invariant.

Therefore, we have introduced a 2D model with on-site Z_2 symmetry whose ground state does not break the symmetry and is short-range entangled. We can add small perturbation to the system which satisfies the symmetry and the system is going to remain gapped and the ground state short range entangled and symmetric. It seems that the system is quite trivial and boring. However, we are going to show that surprising things happen if the system has a boundary and because of these special features the system cannot be smoothly connected to a trivial phase even if translation symmetry is not required.

7.1.3 CZX model on the boundary

The non-trivialness of this model shows up on the boundary. Suppose that we take a simply connected disk from the lattice, as shown in Fig.7-2(a).

The reduced density matrix of spins in this region is invariant under on-site symmetry in this region. The reduced density matrix is a tensor product of individual terms on each full plaquette, half plaquette and corner of plaquette respectively. On a full plaquette

$$\rho_4 = (|0000\rangle + |1111\rangle)(\langle 0000| + \langle 1111|) \tag{7.9}$$

On a half plaquette

$$\rho_2 = |00\rangle\langle 00| + |11\rangle\langle 11| \tag{7.10}$$

On a corner of a plaquette

$$\rho_1 = |0\rangle\langle 0| + |1\rangle\langle 1| \tag{7.11}$$

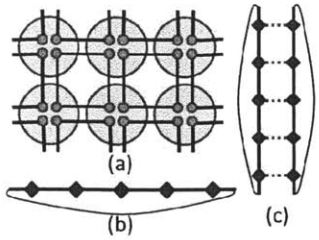

Figure 7-2: (a)CZX model on a disk with boundary (b) boundary effective degrees of freedom form a 1D chain which cannot have a SRE symmetric state (c) two boundaries together can have a SRE symmetric state which is a product of entangled pairs between effective spins connected by a dashed line.

The state of spins on the plaquettes totally inside this region is completely fixed. But on the boundary there are free degrees of freedom. However, unlike in the bond state, only part of the total Hilbert space of the spins on the boundary is free. In particular, two spins in a half plaquette on the boundary are constrained to the two-dimensional subspace $|00\rangle\langle 00| + |11\rangle\langle 11|$ and form an effective spin degree of freedom if we map $|00\rangle$ to $|\tilde{0}\rangle$ and $|11\rangle$ to $|\tilde{1}\rangle$.

In Fig. 7-2(b), we show the effective degrees of freedom on the boundary as diamonds on a line. Projecting the total symmetry operation on the disk to the space supporting reduced density matrix, we find that the effective symmetry operation on the boundary effective spins is $\tilde{U}_{CZX} = \prod_{i=1}^{N} \tilde{X}_i \prod_{i=1}^{N} \tilde{CZ}_{i,i+1}$, with Pauli $\tilde{X}$ on each effect spin and $\tilde{CZ}$ operation between neighboring effective spins. The boundary is periodic and $\tilde{CZ}_{N,N+1}$ acts on effective spin N and 1. This operator generates a Z_2 symmetry group.

This is a very special symmetry on a 1D system. First it is not an on-site symmetry. In fact, no matter how we locally group sites and take projections, the symmetry operations are not going to break down into an on-site form. Moreover, no matter what interactions we add to the boundary, as long as it preserves the symmetry, the boundary cannot have a gapped symmetric ground state. We can start by considering some simple cases. The simplest interaction term preserving this symmetry is $Z_i Z_{i+1}$. This is an Ising interaction term and its ground state breaks the Z_2 symmetry. In the transverse Ising model, the system goes to a symmetric phase if magnetic field in the x direction is increased. However, X_i breaks the Z_2 symmetry $\tilde{U}_{CZX}$ on the boundary and therefore cannot be added to the Hamiltonian. In fact, we are going to prove that the boundary cannot have SRE symmetric ground state (actually a more generalized version of it) in the next section.

The special property on the boundary only shows up when there is an isolated single boundary. If we put two such boundaries together and allow interactions between them, everything is back to normal. As shown in Fig.7-2(c), if we have two boundaries together, there is indeed a SRE symmetric state on the two boundaries. The state is a product of entangled pairs of effective spins connected by a dashed line. The entangled pair can be chosen as $|\tilde{0}\tilde{0}\rangle + |\tilde{1}\tilde{1}\rangle$. In contrast to the single boundary case, we can locally project the two effective spins connected by a dashed line to the subspace $|\tilde{0}\tilde{0}\rangle\langle\tilde{0}\tilde{0}| + |\tilde{1}\tilde{1}\rangle\langle\tilde{1}\tilde{1}|$ and on this subspace, the symmetry acts in an on-site fashion.

This result should be expected because if we have two pieces of sheet with boundary and glue them back into a surface without boundary, we should have the original SRE 2D

state back. Indeed if we map the effective spins back to the original degrees of freedom $|\tilde{0}\rangle \to |00\rangle$ and $|\tilde{1}\rangle \to |11\rangle$, we see that the SRE state between two boundaries is just the a chain of plaquettes $|0000\rangle + |1111\rangle$ in the original state.

This model serves as an example of non-trivial SPT order in 2D SRE states that only needs to be protected by on-site symmetry. In order to prove the special property on the boundary of CZX model and have a more complete understanding of possible SPT orders in 2D SRE states with on-site symmetry, we are going to introduce a mathematical tool called Matrix Product Unitary Operator. We will show that 2D SPT phases are related to elements in $\mathcal{H}^3(G, U(1))$ which emerge in the transformation structure of the matrix product unitary operators. The definition of matrix product unitary operator and some basic properties are given in section 7.4.3. The discussion in the next section is general, but we will work out the CZX example explicitly for illustration.

7.1.4 Matrix Product Unitary Operators and its relation to 3 cocycle

In this section, we discuss the matrix product unitary operator (MPUO) formalism and show how the effective symmetry operation on the boundary of CZX model can be expressed as MPUO. Moreover, we are going to relate MPUO of a symmetry group to the 3-cocycle of the group and in particular, we are going to show that the CZX model corresponds to a nontrivial 3-cocycle of the Z_2 group.

A matrix product operator acting on a 1D system is given by,[PMCV10]

$$O = \sum_{\{i_k\},\{i'_k\}} Tr(T^{i_1,i'_1} T^{i_2,i'_2} ... T^{i_N,i'_N}) |i'_1 i'_2 ... i'_N\rangle\langle i_1 i_2 ... i_N| \tag{7.12}$$

where for fixed i and i', $T^{i,i'}$ is a matrix with index α and β. Here we want to use this formalism to study symmetry transformations, therefore we restrict O to be a unitary operator U. Using matrix product representation, U does not have to be an on-site symmetry. U is represented by a rank-four tensor $T^{i,i'}_{\alpha,\beta}$ on each site, where i and i' are input and output physical indices and α, β are inner indices. Basic properties of matrix product unitary operators are given in section 7.4.3.

In particular, the symmetry operator U_{CZX} (we omit the $\sim$ label for effective spins in following discussions) on the boundary of the CZX model can be represented by tensors

$$\begin{aligned} &T^{0,1}(CZX) = |0\rangle\langle +|, \quad T^{1,0}(CZX) = |1\rangle\langle -|, \\ &\text{other terms are zero} \end{aligned} \tag{7.13}$$

where $|+\rangle = |0\rangle + |1\rangle$ and $|-\rangle = |0\rangle - |1\rangle$. It is easy to check that this tensor indeed gives $U_{CZX} = CZ_{12}...CZ_{N1}X_1...X_N$.

The other element in the Z_2 group–the identity operation–can also be represented as MPUO with tensors

$$\begin{aligned} &T^{0,0}(I) = |0\rangle\langle 0|, \qquad T^{1,1}(I) = |0\rangle\langle 0|, \\ &\text{other terms are zero} \end{aligned} \tag{7.14}$$

These two tensors are both in the canonical form as defined in section 7.4.3.

If two MPUO $T(g_2)$ and $T(g_1)$ are applied subsequently, their combined action should be equivalent to $T(g_1 g_2)$. However, the tensor $T(g_1, g_2)$ obtained by contracting the output physical index of $T(g_2)$ with the input physical index of $T(g_1)$, see Fig. 7-3, is usually more redundant than $T(g_1 g_2)$ and might not be in the canonical form. It can only be reduced to

$T(g_1 g_2)$ if certain projection P_{g_1,g_2} is applied to the inner indices (see Fig. 7-3).

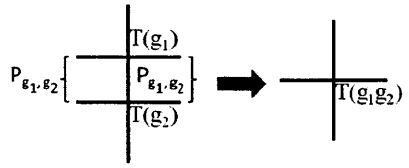

Figure 7-3: Reduce combination of $T(g_2)$ and $T(g_1)$ into $T(g_1 g_2)$.

P_{g_1,g_2} is only defined up to an arbitrary phase factor $e^{i\theta(g_1,g_2)}$. If the projection operator on the right side P_{g_1,g_2} is changed by the phase factor $e^{i\theta(g_1,g_2)}$, the projection operator $P^\dagger_{g_1,g_2}$ on the left side is changed by phase factor $e^{-i\theta(g_1,g_2)}$. Therefore the total action of P_{g_1,g_2} and $P^\dagger_{g_1,g_2}$ on $T(g_1,g_2)$ does not change and the reduction procedure illustrated in Fig.7-3 still works. Moreover, from the discussion in the section 7.4.3, we know that this is the only degree of freedom in P_{g_1,g_2}. Up to a phase factor, P_{g_1,g_2} is unique (on the unique block in the canonical form of $T(g_1,g_2)$).

Let us illustrate how the reduction is done for the symmetry group (I, U_{CZX}). For example, if we apply $U_{CZX}U_{CZX}$ the totally action should be equivalent to I. However the tensor $T(CZX,CZX)$ is given by

$$\begin{array}{l} T^{0,0}(CZX,CZX) = |01\rangle\langle +-|, \quad T^{1,1}(CZX,CZX) = |10\rangle\langle -+|, \\ \text{other terms are zero} \end{array} \tag{7.15}$$

This tensor is reduced to $T(I)$ if projection

$$P_{CZX,CZX} = (|01\rangle - |10\rangle)\langle 0| \tag{7.16}$$

and its Hermitian conjugate are applied to the right and left of $T(CZX,CZX)$ respectively.[2] Adding an arbitrary phase factor $e^{i\theta(CZX,CZX)}$ to $P_{CZX,CZX}$ does not affect the reduction at all. By writing $P_{CZX,CZX}$ in the above form, we have made a particular choice of phase.

Below we list the (right) projection operators for all possible combinations of g_1 and g_2 of this Z_2 group.

$$\begin{array}{llll} P_{I,I} = |00\rangle\langle 0| & P_{CZX,I} = |00\rangle\langle 0| + |10\rangle\langle 1| \\ P_{I,CZX} = |00\rangle\langle 0| + |10\rangle\langle 1| & P_{CZX,CZX} = (|01\rangle - |10\rangle)\langle 0| \end{array} \tag{7.17}$$

Note that in giving P_{g_1,g_2} we have picked a particular choice of phase factor $e^{i\theta(g_1,g_2)}$. In general, any phase factor is allowed.

Nontrivial phase factors appear when we consider the combination of three MPUO's. See Fig. 7-4.

There are two different ways to reduce the tensors. We can either first reduce the combination of $T(g_1)$, $T(g_2)$ and then combine $T(g_3)$ or first reduce the combination of $T(g_2)$,$T(g_3)$ and then combine $T(g_1)$. The two different ways should be equivalent. More specifically, they should be the same up to phase on the unique block of Tg_1, g_2, g_3. Denote

[2]The mapping actually reduces $T(CZX,CZX)$ to $-T(I)$. But this is not a problem as we can redefine $\tilde{T}(CZX) = iT(CZX)$ and the extra minus sign would disappear.

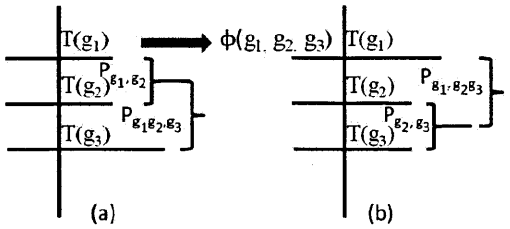

Figure 7-4: Different ways to reduce combination of $T(g_3)$, $T(g_2)$ and $T(g_1)$ into $T(g_1g_2g_3)$. Only the right projection operators are shown. Their combined actions differ by a phase factor $\phi(g_1, g_2, g_3)$.

the projection onto the unique block of $T(g_1, g_2, g_3)$ as Q_{g_1,g_2,g_3}. We find that

$$Q_{g_1,g_2,g_3}(I_3 \otimes P_{g_1,g_2})P_{g_1g_2,g_3} = \phi(g_1, g_2, g_3)Q_{g_1,g_2,g_3}(P_{g_2,g_3} \otimes I_1)P_{g_1,g_2g_3} \tag{7.18}$$

From this we see that the reduction procedure is associative up to a phase factor $\phi(g_1, g_2, g_3)$. According to the definition of cocycles in section 7.4.1, we see that $\phi(g_1, g_2, g_3)$ forms a 3-cocycle of group G. That is, $\phi(g_1, g_2, g_3)$ satisfies

$$\frac{\phi(g_2, g_3, g_4)\phi(g_1, g_2g_3, g_4)\phi(g_1, g_2, g_3)}{\phi(g_1g_2, g_3, g_4)\phi(g_1, g_2, g_3g_4)} = 1 \tag{7.19}$$

Let's calculate $\phi(g_1, g_2, g_3)$ explicitly for the group generated by U_{CZX}.

$$\begin{array}{ll} \phi(I,I,I) = 1 & \phi(I,I,CZX) = 1 \\ \phi(I,CZX,I) = 1 & \phi(CZX,I,I) = 1 \\ \phi(I,CZX,CZX) = 1 & \phi(CZX,CZX,I) = 1 \\ \phi(CZX,I,CZX) = 1 & \phi(CZX,CZX,CZX) = -1 \end{array} \tag{7.20}$$

We can check that ϕ is indeed a 3-cocycle. The last term shows a nontrivial -1. This minus one cannot be removed by redefining the phase of P_{g_1,g_2} in any way. Therefore ϕ corresponds to a nontrivial 3-cocycle for the Z_2 group.

What does this nontrivial mathematical structure imply about the physics of the CZX model? In the next section we are going to answer this question by proving that MPUO related to a nontrivial 3-cocycle cannot have a short range entangled symmetric state. That is, the boundary of the CZX model cannot have a gapped symmetric ground state. It either breaks the symmetry or is gapless.

7.1.5 Nontrivial 3-cocycle of MPUO and nonexistence of SRE symmetric state

In this section we will show that a symmetry defined by a MPUO on a 1D chain can have a SRE symmetric state only if the MPUO corresponds to a trivial 3-cocycle. Therefore, the boundary of the CZX model must be gapless or have symmetry breaking. For this proof, we will be using the matrix product state representation of SRE states.

Suppose that the symmetry on a 1D chain is represented by tensors $T^{i,i'}_{\alpha,\beta}(g)$. WLOG, $T(g)$ is single-blocked and in the canonical form as defined in section 7.4.3. Assume that it

has a SRE symmetric state represented by matrices $A^i_{\lambda,\eta}$ which is also single-blocked and in the canonical form. For a review of matrix product state formalism including its canonical form and single-block property see section 7.4.2.

Based on the result in [PGVWC07] and [PGWS+08] we can show that (see section 7.4.3)

$$A^i = V^\dagger(\sum_{i'} T^{i,i'}(g)A^{i'})V \tag{7.21}$$

where $V^\dagger V = I$ and V is unique on the single block of $\sum_{i'} T^{i,i'}(g)A^{i'}$ up to phase. This is saying that we can reduce the MPS obtained from $\sum_{i'} T^{i,i'}(g)A^{i'}$ back to the original form A^i by applying $V^\dagger$ and V to the left and right of the matrices respectively. See Fig. 7-5.

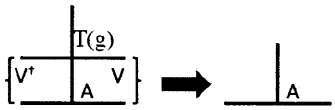

Figure 7-5: Reduction of the combination of $T(g)$ and A into A. Here $T^{i,i'}(g)$ is a MPUO, A^i is a matrix product state symmetric under $T^{i,i'}(g)$.

For a fixed representation of the SRE state A^i and fixed representation of the MPUO symmetry $T(g)$, V is fixed up to phase. We can pick a particular choice of phase for V.

Now we consider the combined operation of $T(g_1)$ and $T(g_2)$ on A. See Fig.7-6.

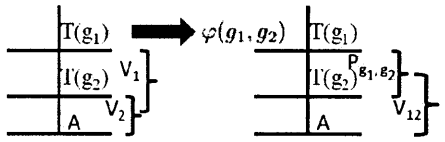

Figure 7-6: Two ways of reducing the combination of $T(g_2)$, $T(g_1)$ and A into A. Only the right projection operators are shown. Their combined actions differ by a phase factor $\varphi(g_1, g_2)$.

We can either first combine $T(g_2)$ and A and then combine $T(g_1)$ and A or first combine $T(g_1)$ and $T(g_2)$ and then combine $T(g_1g_2)$ and A. The right projection operator for these two methods differ by a phase factor $\varphi(g_1, g_2)$. This phase factor can be arbitrarily changed by changing the phase of P_{g_1,g_2}. For following discussions, we fix the phase of P_{g_1,g_2} and hence $\varphi(g_1, g_2)$.

This is all the freedom we can have. If we are to combine three or more T's with A, different reduction methods differ by a phase factor but the phase factor are all determined by $\varphi(g_1, g_2)$. Consider the situation in Fig. 7-7, where we are to combine $T(g_3)$, $T(g_2)$ and $T(g_1)$ with A.

To change the reduction procedure in Fig.7-7(a) to that in Fig.7-7(c), we can either go through step (b) or steps (d) and (e). If we go through step (b), the phase difference in the right projection operators is

$$\varphi^{-1}(g_1g_2, g_3)\varphi^{-1}(g_1, g_2) \tag{7.22}$$

On the other hand, if we go through steps (d) and (e), the phase difference in the right

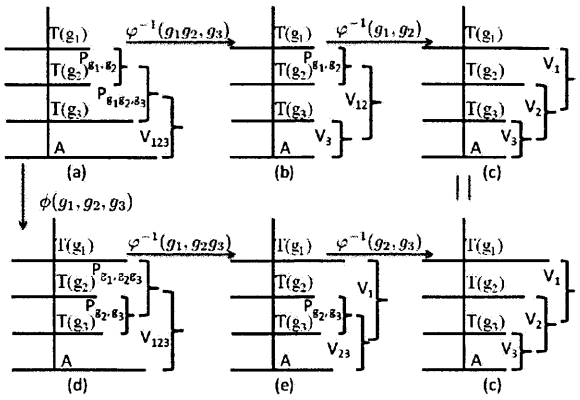

Figure 7-7: Different ways of reducing the combination of $T(g_3)$, $T(g_2)$, $T(g_1)$ and A into A. Only the right projection operators are shown. Their combined actions differ by a phase factor written on the arrow.

projection operators is

$$\phi(g_1, g_2, g_3)\varphi^{-1}(g_1, g_2g_3)\varphi^{-1}(g_2, g_3) \tag{7.23}$$

But these two procedures should be equivalent as the initial and final configurations are the same whose phases have been fixed previously. Therefore, we find that

$$\phi(g_1, g_2, g_3) = \frac{\varphi(g_1, g_2g_3)\varphi(g_2, g_3)}{\varphi(g_1g_2, g_3)\varphi(g_1, g_2)} \tag{7.24}$$

and $\phi(g_1, g_2, g_3)$ must be a trivial 3-cocycle (see Eq. 7.66).

This finishes the proof that: *A 1D system with symmetry defined by matrix product unitary operators can have a gapped symmetric ground state only if the matrix product unitary operator corresponds to a trivial 3-cocycle.*

Because we have shown that the symmetry on the boundary of the CZX model corresponds to a nontrivial 3-cocycle of the Z_2 group, the system with boundary cannot have a gapped symmetric ground state. This shows that the CZX model has nontrivial SPT order protected by on-site Z_2 symmetry as we have promised in section 7.1.2.

7.2 Systematic construction of SPT phases in two and higher dimensions

The construction of the CZX model signifies the close relation between SPT phases and nontrivial cocycles of the symmetry group. This idea is not limited to two dimensional systems. In this section, we generalize the formalism and construct nontrivial SPT phases in any d dimension with on-site unitary and anti-unitary symmetries G based on $(d+1)$-cocycles of G. We expect that this construction gives a complete classification of d-dimensional SPT phases.

In section 7.2.1, we first argue that the plaquette structure in the ground state of the CZX model is actually generic in short range entangled states. Then based on this structure, we construct SPT phases from group cocycles for interacting bosonic systems in any dimension

and with any symmetry by giving their Hamiltonian, ground state and symmetry action, as we did in the last section. The SPT orders in these models are hence established in a similar way as the CZX model. In section 7.2.2, we take a different point of view and construct the path integral of these systems using group cocycle. Such a construction makes explicit how the SPT phase emerges from topological terms in the path integral and shows the close relation between our construction and nonlinear sigma models. Also we will show that the Hamiltonian and Lagrangian formulations are equivalent.

7.2.1 Construction of SPT phases in Hamiltonian formulation

Generic structure of SRE ground states

Consider a short range entangled ground state. By definition in Chapter 5, a short range entangled state is one that can be mapped to a product state with local unitary transformations, either in the form of finite time local unitary evolution or finite depth quantum circuit. If the system under consideration has certain symmetry, then the local unitary transformation must preserve the symmetry and it is possible that under this constraint a short range entangled state cannot be be totally disentangled. In one dimension, we have seen that all short range entangled states can be reduced to a dimer form, even under symmetry constraint, but it is not always possible to disentangle the dimers without breaking symmetry. In higher dimensions, we expect that similar conclusions can be drawn that all short range entangled states can be reduced to a product of local few-body entangled states without breaking the symmetry. Whether the local few-body entanglement can be further removed depends on the SPT order in the state. We do not have a rigorous proof of this fact as in 1D, but we will show that there is strong intuitive reason to believe that this is true.

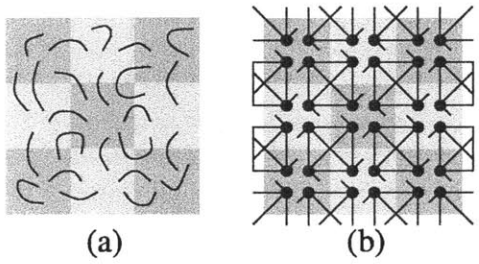

Figure 7-8: Transforming a SRE state to a tensor-network state which take simple canonical form. (a) A SRE state. (b) Using the unitary transformations that act within each block, we can transform the SRE state to a tensor-network state. Entanglements exist only between the degrees of freedom on the connected tensors.

Consider a 2D state with short range entanglement. If the system has certain on-site symmetry, then the degrees of freedom on each site should form a representation of the symmetry. First group sites together and divide our system into patches of size l as in Fig. 7-8a. The degrees of freedom in each patch should still form representations of the symmetry. If l is large enough, entanglement only exists between regions that share an edge or a corner. In this case, we can use LU transformation to transform the state in Fig. 7-8a into a state with many unentangled regions (see Fig. 7-8b). For example, some degrees of

freedom in the middle square in Fig. 7-8a may be entangled with the degrees of freedom in the three squares below, to the right, and to the lower-right of the middle square. We can use the LU transformation inside the middle square to move all those degrees of freedom to the lower-right corner of the middle square. Similarly, we can use the LU transformation to move all the degrees of freedom that are entangled with the three squares below, to the left, and to the lower-left of the middle square to the lower-left corner of the middle square, etc. Repeat such operation to every square and we obtain a state described by Fig. 7-8b. For stabilizer states, such reduction procedure has been established explicitly.[3] Note that the process of moving degrees of freedom around within a patch does not affect the on-site symmetry acting on the patch. Therefore, after the reduction procedure, the state is till symmetric under the on-site symmetry acting on each patch. One possible intermediate step involved in the reduction is to project the degrees of freedom on each patch to the support space on the patch. This does not break the on-site symmetry of the system as the support space on each patch in a symmetric state should always form a representation of the on-site symmetry.

After the reduction, we have a state as shown in Fig. 7-8b, which is a graphic representation of a tensor-network description of the state. In the graphic representation, a dot with n legs represents a rank n tensor. If two legs are connected, the indexes on those legs will take the same value and are summed over. In the tensor-network representation of states, we can see the entanglement structure. The disconnected parts of tensor-network are not entangled. In particular, the tensor-network state Fig. 7-8b is a direct product state of local entangled plaquette states. The four degrees of freedom in a patch form a representation of the on-site symmetry although each one of them may not be.

If there is no symmetry, we can further decompose the plaquettes into product states. But with symmetry, we might not be able to simplify the state further. We will take this plaquette structure as the canonical form of 2D SRE states and use it as the starting point for our construction of generic SPT phases. We would like to point out that although in Fig. 7-8b, we only present a 2D tensor-network state in canonical form, a similar reduction can be done in any dimensions. In general dimensions, the canonical form of SRE states is a product of local entangled cubes shared between neighboring sites.

It is strange to think that different SPT phases can all be constructed out of states with the same structure. One may ask, if the ground states of two systems have the same structure, wouldn't their physical property also be the same and hence be in the same phase? The answer to this question is yes only if symmetry in the two systems acts in the same way. If symmetry acts differently, even systems with the same ground state can have very different response to the symmetry and hence be in different phases.

The transverse Ising model provides a good example. Consider a system with ground state $|\uparrow\uparrow ... \uparrow\rangle$. If symmetry acts as spin flip $\uparrow\to\downarrow$ and $\downarrow\to\uparrow$, then this ground state breaks the symmetry and therefore the system is in a symmetry breaking phase. On the other hand, if the symmetry acts as $\uparrow\to\uparrow$ and $\downarrow\to -\downarrow$, which is again a Z_2 symmetry, then the ground state is symmetric and the system is in a symmetric phase. The difference between the two symmetries is just a change of basis from σ_z basis to σ_x basis. Without knowing exactly how the symmetry acts, the ground state alone cannot tell us which phase the system is in. On the other hand, starting from the same ground state and putting different symmetry requirements on the system could result in different phases.

We will attempt to do the same for SPT phases in the following sections. We will

[3] private communication with Sergey Bravyi

start with SRE ground states all in the same canonical form $|\Psi_{\text{pSRE}}\rangle$, put different on-site symmetry constraints on the system and find out which SPT phase they lead to. The on-site symmetry is designed such that the ground state is invariant under the symmetry

$$\otimes_i U^i |\Psi_{\text{pSRE}}\rangle = |\Psi_{\text{pSRE}}\rangle \tag{7.25}$$

hence we are focusing on the topological phases. In the following, we are going to construct solutions to this equation using the cocycles of the symmetry group. We will start from the 1D case where we already know what the SPT phases look like, from Chapter 6.

1+1D case

Let us discuss the 1D case first. We will choose the 1D SPT wave function to have a fixed form of a "dimer crystal" (see Fig. 7-9):

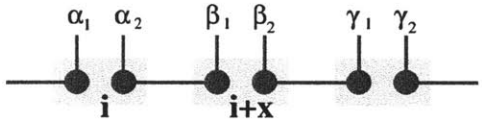

Figure 7-9: The canonical tensor network representation for 1D SRE state $|\Psi_{\text{pSRE}}\rangle$. The two dots in each rectangle represent a physical site.

$$|\Psi_{\text{pSRE}}\rangle = ... \otimes (\sum_{g\in G} |\alpha_2 = g, \beta_1 = g\rangle) \otimes (\sum_{g\in G} |\beta_2 = g, \gamma_1 = g\rangle) \otimes ... \tag{7.26}$$

where we have assumed that physical states on each dot in Fig. 7-9 are labeled by the elements of the symmetry group G: $\alpha_i, \beta_i \in G$. The dimmer in Fig. 7-9 corresponds to a maximally entangled state $\sum_{g\in G} |\alpha_2 = g, \beta_1 = g\rangle$.

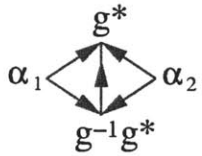

Figure 7-10: The graphic representation of Eq. (7.28). $f_2(\alpha_1, \alpha_2, g, g^*)$ is represented by the polygon with a branching structure as represented by the arrows on the edge which never form a oriented loop on any triangle. $\nu_2(\alpha_1, g^{-1}g^*, g^*)$ and $\nu_2(\alpha_2, g^{-1}g^*, g^*)$ are represented by the two triangles as in Fig. 7-21a. The value of the cocycle ν_2 on a triangle (say $\nu_2(\alpha_1, g^{-1}g^*, g^*)$) can be viewed as flux going through the corresponding triangle.

Next, we need to choose an on-site symmetry transformation Eq. (7.25) such that the state $|\Psi_{\text{pSRE}}\rangle$ is invariant (where the two dots in each shaded box represent a site). We note that $U^i(g)$ acts on the states on the i site which are linear combinations of $|\alpha_1, \alpha_2\rangle$ in Fig. 7-9. Note that $\alpha_1, \alpha_2 \in G$. So we can choose the action of $U^i(g)$ to be (see Fig. 7-10)

$$U^i(g)|\alpha_1, \alpha_2\rangle = f_2(\alpha_1, \alpha_2, g, g^*)|g\alpha_1, g\alpha_2\rangle \tag{7.27}$$

where $f_2(\alpha_1, \alpha_2, g, g^*)$ is a phase factor $|f_2(\alpha_1, \alpha_2, g, g^*)| = 1$. We will use a 2-cocycle $\nu_2 \in \mathcal{H}^2[G, U_T(1)]$ for the symmetry group G to construct the phase factor f_2. (A discussion of the group cocycles is given in the section 7.4.1.)

Using a 2-cocycle ν_2, we construct the phase factor f_2 as the follows (see Fig. 7-10):

$$f_2(\alpha_1, \alpha_2, g, g^*) = \frac{\nu_2(\alpha_1, g^{-1}g^*, g^*)}{\nu_2(\alpha_2, g^{-1}g^*, g^*)}. \tag{7.28}$$

Here g^* is a fixed element in G. For example we may choose $g^* = 1$. In section 7.4.4, we will show that $U^i(g)$ defined above is indeed a linear representation of G that satisfies Eq. (7.25). In this way, we obtain a SPT phase described by $|\Psi_{\text{pSRE}}\rangle$ that transforms as $U^i(g)$.

Note that here we only discussed a fixed SRE wave function. If we choose different cocycles in Eq. (7.28), the same wave function Eq. (7.26) can indeed represent different phases. One may wonder how a fixed SRE wave function can represent different quantum phases.

To see this, let us examine how the state varies under the symmetry group. Notice that the phase factor $f_2(\alpha_1, \alpha_2, g, g^*)$ is factorized on the two dots and the basis $|\alpha_1\rangle$ of one dot varies as

$$M(g)|\alpha_1\rangle = \nu_2(\alpha_1, g^{-1}g^*, g^*)|g\alpha_1\rangle. \tag{7.29}$$

The states $|\alpha_1\rangle$ form a representation of G itself, and the operator g transforms a state into another. The representation matrix element is given as $M(g)_{\alpha_1, g\alpha_1} = \nu_2(g^{-1}g^*, g^*, \alpha_1)$, and eqn.(7.28) can be rewritten as $f_2(\alpha_1, \alpha_2, g, g^*) = M(g)_{\alpha_1, g\alpha_1}[M(g)_{\alpha_2, g\alpha_2}]^\dagger$. From eqn.(7.27) we have $U^i(g) = M(g) \otimes [M(g)]^\dagger$. Actually, this matrix $M(g)$ is a projective representation of the group G, corresponding to the 2-cocycle ν_2.

Different classes of cocycles ν_2 correspond to different projective representations. In the trivial case, where $\nu_2(\alpha_1, g^{-1}g^*, g^*) = 1$, $M(g)$ can be reduced into linear representations, and the corresponding SPT phase is a trivial phase.

We will also show, in section 7.4.4, that on a finite segment of chain, the state $|\Psi_{\text{pSRE}}\rangle$ has low energy excitations on the chain end. The excitations on one end of the chain form a projective representation described by the same cocycle ν_2 that is used to construct the solution $U^i(g)$. The end states and their projective representation describe the universal properties of bulk SPT phase.

The different solutions of Eq. (7.25) constructed from different 2-cocycles do not always represent different SPT phases. If $\nu_2(g_0, g_1, g_2)$ satisfies Eq. (7.67) and Eq. (7.76), then

$$\nu_2'(g_0, g_1, g_2) = \nu_2(g_0, g_1, g_2)\frac{\mu_1(g_1, g_2)\mu_1(g_0, g_1)}{\mu_1(g_0, g_2)} \tag{7.30}$$

also satisfies Eq. (7.67) and Eq. (7.76), for any $\mu_1(g_0, g_1)$ satisfying $\mu_1(gg_0, gg_1) = \mu_1^{s(g)}(g_0, g_1)$, $g \in G$. So $\nu_2'(g_0, g_2, g_3)$ also gives rise to a solution of Eq. (7.25). But the two solutions constructed from $\nu_2(g_0, g_1, g_2)$ and $\nu_2'(g_0, g_1, g_2)$ are related by a symmetric LU transformations (for details, see discussion near the end of section 7.4.3). They are also smoothly connected since we can smoothly deform $\mu_1(g_0, g_1)$ to $\mu_1(g_0, g_1) = 1$. So we say that the two solutions obtained from $\nu_2(g_0, g_2, g_3)$ and $\nu_2'(g_0, g_2, g_3)$ are equivalent. We note that $\nu_2(g_0, g_2, g_3)$ and $\nu_2'(g_0, g_2, g_3)$ differ by a 2-coboundary $\frac{\mu_1(g_1, g_2)\mu_1(g_0, g_1)}{\mu_1(g_0, g_2)}$. So the set of equivalence classes of

$\nu_2(g_0, g_2, g_3)$ is nothing but the cohomology group $\mathcal{H}^2[G, U_T(1)]$. Therefore, the different SPT phases are classified by $\mathcal{H}^2[G, U_T(1)]$, which reproduces the result we had in Chapter 6.

We see that, in our approach here, the different SPT phases are not encoded in the different wave functions, but encoded in the different symmetry transformations $U^i(g)$.

Finally, a symmetric gapped Hamiltonian can be easily constructed for the ground state, which is a sum of commuting projectors onto the dimers

$$H = -\sum_i (\sum_{g\in G} |g, g\rangle_{i,i+1})(\sum_{g\in G} {}_{i,i+1}\langle g, g|) \tag{7.31}$$

(2+1)D case

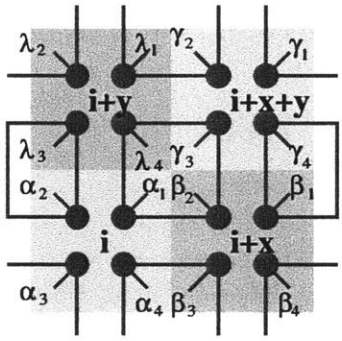

Figure 7-11: The canonical tensor network representation for 2D SRE state $|\Psi_{\text{pSRE}}\rangle$. The four dots in each square represent a physical site.

The above discussion and result can be generalized to higher dimensions. Here we will discuss 2D SPT state as an example. We choose the 2D SPT state to be a "plaquette state" (see Fig. 7-11)

$$|\Psi_{\text{pSRE}}\rangle = \otimes_{\text{squares}}(\sum_{g\in G} |\alpha_1 = g, \beta_2 = g, \gamma_3 = g, \lambda_4 = g\rangle) \tag{7.32}$$

where we have assumed that physical states on each dot in Fig. 7-11 are labeled by the elements of the symmetry group G: $\alpha_i, \beta_i, ... \in G$. The four dots in a linked square in Fig. 7-11 form a maximally entangled state $\sum_{g\in G} |\alpha_1 = g, \beta_2 = g, \gamma_3 = g, \lambda_4 = g\rangle$. We require that the state $|\Psi_{\text{pSRE}}\rangle$ is invariant under an on-site symmetry transformation Eq. (7.25) (where the four dots in each shaded square represent a site).

To construct an on-site symmetry transformation Eq. (7.25), in 2 dimensions, the action of U^i is chosen to be

$$U^i(g)|\alpha_1, \alpha_2, \alpha_3, \alpha_4\rangle = f_3(\alpha_1, \alpha_2, \alpha_3, \alpha_4, g, g^*)|g\alpha_1, g\alpha_2, g\alpha_3, g\alpha_4\rangle. \tag{7.33}$$

Here $f_3(\alpha_1, \alpha_2, \alpha_3, \alpha_4, g, g^*)$ is a phase factor that corresponds to the value of a 3-cocycle

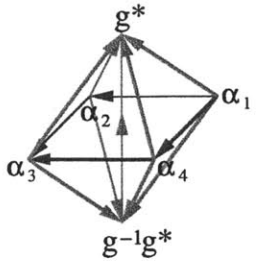

Figure 7-12: The graphic representation of the phase factor $f_3(\alpha_1, \alpha_2, \alpha_3, \alpha_4, g, g^*)$ in Eq. (7.33). The arrows on the edges that never form a oriented loop on any triangle represent the branching structure on the complex. The four tetrahedrons give rise to $\nu_3(\alpha_1, \alpha_2, g^{-1}g^*, g^*)$, $\nu_3(\alpha_2, \alpha_3, g^{-1}g^*, g^*)$, $\nu_3^{-1}(\alpha_4, \alpha_3, g^{-1}g^*, g^*)$, and $\nu_3^{-1}(\alpha_1, \alpha_4, g^{-1}g^*, g^*)$

$\nu_3 \in \mathcal{H}^3[G, U_T(1)]$ evaluated on the complex with a branching structure in Fig. 7-12:

$$f_3(\alpha_1, \alpha_2, \alpha_3, \alpha_4, g, g^*) = \frac{\nu_3(\alpha_1, \alpha_2, g^{-1}g^*, g^*)\nu_3(\alpha_2, \alpha_3, g^{-1}g^*, g^*)}{\nu_3(\alpha_4, \alpha_3, g^{-1}g^*, g^*)\nu_3(\alpha_1, \alpha_4, g^{-1}g^*, g^*)}. \tag{7.34}$$

In section 7.4.5, we will show that $U^i(g)$ defined above is indeed a linear representation of G that satisfies Eq. (7.25). We will also show that (see section 7.4.6 and [CLW11]) *in a basis where the many-body ground state is a simple product state, although $\otimes_i U^i(g)$ is an on-site symmetry transformation when acting on the bulk state, it cannot be an on-site symmetry transformation when viewed as a symmetry transformation acting on the effective low energy degrees of freedom on the boundary when the 3-cocycle ν_3 is non-trivial.*

In section 7.4.6 we show that the effective symmetry action on the boundary can again be written as a matrix product unitary operator, like in the CZX model, whose transformation is related to the 3-cocycle ν_3. As shown in section 7.1, if ν_3 is nontrivial, the boundary must be gapless if symmetry is not broken, hence proving the non-trivialness of the SPT order in the state. On the other hand, different classes of 3-cocycles cannot smoothly change into each other, hence lead to different SPT phases. Therefore, in our construction, there is a one to one correspondence between equivalence classes of 3-cocycles in $\mathcal{H}[G, U(1)]$ and SPT phases in 2D bosonic systems.

The Hamiltonian of the system can be constructed in a similar way as in the CZX model to be a sum of commuting projectors onto each plaquette. We will not repeat it here.

This construction from $|\Psi_{\text{pSRE}}\rangle$ and group cocycles to SPT phases works generically in any dimension.

7.2.2 Construction of SPT phases in Lagrangian formulation

In this section, we are going to present the Lagrangian formulation of our construction of SPT phases. As we will show, it is equivalent to the Hamiltonian formulation, yet simpler in presentation.

Fixed point action amplitude from group cocycles

The field theory approach[AS06] to topological phases is to write down the imaginary time path integral over the $d+1$ dimensional field configuration $\boldsymbol{n}(\boldsymbol{x},\tau)$ of the system.

$$Z = \int D\boldsymbol{n}\ \mathrm{e}^{-\int \mathrm{d}^d\boldsymbol{x}\mathrm{d}\tau\ \mathcal{L}[\boldsymbol{n}(\boldsymbol{x},\tau)]}. \tag{7.35}$$

where $\mathcal{L}[\boldsymbol{n}(\boldsymbol{x},\tau)]$ is the Lagrangian density of the system. As we will be interested in gapped quantum phases with finite correlation length, the low energy effective description of the system should not depend on a particular length or energy scale. Therefore, the fixed point action

$$S = \int \mathrm{d}^d\boldsymbol{x}\mathrm{d}\tau\ \mathcal{L}_{\text{fix}}[\boldsymbol{n}(\boldsymbol{x},\tau)] \tag{7.36}$$

or equivalently its exponential, which we call the action amplitude

$$\mathrm{e}^{-\int \mathrm{d}^d\boldsymbol{x}\mathrm{d}\tau\ \mathcal{L}_{\text{fix}}[\boldsymbol{n}(\boldsymbol{x},\tau)]} \tag{7.37}$$

should not depend on space-time metric. Such a quantum field theory is called topological.

A trivial topological phase is described by $\mathcal{L}_{\text{fix}}[\boldsymbol{n}(\boldsymbol{x},\tau)] = 0$, while in general $\mathcal{L}_{\text{fix}}[\boldsymbol{n}(\boldsymbol{x},\tau)]$ can be nonzero. One possible form of of a nonzero fixed point Lagrangian $\mathcal{L}_{\text{fix}}[\boldsymbol{n}(\boldsymbol{x},\tau)]$ giving rise to metric independent action amplitude $\mathrm{e}^{-\int \mathrm{d}^d\boldsymbol{x}\mathrm{d}\tau\ \mathcal{L}_{\text{fix}}[\boldsymbol{n}(\boldsymbol{x},\tau)]}$ is the topological θ term in non-linear sigma models, where the action amplitude only depends on the mapping class from the space-time manifold to the target manifold that $\boldsymbol{n}$ lives in. Note that such a topological θ term requires both continuous space-time manifold and continuous target manifold.

On the other hand, we are considering quantum disordered states that do not break any symmetry. So the field $\boldsymbol{n}(\boldsymbol{x},\tau)$ fluctuates strongly at all length scale. The low energy effective theory has no smooth continuum limit. Therefore, the low energy effective theory must be one defined on discrete space-time. For discrete space-time, we no longer have non-trivial mapping class from space-time to target manifold, and we no longer have topological θ-term in their usual form. In this section we will show that we can define a new topological θ term on discrete space time.

This new term is similar to the usual topological θ term in non-linear sigma models in the following ways

1. It is a fixed point term in the sense that the action amplitude does not change under renormalization transformations of the (discrete) space-time
2. The term has a symmetry as we are describing topological phases in systems with symmetry

It is also very different from the usual topological θ term in non-linear sigma models

1. It is defined on discrete space time
2. Its field (on each discrete space time point) takes value in the full symmetry group $g \in G$
3. It applies to discrete group G also.
4. The action amplitude on a closed manifold is always equal to 1 or 'quantized'

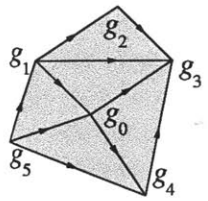

Figure 7-13: The graphic representation of the action-amplitude $\mathrm{e}^{-S(\{g_i\})}$ on a 1+1D complex with a branching structure represented by the arrows on the edge. The vertices of the complex are labeled by i. Note that the arrows never form a loop on any triangle.

Because of these, we call this term the 'quantized topological θ term' on discrete space-time.

More specifically, we discretize the space-time into a complex with a branching structure (such as the complex obtained by a triangularization of the space-time manifold, see Fig. 7-13 for example). The path integral then can be rewritten as

$$Z = |G|^{-N_v} \sum_{\{g_i\}} \mathrm{e}^{-S(\{g_i\})}$$
$$\mathrm{e}^{-S(\{g_i\})} = \prod_{\{ij...k\}} \nu_{1+d}^{s_{ij...k}}(g_i, g_j, ..., g_k) \tag{7.38}$$

Here on each vertex of the space-time complex, we have a $g_i \in G$. g_i corresponds to the field $\boldsymbol{n}(\boldsymbol{x}, t)$ and $\sum_{\{g_i\}}$ corresponds to the path integral $\int D\boldsymbol{n}$ in the continuous non-linear σ-model. $|G|$ is the number of elements in G, N_v is the number of vertices in the complex. $\mathrm{e}^{-S(\{g_i\})}$ is the action-amplitude on the discretized space-time that corresponds to $\mathrm{e}^{-\int \mathrm{d}^d\boldsymbol{x}\,\mathrm{d}\tau\, \mathcal{L}[\boldsymbol{n}(\boldsymbol{x},\tau)]}$ of the continuous non-linear σ-model, and $\nu_{1+d}^{s_{ij...k}}(g_i, g_j, ..., g_k)$ corresponds to the action-amplitude $\mathrm{e}^{-\int_{(i,j,...,k)} \mathrm{d}^d\boldsymbol{x}\,\mathrm{d}\tau\, \mathcal{L}[\boldsymbol{n}(\boldsymbol{x},\tau)]}$ on a single simplex $(i, j, ..., k)$. Also, $s_{ij...k} = \pm 1$ depending on the orientation of the simplex.

The requirement that this topological term be quantized(equal to 1 on closed manifold) translates to

$$\prod_{\{ij...k\}} \nu_{1+d}^{s_{ij...k}}(g_i, g_j, ..., g_k) = 1 \tag{7.39}$$

on every closed space-time complex without boundary. As we will show, this is satisfied by cocycles which satisfy the condition given by Eqn. 7.74.

For example, in 1+1D, the quantization condition on action amplitude is given by

$$\mathrm{e}^{-S(\{g_i\})} = \prod_{\{ijk\}} \nu_2^{s_{ijk}}(g_i, g_j, g_k) = 1 \tag{7.40}$$

on closed space-time complex without boundary, in particular, on a tetrahedron with four triangles (see Fig. 7-21):

$$\mathrm{e}^{-S(\{g_i\})} = \prod_{\{ijk\}} \nu_2^{s_{ijk}}(g_i, g_j, g_k) = \frac{\nu_2(g_1, g_2, g_3)\nu_2(g_0, g_1, g_3)}{\nu_2(g_0, g_1, g_2)\nu_2(g_0, g_2, g_3)} = 1 \tag{7.41}$$

which is exactly the cocycle condition in Eqn. 7.75. Putting the tetrahedrons together we find that Eqn. 7.40 is satisfied for arbitrary closed surface. Similar equality holds in higher dimensions.

Therefore, by putting cocycles $\nu_{d+1}(g_0, g_1 ... g_{d+1})$ onto the simplexes of the discrete space time and multiply them together, we obtain the quantized topological θ term on discrete space time.

We need to verify that the path integral written in this way is symmetric under the symmetry group G and is a fixed point under renormalization transformation. First note that (see Eqn. 7.67)

$$\nu_{d+1}^{s(g)}(g_0, g_1, ..., g_{d+1}) = \nu_{d+1}(gg_0, gg_1, ..., gg_{d+1}), g \in G \tag{7.42}$$

therefore,

$$\begin{aligned} e^{-S(\{g_i\})} &= e^{-S(\{gg_i\})}, \text{ if } g \text{ contains no T} \\ \left(e^{-S(\{g_i\})}\right)^\dagger &= e^{-S(\{gg_i\})}, \text{ if } g \text{ contains one T} \end{aligned} \tag{7.43}$$

where T is the time-reversal transformation. This guarantees the symmetry of the path integral.

The fact that Eqn. 7.38 gives a fixed point action amplitude can be seen from the cocycle condition Eqn. 7.74. The cocycle condition leads to a renormalization flow in the discrete space time. For example in 1+1D, from the geometrical picture of the cocycles (see Fig.

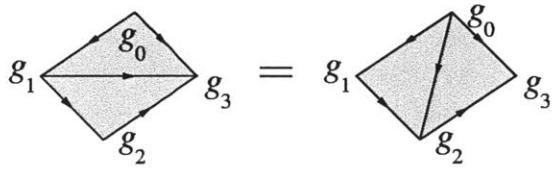

Figure 7-14: Graphic representation of $\nu_2(g_0, g_1, g_2)\nu_2(g_0, g_2, g_3) = \nu_2(g_1, g_2, g_3)\nu_2(g_0, g_1, g_3)$. The arrows on the edges represent the branching structure.

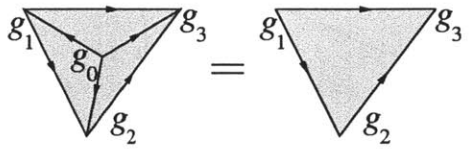

Figure 7-15: Graphic representation of $\nu_2(g_1, g_2, g_3) = \nu_2(g_0, g_1, g_2)\nu_2(g_0, g_2, g_3)\nu_2^{-1}(g_0, g_1, g_3)$. The arrows on the edges represent the branching structure.

7-21), we have the following relations: $\nu_2(g_0, g_1, g_2)\nu_2(g_0, g_2, g_3) = \nu_2(g_1, g_2, g_3)\nu_2(g_0, g_1, g_3)$ (see Fig. 7-14) and $\nu_2(g_1, g_2, g_3) = \nu_2(g_0, g_1, g_2)\nu_2(g_0, g_2, g_3)\nu_2^{-1}(g_0, g_1, g_3)$. (see Fig. 7-15). We can use those two basic moves to generate a renormalization flow that induces a coarse-grain transformation of the complex. The two relations Fig. 7-14 and Fig. 7-15 imply that the action-amplitude is invariant under the renormalization flow. In 2+1D, the

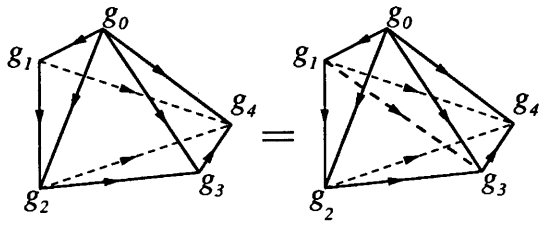

Figure 7-16: Two solid tetrahedrons $g_0g_1g_2g_4$, $g_0g_2g_3g_4$ and three solid tetrahedrons $g_0g_1g_2g_3$, $g_0g_1g_3g_4$, $g_1g_2g_3g_4$ occupy the same volume, which leads to the graphic representation of $\nu_3(g_0,g_1,g_2,g_4)\nu_3(g_0,g_2,g_3,g_4) = \nu_3(g_0,g_1,g_2,g_3)\nu_3(g_0,g_1,g_3,g_4)\nu_3(g_1,g_2,g_3,g_4)$ (see Eq. (7.77)). The arrows on the edges represent the branching structure.

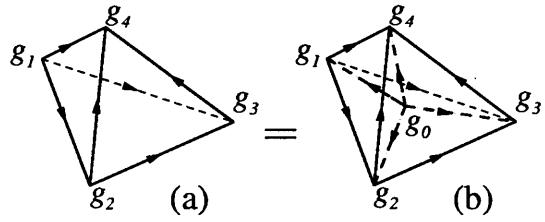

Figure 7-17: One solid tetrahedron $g_1g_2g_3g_4$, and four solid tetrahedrons $g_0g_1g_2g_4$, $g_0g_2g_3g_4$, $g_0g_1g_3g_4$, $g_1g_1g_2g_3$ occupy the same volume, which leads to the graphic representation of $\nu_3(g_1,g_2,g_3,g_4) = \nu_3(g_0,g_1,g_2,g_4)\nu_3(g_0,g_2,g_3,g_4)\nu_3^{-1}(g_0,g_1,g_3,g_4)\nu_3^{-1}(g_0,g_1,g_2,g_3)$ (see Eq. (7.77)). The arrows on the edges represent the branching structure.

conditions of 3-cocycle lead to the two relations in Fig. 7-16 and Fig. 7-17. These lead to a renormalization flow of the complex in which the action-amplitude is again a fixed-point action-amplitude. Similar arguments hold in higher dimensions.

To summarize, with cocycles ν_{d+1} of group G, we can write a quantized topological θ term on discrete $d+1$ dimensional space time. The action amplitude is symmetric under the action of G, a fixed point under renormalization flow and is always equal to 1 on a closed manifold. When the space-time complex has a boundary, the action-amplitude will not always be equal to 1 and is not trivial. We note that, due to the cocycle condition on $\nu_{1+d}^{s_{ij...k}}(g_i, g_j, ..., g_k)$, such an action-amplitude will only depend on g_i's on the boundary of the space-time complex. Thus such an action-amplitude can be viewed as an action-amplitude of the boundary theory but defined on an extended space, which is a generalization of the WZW topological term for continuous non-linear σ-models to discrete non-linear σ-models.

From fixed point action amplitude to ground state wave function

So what kind of phases do these topological terms represent? We will find out about this from the ground state wave-function. In particular, we will find the ground state wave-function from the quantized topological θ term and see

1. The ground state is symmetric and short range entangled, therefore the quantized topological θ term describes a SPT phase.

2. Cocycles in the same class represent the same SPT phase; Cocyles in different classes represent different SPT phases.

3. The wave-function is (under a duality transformation) the same as the canonical form we used in the Hamiltonian formulation, therefore the two formulations are equivalent.

The ground state wave-function can be obtained from imaginary time evolution from time $-\infty$ until time 0. In our formulation, this is equivalent to imaginary time path integral on a space-time geometry with a boundary (at time 0). Denote the boundary manifold as M and the whole manifold as M_{ext}. As we are considering a fixed point path integral, it does not matter how big the interior of M_{ext} is and we can reduce it, for example, to just one point as shown in Fig. 7-18 for 1+1D systems.

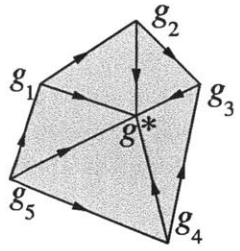

Figure 7-18: The graphic representation of Eq. (7.44). The boundary is the complex M, and the whole complex M_{ext} is an extension of M.

To obtain the ground state wave function, we fix the degrees of freedom on M and choose an arbitrary configuration for degrees of freedom in the interior of M_{ext}.

$$\Psi_M(\{g_i\}_M) = \prod_{\{ij...*\}} \nu_{1+d}^{s_{ij...*}}(g_i, g_j, ..., g^*). \tag{7.44}$$

where $\{g_i\}_M$ are on the vertices on M and g^* is on the vertex inside the complex M_{ext}. Also $\prod_{\{ij...*\}}$ is product over all simplices on M_{ext}. The state on M (the boundary of Fig. 7-18) does not depend on the choice of g^*.

Using the above expression, we can show that the ground state wave function of our fixed-point model is SRE state with no intrinsic topological orders. Let us first write the ground state of our fixed-point model in a form

$$|\Psi_M\rangle = \sum_{\{g_i\}_M} \prod_{\{ij...*\}} \nu_{1+d}^{s_{ij...*}}(g_i, g_j, ..., g^*)|\{g_i\}_M\rangle, \tag{7.45}$$

where $|\{g_i\}_M\rangle$ form a basis of our model on d-dimensional complex M. The on-site symmetry acts in a simple way:

$$g: \ |\{g_i\}_M\rangle \to |\{gg_i\}_M\rangle, \ g \in G \tag{7.46}$$

As $\prod_{\{ij...*\}} \nu_{1+d}^{s_{ij...*}}(g_i, g_j, ..., g^*) = \prod_{\{ij...*\}} \nu_{1+d}^{s_{ij...*}}(gg_i, gg_j, ..., g^*)$, the ground state is symmetric under the symmetry action.

We note that if we choose the particular form of M_{ext} in Fig. 7-18 to obtain state Φ_M on M, the phase factor $\prod_{\{ij...*\}} \nu_{1+d}^{s_{ij...*}}(g_i, g_j, ..., g^*)$ can be viewed as a LU transformation. We can write $|\Psi_M\rangle$ in a new basis $|\{g_i\}_M\rangle' = \prod_{\{ij...*\}} \nu_{1+d}^{s_{ij...*}}(g_i, g_j, ..., g^*)|\{g_i\}_M\rangle$:

$$|\Psi_M\rangle = \sum_{\{g_i\}_M} |\{g_i\}_M\rangle'. \tag{7.47}$$

The two basis differ by local unitary transformations given by the cocycles. Thus, on any complex M that can be viewed as a boundary of another complex M_{ext}, the state on M can be transformed by an LU transformation into a state that is the equal weight superposition of all possible states $|\{g_i\}_M\rangle$ on M. The wave function in the new bases is very simple, which is actually a product state.

We have used the $(1+d)$-cocycles in $\mathcal{H}^{1+d}[G, U_T(1)]$ to construct our fixed-point models which have ground state wave functions that also depend on the $(1+d)$-cocycles. In the above, we have shown that all those states can be mapped to the same simple product state via LU transformations. Does this mean that those states from different $(1+d)$-cocycles all belong to the same phase? The answer depends on if symmetry is included or not.

If we do not include any symmetry, those states from different $(1+d)$-cocycles indeed all belong to the same trivial phase. Thus our fixed-point states constructed from different $(1+d)$-cocycles all have trivial intrinsic topological order. They can only have nontrivial SPT order.

On the other hand, if we include the on-site symmetry G, states from different $(1+d)$-cocycles belong to the different phases which correspond to different SPT phases. This is because the LU transformation represented by $\prod_{\{ij...*\}} \nu_{1+d}^{s_{ij...*}}(g_i, g_j, ..., g^*)$ is not a symmetric LU transformation under the on-site symmetry G. To see this, we first note that the LU transformation $\prod_{\{ij...*\}} \nu_{1+d}^{s_{ij...*}}(g_i, g_j, ..., g^*)$ contains several layers of non-overlapping terms.

For example, for the (1+1)D system in Fig. 7-18, the LU transformation has two layers

$$\prod_{\{ijk\}} \nu_2(g_i,g_j,g_k) = [\nu_2(g_3,g_2,g^*)\nu_2(g_5,g_4,g^*)]\times \\ [\nu_2(g_2,g_1,g^*)\nu_2(g_4,g_3,g^*)\nu_2(g_1,g_5,g^*)] \tag{7.48}$$

In order for the LU transformation to be a symmetric, each local term, such as $\nu_2(g_2,g_1,g^*)$, must transform as

$$\nu_2^{s(g)}(g_2,g_1,g^*) = \nu_2(gg_2,gg_1,g^*) \tag{7.49}$$

under the on-site symmetry transformation generated by $g \in G$: Although $\nu_2^{s(g)}(g_2,g_1,g^*) = \nu_2(gg_2,gg_1,gg^*)$, in general $\nu_2^{s(g)}(g_2,g_1,g^*) \neq \nu_2(gg_2,gg_1,g^*)$. In fact, only trivial cocycle in $\mathcal{H}^{1+d}[G,U_T(1)]$ can satisfy $\nu_{1+d}^{s(g)}(g_1,g_2,..,g_{1+d},g^*) = \nu_{1+d}(gg_1,gg_2,..,gg_{1+d},g^*)$. Thus the fixed-point states from nontrivial (1+d)-cocycles belong to nontrivial SPT phases. Similarly we can find that fixed point states from cocycles in different classes belong to different SPT phases.

On the other hand, we can show that cocycles within the same equivalence class give rise to the same SPT phase. In particular, consider the ground state wave function $\Psi_M(\{g_i\}_M)$ of a SPT phase is constructed from a cocycle ν_{1+d} as in Eq. (7.44). Let ν'_{1+d} be a cocycle that is equivalent to ν_{1+d}. That is ν_{1+d} and ν'_{1+d} only differ by a coboundary

$$\nu'_{1+d}(g_0,...,g_{1+d}) = \nu_{1+d}(g_0,...,g_{1+d}) \prod_{i=0}^{1+d} \mu_d^{(-)^i}(...,g_i,g_{i+1},...) \tag{7.50}$$

where $\mu_d(g_0,...,g_d)$ is a d-cochain. Then ν'_{1+d} will give rise to a new ground state wave function $\Psi'_M(\{g_i\}_M)$ of a SPT phase. One can show that $\Psi_M(\{g_i\}_M)$ and $\Psi'_M(\{g_i\}_M)$ are related:

$$\Psi'_M(\{g_i\}_M) = \Psi_M(\{g_i\}_M) \prod_{\{ij...\}} \mu_d^{s_{ij...}}(g_i,g_j,...) \tag{7.51}$$

where $\prod_{\{ij...\}}$ multiply over all the d-simplices in M. Note that, when we calculate the wave function $\Psi'_M(\{g_i\}_M)$, the terms $\mu_d(g_i,g_j,...,g^*)$ containing g^* all cancel out. Due to the cochain condition Eq. (7.67) satisfied by μ_d, the factor $\prod_{\{ij...\}} \mu_d^{s_{ij...}}(g_i,g_j,...)$ actually represents a *symmetric* LU transformation. So the two wave functions $\Psi_M(\{g_i\}_M)$ and $\Psi'_M(\{g_i\}_M)$ are connected by symmetric LU transformations and belong to the same SPT phase. Hence equivalent cocycles give rise to the same SPT phase, and different SPT phases are classified by the equivalence classes of cocycles which form $\mathcal{H}^{1+d}[G,U(1)]$.

Finally we will show that the ground state wave function (7.47) in the Lagrangian formalism is dual to the ground state wave function $|\Psi_{\text{pSRE}}\rangle$ (7.26,7.32) in the Hamiltonian formalism discussed in Sec. 7.2.1. Furthermore, after the duality transformation, the the symmetry representations (7.46) are the same as that defined in eqn. (7.27) or Eq. (7.33).

Let us illustrate above result in 1D. Firstly, we introduce the dual transformation which maps a state to its dual wave function living on the dual lattice. In the dual transformation, the bases $|g_i\rangle$ at site i correspond to the bond $|g_i^r, g_{i+1}^l\rangle$ in the dual lattice (see Fig. 7-19), where $g_i^r = g_{i+1}^l = g_i$ and the amplitude of the configuration remains unchanged. In this

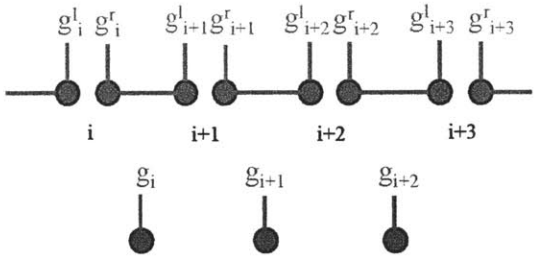

Figure 7-19: (Color online) The dual transformation in the new bases in 1D.

way, we obtain the dual wave function $\Psi_d(\{g_i^l, g_i^r\})$ of $\Psi(\{g_i\})$.

Now we introduce the new bases $|\{g_i^l, g_i^r\}\rangle'$ through the LU transformation introduced in eqn. (7.47),

$$\begin{aligned} |\{g_i^l, g_i^r\}\rangle' &= \prod_i \nu_2(g_i, g_{i+1}, g^*)|\{g_i^l, g_i^r\}\rangle \\ &= \prod_i \nu_2(g_i^r, g_{i+1}^r, g^*)|\{g_i^l, g_i^r\}\rangle \\ &= \prod_i \left[\nu_2(g_{i+1}^l, g_{i+1}^r, g^*)|g_{i+1}^l, g_{i+1}^r\rangle\right] \end{aligned} \tag{7.52}$$

In the new bases, the fixed point state in the dual lattice becomes a direct product of bonds. Notice that the previous local unitary transformation in eqn. (7.47) becomes on-site unitary transformation. Furthermore, in the new bases the symmetry representation also becomes on-site and is fractionalized into two 'projective' operations:

$$\begin{aligned} & \otimes_i U^i(g)|\{g_i^l, g_i^r\}\rangle' \\ = & \prod_i \nu_2(g_{i+1}^l, g_{i+1}^r, g^*)|\{gg_{i+1}^l, gg_{i+1}^r\}\rangle \\ = & \prod_i \frac{\nu_2(g_{i+1}^l, g_{i+1}^r, g^*)}{\nu_2(g_{i+1}^l, g_{i+1}^l, g^{-1}g^*)}|\{gg_{i+1}^l, gg_{i+1}^r\}\rangle' \\ = & \prod_i \frac{\nu_2(g_{i+1}^l, g^{-1}g^*, g^*)}{\nu_2(g_{i+1}^r, g^{-1}g^*, g^*)}|\{gg_{i+1}^l, gg_{i+1}^r\}\rangle' \end{aligned} \tag{7.53}$$

Above formula is the same as eqn. (7.28).

Similarly, we can illustrate the result in 2D. Now the basis $|g_i\rangle$ correspond to the state $|g_i^1, g_{i+x}^2, g_{i+x+y}^3, g_{i+y}^4\rangle$ in the dual lattice (see Fig. 7-20). After the dual transformation, the wave function $\Psi(\{g_i\})$ becomes $\Psi_d(\{g_i^1, g_i^2, g_i^3, g_i^4\})$ (here $g_i^1 = g_{i+x}^2 = g_{i+x+y}^3 = g_{i+y}^4 = g_i$). Again, we introduce the LU transformation

$$\begin{aligned} & |\{g_i^1, g_i^2, g_i^3, g_i^4\}\rangle' \\ = & \prod_i \frac{\nu_3(g_i, g_{i+x}, g_{i+y}, g^*)}{\nu_3(g_{i+x}, g_{i+y}, g_{\bar{i}}, g^*)}|\{g_i^1, g_i^2, g_i^3, g_i^4\}\rangle \\ = & \prod_i \frac{\nu_3(g_{\bar{i}}^3, g_{\bar{i}}^4, g_{\bar{i}}^2, g^*)}{\nu_3(g_{\bar{i}}^4, g_{\bar{i}}^2, g_{\bar{i}}^1, g^*)}|\{g_i^1, g_{\bar{i}}^2, g_{\bar{i}}^3, g_{\bar{i}}^4\}\rangle \end{aligned} \tag{7.54}$$

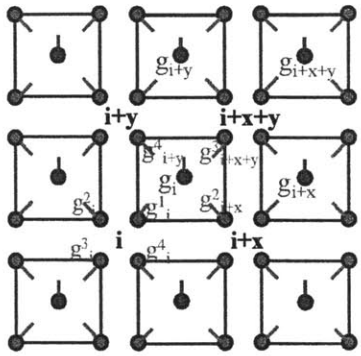

Figure 7-20: (Color online) The duality transformation in 2-dimension. The green dots represent the dual lattice of the red dots. In the new bases, the wave function in the green lattice is the same as the one introduced in Sec. III and IV.

where $\tilde{i} = i + x + y$. The LU transformation between the old bases and the new ones is on-site. In the new bases, the fixed point wave function is a direct product of plaquettes. The symmetry operation now becomes

$$\begin{aligned}
& \otimes_i U^i(g) |\{g_i^1, g_i^2, g_i^3, g_i^4\}\rangle' \\
= & \prod_i \frac{\nu_3(g_{\tilde{i}}^3, g_{\tilde{i}}^4, g_{\tilde{i}}^2, g^*)}{\nu_3(g_{\tilde{i}}^4, g_{\tilde{i}}^2, g_{\tilde{i}}^1, g^*)} |\{g g_{\tilde{i}}^1, g g_{\tilde{i}}^2, g g_{\tilde{i}}^3, g g_{\tilde{i}}^4\}\rangle \\
= & \prod_i \frac{\nu_3(g_{\tilde{i}}^3, g_{\tilde{i}}^4, g_{\tilde{i}}^2, g^*)}{\nu_3(g_{\tilde{i}}^4, g_{\tilde{i}}^2, g_{\tilde{i}}^1, g^*)} \prod_i \frac{\nu_3(g_{\tilde{i}}^4, g_{\tilde{i}}^2, g_{\tilde{i}}^1, g^{-1}g^*)}{\nu_3(g_{\tilde{i}}^3, g_{\tilde{i}}^4, g_{\tilde{i}}^2, g^{-1}g^*)} |\{g g_{\tilde{i}}^1, g g_{\tilde{i}}^2, g g_{\tilde{i}}^3, g g_{\tilde{i}}^4\}\rangle' \\
= & \prod_i \frac{\nu_3(g_{\tilde{i}}^3, g_{\tilde{i}}^4, g^{-1}g^*, g^*)\nu_3(g_{\tilde{i}}^4, g_{\tilde{i}}^1, g^{-1}g^*, g^*)}{\nu_3(g_{\tilde{i}}^3, g_{\tilde{i}}^2, g^{-1}g^*, g^*)\nu_3(g_{\tilde{i}}^2, g_{\tilde{i}}^1, g^{-1}g^*, g^*)} |\{g g_{\tilde{i}}^1, g g_{\tilde{i}}^2, g g_{\tilde{i}}^3, g g_{\tilde{i}}^4\}\rangle' \qquad (7.55)
\end{aligned}$$

The above equation agrees with eqn. (7.34).

From above examples, we can see that after the 'dual transformation' the ground state wave function and its symmetry representation in the Lagrangian formalism are the same as the Hamiltonian formalism as we discussed in Sec.7.2.1.

7.3 Summary of result

Finally, we will summarize our systematic construction of SPT phases in interacting bosonic systems in the following table. Each entry in the table is the $(d+1)$th cohomology group of the symmetry group, whose different group elements label different SPT phases. The identify element labels the trivial phase, while the nontrivial elements label nontrivial SPT phases.

The $U(1) \rtimes Z_2^T$ line describes the SPT phases for interacting bosons with time reversal symmetry Z_2^T and boson number conservation (symmetry group $= U(1) \rtimes Z_2^T$, where time reversal T and $U(1)$ transformations U_θ satisfy $TU_\theta = U_{-\theta}T$). Those phases are bosonic analogues of free fermion topological insulators protected by the same symmetry. From $\mathcal{H}^{1+d}[U(1) \rtimes Z_2^T, U(1)]$, we find one kind of non-trivial bosonic topological insulators in 1D or 2D, and three kinds in 3D. The only non-trivial topological insulator in 1D is the same

Symm. group	$d=0$	$d=1$	$d=2$	$d=3$
$U(1) \rtimes Z_2^T$	$\mathbb{Z}$	$\mathbb{Z}_2$	$\mathbb{Z}_2$	$\mathbb{Z}_2^2$
$U(1) \times Z_2^T$	$\mathbb{Z}_1$	$\mathbb{Z}_2^2$	$\mathbb{Z}_1$	$\mathbb{Z}_2^3$
Z_2^T	$\mathbb{Z}_1$	$\mathbb{Z}_2$	$\mathbb{Z}_1$	$\mathbb{Z}_2$
$U(1)$	$\mathbb{Z}$	$\mathbb{Z}_1$	$\mathbb{Z}$	$\mathbb{Z}_1$
$SO(3)$	$\mathbb{Z}_1$	$\mathbb{Z}_2$	$\mathbb{Z}$	$\mathbb{Z}_1$
$SO(3) \times Z_2^T$	$\mathbb{Z}_1$	$\mathbb{Z}_2^2$	$\mathbb{Z}_2$	$\mathbb{Z}_2^3$
Z_n	$\mathbb{Z}_n$	$\mathbb{Z}_1$	$\mathbb{Z}_n$	$\mathbb{Z}_1$
$Z_n \times Z_2^T$	$\mathbb{Z}_{(2,n)}$	$\mathbb{Z}_2 \times \mathbb{Z}_{(2,n)}$	$\mathbb{Z}^2_{(2,n)}$	$\mathbb{Z}_2 \times \mathbb{Z}^2_{(2,n)}$
$Z_n \rtimes Z_2^T$	$\mathbb{Z}_n$	$\mathbb{Z}_2 \times \mathbb{Z}_{(2,n)}$	$\mathbb{Z}^2_{(2,n)}$	$\mathbb{Z}_2 \times \mathbb{Z}^2_{(2,n)}$
$D_2 \times Z_2^T = D_{2h}$	$\mathbb{Z}_2^2$	$\mathbb{Z}_2^4$	$\mathbb{Z}_2^6$	$\mathbb{Z}_2^9$
$U(1) \times Z_2$	$\mathbb{Z} \times \mathbb{Z}_2$	$\mathbb{Z}_1$	$\mathbb{Z} \times \mathbb{Z}_2^2$	$\mathbb{Z}_1$
$U(1) \rtimes Z_2$	$\mathbb{Z}_2$	$\mathbb{Z}_2$	$\mathbb{Z} \times \mathbb{Z}_2$	$\mathbb{Z}_2$

Table 7.1: SPT phases of interacting bosonic systems in d-spatial dimensions protected by some simple symmetries. Here $\mathbb{Z}_1$ means that our construction only gives rise to the trivial phase. $\mathbb{Z}_n$ means that the constructed non-trivial SPT phases plus the trivial phase are labeled by the elements in $\mathbb{Z}_n$. Z_2^T represents time reversal symmetry, $U(1)$ represents $U(1)$ symmetry, Z_n represents cyclic symmetry, etc. Also (m,n) is the greatest common divisor of m and n. The red rows are for strong bosonic topological insulators and the blue rows strong bosonic topological superconductors.

as the Haldane phase.

The $U(1) \times Z_2^T$ line describes the SPT phases for integer spin systems with time reversal and $U(1)$ spin rotation symmetries (symmetry group $= U(1) \times Z_2^T$, where time reversal T and $U(1)$ transformations U_θ satisfy $TU_\theta = U_\theta T$). From $\mathcal{H}^{1+d}[U(1) \times Z_2^T, U(1)]$, we find three non-trivial SPT phases in 1D, none in 2D, and seven in 3D.

The Z_2^T line describes interacting bosonic analogues of free fermion topological superconductors [SMF99, RG00, Roy06, QHRZ09, SF09] with only time reversal symmetry, Z_2^T . Since $\mathcal{H}^{1+d}[Z_2^T, U(1)] = \mathbb{Z}_2$ for odd d and $\mathcal{H}^{1+d}[Z_2^T, U(1)] = \mathbb{Z}_1$ for even d, we find one kind of "bosonic topological superconductors" or non-trivial SPT phases in every odd dimensions (for the spin/boson systems with only time reversal symmetry).

We also find that $\mathcal{H}^{1+d}[Z_n, U(1)] = \mathbb{Z}_n$ for even d and $\mathcal{H}^{1+d}[Z_n, U(1)] = \mathbb{Z}_1$ for odd d. So spin/boson systems with Z_n on-site symmetry have $n-1$ kinds of non-trivial SPT phases in $d =$ even dimensions.

From $\mathcal{H}^{1+d}[U(1), U(1)] = \mathbb{Z}$ for even d and $\mathcal{H}^{1+d}[U(1), U(1)] = \mathbb{Z}_1$ for odd d, we find that spin/boson systems with $U(1)$ on-site symmetry have infinite non-trivial SPT phases labeled by non-zero integer in $d =$ even dimensions. This generalizes a result obtained by Levin for $d = 2$.[LG12]

For integer spin systems with D_{2h} symmetry but no translation symmetry, we discover 15 new SPT phases in 1D,[CGW11b, LCW11] 63 new SPT phases in 2D, and 511 new SPT phases in 3D.

For integer spin systems with the full $SO(3)$ spin rotation symmetries, the symmetry group is $SO(3)$. From $\mathcal{H}^{1+d}[SO(3), U(1)]$, we find one non-trivial SPT phase in 1D and infinite many in 2D.

For integer spin systems with time reversal and the full $SO(3)$ spin rotation symmetries, the symmetry group is $SO(3) \times Z_2^T$. From $\mathcal{H}^{1+d}[SO(3) \times Z_2^T, U_T(1)]$, we find one non-trivial

SPT phase in 2D and seven in 3D.

7.4 Supplementary materials for the systematic construction

7.4.1 Group cohomology

The above discussion on the factor system of a projective representation can be generalized which give rise to a cohomology theory of group. In this section, we will briefly describe the group cohomology theory.

For a group G, let M be a G-module, which is an abelian group (with multiplication operation) on which G acts compatibly with the multiplication operation (i.e. the abelian group structure) on M:

$$g \cdot (ab) = (g \cdot a)(g \cdot b), \quad g \in G, \quad a, b \in M. \tag{7.56}$$

For the cases studied in this chapter, M is simply the $U(1)$ group and a an $U(1)$ phase. The multiplication operation ab is the usual multiplication of the $U(1)$ phases. The group action is trivial: $g \cdot a = a$, $g \in G$, $a \in U(1)$.

Let $\omega_n(g_1, ..., g_n)$ be a function of n group elements whose value is in the G-module M. In other words, $\omega_n : G^n \to M$. Let $\mathcal{C}^n(G, M) = \{\omega_n\}$ be the space of all such functions. Note that $\mathcal{C}^n(G, M)$ is an Abelian group under the function multiplication $\omega_n''(g_1, ..., g_n) = \omega_n(g_1, ..., g_n)\omega_n'(g_1, ..., g_n)$. We define a map d_n from $\mathcal{C}^n[G, U(1)]$ to $\mathcal{C}^{n+1}[G, U(1)]$:

$$\begin{aligned}(d_n\omega_n)(g_1, ..., g_{n+1}) = \quad & g_1 \cdot \omega_n(g_2, ..., g_{n+1})\omega_n^{(-1)^{n+1}}(g_1, ..., g_n) \\ & \times \prod_{i=1}^{n} \omega_n^{(-1)^i}(g_1, ..., g_{i-1}, g_i g_{i+1}, g_{i+2}, ...g_{n+1})\end{aligned} \tag{7.57}$$

Let

$$\mathcal{B}^n(G, M) = \{\omega_n | \omega_n = d_{n-1}\omega_{n-1} | \omega_{n-1} \in \mathcal{C}^{n-1}(G, M)\} \tag{7.58}$$

and

$$\mathcal{Z}^n(G, M) = \{\omega_n | d_n\omega_n = 1, \omega_n \in \mathcal{C}^n(G, M)\} \tag{7.59}$$

$\mathcal{B}^n(G, M)$ and $\mathcal{Z}^n(G, M)$ are also Abelian groups which satisfy $\mathcal{B}^n(G, M) \subset \mathcal{Z}^n(G, M)$ where $\mathcal{B}^1(G, M) \equiv \{1\}$. The n-cocycle of G is defined as

$$\mathcal{H}^n(G, M) = \mathcal{Z}^n(G, M)/\mathcal{B}^n(G, M) \tag{7.60}$$

Let us discuss some examples. We choose $M = U(1)$ and G acts trivially: $g \cdot a = a$, $g \in G$, $a \in U(1)$. In this case $\omega_n(g_1, ..., g_n)$ is just a phase factor. From

$$(d_1\omega_1)(g_1, g_2) = \omega_1(g_2)\omega_1(g_1)/\omega_1(g_1 g_2) \tag{7.61}$$

we see that

$$\mathcal{Z}^1(G, U(1)) = \{\omega_1 | \omega_1(g_2)\omega_1(g_1) = \omega_1(g_1 g_2)\}. \tag{7.62}$$

In other words, $\mathcal{Z}^1(G, U(1))$ is the set formed by all the 1D representations of G. Since

$\mathcal{B}^1(G,U(1)) \equiv \{1\}$ is trivial. $\mathcal{H}^1(G,U(1)) = \mathcal{Z}^1(G,U(1))$ is also the set of all the 1D representations of G.

From

$$(d_2\omega_2)(g_1,g_2,g_3) = \omega_2(g_2,g_3)\omega_2(g_1,g_2g_3)/\omega_2(g_1g_2,g_3)\omega_2(g_1,g_2) \tag{7.63}$$

we see that

$$\mathcal{Z}^2(G,U(1)) = \{\omega_2|\omega_2(g_2,g_3)\omega_2(g_1,g_2g_3) = \omega_2(g_1g_2,g_3)\omega_2(g_1,g_2)\}.$$

and

$$\mathcal{B}^2(G,U(1)) = \{\omega_2|\omega_2(g_1,g_2) = \omega_1(g_2)\omega_1(g_1)/\omega_1(g_1g_2)\}. \tag{7.64}$$

The 2-cocycle $\mathcal{H}^2(G,U(1)) = \mathcal{Z}^2(G,U(1))/\mathcal{B}^2(G,U(1))$ classify the projective representations discussed in section 6.5.1.

From

$$(d_3\omega_3)(g_1,g_2,g_3,g_4) = \frac{\omega_3(g_2,g_3,g_4)\omega_3(g_1,g_2g_3,g_4)\omega_3(g_1,g_2,g_3)}{\omega_3(g_1g_2,g_3,g_4)\omega_3(g_1,g_2,g_3g_4)} \tag{7.65}$$

we see that

$$\mathcal{Z}^3(G,U(1)) = \{\omega_3|\frac{\omega_3(g_2,g_3,g_4)\omega_3(g_1,g_2g_3,g_4)\omega_3(g_1,g_2,g_3)}{\omega_3(g_1g_2,g_3,g_4)\omega_3(g_1,g_2,g_3g_4)} = 1\}.$$

and

$$\mathcal{B}^3(G,U(1)) = \{\omega_3|\omega_3(g_1,g_2,g_3) = \frac{\omega_2(g_2,g_3)\omega_2(g_1,g_2g_3)}{\omega_2(g_1g_2,g_3)\omega_2(g_1,g_2)}\}, \tag{7.66}$$

which give us the 3-cocycle $\mathcal{H}^3(G,U(1)) = \mathcal{Z}^3(G,U(1))/\mathcal{B}^3(G,U(1))$.

In the following, we will describe a geometric interpretation of group cohomology. First, let us introduce the map $\nu_n : G^{n+1} \to M$ that satisfy

$$|\nu_d(g_0,g_1,...,g_d)| = 1, \nu_d^{s(g)}(g_0,g_1,...,g_d) = \nu_d(gg_0,gg_1,...,gg_d), g \in G \tag{7.67}$$

where $s(g) = 1$ if g contains no anti-unitary time reversal transformation T and $s(g) = -1$ if g contains one anti-unitary time reversal transformation T.

We will call such a map ν_n a n-cochain:

$$\mathcal{C}^n(G,M) = \{\nu_n|\nu_d^{s(g)}(g_0,g_1,...,g_d) = \nu_d(gg_0,gg_1,...,gg_d)\}. \tag{7.68}$$

ω_n discussed above is one-to-one related to ν_n through

$$\begin{aligned}\omega_n(g_1,...,g_n) &= \nu_n(1,g_1,g_1g_2,...,g_1\cdots g_n)\\ &= \nu_n(1,\tilde{g}_1,\tilde{g}_2,...,\tilde{g}_n)\end{aligned} \tag{7.69}$$

where $\tilde{g}_i = g_1g_2\cdots g_i$.

We can rewrite the d_n map, $d_n : \omega_n \to \omega_{n+1}$, as $d_n : \nu_n \to \nu_{n+1}$:

$$(d_n\nu_n)(g_0, g_1, ..., g_{n+1}) = \prod_{i=0}^{n+1} \nu_n^{(-1)^i}(g_0, .., g_{i-1}, g_{i+1}, ..., g_{n+1}) \tag{7.70}$$

which is a more compact and a nicer expression of the d_n operation.

When $n = 1$, we have

$$(d_1\nu_1)(g_0, g_1, g_2) = \nu_1(g_1, g_2)\nu_1(g_0, g_1)/\nu_1(g_0, g_2) \tag{7.71}$$

For $n = 2$:

$$(d_2\nu_2)(g_0, g_1, g_2, g_3) = \frac{\nu_2(g_1, g_2, g_3)\nu_2(g_0, g_1, g_3)}{\nu_2(g_0, g_2, g_3)\nu_2(g_0, g_1, g_2)} \tag{7.72}$$

and for $n = 3$:

$$(d_3\nu_3)(g_0, g_1, g_2, g_3, g_4) = \frac{\nu_3(g_1, g_2, g_3, g_4)\nu_3(g_0, g_1, g_3, g_4)\nu_3(g_0, g_1, g_2, g_3)}{\nu_3(g_0, g_2, g_3, g_4)\nu_3(g_0, g_1, g_2, g_4)} \tag{7.73}$$

The d-cocycles are special d-cochains that satisfy

$$\prod_{i=0}^{d+1} \nu_d^{(-1)^i}(g_0, .., g_{i-1}, g_{i+1}, ..., g_{d+1}) = 1 \tag{7.74}$$

For $d = 1$, the 1-cocycles satisfy

$$\nu_1(g_1, g_2)\nu_1(g_0, g_1)/\nu_1(g_0, g_2) = 1 \tag{7.75}$$

The 2-cocycles satisfy

$$\frac{\nu_2(g_1, g_2, g_3)\nu_2(g_0, g_1, g_3)}{\nu_2(g_0, g_2, g_3)\nu_2(g_0, g_1, g_2)} = 1 \tag{7.76}$$

and the 3-cocycles satisfy

$$\frac{\nu_3(g_1, g_2, g_3, g_4)\nu_3(g_0, g_1, g_3, g_4)\nu_3(g_0, g_1, g_2, g_3)}{\nu_3(g_0, g_2, g_3, g_4)\nu_3(g_0, g_1, g_2, g_4)} = 1 \tag{7.77}$$

The d-coboundaries λ_d are special d-cocycles that can be constructed from the $(d-1)$-cochains μ_{d-1}:

$$\lambda_d(g_0, ..., g_d) = \prod_{i=0}^{d} \mu_{d-1}^{(-1)^i}(g_0, .., g_{i-1}, g_{i+1}, ..., g_d). \tag{7.78}$$

For $d = 1$, the 1-coboundaries are given by

$$\lambda_1(g_0, g_1) = \mu_0(g_1)/\mu_0(g_0) \tag{7.79}$$

The 2-coboundaries are given by

$$\lambda_2(g_0, g_1, g_2) = \mu_1(g_1, g_2)\mu_1(g_0, g_1)/\mu_1(g_0, g_2), \tag{7.80}$$

and the 3-coboundaries by

$$\lambda_3(g_0, g_1, g_2, g_3) = \frac{\mu_2(g_1, g_2, g_3)\mu_2(g_0, g_1, g_3)}{\mu_2(g_0, g_2, g_3)\mu_2(g_0, g_1, g_2)}. \tag{7.81}$$

Two d-cocycles, ν_d and ν'_d, are said to be equivalent iff they differ by a coboundary λ_d: $\nu_d = \nu'_d\lambda_d$. The equivalence classes of cocycles give rise to the d-cohomology group $\mathcal{H}^d[G, U_T(1)]$.

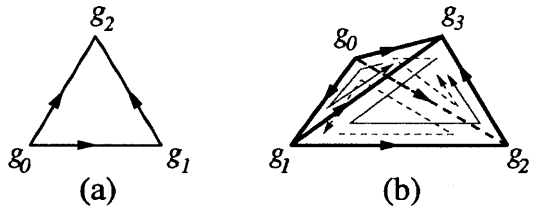

Figure 7-21: (a) The line from g_0 to g_1 is a graphic representation of $\nu_1(g_0, g_1)$. The triangle (g_0, g_1, g_2) with a branching structure is a graphic representation of $\nu_2(g_0, g_1, g_2)$. Note that, for the first variable, the g_0-vertex is connected to two outgoing edges, and for the last variable, the g_2-vertex is connected to two incoming edges. (a) can also be viewed as the graphic representation of Eq. (7.75) and Eq. (7.71). The triangle corresponds to $(\mathrm{d}_1\nu_1)(g_0, g_1, g_2)$ in Eq. (7.71) and the three edges correspond to $\nu_1(g_1, g_2)$, $\nu_1(g_0, g_1)$ and $\nu_1^{-1}(g_0, g_2)$. (b) The tetrahedron (g_0, g_1, g_2, g_3) with a branching structure is a graphic representation of $\nu_3(g_0, g_1, g_2, g_3)$. (b) can also be viewed as the graphic representation of Eq. (7.76) and Eq. (7.72). The tetrahedron corresponds to $(\mathrm{d}_2\nu_2)(g_0, g_1, g_2, g_3)$ in Eq. (7.72), and the four faces correspond to $\nu_2(g_1, g_2, g_3)$, $\nu_2(g_0, g_1, g_3)$, $\nu_2^{-1}(g_0, g_2, g_3)$, and $\nu_2^{-1}(g_0, g_1, g_2)$.

A d-cochain can be represented by a d-dimensional simplex with a branching structure (see Fig. 7-21). A branching structure is represented by arrows on the edges of the simplex that never form an oriented loop on any triangles. We note that the first variable g_0 in $\nu_d(g_0, g_1, ..., g_d)$ corresponds to the vertex with no incoming edge, the second variable g_1 to the vertex with one incoming edge, and the third variable g_2 to the vertex with two incoming edges, etc. The conditions Eq. (7.75) and Eq. (7.76) can also be represented as in Fig. 7-21. For example, Fig. 7-21a has three edges which correspond to $\nu_1(g_1, g_2)$, $\nu_1(g_0, g_1)$ and $\nu_1^{-1}(g_0, g_2)$. The evaluation of a 1-cochain ν_1 on the complex Fig. 7-21a is given by the product of the factors $\nu_1(g_1, g_2)$, $\nu_1(g_0, g_1)$ and $\nu_1^{-1}(g_0, g_2)$. Such an evaluation will be 1 if ν_1 is a cocycle. Similarly, the value of a 2-cocycle ν_2 on the closed surface (such as a tetrahedron) is also 1. In general, the evaluations of cocycles on any complex without boundary are 1. In this way, we obtain a graphical representation of eqn. (7.71) and Eq. (7.72) as in Fig. 7-21.

Let us choose $M = U(1)$ and consider a 1-form Ω_1 on the plane in Fig. 7-21a. Then the

differential form expression

$$\int_{(g_0,g_1,g_2)} \mathrm{d}\Omega_1 = \int_{g_0}^{g_1} \Omega_1 - \int_{g_0}^{g_2} \Omega_1 + \int_{g_1}^{g_2} \Omega_1 \tag{7.82}$$

give us Eq. (7.71) if we set

$$(d_1\nu_1)(g_0,g_1,g_2) = \exp\Big(\mathrm{i}\int_{(g_0,g_1,g_2)} \mathrm{d}\Omega_1\Big) \tag{7.83}$$

and

$$\nu_1(g_i,g_j) = \exp\Big(\mathrm{i}\int_{g_i}^{g_j} \Omega_1\Big). \tag{7.84}$$

Here $\int_{(g_0,g_1,g_2)}$ is the integration on the triangle (g_0,g_1,g_2) in Fig. 7-21a. Similarly the differential form expression

$$\int_{(g_0,g_1,g_2,g_3)} \mathrm{d}\Omega_2 = \int_{(g_1,g_2,g_3)} \Omega_2 - \int_{(g_0,g_2,g_3)} \Omega_2 + \int_{(g_0,g_1,g_3)} \Omega_2 - \int_{(g_0,g_1,g_2)} \Omega_2 \tag{7.85}$$

give us Eq. (7.72) if we set

$$(d_2\nu_2)(g_0,g_1,g_2,g_3) = \exp\Big(\mathrm{i}\int_{(g_0,g_1,g_2,g_3)} \mathrm{d}\Omega_2\Big) \tag{7.86}$$

and

$$\nu_2(g_i,g_j,g_k) = \exp\Big(\mathrm{i}\int_{(g_i,g_j,g_k)} \Omega_2\Big). \tag{7.87}$$

This leads to a geometric picture of group cohomology. For example, if Ω_2 is a closed form, $\mathrm{d}\Omega_2 = 0$, the corresponding $\nu_2(g_i,g_j,g_k)$ will be a cocycle. If Ω_2 is an exact form, $\Omega_2 = \mathrm{d}\Omega_1$, the corresponding $\nu_2(g_i,g_j,g_k)$ will be a coboundary.

7.4.2 Review: obtaining canonical form of MPS

In this section we review how to obtain the canonical form of MPS which was first derived in [PGVWC07]. Similar ideas are going to be used in the study of matrix product unitary operators.

A matrix product representation of 1D state is

$$|\psi\rangle = \sum_{i_1 i_2 \ldots i_N} Tr(A_{i_1} A_{i_2} \ldots A_{i_N}) |i_1 i_2 \ldots i_N\rangle \tag{7.88}$$

A_i's are $D \times D$ matrices.

Define double tensor E for the MPS as

$$E = \sum_i A_i \otimes A_i^* \tag{7.89}$$

Equivalently, E can be expressed as a completely positive quantum channel $\mathcal{E}$ as

$$\mathcal{E}(X) = \sum_i A_i X A_i^\dagger \tag{7.90}$$

and the corresponding dual channel $\mathcal{E}^*$ as

$$\mathcal{E}^*(X) = \sum_i A_i^\dagger X A_i \tag{7.91}$$

The correspondence between E and $\mathcal{E}$, $\mathcal{E}^*$ is as follows. Suppose that X and Y are $D \times D$ matrices which satisfy

$$Y = \mathcal{E}(X) \tag{7.92}$$

Combine the two indices of the matrices into one and write them as vectors

$$(V_X)_{(\alpha-1)D+\beta} = X_{\alpha,\beta} \;\; (V_Y)_{(\alpha-1)D+\beta} = Y_{\alpha,\beta} \tag{7.93}$$

V_X and V_Y are then related by E as

$$EV_X = V_Y \tag{7.94}$$

Similarly, if

$$Y = \mathcal{E}^*(X) \tag{7.95}$$

then

$$V_X^\dagger E = V_Y^\dagger \tag{7.96}$$

We will use E and $\mathcal{E}$, $\mathcal{E}^*$ inter-changeably, whichever is more convenient.

From the structure of $\mathcal{E}$ and $\mathcal{E}^*$ we can put A_i's into a canonical form. Suppose that the largest magnitude of the eigenvalues of $\mathcal{E}$ is $\lambda_1 > 0$. There could be multiple eigenvalues $\lambda_1 e^{i\theta_k}$ of this magnitude. As shown in [FNW92b], $e^{i\theta_k}$ form a group and they are the pth root of unity. To get rid of this, we can just group p sites together and the eigenvalues of the largest magnitude will all be real and positive. We still label them as λ_1.

Because $\mathcal{E}$ is a completely positive channel, at least one of corresponding fixed points Λ

$$\mathcal{E}(\Lambda) = \lambda_1 \Lambda \tag{7.97}$$

is positive-semidefinite. Denote the support space of Λ as P. It can be shown that $A_i P = PA_iP$.[PGVWC07] Decompose each A_i into four parts $A_i = PA_iP + PA_iP_\perp + P_\perp A_i P + P_\perp A_i P_\perp$. $P_\perp A_i P = 0$. $PA_iP_\perp$ may not be zero. However, it does not contribute to the MPS, therefore we can remove it safely. After doing this, A_i is decomposed into two blocks and Λ is a full rank positive fixed point of $\mathcal{E}_P(X) = \sum_i (PA_iP)X(PA_iP)^\dagger$ with eigenvalue λ_1.

Because

$$\mathcal{E}_P(X) = \sum_i (PA_iP)X(PA_iP)^\dagger = \sum_i (A_iP)X(A_iP)^\dagger \tag{7.98}$$

every fixed point of $\mathcal{E}_P$(within space P) is also a fixed point of $\mathcal{E}$ with the same eigenvalue. Therefore, λ_1 is also the largest eigenvalue of $\mathcal{E}_P$. Suppose that $\mathcal{E}_P$ has another fixed point Z of eigenvalue λ_1 which is not proportional to Λ. WLOG, we can choose Z to be Hermitian. (This is because $\sum_i (A_iP)Z(A_iP)^\dagger = \lambda_1 Z$, therefore $\sum_i (A_iP)Z^\dagger(A_iP)^\dagger = \lambda_1 Z^\dagger$.

And because Z is not proportional to Λ, at least one of the Hermitian matrices $Z + Z^\dagger$ or $i(Z - Z^\dagger)$ is not proportional to Λ.) Diagonalize the Hermitian matrix $\Lambda^{-1/2} Z \Lambda^{-1/2}$ and get eigenvalues $z_1 > z_2 > ...$ It is easy to see that $\Lambda - \frac{1}{z_1} Z$ is another non full rank positive fixed point of $\mathcal{E}_P$ with eigenvalue λ_1. Therefore we can repeat the previous process and turn PA_iP into smaller blocks.

Repeat this process for every block until (1) the channel $\mathcal{E}_{P_k}$ of every block k has a largest positive eigenvalue λ_k. There is a positive full rank fixed point Λ_{P_k} within subspace P_k. (2) There is no other fixed point within P_k of the same eigenvalue. (3) The block $P_\perp = I - \sum_k P_k$ which does not have a positive fixed point for largest eigenvalue must only have zero eigenvalue. The block could be non-zero in general, but it does not contribute to MPS. Note that $\sum_k P_k + P_\perp = I$, $A_i P_k = P_k A_i P_k$. Written in the blocks P_k and $P_\perp$, A_i is upper(or lower) triangular.

Now we look at each block k separately but from the dual channel perspective. We can similarly block diagonalize A_i^k if non full rank positive fixed point exists for the largest eigenvalue of $\mathcal{E}^*_{P_k}$. For each sub-block projection $P_{k,l}$, $P_{k,l} A_i^k = P_{k,l} A_i^k P_{k,l}$. A_i^k can be turned into sub-blocks $A_i^{k,l} = P_{k,l} A_i^k P_{k,l}$. Note that, if $\Lambda_{P_{k,l}} = P_{k,l} \Lambda_{P_k} P_{k,l}$,

$$\begin{aligned} \sum_i A_i^{k,l} \Lambda_{P_{k,l}} (A_i^{k,l})^\dagger &= A_i^{k,l} \Lambda_{P_k} (A_i^{k,l})^\dagger \\ &= P_{k,l} A_i^k \Lambda_{P_k} (A_i^k)^\dagger P_{k,l} \\ &= \lambda_k \Lambda_{P_{k,l}} \end{aligned} \tag{7.99}$$

Therefore, within each sub-block, $\Lambda_{P_{k,l}}$ is still a positive full rank fixed point of $\mathcal{E}_{P_{k,l}}$ with eigenvalue λ_k. As there cannot be positive fixed points of other eigenvalue, λ_k must be the largest. Similarly, if X_k is a fixed point of $\mathcal{E}_{P_k}$, $P_{k,l} X_k P_{k,l}$ is a fixed point of $\mathcal{E}_{P_{k,l}}$ with the same eigenvalue.

Proceed similarly as for $\mathcal{E}$, we can block diagonalize A_i^k into $A_i^{k,l}$ such that $\mathcal{E}^*_{P_{k,l}}$ has only one fixed point for its largest eigenvalue which is full rank positive.

Finally, we arrive at a canonical form, which is composed of blocks P_k and sub-blocks $P_{k,l}$. Within each sub-block, the matrices satisfy (1) the channel $\mathcal{E}_{P_{k,l}}$ has a largest positive eigenvalue. The corresponding fixed point is full rank positive. (2) There is no other fixed point within the sub-block of the same eigenvalue. (3) the dual channel $\mathcal{E}^*_{P_{k,l}}$ also has a largest positive eigenvalue. The corresponding fixed point is full rank positive. (4) There is no other fixed point within the sub-block of the same eigenvalue.

A generic matrix product state has only one block in its canonical form.[PGVWC07] We will call these MPS single-blocked MPS. Single-blocked MPS represents gapped, short range correlated 1D states. The single-block property is a generalization of the injectivity condition for MPS.[PGVWC07] A single-blocked MPS is injective if the dimension of the matrices equals that in the canonical form. On the other hand, a single-blocked MPS might not be written in a canonical form. It is in general more redundant. To do the reduction, necessary steps involves projection onto the single block and re-labeling the basis. Any invertible operation within the projected space might be added. However, if the resulting canonical form is fixed, the reduction operation is unique within the projected space up to an arbitrary phase factor.

7.4.3 Matrix Product Unitary Operators

Similarly to MPS, a matrix product representation of operators acting on a 1D system is given by,[PMCV10]

$$O = \sum_{\{i_k\},\{i'_k\}} Tr(T^{i_1,i'_1}T^{i_2,i'_2}...T^{i_N,i'_N})|i'_1 i'_2...i'_N\rangle\langle i_1 i_2...i_N| \tag{7.100}$$

Here we restrict to unitary operators U as we want to discuss symmetry operations. Using matrix product representation, U does not have to be an on-site symmetry. U is represented by a rank-four tensor $T^{i,i'}_{\alpha,\beta}$ on each site, where i and i' are input and output physical indices and α, β are inner indices.

Just like every matrix product state can be reduced to a canonical form.[PGVWC07] every matrix product operator can be reduced to a canonical form also. To do so, we just need to treat the two physical indices as one and apply the procedure described in section 2.1. Similar to MPS, we can also define double tensor/ quantum channel for each matrix product operator. The double tensor of T is

$$E = \sum_{i,i'} T^{i,i'} \otimes (T^{i,i'})^* \tag{7.101}$$

The fact that T represents a unitary operator puts strong constraint on the form of T. $U^\dagger U = I \otimes ... \otimes I$ is represented on each site by tensor

$$\mathbb{T}^{i,i''}_{\alpha\alpha',\beta\beta'} = \sum_{i'} T^{i,i'}_{\alpha,\beta}(T^{i'',i'}_{\alpha',\beta'})^* \tag{7.102}$$

$\mathbb{T}$ must be equivalent to $\delta_{i,i''}$ on each site. We can reduce $\mathbb{T}$ to the canonical form. The canonical form of $\mathbb{T}$ could contain multiple blocks, but each block must represent the same operator $I \otimes ... \otimes I$ and takes the form $\lambda_k \delta_{i,i''}|k\rangle\langle k|$. $|k\rangle\langle k|$ is the projection onto the kth block, λ_k is a number. Later we will impose further constraints on U to get rid of multi-block.

First we want to show that we can write every MPUO in an single-blocked canonical form. That is, the canonical form contains only one block. Suppose that we start with a canonical representation of the symmetry operation. In general, the canonical representation could have multiple blocks. We are going to show that this is not necessary as different blocks represent the same unitary operation.

Suppose that a canonical MPUO contains two blocks

$$T^{ii'} = T^{ii'}_{[1]} \oplus T^{ii'}_{[2]} \tag{7.103}$$

$T_{[1]}$ represents MPO O_1 and $T_{[2]}$ represents MPO O_2 (not necessarily unitary). $U = O_1 + O_2$.

The corresponding $\mathbb{T}$ contains four blocks

$$\begin{aligned} \mathbb{T}^{i,i''} &= \textstyle\sum_{i'} T^{ii'} \otimes (T^{i''i'})^* \\ &= \mathbb{T}^{i,i'}_{[11]} \oplus \mathbb{T}^{i,i'}_{[12]} \oplus \mathbb{T}^{i,i'}_{[21]} \oplus \mathbb{T}^{i,i'}_{[22]} \end{aligned} \tag{7.104}$$

$\mathbb{T}_{[kk']}$ represent MPO $O_k O^\dagger_{k'}$. Because $\mathbb{T}$ represents $I \otimes I... \otimes I$, each of its block must also do. Therefore,

$$O_1 O_1^\dagger = O_1 O_2^\dagger = O_2 O_1^\dagger = O_2 O_2^\dagger = I \otimes I... \otimes I \tag{7.105}$$

That is, O_1 and O_2 represent the same unitary operator and there is no need for multiple blocks. In the following we will always assume that T is written in a canonical form with only one block. We will call this the single-block condition for MPUO.

With the MPUO representation defined for each symmetry operation, we now want to know how the representation changes when two or more operations are combined.

First let's consider what happens when U is combined with $U^\dagger$. As we discussed before, this is represented by $\mathbb{T}$ which could contain multiple blocks $\lambda_k \delta_{i,i''} |k\rangle\langle k|$ in the canonical form. Correspondingly, the double tensor of T

$$E = \sum_{i,i'} T^{i,i'} \otimes (T^{i,i'})^* = \sum_i \mathbb{T}^{i,i} \tag{7.106}$$

has multiple eigenvectors $|k\rangle$ with corresponding eigenvalues λ_k.

Define the correlator between two sets of operator pairs $\{o_1^m, \tilde{o}_1^m\}$ and $\{o_2^n, \tilde{o}_2^n\}$ to be

$$\begin{array}{rcl} (o_1, o_2)_U & = & \sum_{mn} \mathrm{Tr}(o_1^m o_2^n U \tilde{o}_1^m \tilde{o}_2^n U^\dagger) \\ & & -(\sum_m \mathrm{Tr}(o_1^m U \tilde{o}_1^m U^\dagger))(\sum_n \mathrm{Tr}(o_2^n U \tilde{o}_2^n U^\dagger)) \end{array} \tag{7.107}$$

On the one hand, written in terms of tensors, the correlator is expressed as

$$\begin{array}{rcl} (o_1, o_2)_U & = & \mathrm{Tr}(E..E[o_1]..E[o_2]..E) \\ & - & \mathrm{Tr}(E..E[o_1]..E)\mathrm{Tr}(E..E[o_2]..E) \end{array} \tag{7.108}$$

where

$$\begin{array}{l} E_{[o_1]} = \sum_{m,i} (o_1^m)^{i_2,i_3} (\tilde{o}_1^m)^{i_4,i_1} T^{i_1,i_2} \otimes (T^{i_4,i_3})^* \\ E_{[o_2]} = \sum_{n,i} (o_2^n)^{i_2,i_3} (\tilde{o}_2^n)^{i_4,i_1} T^{i_1,i_2} \otimes (T^{i_4,i_3})^* \end{array} \tag{7.109}$$

This is the same form as the correlation function of operators $o_1 = \sum_m o_1^m \otimes \tilde{o}_1^m$ and $o_2 = \sum_n o_2^n \otimes \tilde{o}_2^n$ in a matrix product state with double tensor E. From our knowledge of MPS, we know that the correlator decays as $(\lambda_2/\lambda_1)^l$.

On the other hand, we consider for simplicity only unitaries U which preserve locality of operators exactly. That is, if o is supported on a finite number of sites, $UoU^\dagger$ is also supported on a finite number of sites, though the number may be larger. We do not consider the local operators with exponentially decaying tails. [4] Under this restriction, it follows that when $\{o_1^m, \tilde{o}_1^m\}$ and $\{o_2^n, \tilde{o}_2^n\}$ are far apart

$$\begin{array}{l} \sum_{mn} \mathrm{Tr}(o_1^m o_2^n U \tilde{o}_1^m \tilde{o}_2^n U^\dagger) \\ = \sum_{mn} \mathrm{Tr}(o_1^m o_2^n U \tilde{o}_1^m U U^\dagger \tilde{o}_2^n U^\dagger) \\ = \sum_{mn} \mathrm{Tr}((o_1^m U \tilde{o}_1^m U^\dagger)) \otimes (o_2^n U \tilde{o}_2^n U^\dagger)) \\ = \sum_{mn} \mathrm{Tr}(o_1^m U \tilde{o}_1^m U^\dagger) \mathrm{Tr}(o_2^n U \tilde{o}_2^n U^\dagger) \end{array} \tag{7.110}$$

the correlator $(o_1, o_2)_U$ must be zero if the separation is large enough. Therefore, $\lambda_2 = 0$. E has only one eigenvector and $\mathbb{T}$ has only one block in its canonical form.

Now we want to use this property to show that the single-block condition is stable under combination of MPUO's. That is, if we start with two MPUO represented by T^a and T^b

[4] This is a reasonable restriction because we want to study systems at fixed point where the correlation length in the bulk is zero. Any exactly local operator in the bulk becomes an exactly local effective operator on the boundary.

with only one block in the canonical form, their combination

$$T^{c,ii''}_{\alpha\alpha',\beta\beta'} = \sum_{i'} T^{a,ii'}_{\alpha,\beta} T^{b,i'i''}_{\alpha',\beta'} \tag{7.111}$$

also has only one block in its canonical form. Of course, written as above, T^c is not necessarily in the canonical form. Note that the discussion in the previous paragraphs is actually on the special case where $T^{b,ii'} = (T^{a,i'i})^*$.

In order to see this, we take the double tensor of T^c

$$\begin{aligned} E^c &= \textstyle\sum_{i,i''} T^{c,ii''} \otimes (T^{c,ii''})^* \\ &= \textstyle\sum_{i,i''} (\sum_{i'_1} T^{a,ii'_1} \otimes T^{b,i'_1 i''}) \otimes (\sum_{i'_2} T^{a,ii'_2} \otimes T^{b,i'_2 i''})^* \\ &= \textstyle\sum_{i'_1,i'_2} \mathbb{T}^{a,i'_1 i'_2} \otimes \mathbb{T}^{b,i'_1 i'_2} \end{aligned} \tag{7.112}$$

$\mathbb{T}^a$ and $\mathbb{T}^b$ both have one block in their canonical form. Denote the projection onto the blocks as P_a and P_b.

$$P_a = |\psi^a_{\alpha\tilde{\alpha}}\rangle\langle\psi^a_{\beta\tilde{\beta}}|,\ P_b = |\psi^b_{\alpha'\tilde{\alpha}'}\rangle\langle\psi^b_{\beta'\tilde{\beta}'}| \tag{7.113}$$

Being the only eigenvector of E^a and E^b, $|\psi^a_{\alpha\tilde{\alpha}}\rangle$ and $|\psi^b_{\alpha'\tilde{\alpha}'}\rangle$ are positive full rank if written as matrices $\Lambda^a_{\alpha,\tilde{\alpha}}$, $\Lambda^b_{\alpha',\tilde{\alpha}'}$. The only term that contributes to the trace of E^c is

$$(|\psi^a\rangle \otimes |\psi^b\rangle)(\langle\psi^a| \otimes \langle\psi^b|) \tag{7.114}$$

This is also true for any power of E^c.

This special property of E^c tells us that E^c has only a single non-zero eigenvalue. Suppose $E^c = \lambda_0|0\rangle\langle 0| + M$, $|0\rangle$ is short for $|\psi^a\rangle \otimes |\psi^b\rangle$. $\mathrm{Tr}(E^c) = \lambda_0$. Moreover, $\mathrm{Tr}(E^c)^k = \lambda_0^k$. Because $\mathrm{Tr}(E^c)^k = \sum_i (\lambda_i)^k$, it can be shown that $\lambda_i = 0, \forall i > 0$. The fact that E^c has a single eigenvalue in turn tells us that T^c contains only one block in its canonical form, because otherwise, E^c would have at least n^2 non-zero eigenvalues with n being the block number.

Therefore, we have shown that if we start with the canonical single-blocked tensor representation of some unitary operators, the tensor obtained from their concatenation still has only one block in its canonical form and is hence single-blocked. For single-blocked T we can always apply the procedure in [PGVWC07] (also discussed in detail in section 2.1) to reduce it to a canonical form. If we have multiple ways to do the reduction, they must be equivalent. More specifically, projected onto the unique block, the reduction operation is unique up to phase (if the final canonical form is fixed, not up to gauge). This phase factor is going to play an important role in our study of SPT orders.

Similar reduction procedure applies when a matrix product unitary operator acts on a matrix product state. In particular, suppose $T^{i,i'}$ is a MPUO and A^i represents a MPS which is symmetric under it. Suppose that $T^{i,i'}$ and A^i are both in the canonical form and have only one block. Because $T^{i,i'}$ represents a symmetry of A^i

$$\tilde{A}^i = \sum_{i'} T^{i,i'} \otimes A^{i'} \tag{7.115}$$

represent the same matrix product state as A^i. Moreover, because A^i is short range correlated and $T^{i,i'}$ does not increase correlation length, $\tilde{A}^i$ is still short range correlated and it also contains one block in its canonical form. However, note that $T^{i,i'}$ is a matrix and the

inner dimension of $\tilde{A}^i$ is in general larger than that of A^i. Therefore $\tilde{A}^i$ may no longer be in the canonical form. Some reduction procedure needs to be done to bring $\tilde{A}^i$ back to the canonical form.

Suppose that P is the projection onto the single block in the canonical form of $\tilde{A}^i$. Due to the uniqueness of the canonical form of a MPS, P must be of the same dimension as A^i and $P\tilde{A}^iP$ must be equivalent to A^i up an invertible transformation Q.[PGVWC07, PGWS+08] That is

$$A^i = QP^\dagger \tilde{A}^i PQ^{-1} \tag{7.116}$$

Denote $V_r = PQ^{-1}$ and $V_l = QP$, we get $A^i = V_l \tilde{A}^i V_r$. Moreover, $V_l V_r = I$, the identity on the inner dimensions of A^i. As Q is unique up to phase, V_l and V_r are unique on the single block of $\tilde{A}^i$ up to a conjugate phase factor. With slight abuse of notation, we will denote V_r as V and V_l as $V^\dagger$ and we have

$$A^i = V^\dagger \tilde{A}^i V \tag{7.117}$$

7.4.4 (1+1)D solutions of Eq. (7.25)

$U^i(g)$ is a linear representation

To show that $U^i(g)$ defined in Eq. (7.28) is a linear representation of G, let us compare the combined actions of $U^i(g)$ and $U^i(g'g^{-1})$ with the action of $U^i(g')$ which are given by (see Fig. 7-22)

$$U^i(g'g^{-1})U^i(g)|\alpha_1,\alpha_2\rangle = f_2(\alpha_1,\alpha_2,g,g^*)f_2(g\alpha_1,g\alpha_2,g'g^{-1},g^*)|g'\alpha_1,g'\alpha_2\rangle \tag{7.118}$$

and

$$U^i(g')|\alpha_1,\alpha_2\rangle = f_2(\alpha_1,\alpha_2,g',g^*)|g'\alpha_1,g'\alpha_2\rangle \tag{7.119}$$

We see that

$$\begin{aligned} & f_2(\alpha_1,\alpha_2,g,g^*)f_2(g\alpha_1,g\alpha_2,g'g^{-1},g^*)f_2^{-1}(\alpha_1,\alpha_2,g',g^*) \\ =& \frac{\nu_2(\alpha_1,g^{-1}g^*,g^*)}{\nu_2(\alpha_2,g^{-1}g^*,g^*)}\frac{\nu_2(g\alpha_1,gg'^{-1}g^*,g^*)}{\nu_2(g\alpha_2,gg'^{-1}g^*,g^*)}\frac{\nu_2(\alpha_2,g'^{-1}g^*,g^*)}{\nu_2(\alpha_1,g'^{-1}g^*,g^*)} \\ =& \frac{\nu_2(\alpha_1,g^{-1}g^*,g^*)}{\nu_2(\alpha_2,g^{-1}g^*,g^*)}\frac{\nu_2(\alpha_1,g'^{-1}g^*,g^{-1}g^*)}{\nu_2(\alpha_2,g'^{-1}g^*,g^{-1}g^*)}\frac{\nu_2(\alpha_2,g'^{-1}g^*,g^*)}{\nu_2(\alpha_1,g'^{-1}g^*,g^*)} \end{aligned} \tag{7.120}$$

The above expression can be represented as Fig. 7-22 which indicates that the expression is equal to 1. Thus $U^i(g)$ defined in Eq. (7.27) form a unitary representation of G.

$U^i(g)$ satisfies Eq. (7.25)

The action of $\otimes U^i(g)$ on the 1D state on a ring in Fig. 7-23 is given by

$$\otimes_i U^i(g)|\alpha,\beta;\beta,\gamma;\gamma,\alpha\rangle = f_2(\alpha,\beta,g,g^*)f_2(\beta,\gamma,g,g^*)f_2(\gamma,\alpha,g,g^*) \times |g\alpha,g\beta;g\beta,g\gamma;g\gamma,g\alpha\rangle$$

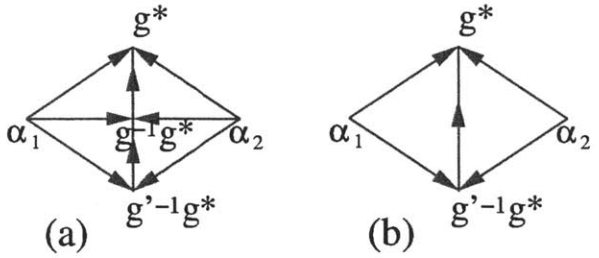

Figure 7-22: The evaluation of the 2-cocycle ν_2 on the above two complexes with branching structure gives rise to two phase factors in Eq. (7.118) and Eq. (7.119), which shows that the ratio of the two factors, Eq. (7.120), is equal to 1, since the complexes in (a) and (b) overlap.

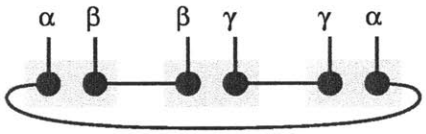

Figure 7-23: The 1D state Eq. (7.26) on a ring. The degrees of freedom form maximally entangled dimer states.

From Eq. (7.28), we see that

$$\begin{aligned} & f_2(\alpha,\beta,g,g^*)f_2(\beta,\gamma,g,g^*)f_2(\gamma,\alpha,g,g^*) \\ = & \frac{\nu_2(\alpha,g^{-1}g^*,g^*)}{\nu_2(\beta,g^{-1}g^*,g^*)}\frac{\nu_2(\beta,g^{-1}g^*,g^*)}{\nu_2(\gamma,g^{-1}g^*,g^*)}\frac{\nu_2(\gamma,g^{-1}g^*,g^*)}{\nu_2(\alpha,g^{-1}g^*,g^*)} \\ = & 1 \end{aligned} \tag{7.121}$$

We find that

$$\otimes_i U^i(g)|\alpha,\beta;\beta,\gamma;\gamma,\alpha\rangle = |g\alpha,g\beta;g\beta,g\gamma;g\gamma,g\alpha\rangle.$$

The state $|\Psi_{\text{pSRE}}\rangle$ on a ring is invariant under the symmetry transformation. So, U^i defined in Eq. (7.27) is indeed a solution of Eq. (7.25). We can obtain one solution for every cocycle in $\mathcal{H}^2(G,U(1))$ and each solution correspond to a SPT phase in 1 dimensions.

States at the chain end form a projective representation

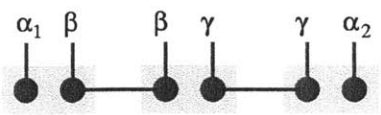

Figure 7-24: A segment of 1D chain with open ends. The degrees of freedom not on the end form maximally entangled dimer states.

Now let us consider the action of on-site symmetry transformation $\otimes_i U^i(g)$ on a segment with boundary (see Fig. 7-24):

$$\begin{aligned} &\otimes_i U^i(g)|\alpha_1,\beta;\beta,\gamma;\gamma,\alpha_2\rangle \\ &= f_2(\alpha_1,\beta,g,g^*)f_2(\beta,\gamma,g,g^*)|g\alpha_1,g\beta;g\beta,g\gamma;g\gamma,g\alpha_2\rangle \\ &= \frac{\nu_2(\alpha_1,g^{-1}g^*,g^*)}{\nu_2(\alpha_2,g^{-1}g^*,g^*)}|g\alpha_1,g\beta;g\beta,g\gamma;g\gamma,g\alpha_2\rangle. \end{aligned} \tag{7.122}$$

or

$$\otimes_i U^i(g)|\alpha_1,\alpha_2\rangle_0 = \frac{\nu_2(\alpha_1,g^{-1}g^*,g^*)}{\nu_2(\alpha_2,g^{-1}g^*,g^*)}|g\alpha_1,g\alpha_2\rangle_0, \tag{7.123}$$

where

$$|\alpha_1,\alpha_2\rangle_0 = \sum_{\beta,\gamma}|\alpha_1,\beta;\beta,\gamma;\gamma,\alpha_2\rangle. \tag{7.124}$$

Eqn. (7.123), is the same as Eq. (7.27) and Eq. (7.28). Thus, $\otimes_i U^i(g)$ form a linear representation of G.

Note that $|\alpha_1,\alpha_2\rangle_0$ is the ground state of our fixed-point model on a segment of chain, where all the internal degrees of freedom form the maximally entangled dimers (just like the ground state on a ring), while the boundary degrees of freedom are labeled by α_1 and α_2 on the chain ends. α_1 and α_2 label the effective low energy degrees of freedom $|\alpha_1,\alpha_2\rangle_0$. Those low energy degrees of freedom form a linear representation of the symmetry transformation as expected. Eqn. (7.123) describe how the boundary low energy degrees of freedom $|\alpha_1,\alpha_2\rangle_0$ transform under the symmetry transformation.

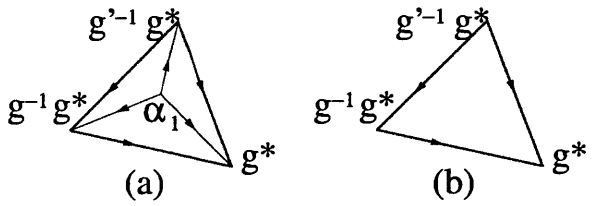

Figure 7-25: (a) The graphic representation of $\frac{\nu_2(\alpha_1,g'^{-1}g^*,g^{-1}g^*)\nu_2(\alpha_1,g^{-1}g^*,g^*)}{\nu_2(\alpha_1,g'^{-1}g^*,g^*)}$. (b) The graphic representation of $\nu_2(g'^{-1}g^*,g^{-1}g^*,g^*)$ which allows us to show $\frac{\nu_2(\alpha_1,g'^{-1}g^*,g^{-1}g^*)\nu_2(\alpha_1,g^{-1}g^*,g^*)}{\nu_2(\alpha_1,g'^{-1}g^*,g^*)} = \nu_2(g'^{-1}g^*,g^{-1}g^*,g^*)$.

On the other hand, the symmetry transformation $\otimes_i U^i(g)$ factorize (see Eq. (7.123)), also as expected. This is because the degrees of freedom labeled by α_1 and α_2 are located far apart and decouple. We have (on the end whose states are labeled by α_1)

$$\otimes_i U^i(g)|\alpha_1\rangle_0 = \nu_2(\alpha_1,g^{-1}g^*,g^*)|g\alpha_1\rangle_0. \tag{7.125}$$

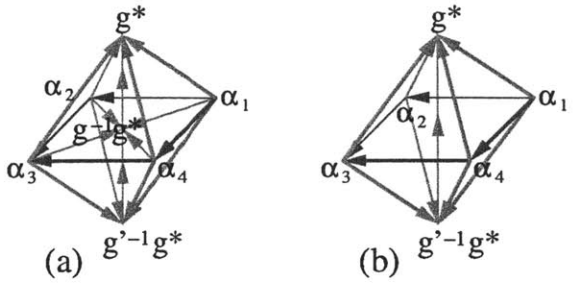

Figure 7-26: (a) The graphic representation of the phase factor Eq. (7.127). (b) The graphic representation of the phase factor Eq. (7.128). The graphic representations indicate that the two phases are the same.

Such transformation satisfies (see Fig. 7-25)

$$\begin{aligned}
&\otimes_i U^i(g'g^{-1}) \otimes_i U^i(g)|\alpha_1\rangle_0 \\
&= \frac{\nu_2(g\alpha_1, gg'^{-1}g^*, g^*)\nu_2(\alpha_1, g^{-1}g^*, g^*)}{\nu_2(\alpha_1, g'^{-1}g^*, g^*)} \otimes_i U^i(g')|\alpha_1\rangle_0 \\
&= \frac{\nu_2(\alpha_1, g'^{-1}g^*, g^{-1}g^*)\nu_2(\alpha_1, g^{-1}g^*, g^*)}{\nu_2(\alpha_1, g'^{-1}g^*, g^*)} \otimes_i U^i(g')|\alpha_1\rangle_0 \\
&= \nu_2(g'^{-1}g^*, g^{-1}g^*, g^*) \otimes_i U^i(g')|\alpha_1\rangle_0. \qquad (7.126)
\end{aligned}$$

We see that the degrees of freedom on one end form a projective representation labeled by the 2-cocycle ν_2, the same 2-cocycle ν_2 that characterize the symmetry transformation of the SRE state.

7.4.5 (2+1)D solutions of Eq. (7.25)

$U^i(g)$ is a linear representation

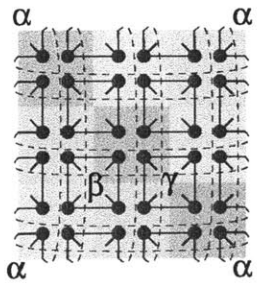

Figure 7-27: A 2D $|\Psi_{\text{pSRE}}\rangle$ state on a torus. In $|\Psi_{\text{pSRE}}\rangle$, the linked dots carry the same index $\alpha, \beta, \gamma, ...$

To show that U^i defined in Eq. (7.33) is a linear representation of G, let us compare the action of two symmetry transformations: $U^i(g)U^i(g^{-1}g')$ with the action of $U^i(g')$, which

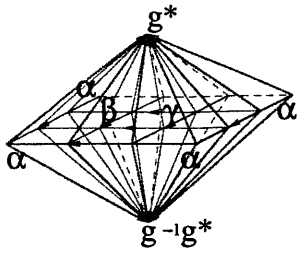

Figure 7-28: The graphic representation of the phase F_3 in Eq. (7.129). F_3 is the value of a 3-cocycle ν_3 on the above complex with a branching structure. Note that the top pyramid and the bottom pyramid each form a solid torus (due to the periodic boundary condition) and the whole complex is a sphere. So $F_3 = 1$. Note that the two pyramids on top and blow each small square represent the phase factor f_3 in Eq. (7.33).

changes $|\alpha_1, \alpha_2, \alpha_3, \alpha_4\rangle$ to $|g'\alpha_1, g'\alpha_2, g'\alpha_3, g'\alpha_4| >$. One has a phase factor

$$\begin{aligned}
&\frac{\nu_3(\alpha_1, \alpha_2, g^{-1}g^*, g^*)\nu_3(\alpha_2, \alpha_3, g^{-1}g^*, g^*)}{\nu_3(\alpha_4, \alpha_3, g^{-1}g^*, g^*)\nu_3(\alpha_1, \alpha_4, g^{-1}g^*, g^*)} \frac{\nu_3(g\alpha_1, g\alpha_2, gg'^{-1}g^*, g^*)\nu_3(g\alpha_2, g\alpha_3, gg'^{-1}g^*, g^*)}{\nu_3(g\alpha_4, g\alpha_3, gg'^{-1}g^*, g^*)\nu_3(g\alpha_1, g\alpha_4, gg'^{-1}g^*, g^*)} \\
&= \frac{\nu_3(\alpha_1, \alpha_2, g^{-1}g^*, g^*)\nu_3(\alpha_2, \alpha_3, g^{-1}g^*, g^*)}{\nu_3(\alpha_4, \alpha_3, g^{-1}g^*, g^*)\nu_3(\alpha_1, \alpha_4, g^{-1}g^*, g^*)} \frac{\nu_3(\alpha_1, \alpha_2, g'^{-1}g^*, g^{-1}g^*)\nu_3(\alpha_2, \alpha_3, g'^{-1}g^*, g^{-1}g^*)}{\nu_3(\alpha_4, \alpha_3, g'^{-1}g^*, g^{-1}g^*)\nu_3(\alpha_1, \alpha_4, g'^{-1}g^*, g^{-1}g^*)}
\end{aligned} \tag{7.127}$$

and the other has a phase factor

$$\frac{\nu_3(\alpha_1, \alpha_2, g'^{-1}g^*, g^*)\nu_3(\alpha_2, \alpha_3, g'^{-1}g^*, g^*)}{\nu_3(\alpha_4, \alpha_3, g'^{-1}g^*, g^*)\nu_3(\alpha_1, \alpha_4, g'^{-1}g^*, g^*)} \tag{7.128}$$

From their graphic representations Fig. 7-26, we see that the two phases are the same. Thus $U^i(g)$ form an unitary representation of the symmetry group G.

$U^i(g)$ satisfies Eq. (7.25)

Following a similar approach as for the (1+1)D case, we can also show that the state $|\Psi_{\text{pSRE}}\rangle$ on a 2D complex (see Fig. 7-27) that is a boundary of another graph is invariant under the symmetry transformation $\otimes_i U^i$ (see Fig. 7-28):

$$\otimes_i U^i |\Psi_{\text{pSRE}}\rangle = F_3 |\Psi_{\text{pSRE}}\rangle = |\Psi_{\text{pSRE}}\rangle \tag{7.129}$$

So, U^i defined in Eq. (7.33) is indeed a solution of Eq. (7.25). We can obtain one solution for every cocycle in $\mathcal{H}^3(G, U_T(1))$ and each solution correspond to a SPT phase in 2 dimensions.

The action of $\otimes U^i(g)$ on $|\Psi_{\text{pSRE}}\rangle$ with boundary

Now let us consider the action of $\otimes_i U^i$ on a state in Fig. 7-29 with a boundary (see Fig. 7-30):

$$\otimes_i U^i(g) |\alpha_1, \alpha_2, \beta, \gamma, ...\rangle = \tilde{F}_3(g, g^*; \alpha_1, \alpha_2, \beta, \gamma, ...) |g\alpha_1, g\alpha_2, g\beta, g\gamma, ...\rangle \tag{7.130}$$

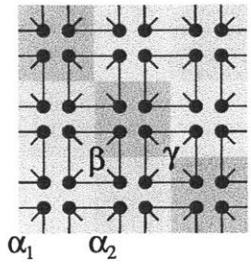

Figure 7-29: A 2D $|\Psi_{\text{pSRE}}\rangle$ state on an open square. In $|\Psi_{\text{pSRE}}\rangle$, the linked dots carry the same index $\alpha_1, \alpha_2, \beta, \gamma, ...$ The indices on the boundary are given by $\alpha_1, \alpha_2, ...$ The indices inside the square are given by $\beta, \gamma, ...$

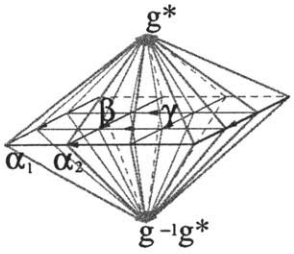

Figure 7-30: The graphic representation of the phase $\tilde{F}_3(g, g^*; \alpha_1, \alpha_2, \beta, \gamma, ...)$ in Eq. (7.130). Compared to the complex in Fig. 7-28, the above complex do not have the periodic boundary condition.

From the Fig. 7-30 and the geometric meaning of the cocycles, we find that

$$\tilde{F}_3(g,g^*;\alpha_1,\alpha_2,\beta,\gamma,...) = \prod_{\langle ij\rangle} \nu_3^{s_{ij}}(\alpha_i,\alpha_j,g^{-1}g^*,g^*) \tag{7.131}$$

where $\prod_{\langle ij\rangle}$ is a product over the nearest neighbor bonds $\{ij\}$, $|i-j|=1$, around the boundary. The direction $i \to j$ is the direction of the bond and $s_{ij} = 1$ f $i > j$, $s_{ij} = -1$ f $i < j$. Since $\tilde{F}_3$ is independent of the indices $\beta, \gamma, ...$ that are not on the boundary, we find

$$\otimes_i U^i(g)|\{\alpha_i\}\rangle_0 = \prod_{\langle ij\rangle} \nu_3^{s_{ij}}(\alpha_i,\alpha_j,g^{-1}g^*,g^*)|\{g\alpha_i\}\rangle_0 \tag{7.132}$$

where $|\{\alpha_i\}\rangle_0$ is the SPT state with a boundary which depends on the indices $\{\alpha_i\}$ on the boundary:

$$|\{\alpha_i\}\rangle_0 = \sum_{\beta,\gamma,...\in G} |\alpha_1,\alpha_2,\beta,\gamma,...\rangle. \tag{7.133}$$

We see that the action of $\otimes_i U^i(g)$ on $|\{\alpha_i\}\rangle_0$ is very similar to the action of a single $U^i(g)$ on a single site (compare Figs. 7-12 and 7-30). Using a similar approach, we can show that $\otimes_i U^i(g)$ indeed form a linear representation (see Fig. 7-26), when viewed as an operator $U_b(g)$ acting on the boundary state $|\{\alpha_i\}\rangle_0$.

To summarize, we discussed the form of on-site symmetry transformations $\otimes_i U^i(g)$ in a basis where the many-body ground state is a simple product state. We find that different on-site symmetry transformations can be constructed from each 3-cocycle ν_3 in $\mathcal{H}^3[G, U_T(1)]$.

We would like to stress that, in such a simple basis, the symmetry transformation $\otimes_i U^i(g)$ on the boundary Eq. (7.132) has a very unusual locality property: Due to the non-trivial phase factor $\prod_{\langle ij\rangle} \nu_3^{s_{ij}}(\alpha_i,\alpha_j,g^{-1}g^*,g^*)$, we cannot view $U_b(g)$ (acting on the boundary state $|\{\alpha_i\}\rangle_0$) as a direct product of local operators acting on each boundary sites $|\alpha_i\rangle$. (Note that we can view the boundary state $|\{\alpha_i\}\rangle_0$ as $|\{\alpha_i\}\rangle_0 = \otimes_{i\in\text{boundary}}|\alpha_i\rangle$.) Therefore, $U_b(g)$ is *not* a on-site symmetry transformation on the *boundary*.

In the above, we have viewed i as effective sites on the boundary with physical states $|\alpha_i\rangle$ on each site. We see that the symmetry transformation is not an on-site symmetry transformation. If we view, instead, each nearest neighbor bond $\langle ij\rangle$ as an effective site with physical states $|\alpha_i\alpha_j\rangle$ on each site, then the symmetry transformation will be an "on-site" symmetry transformation, but the states on different bounds are not independent and $|\{\alpha_i\}\rangle_0 \neq \otimes_{\langle ij\rangle\in\text{boundary}}|\alpha_i\alpha_j\rangle$.

Thus in a basis where the many-body ground state is a simple product state, although $\otimes_i U^i(g)$ is an on-site symmetry transformation when acting on the bulk state, it cannot be an on-site symmetry transformation when viewed as a symmetry transformation acting on the effective low energy degrees of freedom on the boundary when the 3-cocycle ν_3 is non-trivial. This is the non-trivial physical properties that characterize a non-trivial SPT phase in (2+1)D (see section 7.1 and [CLW11] for more details).

7.4.6 $(2+1)D$ SPT states constructed from 3-cocycles and matrix product unitary operator

In this section, we are going to apply the MPUO method to the general models constructed in section 7.2.1 and show that for the model constructed from a 3-cocycle $\nu_3(g_0,g_1,g_2,g_3)$, the effective MPUO on the boundary transform with the same 3-cocycle. Therefore, according to the result in [CLW11] or section 7.1, models constructed from nontrivial $\nu_3(g_0,g_1,g_2,g_3)$ must either break the symmetry or have gapless excitations if the system has a boundary. Moreover, we can show the contrary for models constructed from trivial $\nu_3(g_0,g_1,g_2,g_3)$. That is, for models constructed from trivial $\nu_3(g_0,g_1,g_2,g_3)$ we are going to explicitly construct a short range entangled symmetric state for the effective symmetry on the boundary. For basic definition and properties of MPUO, see section 7.4.3.

In general, the effective symmetry on the 1D boundary of a 2D model can be written as a matrix product unitary operator

$$U=\sum_{\{i_k\},\{i'_k\}}\mathrm{Tr}(T^{i_1,i'_1}T^{i_2,i'_2}...T^{i_N,i'_N})|i'_1i'_2...i'_N\rangle\langle i_1i_2...i_N| \tag{7.134}$$

where i and i' are input and output physical indices and for fixed i and i', $T^{i,i'}$ is a matrix.

For the models defined in section 7.2.1, the effective symmetry $\tilde{U}(g)$ on the boundary takes the form(see section 7.4.5)

$$\tilde{U}(g)|\{\alpha_i\}\rangle=\prod_{i,j}\nu_3^{s_{ij}}(\alpha_i,\alpha_j,g^{-1}g^*,g^*)|\{g\alpha_i\}\rangle \tag{7.135}$$

where $\prod_{ij}$ is a product over the nearest neighbor bonds $\{ij\}$, $|i-j|=1$, around the boundary. The direction $i\to j$ is the direction of the bond and $s_{ij}=1$ if $i>j$, $s_{ij}=-1$ if $i<j$. This symmetry operator on a 1D chain can be expressed as a MPUO. If the bond goes from α_i to α_{i+1}

$$\begin{aligned}&T_i^{\alpha_i,g\alpha_i}(g)=\textstyle\sum_{\alpha_{i+1}}\nu_3^{-1}(\alpha_i,\alpha_{i+1},g^{-1}g^*,g^*)|\alpha_i\rangle\langle\alpha_{i+1}|\ ,\forall\alpha_i\\&\text{other terms are zero}\end{aligned} \tag{7.136}$$

If the bond goes from α_{i+1} to α_i,

$$\begin{aligned}&T_i^{\alpha_i,g\alpha_i}(g)=\textstyle\sum_{\alpha_{i+1}}\nu_3(\alpha_{i+1},\alpha_i,g^{-1}g^*,g^*)|\alpha_i\rangle\langle\alpha_{i+1}|\ ,\forall\alpha_i\\&\text{other terms are zero}\end{aligned} \tag{7.137}$$

Now we compose multiple MPUOs and find their reduction rule. We will see that the reduction rule is related to the same ν_3. First, the combination of $T_i(g_2)$ and $T_i(g_1)$ gives (if the bond goes from α_i to α_{i+1})

$$\begin{aligned}&T_i(g_1,g_2)^{\alpha_i,g_1g_2\alpha_i}=\textstyle\sum_{\alpha_{i+1},\alpha'_{i+1}}\nu_3^{-1}(\alpha_i,\alpha_{i+1},g_2^{-1}g^*,g^*)\times\\&\nu_3^{*s(g_2)}(g_2\alpha_i,\alpha'_{i+1},g_1^{-1}g^*,g^*)|\alpha_i,g_2\alpha_i\rangle\langle\alpha_{i+1},\alpha'_{i+1}|\end{aligned} \tag{7.138}$$

This can be reduced to

$$T_i(g_1g_2)^{\alpha_i,g_1g_2\alpha_i}=\sum_{\alpha_{i+1}}\nu_3^{-1}(\alpha_i,\alpha_{i+1},g_2^{-1}g_1^{-1}g^*,g^*)|\alpha_i\rangle\langle\alpha_{i+1}| \tag{7.139}$$

by applying the following projection operator to the right side of the matrices

$$P^r_{g_1,g_2} = \sum_{\alpha_{i+1}} \nu_3^{-1}(\alpha_{i+1}, g_2^{-1}g_1^{-1}g^*, g_2^{-1}g^*, g^*)|\alpha_{i+1}, g_2\alpha_{i+1}\rangle\langle\alpha_{i+1}|$$

and the hermitian conjugate of

$$P^l_{g_1,g_2} = \sum_{\alpha_i} \nu_3^{-1}(\alpha_i, g_2^{-1}g_1^{-1}g^*, g_2^{-1}g^*, g^*)|\alpha_i, g_2\alpha_i\rangle\langle\alpha_i| \tag{7.140}$$

to the left side of the matrices. This is because,

$$\nu_3(g_2\alpha_i, g_2\alpha_{i+1}, g_1^{-1}g^*, g^*) = \nu_3^{s(g_2)}(\alpha_i, \alpha_{i+1}, g_2^{-1}g_1^{-1}g^*, g_2^{-1}g^*) \tag{7.141}$$

and the 3-cocycle condition of ν_3

$$\begin{aligned}&\nu_3(\alpha_i, \alpha_{i+1}, g_2^{-1}g^*, g^*)\nu_3(\alpha_i, \alpha_{i+1}, g_2^{-1}g_1^{-1}g^*, g_2^{-1}g^*)\times\\ &\nu_3^{-1}(\alpha_i, g_2^{-1}g_1^{-1}g^*, g_2^{-1}g^*, g^*)\nu_3(\alpha_{i+1}, g_2^{-1}g_1^{-1}g^*, g_2^{-1}g^*, g^*)\\ &= \nu_3(\alpha_i, \alpha_{i+1}, g_2^{-1}g_1^{-1}g^*, g^*)\end{aligned} \tag{7.142}$$

It is easy to check that the same reduction procedure applies when the bond goes from α_{i+1} to α_i. The above definition of P^l and P^r has picked a particular gauge choice of phase for P^l and P^r.

Next we consider the combination of three MPUOs and find the corresponding 3-cocycle associated with different ways of combining the three MPUOs into one. If we combine $T(g_2)$,$T(g_1)$ first and then combine $T(g_1g_2)$ with $T(g_3)$, the combined operation of P_{g_1,g_2} and $P_{g_1g_2,g_3}$ is (we omit the site label i)

$$\begin{aligned}&(P_{g_1,g_2}\otimes I)P_{g_1g_2,g_3}\\ &= \sum_{\alpha} \nu_3(\alpha, g_3^{-1}g_2^{-1}g_1^{-1}g^*, g_3^{-1}g_2^{-1}g^*, g_3^{-1}g^*)\times\\ &\quad \nu_3(\alpha, g_3^{-1}g_2^{-1}g_1^{-1}g^*, g_3^{-1}g^*, g^*)|\alpha, g_3\alpha, g_2g_3\alpha\rangle\langle\alpha|.\end{aligned} \tag{7.143}$$

On the other hand, if we combine $T(g_3)$,$T(g_2)$ first and then combine $T(g_2g_3)$ with $T(g_1)$, the combined operator of P_{g_2,g_3} and P_{g_1,g_2g_3} is

$$\begin{aligned}&(I\otimes P_{g_2,g_3})P_{g_1,g_2g_3} =\\ &\textstyle\sum_\alpha \nu_3(\alpha, g_3^{-1}g_2^{-1}g^*, g_3^{-1}g^*, g^*)\times\\ &\nu_3(\alpha, g_3^{-1}g_2^{-1}g_1^{-1}g^*, g_3^{-1}g_2^{-1}g^*, g^*)|\alpha, g_3\alpha, g_2g_3\alpha\rangle\langle\alpha|\end{aligned} \tag{7.144}$$

These two differ by a phase factor

$$\nu_3(g_3^{-1}g_2^{-1}g_1^{-1}g^*, g_3^{-1}g_2^{-1}g^*, g_3^{-1}g^*, g^*) \tag{7.145}$$

Hence we see that, the reduction procedure of T's is associative up to phase. The phase factor is the same 3-cocycle that we used to construct the model. From the result in [CLW11] we know that if ν_3 is nontrivial, the model we constructed has a nontrivial boundary which cannot have a gapped symmetric ground state. It must either break the symmetry or be gapless. Therefore, the model constructed with nontrivial 3-cocycles belong to nontrivial SPT phases.

On the other hand, if the model is constructed from a trivial 3-cocycle, the boundary effective symmetry does allow SRE symmetric state. Actually, the SRE symmetric state on the boundary can be constructed explicitly for the models discussed here. If ν_3 is trivial, it takes the form of a 3-coboundary

$$\nu_3(g_0,g_1,g_2,g_3)=\frac{\mu_2(g_1,g_2,g_3)\mu_2(g_0,g_1,g_3)}{\mu_2(g_0,g_2,g_3)\mu_2(g_0,g_1,g_2)} \tag{7.146}$$

where μ_2 is an arbitrary 2-cochain. Note that it is not necessarily a cocycle. The effective symmetry on the boundary can hence be written as

$$\tilde{U}(g)|\{\alpha_i\}\rangle=\prod_{i,j}\left(\frac{\mu_2(\alpha_j,g^{-1}g^*,g^*)\mu_2(\alpha_i,\alpha_j,g^*)}{\mu_2(\alpha_i,g^{-1}g^*,g^*)\mu_2(\alpha_i,\alpha_j,g^{-1}g^*)}\right)^{s_{ij}}|\{g\alpha_i\}\rangle \tag{7.147}$$

The $\mu_2(\alpha_i,g^{-1}g^*,g^*)$ terms cancel out in the product of phase factors, and the remaining terms can be grouped into two sets $\prod_{ij}\mu_2^{s_{ij}}(\alpha_i,\alpha_j,g^*)$ and $\prod_{ij}\mu_2^{-s_{ij}}(\alpha_i,\alpha_j,g^{-1}g^*)=\prod_{ij}\mu_2^{-s_{ij}s(g)}(g\alpha_i,g\alpha_j,g^*)$. Define $\Theta(g)=\prod_{ij}\sum_{\alpha_i,\alpha_j}\mu_2^{s_{ij}}(\alpha_i,\alpha_j,g^*)|\alpha_i\alpha_j\rangle\langle\alpha_i\alpha_j|$. $\Theta(g)$ is a product of local unitaries. It is easy to see that

$$\tilde{U}(g)=\Theta^\dagger(g)\left(\sum_{\{\alpha_i\}}|\{g\alpha_i\}\rangle\langle\{\alpha_i\}|\right)\Theta(g) \tag{7.148}$$

(a complex conjugation operation needs to be added if $\tilde{U}(g)$ is anti-unitary). The term in the middle is an on-site operation which permutes the basis. It has a simple symmetric state which is a product state $\otimes_i(\sum_{\alpha_i}|\alpha_i\rangle)$. Therefore $\Theta^\dagger(g)\otimes_i(\sum_{\alpha_i}|\alpha_i\rangle)$ is a symmetric state of $\tilde{U}(g)$. Because $\otimes_i(\sum_{\alpha_i}|\alpha_i\rangle)$ is a product state and $\Theta^\dagger(g)$ is a product of local unitaries, this is a short range entangled state. Therefore, we have explicitly constructed a short range entangled symmetric state on the boundary if the model is constructed from a trivial 3-cocycle ν_3.

Part IV

Application to Quantum Computation

With an efficient tool to study many-body entangled quantum states in physical systems (the tensor network representation) and a better understanding of possible many-body entanglement structures, we now want to address the question of which many-body entangled states are useful for quantum computation. The answer to this question depends largely on the specific method one chooses to build the quantum computer. For example, in the topological quantum computation model, it is known that quantum states with intrinsic topological order, hence long range entanglement, are necessary. Moreover, there are special requirements on the fractional statistics of the quasi particles of the system in order to achieve the full power of quantum computation. First of all nonabelian statistics is necessary and it has been shown that the $\nu = 5/2$ fractional quantum Hall state is sufficient to realize universal quantum computation in the topological model. In this part, we focus on a different model of quantum computation – the Measurement-based Quantum Computation (MBQC) and ask what many-body entanglement resource is useful. It turns out that a very different kind of many-body entanglement is needed for MBQC compared to the topological model. In particular, short range entanglement is sufficient for the realization of measurement-based quantum computation.[5] In Chapter 8, we review the measurement-based quantum computation model and focus on its relation to the tensor network representation of many-body entangled states studied in previous works. Such a connection allows us to find physically more realistic many-body entangled resource states for measurement-based quantum computation in Chapter 9 and generalize the measurement-based quantum computation model to fermionic systems in Chapter 10.

[5]Of course the fault-tolerance property of topological quantum computation model is lost.

Chapter 8

Measurement-based quantum computation and tensor product states

An important application of our understanding of many-body entanglement is to design better quantum computation schemes. Many-body entanglement is an essential ingredient in the successful and efficient implementation of quantum computation but its creation and maintenance also leads to a major difficulty in experimental realization. It is highly desirable to find experimentally feasible ways to achieve the many-body entanglement necessary for useful quantum computation.

Different models of quantum computation require different forms of many-body entanglement patterns. We focus on the model of measurement-based quantum computation. Measurement-based quantum computation implements the whole computational process with only single particle measurements on a proper many-body entangled resource state. The key to the successful realization of the computational model hence lies in finding and generating a proper many-body entangled state. In this chapter, we review the measurement-base quantum computation model. We start in section 8.1 from the first and best known proposal of measurement-based quantum computation based on the so-called 'cluster' state. After its first proposal, a lot of progress was made both theoretically and experimentally on this model of quantum computation. In particular, we review in section 8.2 how the tensor network representation of the resource state reveals the entanglement assisted information flow generated by the measurement operations. After such a connection was established, many-body resource states were found for measurement-based quantum computation beyond the 'cluster' state model. This is the basis for our construction of experimentally more realistic resource states in the next two chapters. This chapter is based on previous works[RB01, GE07].

8.1 Measurement-based quantum computation

In the usual circuit model of quantum computation, a quantum computer runs in a very similar way to the classical computers we use today. The computation starts with a bunch of 'fresh' quantum mechanical bits (qubits), which are initialized in certain product states (for example with all spins pointing in the $+z$ direction for spin 1/2 particles). The qubits are then sent individually or in pairs through unitary gates (the equivalents of And, OR gates

in classical computers) and get entangled. Finally, the qubits are measured in certain basis which yields the computation result. The necessary components for the circuit model of quantum computation include then the supply of fresh qubits (in product states), coherent unitary operations on single and two qubits, and measurement operations on individual qubits. The hardest part in experiment, as it turns out, is the realization of coherent unitary operations, especially on two qubits. A great deal of effort has been put into this and until now the best record for the realization of two qubit unitary gates has been set in trapped ion system, with fidelity $> 99\%$[BKRB08]. The challenge lies in keeping or increasing the fidelity while scaling the computation scheme up to hundreds or thousands of qubits.

Measurement-based quantum computation [RB01], also called the one-way quantum computation model, provides an alternative way to realize quantum computation, one that does not require coherent unitary operations. In the measurement-based quantum computation model, we start with a many-body entangled state called the resource state and implement the computation algorithm with only a series of adaptive single particle measurements which simulate the initialization, the unitary gate operations and the readout processes in the circuit model (see Fig. 8-1). Such a setup could potentially greatly reduce the experimental difficulty for building a quantum computer, as coherent unitary operations are not necessary at all!

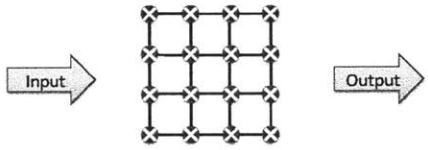

Figure 8-1: Measurement-based quantum computation. The whole computational process, including initialization, unitary operation and readout, is carried out with single site measurements on a many-body entangled state.

The first resource state proposed in the original work of Raussendorf and Briegel [RB01] was the cluster state (also called the graph state in some literature) on a two dimensional square lattice. The cluster state on a lattice is composed of qubits and is a stabilizer state (which means it is the eigenvalue 1 eigenstates of a set of commuting Pauli operators [NC00]) with stabilizers

$$X_i \prod_{n_i} Z_{n_i} \tag{8.1}$$

where i labels different sites in the lattice and n_i are the neighboring sites of i. For example, on a 2D square lattice, n_i includes the sites above, below, to the left and to the right of i. The cluster state $|\psi_{\text{cluster}}\rangle$ hence satisfies

$$X_i \prod_{n_i} Z_{n_i} |\psi_{\text{cluster}}\rangle = |\psi_{\text{cluster}}\rangle\,, \ \forall i \tag{8.2}$$

Such a definition yields a unique many-body entangled state $|\psi_{\text{cluster}}\rangle$ and applies to any graph (hence the name graph state). In [RB01] it was shown that single qubit measurements on a 2D square lattice cluster state can be used to simulate all the necessary computational steps in the circuit model quantum computation. Actually the two models have the same

computational power in that each can simulate the other efficiently.

The model appeared quite surprising at first. As measurement operations are usually used to extract information from the computation ensemble, it seems that the cluster state 'knows' the answer to all quantum algorithms and encodes them all in its wave-function, which sounds quite impossible. Soon it was realized that the measurement-based quantum computation is related to teleportation[Nie06], where measurement can be used to transmit information (and change it along the way) with the help of entanglement[GC99]. Based on such an understanding, the measurement-based quantum computation model was generalized to many other lattice structures, for the purpose of resistance against error and randomness[RHG05, RBB02].

The key challenge in the experimental realization of this computational model is in building a large scale cluster state. Small scale cluster states with < 10 qubits have been successfully generated[LZG+07], by entangling individual qubits with coherent quantum gates into a big entangled state. However, scaling this process up to hundreds or even thousands of qubits seems extremely difficult, as decoherence sets in before much of the entangling process is done. An alternative approach to generate large scale many-body entangled states is to trap a large number of particles together, engineer the necessary interactions among them such that the desired state exists as a gapped ground state and then cool the system down to below its excitation energy. This approach, if realized, would be much easier to scale up and the generated many-body entangled state would be more stable against decoherence and noise due to the existence of a gap in the system. The cluster state does exist as the gapped ground state of local interactions, but unfortunately the interaction involves at least four particles which is physically unrealistic[Nie06, VdNLDB08]. If we relax the requirement and allow perturbative construction, then a two-body Hamiltonian can be found which has the cluster state as its perturbative ground state at fourth order perturbation[BR06].

8.2 MBQC in tensor product states

A major development in the theory of measurement-based quantum computation was achieved by Gross and Eisert [GE07]. They proposed a much more general way to construct resource states beyond the cluster state based on the relation between measurement-based quantum computation and the tensor network representation of the state. In this section, we review such a connection. It serves as the basis for our construction in the next two chapters.

8.2.1 Teleportation

The basic building block of measurement-based quantum computation is teleportation, which is a process of transmitting and processing quantum information with measurement operations with the help of entangled pair states[BBC+93, GC99].

First, to see how teleportation transmits information, consider the following setup that involves an input qubit $|\psi\rangle$ to be teleported and an entangled pair $|E\rangle = |00\rangle + |11\rangle$ (suppressing normalization) shared between the input end and the output end. The information in $|\psi\rangle$ is transmitted to the output end when one measures $|\psi\rangle$ and half of the entangled pair jointly. Furthermore, by choosing different measurement bases, different gates can be performed on $|\psi\rangle$ while it is teleported to the output end.

To see this, consider an input qubit

$$|\psi_1\rangle = m_0 |0\rangle + m_1 |1\rangle , \tag{8.3}$$

with $|m_0|^2 + |m_1|^2 = 1$, and an entangled pair $|E_{23}\rangle$, as shown in Fig. 8-2. Qubit 1 and 2 belong to the input end. Qubit 3 belongs to the output end.

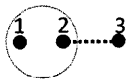

Figure 8-2: Teleportation of one-qubit unitary gates. The qubits are denoted by dots and the entangled pair is depicted by a dashed line. The big circle represents the input end and qubits inside it are measured together. After measuring qubit 1,2 together information in qubit 1 flows to qubit 3.

The total wave function of the system is

$$|\psi_{123}\rangle = (m_0 |0\rangle + m_1 |1\rangle) \otimes (|00\rangle + |11\rangle). \tag{8.4}$$

If we measure qubits 1 and 2 in the Bell basis $|\phi_{12}^{\alpha}\rangle = \sigma_\alpha \otimes I(|00\rangle + |11\rangle)$, $\alpha = 0, 1, 2, 3$, where σ_α are Pauli matrices, the wave function of the unmeasured qubit 3 results in $\langle\phi_{12}^{\alpha}|\psi_{123}\rangle = \sigma_\alpha(m_0 |0\rangle + m_1 |1\rangle)$. Thus, one can see that the original information is teleported from qubit 1 to qubit 3 with possible extra Pauli operations.

In general, teleportation not only transmits information, but also implements gates at the same time, as the Pauli gates seen at the output in the example given above. Measuring in a basis of the generic form

$$|\phi_{12}^{\alpha}\rangle = (U^\dagger \sigma_\alpha) \otimes I(|00\rangle + |11\rangle), \tag{8.5}$$

where U is any one-qubit unitary gate, yields at the output

$$\langle\phi_{12}^{\alpha}|\psi_{123}\rangle = \sigma_\alpha U(m_0 |0\rangle + m_1 |1\rangle)_3 = \sigma_\alpha U |\psi_1\rangle . \tag{8.6}$$

For example, we can choose U as the Hadamard operation $H = |0\rangle\langle+| + |1\rangle\langle-|$, where $|\pm\rangle = \frac{1}{\sqrt{2}}(|0\rangle \pm |1\rangle)$, and the phase gate $Z(\theta) = e^{-i\frac{\theta}{2}} |0\rangle\langle 0| + e^{i\frac{\theta}{2}} |1\rangle\langle 1|$ to implement the corresponding one-qubit gates during teleportation.

In addition to one-qubit gates, the requirement of universal quantum computation also involves certain two-qubit gates, for example, the controlled-Z gate together with the Hadamard gates on the two qubits[NC00] which we denote as U_{ph}. Specifically,

$$U_{ph} = |00\rangle\langle++| + |01\rangle\langle+-| + |10\rangle\langle-+| - |11\rangle\langle--| . \tag{8.7}$$

The schematic for teleporting U_{ph} is depicted in Fig. 8-3. It can be interpreted as a generalized version of teleportation which involves a two-qubit input and three entangled pairs[VC04]. It can be checked that measuring qubits 1,2,3 in

$$(\sigma_x)^i \otimes (\sigma_x)^j \otimes I(|0++\rangle \pm |1--\rangle), \tag{8.8}$$

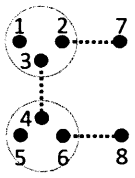

Figure 8-3: Teleportation of the two-qubit controlled operation U_{ph}. As shown in the figure, qubit 1 is the control qubit and qubit 5 is the target qubit. After proper 3-qubit measurements are implemented on qubits $1,2,3$ and $4,5,6$ respectively, U_{ph} gets teleported from qubits 1 and 5 to qubits 7 and 8.

and measuring qubits 4,5,6 in

$$(\sigma_x)^k \otimes (\sigma_x)^l \otimes I(|00+\rangle \pm |11-\rangle), \tag{8.9}$$

with $i,j,k,l = 0,1$, teleports U_{ph} to qubits 7,8 up to Pauli operations on 7,8 separately. Hereby, one can see that teleportation is indeed a way of realizing universal quantum computation, with multi-qubit measurements.

8.2.2 Measurement-based quantum computation as teleportation in projected entangled pair state

The projected entangled pair state (PEPS)[VMC08] (see Chapter 2) representation of many-body entangled states turns out to be very useful for understanding the power of resource states in measurement-based quantum computation. More explicitly, if we imagine the maximally entangled pairs in PEPS as in a virtual space where teleportation can be achieved, and interpret the physical Hilbert space of spins as a projection from many virtual spins, then measurements on the physical spins correspond to teleportation steps in the virtual space and it may be possible that we can implement a universal set of unitary operations on virtual qubits by merely performing single-particle measurements in the physical space[GE07].

For simplicity, let us first consider PEPS on a one-dimensional chain. As depicted in Fig. 8-4, a spatially one-dimensional (1D) virtual space is a chain consisting of maximally entangled pairs shared between nearest-neighbor sites. With D-dimensional virtual spins, the maximally entangled pairs are in state $\sum_{i=0}^{D-1} |ii\rangle$. At the left and right end of the chain, there are boundary states $|L\rangle$ and $|R\rangle$. On every site, there are two virtual spins, each being half of an entangled pair connecting neighboring sites. Shortly, we discuss how virtual and physical spins are related via a projection on each site.

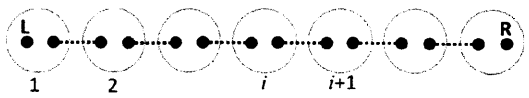

Figure 8-4: Illustration of a 1D PEPS. The virtual space consists of left and right boundaries $|L\rangle$, $|R\rangle$, and virtual spins entangled in $\sum_{i=0}^{D-1} |ii\rangle$. The big circle represents an on-site projection where virtual spins inside are projected together to the physical space.

The wave function for the virtual chain follows

$$|\psi_v\rangle = |L\rangle \prod_{k=1}^{N-1} \left(\sum_{i=0}^{D-1} |ii\rangle_{k,k+1} \right) |R\rangle \tag{8.10}$$

where k labels different sites in the chain.

A PEPS with d-dimensional physical spins is obtained by a local projection P on virtual spins located on each site in the virtual space which maps the virtual space to physical space. In Fig. 8-4, the projections are presented as circles. Note that the projection here is only a map between two Hilbert spaces and is not the usual sense of projection that needs to obey $P^2 = P$. More specifically,

$$|\psi_{PEPS}\rangle = \prod_{k=1}^{N} P_k |L\rangle \prod_{k=1}^{N-1} \left(\sum_{i=0}^{D-1} |ii\rangle_{k,k+1} \right) |R\rangle \tag{8.11}$$

with local projection operators on each site defined as

$$P_k = \sum_{\tilde{i}=0}^{d-1} \sum_{\ell,r=0}^{D-1} |\tilde{i}\rangle A^{\tilde{i}}_{k,\ell r} \langle \ell r| . \tag{8.12}$$

Note that each $|\tilde{i}\rangle$ is a state in the d-dimensional physical space and $A^{\tilde{i}}_{\ell r}$'s are coefficients of P that depend on $|\tilde{i}\rangle$ in the physical space that one wants to project onto. Also note that the physical dimension refers to the internal degrees of freedom of spins and is different from the spatial dimension of the lattice.

Using Eq. 8.11 & 8.12, one can show that the wave function of a 1D PEPS with N sites can be expressed as

$$|\psi_{PEPS}\rangle = \sum_{\tilde{i}_k=0}^{d-1} \langle L| A^{\tilde{i}_1}_1 A^{\tilde{i}_2}_2 .....A^{\tilde{i}_N}_N |R\rangle \left|\tilde{i}_1 \tilde{i}_2 .....\tilde{i}_N\right\rangle . \tag{8.13}$$

The PEPS construction provides a perspective to see the relation between MBQC and teleportation [GE07]. Here we give an explicit example that illustrates this idea. Consider measuring site 1 in $|\phi\rangle = a|\tilde{0}\rangle + b|\tilde{1}\rangle$ (d=2). After the measurement, the wave function of the unmeasured physical spins becomes

$$\langle \phi|\psi_{PEPS}\rangle = \sum_{\tilde{i}_k=0}^{1} \langle L| (a^* A^{\tilde{0}} + b^* A^{\tilde{1}}) A^{\tilde{i}_2}_2 .....A^{\tilde{i}_N}_N |R\rangle \left|\tilde{i}_2 \tilde{i}_3 .....\tilde{i}_N\right\rangle . \tag{8.14}$$

The form of the state remains unchanged while the left boundary gets teleported to site 2 and is changed into $\langle L| (a^* A^{\tilde{0}} + b^* A^{\tilde{1}})$, which can be viewed as a gate acting on the old boundary. From Eq. 8.12, we learned that the physical and virtual space are related by the projection. Given a certain P, we can relate measurements in the physical space to teleportation in the virtual space as well as changes in lattice boundary to unitary operations teleported in the virtual space. Quantum computation could therefore be achieved in the virtual space by choosing appropriate measurement bases in the physical space that correspond to bases for teleporting a universal set of gates in the virtual space.

In the above, we have seen that unitary operations on one spin could be realized with

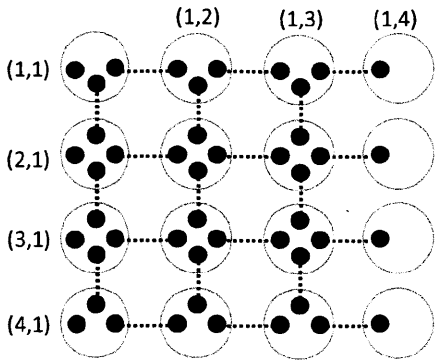

Figure 8-5: Representation of a 2D PEPS with input modes on the left boundaries.

MBQC on a 1D PEPS. With suitably chosen projection P, arbitrary single spin operations could be implemented. Yet, for the universality of quantum computation, entangling operations between two spins must also be feasible; thus a more general 2D lattice is required for MBQC. For this purpose, a 2D PEPS as shown in Fig. 8-5 can be constructed similarly. The only differences are that the virtual space now contains both vertical (between sites (i,j) and $(i+1,j)$) and horizontal (between (i,j) and $(i,j+1)$) entangled pairs $\sum_{i=0}^{D-1}|ii\rangle$, and the on site projection P_{ij} becomes

$$P_{ij}=\sum_{\tilde{i}=0}^{d-1}\sum_{u,l,r,d=0}^{D-1}\left|\tilde{i},\tilde{j}\right\rangle A^{\tilde{i}}_{ij,ulrd}\left\langle ulrd\right|, \tag{8.15}$$

which is almost the same as the 1D projection in Eq. 8.12, except that the number of virtual indices is doubled. Note that $\tilde{i}$ denotes the state of a physical spin as defined in Eq. 8.12. If P is chosen properly, a universal set of gates can be teleported in virtual space with single spin measurements on the physical space.

The cluster state provides a nice illustration of this idea. On a 2D square lattice, the cluster state is given in PEPS construction with inner dimension $D=2$ and physical dimension $d=2$. The on-site projection from virtual spins to physical spins is $P_{uldr}=\left|\tilde{0}\right\rangle\langle 00++|+\left|\tilde{1}\right\rangle\langle 11--|$, where $|\pm\rangle=|0\rangle\pm|1\rangle$ are the eigenstates of X. It was shown in [VC04] that measuring a single physical qubit in $\left|\tilde{\mp}\right\rangle$ state corresponds to teleporting a H gate in virtual space and measuring in $\left|\tilde{0}\right\rangle+e^{i\theta}\left|\tilde{1}\right\rangle$ state corresponds to teleporting HZ_θ gate where $Z_\theta=|0\rangle\langle 0|+e^{i\theta}|1\rangle\langle 1|$. Moreover, measuring two vertically connected physical spins both in $\left|\tilde{\mp}\right\rangle$ state corresponds to teleporting a controlled phase gate $U_{\text{ph}}=I-2|11\rangle\langle 11|$ up to H operations. Putting these together, we get a universal set of gates that can be teleported in virtual space with single qubit measurement in physical space. Of course, in order to achieve full computation, one needs the ability to input information, correct errors in measurement results by adaptively choosing measurement basis in next steps, and finally read out the computational result. It can be checked from the PEPS representation that 2D cluster state satisfy all these requirements and hence serve as a resource state for MBQC. Various other resource states can be constructed using this framework[GE07, GESPG07, GE10], although a general rule is still missing on whether a projected entangled pair state can be used as a resource state or not.

Chapter 9

Measurement-based quantum computation in gapped ground states of two-body Hamiltonian

From the introduction to measurement-based quantum computation in the last chapter (Chapter 8), we see that the key to the experimental realization of measurement-based quantum computation is to find and generate a proper many-body entangled resource state. Ideally, universal resource states of measurement-based quantum computation could be obtained as the unique ground state of a naturally occurring Hamiltonian, one with only nearest-neighbor two-body interactions. If this were the case, especially if an energy gap existed between the ground and first excited states, the one-way quantum computation could be robust against quantum noise and decoherence of the entanglement.

Many efforts have been made to construct the desired many-body entangled state such that it could be the ground state of a naturally occurring Hamiltonian. The cluster state, unfortunately, cannot be the exact ground state of any naturally occurring Hamiltonian[Nie06]. Perturbative approaches providing a Hamiltonian whose ground state approximates that desired have been developed [OT08, VdNLDB08, BR06]. A nice scheme for constructing universal resource states has been proposed and has yielded many interesting examples[GE07]. Based on this, a mixed approach can be taken, using a 1D Hamiltonian to create chains, that are then coupled by two-body unitary operations[GE07, BM08] to form a 2D resource state. Matrix product state techniques allow any measurement of these 1D chains to be computed efficiently, on a classical computer, however, implying that they alone are insufficient for quantum computation. Two-dimensional many-body entangled states are thus likely to be essential for arbitrary quantum computations, but few techniques are presently known for finding local 2D Hamiltonians with the desired ground states. Properties of such states generally remain intrinsically hard to determine [SWVC07].

Here, we present results based on the PEPS representation of many-body entangled states. On the one hand, this representation naturally includes many-body entanglement in its state description[VWPGC06] and hence facilitates understanding of one-way quantum computation schemes[VC04, GE07]. On the other hand, methods have been developed to study the physical properties of PEPS states as ground state of parent Hamiltonians [PGVCW08]. Combining these insights, we are able to construct an example of a system which is both the exact unique ground state of a gapped two-body nearest-neighbor Hamiltonian and a universal resource state for one-way quantum computation. Moreover,

we aim at reducing the dimension of local Hilbert space in the state as much as possible for experimental convenience and we arrive at the 'tri-Cluster' state which is composed of 6-dimensional particles.

In section 9.1, we present the our construction of the resource state in terms of its tensor network representation. In section 9.2, we prove that it is the unique and gapped ground state of a Hamiltonian with only two-body nearest neighbor interactions. Section 9.3 shows the universality of the state for measurement-based quantum computation. Finally in section 9.4 we discuss some more recent developments after our proposal of the 'tri-Cluster' state. This chapter is based on our work [CZG+09].

9.1 Construction of model

9.1.1 Building on PEPS

Consider the state $|\psi^{Sqr}_{\mathrm{PEPS}}\rangle$ defined on a square lattice (Fig. 9-1a) where each pair of nearest-neighbor sites are connected by singlets $|\varphi\rangle = |00\rangle + |01\rangle + |10\rangle - |11\rangle$ (suppressing normalization)[1]. On sufficiently large lattices, starting with $|\psi^{Sqr}_{\mathrm{PEPS}}\rangle$, any quantum circuit can be efficiently simulated by measuring all four qubits at each site (on the boundary, two or three) in appropriate time sequences and measurement bases through teleportation (see Chapter 8).

$|\psi^{Sqr}_{\mathrm{PEPS}}\rangle$ is the unique ground state of a gapped two-body Hamiltonian, as it is simply a tensor product of two-body entangled states. However, the multi-particle measurement required to make this state universal[VC04] is generally disallowed in one-way quantum computation models. Still, if the four qubits at each site were treated as a single 16 dimensional particle, the model could be interpreted as giving the desired result, a universal resource state for one-way quantum computation and also the unique ground state of a gapped two-body Hamiltonian. And while use of 16 dimensional particles is experimentally unrealistic, the idea of using a description in terms of singlet pairs does provide a good starting point for constructing simpler states.

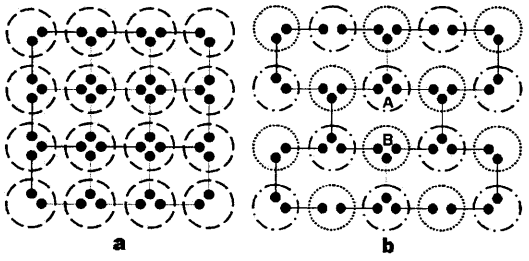

Figure 9-1: Projected Entangled Pair State (PEPS) representation of 2D (a) square $|\psi^{Sqr}_{\mathrm{PEPS}}\rangle$ and (b) hexagonal $|\psi^{Hex}_{\mathrm{PEPS}}\rangle$ lattice states. Filled circles connected by solid lines denote virtual singlet pairs $|\varphi\rangle$. Dashed circles denote projection of virtual qubits into physical states; Dash-dotted and dotted ones correspond to sublattices A and B in hexagonal lattice respectively.

[1]Here we choose the entangled pairs to be slightly different from the ones we used in previous chapters. However, they only differ by a local change of basis and everything can be rephrased using entangled pairs $|00\rangle + |11\rangle$. But with $|\varphi\rangle$ the presentation in this chapter becomes simpler

Specifically, as we discussed earlier, the projector $P^{Sqr}_{Cluster} = |\tilde{0}\rangle\langle 0000| + |\tilde{1}\rangle\langle 1111|$[2] applied to all sites of the square lattice state gives the cluster state on a square lattice [VC04], $|\Psi_{Cluster}\rangle \propto P^{Sqr}_{Cluster}|\psi^{Sqr}_{\rm PEPS}\rangle$, where $|\tilde{0}\rangle$ and $|\tilde{1}\rangle$ are the physical qubits in the cluster state model. Compared with $|\psi^{Sqr}_{\rm PEPS}\rangle$ with 16-dimensional particles, $|\Psi_{Cluster}\rangle$ employs only qubits at each site, and hence is more experimentally accessible. Unfortunately it cannot occur as the exact ground state of nearest-neighbor interactions [VdNLDB08], and the gapped Hamiltonian having it as a unique ground state involves at least five-body interactions. Moreover, it is known that PEPS states composed of lower dimensional particles generally require larger interaction range in their parent Hamiltonian[PGVCW08]. Nevertheless, this line of thought, using PEPS states, can indeed lead to a universal resource state which is the unique ground state of a gapped nearest-neighbor Hamiltonian, while also being composed of particles of relatively low dimension, as we now show.

9.1.2 The tri-Cluster State

The structure of the lattice of singlets, and the choice of projectors, in the construction of PEPS states, provide powerful degrees of freedom for exploring interesting new states. Two specific insights from the above examples illustrate this freedom:

1. Instead of on a square lattice, a cluster state defined on a *hexagonal* lattice $|\Psi^{Hex}_{Cluster}\rangle$ is also universal [VdNMDB06]. On a hexagonal lattice of singlet pairs (Fig. 9-1b), the projector defining this cluster state is $P^{Hex}_{Cluster} = |\tilde{0}\rangle\langle 000| + |\tilde{1}\rangle\langle 111|$, giving $|\Psi^{Hex}_{Cluster}\rangle \propto P^{Hex}_{Cluster}|\psi^{Hex}_{\rm PEPS}\rangle$, where the labels denote left-right-up and left-right-down virtual qubits on sites in sublattices A and B, respectively.

2. An alternative projector can be chosen: $P' = |\tilde{0}\rangle\langle 100| + |\tilde{1}\rangle\langle 011|$ or $P'' = |\tilde{0}\rangle\langle 010| + |\tilde{1}\rangle\langle 101|$; these result in PEPS states different from $|\Psi^{Hex}_{Cluster}\rangle$, but only by local Pauli $\tilde{Z}$ operations, as $\tilde{Z}P = P'(x\otimes z\otimes I) = P''(z\otimes x\otimes I)$ and $|\psi^{Hex}_{PEPS}\rangle$ is invariant with $(x\otimes z\otimes I)$ or $(z\otimes x\otimes I)$ applied to every site. Hence, a modified local measurement scheme still exists, allowing these states to also be universal.

We now introduce a new state, the *tri-Cluster* state $|\Psi_{triC}\rangle$, which is motivated by these two insights, and has properties we desire. This is defined in the PEPS representation on a two-dimensional hexagonal lattice (Fig. 9-1b), with projectors

$$\begin{aligned} P_{triC} &= |\tilde{0}\rangle\langle 000| + |\tilde{1}\rangle\langle 111| \\ &+ |\tilde{2}\rangle\langle 100| + |\tilde{3}\rangle\langle 011| \\ &+ |\tilde{4}\rangle\langle 010| + |\tilde{5}\rangle\langle 101|\,, \end{aligned} \tag{9.1}$$

using the same labeling scheme as above, such that $|\Psi_{triC}\rangle \propto P_{triC}|\psi^{Hex}_{\rm PEPS}\rangle$. Hence, at each lattice site there lives a 6-dimensional particle.

Intuitively, $|\Psi_{triC}\rangle$ is universal because it is closely related to the standard cluster state. Specifically, $|\Psi_{triC}\rangle$ projected into the subspace spanned by $\{|\tilde{0}\rangle, |\tilde{1}\rangle\}$ is the same as $|\Psi_{Cluster}\rangle$, as are also the states given by $|\Psi_{triC}\rangle$ projected into $\{|\tilde{2}\rangle,|\tilde{3}\rangle\}$ and $\{|\tilde{4}\rangle,|\tilde{5}\rangle\}$, up to local Pauli errors. Thus, $|\Psi_{triC}\rangle$ is like a "superposition" of three cluster states. Computational qubits are encoded in the virtual qubits and operated upon by measuring the physical particles. Although the three subspaces of $|\Psi_{triC}\rangle$ cannot be decoupled physically, they may be employed independently in processing encoded qubits with a suitable choice of measurement basis, as detailed later.

[2] which differ from Chapter 8 by local change of basis

The most interesting nontrivial feature of $|\Psi_{triC}\rangle$ is that it is the unique ground state of a gapped two-body Hamiltonian, and we begin with that.

9.2 Uniqueness & Gap of parent Hamiltonian

The fact that $|\Psi_{triC}\rangle$ occurs as the unique ground state of a gapped two-body Hamiltonian is very surprising, as on the one hand the ground states of two-body Hamiltonians are rarely exactly known and on the other hand simply constructed states are not always ground states of simple Hamiltonians. Even the one-dimensional cluster state requires 3-body interactions in its parent Hamiltonian. Below, we give a two-body nearest-neighbor Hamiltonian H_{triC} which has $|\Psi_{triC}\rangle$ as its ground state. Furthermore, we prove that $|\Psi_{triC}\rangle$ is the only ground state of H_{triC} and the Hamiltonian has a constant gap independent of system size.

The central step in constructing H_{triC} and studying its properties is to find the support space S_{ab} of the reduced density matrix of any two nearest-neighbor particles a and b in the state (a, b are in two sublattices A, B respectively). This is accomplished by first finding the corresponding support space S_{ab}^{PEPS} of the six virtual qubits on site a and b, in the PEPS picture, and then computing $S_{ab} \propto P_{triC} S_{ab}^{\text{PEPS}}$. For example, when a is to the left of b (Fig. 9-2), virtual qubits 1 to 6 on those sites are only connected to virtual qubits α,

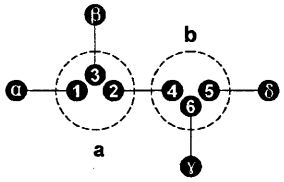

Figure 9-2: One representative site with particles a and b, and neighboring boundary, in the hexagonal lattice of $|\psi_{\text{PEPS}}^{Hex}\rangle$. Filled circles connected by solid lines represent virtual singlets $|\varphi\rangle$ and dashed circles indicate sites projected to obtain the physical state.

β, γ, δ elsewhere. By tracing out α to δ from the 5 singlet pairs, we find S_{ab}^{PEPS} for virtual qubits 1 to 6 to be spanned by $|\pm\rangle_1|\pm\rangle_3|\varphi\rangle_{24}|\pm\rangle_5|\pm\rangle_6$, where $|\pm\rangle = (|0\rangle \pm |1\rangle)/\sqrt{2}$ and $|\varphi\rangle$ is the singlet state. This 16-dimensional space is then projected to give S_{ab} for the depicted lattice site. S_{ab} is different for the three bond directions in a hexagonal lattice, i.e. a to the left of, to the right of, and below b.

Providing a two-body Hamiltonian with $|\Psi_{triC}\rangle$ being a ground state is straightforward. The Hilbert space of two neighboring sites a, b is 36-dimensional, larger than the dimension of S_{ab}. Therefore we may choose any non-negative Hermitian operator h_{ab} on the two sites that has S_{ab} as its null space, such that $h_{ab}|\Psi_{triC}\rangle = 0$ for every h_{ab}. Thus, $|\Psi_{triC}\rangle$ is a ground state of the two-body Hamiltonian $H_{triC} = \sum_{ab} h_{ab}$, where the summation is over all nearest-neighbor pairs. However, the key is to construct H_{triC} such that $|\Psi_{triC}\rangle$ is the *unique* ground state, and it turns out the above procedure does work.

Specifically, let h_{ab} be the projection operator h_{ab}^p which projects onto the $36 - 16 = 20$ dimensional subspace orthogonal to S_{ab}, giving the total Hamiltonian

$$H_{triC} = \sum_{a \in A} \left(h_{ab}^p + h_{ba}^p + h_{\substack{b \\ a}}^p \right) . \tag{9.2}$$

The summation is over sites a in sublattice A and the three terms h^p_{ab}, h^p_{ba}, $h^p_{\substack{b\\a}}$ correspond, respectively, to three bond directions where a is to the left, to the right and below b. The Hamiltonian is hence invariant under translation along sublattice A.

The specific H_{triC} we have presented has $|\Psi_{triC}\rangle$ as its unique ground state. This is shown by verifying the condition [PGVCW08] that for any region R of spins in $|\Psi_{triC}\rangle$, the support space S_R of the reduced density matrix on R satisfies

$$S_R = \bigcap_{\langle ab\rangle} S_{ab} \otimes I_{R\setminus ab}\,, \tag{9.3}$$

where the intersection is taken over all neighboring pairs ab and $I_{R\setminus ab}$ is the full Hilbert space of all spins in region R except a and b. For every possible configuration containing three or four connected sites in $|\Psi_{triC}\rangle$ the condition is confirmed by direct calculation. To check the condition for larger regions, it is useful to notice that any region in $|\Psi_{triC}\rangle$ containing more than one site is *injective* [PGVCW08]. By Lemma 2 of [PGVCW08], 1. if regions R_1 and R_3 are not connected and R_2 and R_3 are injective, then $S_{R_1\cup R_2\cup R_3} = (S_{R_1\cup R_2}\otimes I_{R_3})\cap(S_{R_2\cup R_3}\otimes I_{R_1})$ 2. if regions R_1, R_2, R_3 are all injective, then $S_{R_1\cup R_2\cup R_3} = (S_{R_1\cup R_2}\otimes I_{R_3})\cap(S_{R_2\cup R_3}\otimes I_{R_1})\cap(S_{R_1\cup R_3}\otimes I_{R_2})$. Hence for a region R containing more than 4 sites in $|\Psi_{triC}\rangle$, S_R is the intersection of all four-body support spaces in R. By induction, it follows that condition Eq.(9.3) is satisfied on $|\Psi_{triC}\rangle$ for any R. Therefore, $|\Psi_{triC}\rangle$ is the unique ground state of H_{triC}.

H_{triC} is also gapped; an energy gap η above the ground state exists, which is constant as the system size goes to infinity. The existence of this gap guarantees protection of $|\Psi_{triC}\rangle$ against thermal noise, independent of system size. η can be bounded. First, we show that η is greater than λ, the gap of another Hamiltonian K which also has $|\Psi_{triC}\rangle$ as its unique ground state, but has four-body terms instead of only two-body terms. We then bound λ above a positive constant value.

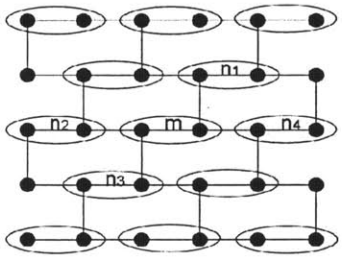

Figure 9-3: Regrouping of lattice sites in tri-Cluster State into disjoint blocks, each containing two sites.

Consider the Hamiltonian K for a re-labeled version of $|\Psi_{triC}\rangle$, in which particles are regrouped into disjoint blocks each containing two nearest-neighbors (Fig. 9-3). Let $K = \sum_{mn} k_{mn}$, where m, n denote two connected blocks, each containing two particles $m^{[l]}, m^{[r]}$ and $n^{[l]}, n^{[r]}$ respectively, and k_{mn} is projection onto the orthogonal space of the four-body reduced density matrix on $m^{[l]}, m^{[r]}, n^{[l]}, n^{[r]}$ (assuming $m^{[r]}$ and $n^{[l]}$ are connected). Then $H_{triC} = \sum_{ab} h^p_{ab} \geq \frac{1}{4}\sum_{mn}\left(h^p_{m^{[l]}m^{[r]}} + h^p_{m^{[r]}n^{[l]}} + h^p_{n^{[l]}n^{[r]}}\right) \geq \frac{1}{4}\sum_{mn}\mu k_{mn} = \frac{1}{4}\mu K$. $\left(h^p_{m^{[l]}m^{[r]}} + h^p_{m^{[r]}n^{[l]}} + h^p_{n^{[l]}n^{[r]}}\right)$ and k_{mn} are both non-negative operators with the same null

space, so the last inequality holds for some positive number μ. Assume that the gaps of the projectors h^p_{ab} and k_{mn} are both 1. Direct calculation gives $\mu = \frac{1}{2}$. As discussed in the uniqueness proof, K also has $|\Psi_{triC}\rangle$ as its unique ground state. Using this, we find $\eta \geq \frac{1}{4}\mu\lambda = \frac{1}{8}\lambda$. The gap λ can be bounded by showing that $K^2 \geq cK$ for some positive constant c. $K^2 = (\sum_{mn} k_{mn})^2 = K + \sum_{mn,m'n'}(k_{mn}k_{m'n'} + k_{m'n'}k_{mn}) \geq K + \sum_{n_i mn_j} k_{mn_i}k_{mn_j} + k_{mn_j}k_{mn_i}$, n_i and n_j are blocks connected to m. The last inequality holds because when region mn and region $m'n'$ do not intersect $k_{mn}k_{m'n'} + k_{m'n'}k_{mn} \geq 0$. Direct calculation shows that (Fig. 9-3) $k_{mn_i}k_{mn_j} + k_{mn_j}k_{mn_i} \geq 0$ for $(i,j) = (1,2),(1,3),(2,4)$ or $(3,4)$ and $k_{mn_i}k_{mn_j} + k_{mn_j}k_{mn_i} \geq -\frac{1}{3}k_{mn_i} - \frac{1}{3}k_{mn_j}$ for $(i,j) = (1,4)$ or $(2,3)$. Summing over all consecutive n_i, m, and n_j gives $\sum_{n_i mn_j} k_{mn_i}k_{mn_j} + k_{mn_j}k_{mn_i} \geq -\frac{2}{3}\sum_{mn} k_{mn}$. Therefore $K^2 \geq \frac{1}{3}K$, giving $\lambda \geq \frac{1}{3}$. Finally, we find a lower bound on the gap η of H_{triC} of $\eta \geq \frac{1}{8}\lambda \geq \frac{1}{24}$.

9.3 Universality for measurement-based quantum computation

$|\Psi_{triC}\rangle$ is a universal resource state, because of properties it inherits from the cluster state. Similar to a cluster state, computational qubits are encoded in the virtual qubits, and the active computational state flows along the lattice as measurements on the physical states are performed. In contrast, however, with $|\Psi_{triC}\rangle$ extra Pauli errors occur, thus necessitating additional analysis. Below, we describe the different steps necessary, focusing on initialization and readout, one-qubit gates, and a two-qubit gate sufficient for universality.

Initialization and readout: Just as with the cluster state, with $|\Psi_{triC}\rangle$, measurement in the six-state basis, $\{|\tilde{0}\rangle \cdots |\tilde{5}\rangle\}$ accomplishes several tasks. First, such measurement detaches unnecessary sites from their neighbors (up to a known Pauli error). Next for state initialization, it gives a post-measurement state with an encoded qubit projected into $|+\rangle$ (when the outcome is $\tilde{0}$, $\tilde{3}$ or $\tilde{4}$) and $|-\rangle$ (for outcomes $\tilde{1}$, $\tilde{2}$ or $\tilde{5}$). At the end of computation, the encoded qubit can also be read out in this way, giving 0 (for $\tilde{0}$, $\tilde{2}$ or $\tilde{5}$), and 1 (for $\tilde{1}$, $\tilde{3}$ or $\tilde{4}$).

One-qubit gates: Similar to gate implementations with the cluster state, once a line in the lattice has been detached from the rest, appropriately measuring a site in the line performs a single qubit rotation, up to a known Pauli error. Specifically, measuring in the basis $\{|\tilde{0}\rangle \pm e^{i\theta}|\tilde{1}\rangle,\ |\tilde{2}\rangle \pm e^{i\theta}|\tilde{3}\rangle,\ |\tilde{4}\rangle \pm e^{-i\theta}|\tilde{5}\rangle\}$ implements operation $\{HZ(\theta), XHZ(\theta), ZHZ(\theta), YHZ(\theta), ZHZ(\theta), YHZ(\theta)\}$, respectively, on the encoded qubit (using standard notation for qubit gates, with $Z(\theta)$ denoting a rotation about $\hat{z}$ by angle θ), up to pre-existing Pauli frame errors from detaching the line.

Two-qubit controlled-Z gate: Measurement of two vertically connected particles a and b implements the final ingredient needed for universality, a controlled-Z gate CZ_{ab}, just as with the cluster state scheme, but with some additional Pauli frame errors. Specifically, measuring in basis $\{\hat{0}\ldots\hat{5}\} = \{|\tilde{0}\rangle \pm |\tilde{1}\rangle,\ |\tilde{2}\rangle \pm |\tilde{3}\rangle,\ |\tilde{4}\rangle \pm |\tilde{5}\rangle\}$ implements the two-qubit operation $\left(X_a^{u_a} Z_a^{v_a} H_a\right)\left(X_b^{u_b} Z_b^{v_b} H_b\right) \otimes \left(X_a^{w_a} X_b^{w_b} CZ_{ab} X_a^{w_a} X_b^{w_b}\right)$ on the two adjacent encoded qubits. For $x \in \{a,b\}$, $u_x = 1$ for x measurement outcomes $\hat{1}$, $\hat{3}$, or $\hat{5}$; $v_x = 1$ for outcomes $\hat{2}$, $\hat{3}$, $\hat{4}$, or $\hat{5}$; $w_x = 1$ for $\hat{4}$, $\hat{5}$; and u_x, v_x, w_x are 0 otherwise. Much like for the cluster state, when embedded in a larger circuit, more complicated configurations arise in implementing a controlled-Z gate , but the principles of propagating a Pauli frame remain the same.

9.4 More recent developments

The tri-Cluster state we find here, which is both universal for one-way quantum computation and the unique ground state of a gapped Hamiltonian, steps closer to physical realizability than previous models. More recently, exciting developments have been achieved based on similar methods which identify the AKLT state as universal for measurement-based quantum computation [Miy11, WAR11]. The AKLT state is the gapped ground state of anti-ferromagnetic Heisenberg interactions between spins, which is physically more realistic and much easier to realize than the interaction in the tri-Cluster model. The remaining challenge in realizing this scheme in experiments is to control errors during the computational process when the quantum state is perturbed away from the exact ground state of the AKLT model.

Chapter 10

Fermionic measurement-based quantum computation

Quantum computation can be realized with different quantum degrees of freedom, for example photons and spins. Fermions, as another major class of quantum particles, have been relatively less explored for their application in quantum computation and can lead to new possibilities. Although it is expected[BK02] that fermions have polynomially equivalent quantum computation power as spins/bosons, it is possible that sub-exponential speedups can be achieved with fermions over spins/bosons in certain computational tasks. For example, the quantum simulation[Fey82, Llo96] of fermionic many-body systems can be much more easily implemented with fermionic degrees of freedom due to the intrinsic sign issue in the simulation of fermions with spins/bosons.

The possibility of using fermions for quantum computation has been studied in a few contexts. It has been shown that the circuit model quantum computation can be implemented with fermions which efficiently simulates quantum circuits with spins[BK02]. On the other hand, topological quantum computation can be realized using certain two dimensional fermion states with strong correlations[Kit03]. In particular, it is known that the fractional quantum Hall state with filling fraction $\nu = 5/2$ can support universal topological quantum computation[Bra06]. Moreover, quantum teleportation[BBC$^+$93], an important quantum protocol for both quantum communication and quantum computation, have also been generalized to fermion systems[MRZ08].

The measurement-based quantum computation model[RB01] as discussed in previous chapters has been extensively studied in spin systems. With the tri-Cluster model presented in the last chapter, we demonstrate that it is possible to do measurement-based quantum computation in the gapped ground state of two-body Hamiltonians. However, the form of the Hamiltonian is still complicated and our pursuit of experimentally feasible resource states does not end here.

With the recent exciting experimental progress in manipulating ultracold fermion gases [KMS$^+$05, KZ08, GPS08], it is then interesting to ask whether similar computational schemes could be implemented in fermion systems, with only single site measurements on a fermionic resource state which ideally can be realized in a controlled way with ultracold fermionic atoms. With the large variety of quantum states that exist in simple free fermion systems, like Fermi liquids, quantum Hall states, and topological insulators, a fermionic version of MBQC may provide new platforms for quantum information processing with reduced experimental complexity while at the same time enjoying the same advantage as in

the spin MBQC model that no coherent quantum operations are needed to carry out the whole computation.

However, no theory exists for fermionic MBQC which studies what fermionic resource states are useful and what single site measurement patterns are necessary to achieve universal quantum computation. Naively, one might expect that a direct Jordan Wigner mapping of spin resource states to fermions would give a useful fermionic resource state for MBQC, but this is not true as the mapping is nonlocal and local spin measurements on the resource state can no longer be implemented with local fermion measurements after the mapping. Moreover, one of the key properties wanted for a MBQC resource state is lost during this mapping. It is highly desirable to have the MBQC resource states be the ground states of local Hamiltonians and many spin resource states are designed to have this property[BR06, CZG+09, BM08, CMDB10, Miy11, WAR11] . Unfortunately this property is not preserved by the nonlocal mapping to fermions and the resulting fermion states can no longer be generated by engineering the appropriate local Hamiltonian terms in the system and then lowering the temperature. Therefore different approaches are needed to construct a useful fermionic MBQC model.

In this chapter, we show that MBQC is possible in local fermion systems by presenting an explicit construction of a fermionic resource state together with the single site measurement patterns necessary to realize universal quantum computation. Our construction is based on the fermionic Projected Entangled Pair States (fPEPS) representation[KSVC10, GVW10], which is known to describe ground states in local fermion systems[PGVCW08]. The construction generalizes the idea of designing spin MBQC resource states based on the spin PEPS representation[GE07, GESPG07] to fermion systems. By encoding the quantum information to be processed into the even parity sector of local fermion modes, we demonstrate how universal quantum computation can be achieved on a fermionic state with only single site measurements. One complication arising from this encoding is the extra fermionic measurement possibilities in the odd parity sector which introduces nonlocal by-products to the computation. We demonstrate further that such by-products in the computation can be properly taken care of by keeping a 'fermionic' frame of the by-products together with the Pauli frame as in the spin MBQC models[RB01, RBB03]. Starting from this explicit construction, we expect that the fPEPS formalism could yield fermionic resource states with simpler encoding scheme and as the ground states of more easily realizable local Hamiltonians. Therefore, we also discuss in general how to design fermion resource states for fMBQC from fPEPS representation.

The chapter is organized as follows: In section 10.1, we start from the basic building block of MBQC–teleportation, and show how it can be realized in fermion systems. Putting the teleportation steps together, we obtain a simple fermionic resource state in section 10.2 A-B and demonstrate in detail how each step in MBQC can be realized on such a state. This example is the starting point of a more general construction based on fPEPS which we present in section 10.2 C. Finally, we conclude and discuss future directions in section 10.3.

10.1 Fermionic teleportation

Our goal in the next sections is to show that on a many-body fermion state single site measurements can be used to simulate the result of any quantum circuit. We achieve this with a similar procedure as that used in spin MBQC: we first construct fermionic telepor-

tation steps for implementing a universal set of gates and then use the fermionic PEPS (fPEPS) representation to map teleportation in the virtual space to single-site measurements in a physical state. However, fermions are very different from spins in two specific ways: 1. fermion operators anti-commute with each other and fermion wave functions are anti-symmetric; 2. the total parity of a fermionic system is always preserved. Therefore, care must be taken in mapping from spins to fermions and the generalization is far from direct. In this section, we start with a fermionic version of teleportation, discuss the necessity of a new encoding scheme for fermionic systems, and finally give a way to achieve universal quantum computation with fermionic teleportation. These serve as the basic building blocks for fermionic MBQC discussed in the next section.

10.1.1 Fermionic teleportation as a generalization of spin teleportation

In quantum computation with spins, the analogy to the bits 0/1 in classical computation is the two-level spin up/down states $|0\rangle$ / $|1\rangle$, or qubits. In the fermionic case, the information is encoded in the wave function of local fermionic modes. It seems straight forward to define the two-level states by the occupation number of the modes. Namely, the analogy of $|0\rangle$ is a state with no fermion in a mode, or vacuum $|\Omega\rangle$, and that of $|1\rangle$ is $\alpha^\dagger|\Omega\rangle$, where $\alpha^\dagger$ is the creation operator for a fermion mode. The maximally entangled spin state $|00\rangle + |11\rangle$ can be replaced accordingly by two entangled modes defined as $(1 + \alpha_1^\dagger\alpha_2^\dagger)|\Omega\rangle$.

However, this naive mapping fails as one attempts to do fermionic teleportation with the configuration shown in Fig. 8-2, where each dot now represents a fermion mode. As fermion parity of a system is always preserved, the input mode 1 cannot be in a superposition state of $(m_0 + m_1\alpha^\dagger)|\Omega\rangle$. In order to deal with this problem, we take a route similar to that in [BK02, MRZ08] by adding extra modes and encoding information in a fixed-parity sector. As depicted in Fig. 10-1, we add an extra mode and a second pair of entangled modes, such that the input defined in Eq. 8.3 becomes $|\psi_{13}\rangle = (m_0|\Omega\rangle + m_1\alpha_1^\dagger\alpha_3^\dagger|\Omega\rangle)_{13}$, which has a definite even parity. To check the feasibility of this strategy, we show in the following that

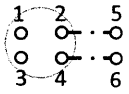

Figure 10-1: Teleportation of two-mode fermionic unitary gates. Fermionic modes are depicted as white dots, and entangled mode pairs are represented by a dashed line. Input modes $(1, 3)$ are in state $|\psi_{13}\rangle = (m_0|\Omega\rangle + m_1\alpha_1^\dagger\alpha_3^\dagger|\Omega\rangle)$, where mode 1 carries the information, and mode 3 preserves the parity of the mode 1.

the input in modes 1 and 3 can be teleported to modes 5 and 6: The total wave function of the system is

$$|\psi\rangle = \sum_{a=0}^{1} m_a(\alpha_1^\dagger\alpha_3^\dagger)^a(\alpha_2^\dagger\alpha_5^\dagger + 1)(\alpha_4^\dagger\alpha_6^\dagger + 1)|\Omega\rangle\,. \tag{10.1}$$

A measurement of modes 1-4 in $\langle\phi| = \langle\Omega|(1 + \alpha_4\alpha_3\alpha_2\alpha_1)$ results in state $\langle\phi|\psi\rangle = (m_0 + m_1\alpha_5^\dagger\alpha_6^\dagger)|\Omega\rangle$ on mode 5 and 6, which is exactly what is desired.

This is the simplest case of a teleportation circuit and illustrates the general strategy we take to deal with the special property of fermions: 1. a proper ordering of all fermion modes needs to be given at the beginning and carried throughout the whole scheme 2. information

is encoded in a fixed parity sector and all operations have fixed parities. In the following, we apply these strategies to the general cases. First we need to specify the encoding scheme of general quantum circuits into fermion modes.

10.1.2 $n \to 2n$ encoding scheme

Due to the parity constraint discussed above, extra modes are needed when encoding spin states into fermion modes to preserve the total fermion parity of a system. Various encoding schemes have been proposed[BK02] which satisfy this constraint. For discussion in this paper, we choose to encode 1 qubit into 2 fermionic modes, or more generally, n qubits into $2n$ fermionic modes. As illustrated in Fig. 10-1 and Fig. 10-2, in our scheme, a 'parity' mode is assigned to every 'info' mode containing the real information to ensure that the total parity of an info mode and the auxiliary parity mode is always fixed. Thus, a spin system with n qubits in state $|\psi_n\rangle = \sum_{\{a_i\}} m_{\{a_i\}} |a_1 a_2 ..... a_n\rangle$, where $\{a_i\} = \{a_1, a_2, ..., a_n\}$ is encoded into a fermionic state with $2n$ modes $|\psi_n\rangle_f = \sum_{\{a_i\}} m_{\{a_i\}} (\alpha_1^\dagger \alpha_{1\,p}^\dagger)^{a_1} (\alpha_2^\dagger \alpha_{2\,p}^\dagger)^{a_2} ... (\alpha_n^\dagger \alpha_{n\,p}^\dagger)^{a_n} |\Omega\rangle$, where $i\ p$ is the parity mode of the info mode i. Note that here we have chosen the order of the modes such that fermionic operators $\alpha_i^\dagger$ always appear in front of $\alpha_j^\dagger$ for $i < j$, and the fermion parity of the state shall always be even.

As a spin state with n qubits is encoded into a fixed parity fermionic state with $2n$ modes, spin gates must also be redesigned accordingly so that an n-qubit spin operator is encoded into a $2n$-mode parity preserving fermion operator and the universal set of spin gates are mapped to a set of fermionic gates which possess the same universality.

A generic one-qubit unitary spin operator

$$U = U_{00} |0\rangle \langle 0| + U_{10} |1\rangle \langle 0| + U_{01} |0\rangle \langle 1| + U_{11} |1\rangle \langle 1| \tag{10.2}$$

is encoded into a 2-mode fermionic gate (where mode 1 is the 'info' mode, and mode 2 is the 'parity' mode of mode 1):

$$U_f = U_{00} \alpha_1 \alpha_1^\dagger \alpha_2 \alpha_2^\dagger + U_{01} \alpha_1^\dagger \alpha_2^\dagger + U_{10} \alpha_1 \alpha_2 + U_{11} \alpha_1^\dagger \alpha_1 \alpha_2^\dagger \alpha_2 \tag{10.3}$$

With this encoding, we have the 2-mode fermionic phase gate

$$Z_f(\theta) = \alpha_1 \alpha_1^\dagger \alpha_2 \alpha_2^\dagger + e^{i\theta} \alpha_1^\dagger \alpha_1 \alpha_2^\dagger \alpha_2, \tag{10.4}$$

and the fermionic Hadamard gate

$$H_f = \alpha_1 \alpha_1^\dagger \alpha_2 \alpha_2^\dagger + \alpha_1^\dagger \alpha_2^\dagger + \alpha_1 \alpha_2 - \alpha_1^\dagger \alpha_1 \alpha_2^\dagger \alpha_2. \tag{10.5}$$

which can be composed to simulate arbitrary unitary gates on a single qubit.

Similarly, the 2-qubit U_{ph} is mapped to $U_{ph;f}$ on 4 consecutive fermionic modes, modes 1, 1p, 2, 2p, where 1,2 are control and target modes, and 1p,2p are parity modes of 1,2 respectively. For simplicity, here we denote fermionic states $|\Omega\rangle$, $\alpha^\dagger |\Omega\rangle$, and $(1 + \alpha_1^\dagger \alpha_2^\dagger) |\Omega\rangle$ as $|0\rangle_f$,$|1\rangle_f$, and $(|00\rangle + |11\rangle)_f$ where we always order the modes as 1, 1p, 2, 2p, etc.

$$\begin{aligned} U_{ph;f} &= |0000\rangle_f (\langle 00| + \langle 11|)_f (\langle 00| + \langle 11|)_f \\ &+ |0011\rangle_f (\langle 00| + \langle 11|)_f (\langle 00| - \langle 11|)_f \\ &+ |1100\rangle_f (\langle 00| - \langle 11|)_f (\langle 00| + \langle 11|)_f \\ &- |1111\rangle_f (\langle 00| - \langle 11|)_f (\langle 00| - \langle 11|)_f. \end{aligned} \tag{10.6}$$

Therefore, with Eqs. 10.4, 10.5 and 10.6, a universal set of fermionic gates for fermionic quantum computation is constructed and can be used to simulate the universal set of spin gates for the original spin quantum computation. Note that the gates discussed here only act on the even fermion parity sector and are unitary only within this sector. However, as information is encoded fully in this sector, these gates are sufficient for quantum computation and are implemented in the MBQC scheme described below. Unlike in the fermionic circuit model of quantum computation[BK02] where fully unitary fermionic gates are necessary, in fermionic MBQC simulating such quasi-unitary operations is sufficient and can be readily realized. The odd fermion parity sector contributes to the fermionic MBQC scheme as computational by-products when the measurement result falls into this sector. As we show below, such computational by-products can be properly dealt without destroying the universality of the computation scheme.

10.1.3 Fermionic teleportation for a universal set of gates

Now that we have defined the encoding of states and the mapping between gates, in the following, we show that the universal set of fermionic gates can be implemented by measuring entangled fermionic states in certain bases, thus achieving universal quantum computation with fermionic teleportation. Note that in the discussion of this section, we always assume that each pair of 'info' mode and 'parity' mode always have even parity. The occurrence of odd parity pairs is considered as computational by-products later.

The schematic for teleporting an arbitrary two-mode parity preserving fermionic gate U_f, the equivalent of a 1-qubit spin gate, is shown in Fig. 10-1. By comparing Figs. 8-2 and 10-1, we can see that the number of inputs as well as that of entangled pairs are both doubled in the fermionic case. The wave function of the state that corresponds to Eq. 8.4 in the spin case is given in Eq. 10.1. It can be checked that the measurement on modes 1-4 in basis

$$|\phi\rangle = (U_{00} - U_{01}\alpha_2^\dagger\alpha_4^\dagger + U_{10}\alpha_1^\dagger\alpha_3^\dagger + U_{11}\alpha_1^\dagger\alpha_2^\dagger\alpha_3^\dagger\alpha_4^\dagger)\,|\Omega\rangle \tag{10.7}$$

teleports U_f to mode 5 and 6.

As for teleporting the 4-mode controlled operation $U_{ph;f}$, the setup depicted in Fig. 10-2 is utilized. The wave function of this state is

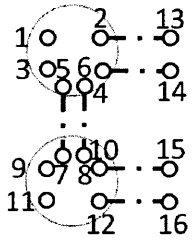

Figure 10-2: Teleportation of the 4-mode controlled operation. Input modes 1 and 9 are the fermionic analogues of the control and target, and modes 3 and 11 are the parity modes corresponding to 1,9 respectively. After measurements on modes $1 \sim 6$ and $7 \sim 12$ are implemented, the gate is teleported to modes $13 \sim 16$.

$$\begin{aligned} |\psi\rangle \;=\; & \textstyle\sum_{a,b=0}^{1} m_{ab}(\alpha_1^\dagger\alpha_3^\dagger)^a(\alpha_9^\dagger\alpha_{11}^\dagger)^b(1+\alpha_2^\dagger\alpha_{13}^\dagger)(1+\alpha_4^\dagger\alpha_{14}^\dagger)\times \\ & (1+\alpha_5^\dagger\alpha_7^\dagger)(1+\alpha_6^\dagger\alpha_8^\dagger)(1+\alpha_{10}^\dagger\alpha_{15}^\dagger)(1+\alpha_{12}^\dagger\alpha_{16}^\dagger)\,|\Omega\rangle\,. \end{aligned}$$

One can check that $U_{ph;f}$ can be teleported by measuring modes 1-6 of the top site in

$$|\phi\rangle_t = (1 - \alpha_2^\dagger\alpha_4^\dagger - \alpha_5^\dagger\alpha_6^\dagger + \alpha_2^\dagger\alpha_4^\dagger\alpha_5^\dagger\alpha_6^\dagger + \alpha_1^\dagger\alpha_3^\dagger - \alpha_1^\dagger\alpha_2^\dagger\alpha_3^\dagger\alpha_4^\dagger + \alpha_1^\dagger\alpha_3^\dagger\alpha_5^\dagger\alpha_6^\dagger - \alpha_1^\dagger\alpha_2^\dagger\alpha_3^\dagger\alpha_4^\dagger\alpha_5^\dagger\alpha_6^\dagger)\,|\Omega\rangle \tag{10.8}$$

and mode 7-12 of the bottom site in

$$|\phi\rangle_b = (1 - \alpha_{10}^\dagger\alpha_{12}^\dagger + \alpha_7^\dagger\alpha_8^\dagger\alpha_9^\dagger\alpha_{11}^\dagger - \alpha_7^\dagger\alpha_8^\dagger\alpha_9^\dagger\alpha_{10}^\dagger\alpha_{11}^\dagger\alpha_{12}^\dagger)\,|\Omega\rangle \tag{10.9}$$

Hereby, we have successfully found a measurement bases corresponding to a universal set of gates and have shown that universal quantum computation can be achieved by teleportation with fermions.

However, our consideration so far is over simplified as we have assumed that the computation always occurs in the even fermion parity sector and the measurements always result in the basis we want. In fact, measurement errors always occur as we can not choose which particular basis among a complete set to measure in. Measurement errors in teleportation steps lead to unwanted by-product operations being teleported. For fermion states, it is also possible to change the parity sector of the states, which seems to pose a serious problem for our scheme. We address these issues in the following sections and show that they can be properly taken care of and will not impede our ability to do MBQC. We refer to the extra operations teleported as 'by-products' instead of 'errors' to emphasize that the former is due to the intrinsic randomness of quantum mechanics and cannot be avoided while the latter is due to noise and perturbation and can in principle be reduced.

10.2 Fermionic Projected Entangled Pair States for MBQC

Even though we have demonstrated the viability of fermionic teleportation for individual gates in the previous section, our ultimate goal is to show that a circuit consisting of multiple operations can be simulated with local measurements, or in other words, to achieve fermionic measurement-based quantum computation (fMBQC). Thus, it is necessary to have a fermionic lattice state similar to the spin lattice state in Fig. 8-5 which allows multiple steps of measurements as the information flows from one place to another.

In this section, we first assemble the teleportation steps and give a simple yet universal example of resource state for fMBQC. We examine in detail the possible by-product operations that occur in the measurement process and show how they can be taken care of with proper measurement schemes. We then discuss the more general fermionic Projected Entangled Pair States (fPEPS) formalism which, like PEPS for spin, allows more possibilities for finding novel fermionic resource states.

10.2.1 A simple example of fermionic resource state

Here we demonstrate that fMBQC can be achieved using a special fermionic resource state on the lattice shown in Fig. 10-3. Like what we have seen in fermionic teleportation, the number of input and entangled pairs are doubled in the fermionic case compared to the spin case; thus, the spin lattice for MBQC (shown in Fig. 8-5), which has 3 or 4 qubits on every site corresponds to the fermion lattice in Fig. 10-3 which has 6 or 8 modes per site and two entangled pairs connecting neighboring sites.

The lattice consists of input mode pairs $\alpha\alpha'$s on the left boundary and entangled pairs $(\beta_{i,j}^\dagger\alpha_{i,j+1}^\dagger + 1)\,|\Omega\rangle$ and $(\beta'^\dagger_{i,j}\alpha'^\dagger_{i,j+1} + 1)\,|\Omega\rangle$ for horizontal bonds, and $(\gamma_{i,j}^\dagger\delta_{i+1,j}^\dagger + 1)\,|\Omega\rangle$ and

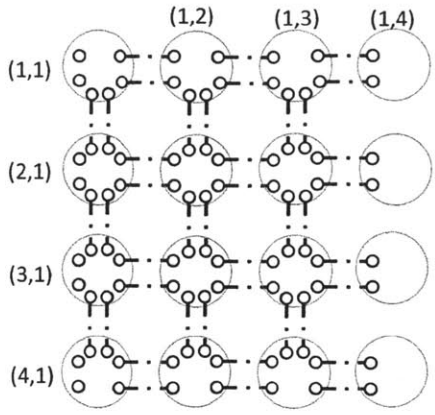

Figure 10-3: Representation of the 2D fPEPS simple example resource state. The lattice consists of boundary modes on the left and entangled mode pairs connecting every site.

$(\gamma'^{\dagger}_{i,j}\delta'^{\dagger}_{i+1,j} + 1)\,|\Omega\rangle$ for vertical bonds. The labeling of modes on a site is shown in Fig. 10-4. When writing the bonds, we define the ordering of sites on the lattice as left (i,j) to right $(i,j+1)$ and top (i,j) to down $(i+1,j)$. This state can be thought of as a fermionic PEPS with a trivial projection on each site. In the following we think of all the modes on each site as one big degree of freedom and discuss how MBQC can be implemented with single site measurements on this state.

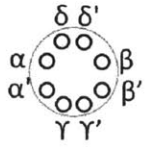

Figure 10-4: Labeling of modes on a site. Modes on the left are labeled α, α', modes on the right are $\beta\beta'$, modes at the top are $\delta\delta'$, and modes at the bottom are $\gamma\gamma'$.

To see the feasibility of fMBQC in this example, we give in detail the procedure to implement each necessary step in fMBQC on this state.

- Assume WLOG that the input modes on the left boundary are all initialized in $|\Omega\rangle$, and measurements are performed on the sites in the first column from top to bottom, and then column by column from left to right so that the information flows to the right.

- Just like in MBQC for spins, the lattice is initially entirely entangled. As one wants to achieve certain operations, for example, two-mode gates or the four-mode controlled operation $U_{ph;f}$, which involve only one or two entangled rows, one needs to isolate the rows and decouple them from other rows. To isolate a row, we remove its entanglement with neighboring upper and lower rows by measuring modes on the sites of the upper and lower rows in the occupation number basis

$$\delta^{\dagger n_\delta}\delta'^{\dagger n_{\delta'}}\alpha^{\dagger n_\alpha}\alpha'^{\dagger n_{\alpha'}}\beta^{\dagger n_\beta}\beta'^{\dagger n_{\beta'}}\gamma^{\dagger n_\gamma}\gamma'^{\dagger n_{\gamma'}}\,|\Omega\rangle$$

for all $n = 0, 1$. Apply this measurement wherever necessary to prepare the lattice for the implementation of a particular circuit.

- After partially decoupling the lattice when necessary in the way introduced above and using the results from Eqs. 10.7, 10.8, 10.9, we see that we can implement a universal set of fermion gates by single site measurements on this state. But this is not enough to claim universality for MBQC as we have not considered the effect of measuring in basis other than the desired one. We discuss how to deal with the computational by-products introduced by the randomness in fermionic measurements in the next section.

- We finally read out the output on the right boundary by measuring the sites in the occupation number bases. Therefore for fermions, we just measure the rightmost column in $(\alpha^\dagger \alpha'^\dagger)^{n_\alpha} |\Omega\rangle$ or $\alpha^{\dagger n_\alpha} \alpha'^{\dagger 1-n_\alpha} |\Omega\rangle$, with $n_\alpha = 0, 1$ to yield the results.

10.2.2 Dealing with measurement randomness in the simple model

In this section, we address the effect of measurement randomness in our scheme. As discussed in the previous section, fMBQC could in principle be achieved with measurements in certain bases; however, measurement results in orthogonal bases that span the rest of the Hilbert space may lead to by-products to the simulated operation. This can be viewed as the fermionic analog of the Pauli by-products that emerge when a Bell measurement is performed. In general, we cannot choose which basis state results from the measurement and whenever a measurement is done, a by-product occurs. Therefore, dealing with by-products becomes a necessity to make sure that there is a finite probability of simulating the wanted operation in order to achieve efficient quantum computation.

So far in our discussion, we have used two important assumptions: 1. we required that the pair of input modes on a site always have even parity as we designed one mode as the parity mode of another; 2. we only mentioned the measurement basis that gives rise to the desired answer without discussing other orthogonal bases that would potentially produce by-products. In general, the fermion parity constraint only requires that the total parity of modes be fixed. Therefore, the input mode pairs could also have odd parity, eg. $m_0 \alpha^\dagger + m_1 \alpha'^\dagger |\Omega\rangle$. Similarly, there are no other constraints on the measurement bases as long as the total parity is fixed. As a result, it may seem that the choice of bases is arbitrary, leading to all kinds of by-products in the simulated operation. Yet, for the consistency of our scheme, we choose a complete set of measurement bases in which the mode pairs ($\alpha\alpha'$, $\beta\beta'$, $\gamma\gamma'$, $\delta\delta'$) each have a fixed parity, which could be either odd or even. Therefore, depending on the parity of the measurement bases, we could characterize the by-products into two categories:

- Parity-preserving by-products: by-products that come from measurements which preserve the parity of the input (i.e. with an even parity measurement basis), such that the parity of the output is the same as the input. These parity preserving local fermionic operations can be mapped to local spin operations and could be corrected locally as spins. To see this more explicitly, we assume on a 1D chain with input of even parity, measurement in the state $(1+\alpha\alpha'\beta\beta') |\Omega\rangle$ simulates the desired operation. Other orthogonal bases that preserve the parity are $(1 - \alpha\alpha'\beta\beta') |\Omega\rangle$, $(\alpha\alpha' + \beta\beta') |\Omega\rangle$ and $(\alpha\alpha' - \beta\beta') |\Omega\rangle$. It is obvious that the by-products on the output for these bases are the fermionic equivalent of Pauli Z, X, and Y respectively. In our simple example,

such by-products can all be incorporated into the next operation to be teleported and hence get corrected.

- Parity-violating by-products: by-products that emerge in measurements which change the parity of the input (i.e. with an odd measurement basis), such that the parity of the output is the opposite of the input. Using the example above, the orthogonal bases in the odd sector are $(\alpha\alpha'\beta \pm \beta')\,|\Omega\rangle$ and $(\alpha\alpha'\beta' \pm \beta)\,|\Omega\rangle$. To keep the information flow, a corresponding encoding of spin states into the odd parity sector needs to be defined, for example by requiring that the 'parity' mode always has the opposite parity to that of the 'info' mode. Moreover, this type of by-products are not the typical spin by-products. Instead they implement odd fermionic operations on the input, which maps back to non-local spin operations. Nevertheless, since in our scheme we have required a fixed parity on each mode pair, the nonlocal part of an odd operation only contributes an overall (± 1) to the total state, and therefore we only need to worry about the local part which is correctable by local measurements. Note that this is a special property of this example. Generally by-products from odd measurement bases are non-local, and we discuss the general case in the next section.

10.2.3 General fPEPS construction for fMBQC

Review of fPEPS formalism

In the previous section, we demonstrated that fMBQC is feasible in principle on a 2D lattice. However, in this model, the on-site measurements involve many degrees of freedom and the resource state may not be readily realizable. Our ultimate goal is to find a resource state which contains few modes per site and is the unique gapped ground state of a simple Hamiltonian, for example a free fermion Hamiltonian. The computational power of such a state is connected to its physical properties through its fPEPS representation. fPEPS, like PEPS for spin, represents many-body fermion states as projections from entangled virtual fermion pairs and provides new possibilities for finding fermionic resource states for quantum computation.

First, we review the fPEPS formalism[KSVC10, GVW10]. A 2D fPEPS is obtained from a lattice of fermionic entangled pairs (for example as shown in Fig. 10-5 or Fig. 10-3) by projecting the fermion modes on each site to a smaller physical Hilbert space. For the simple example given above, the projection is trivial on each site. In a general fPEPS state, the boundary modes and the entangled modes between sites (α, β, γ, δ) are only virtual and we denote the physical modes as c to distinguish them from the virtual ones. The virtual entangled mode pairs are again ordered from left (i,j) to right $(i,j+1)$ and top (i,j) to bottom $(i+1,j)$. The virtual boundaries and mode pairs between sites are denoted as $B_{i,1}$ and $H^k_{ij} = (\alpha^\dagger_{i,j}\beta^\dagger_{i,j+1} + 1)_k\,|\Omega\rangle$ for horizontal bonds and $V^k_{ij} = (\gamma^\dagger_{i,j}\delta^\dagger_{i+1,j} + 1)_k\,|\Omega\rangle$ for vertical bonds respectively, where the integer k labels the number of bonds per direction per site. Fig. 10-3 and Fig. 10-5 represent models with $k = 2$ and $k = 1$ respectively.

The wave function for the virtual space can be expressed as [KSVC10]

$$|\psi\rangle_v = \prod_{i,j,k} B_{i,1} H^k_{ij} V^k_{ij}\,|\Omega\rangle_v\,. \tag{10.10}$$

An on-site projection P_{ij} that maps the virtual space to the physical space with physical modes c_ℓ on every site is defined as [KSVC10]:

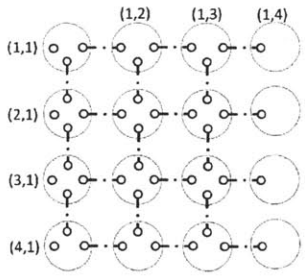

Figure 10-5: Representation of a 2D fPEPS with $k = 1$. The lattice has only one bond per direction.

$$P_{ij} = \sum_{\{n\}=0}^{1} A_{ij}[\{n\}] \prod_{l,k} \left(c_\ell^{\dagger n_\ell} \delta_k^{n_{\delta k}} \beta_k^{n_{\beta k}} \alpha_k^{n_{\alpha k}} \gamma_k^{n_{\gamma k}} \right)_{ij} \tag{10.11}$$

where $\{n\}$ is the set of occupation numbers for every mode, and $A_{ij}[\{n\}]$ depends on the intrinsic properties of the physical state one wants to project to.

P_{ij} is constrained to have a fixed parity for the resulting state to be physical, or

$$\sum_{l,k} (n_\ell + n_{\beta k} + n_{\gamma k} + n_{\alpha k} + n_{\delta k}) \ mod \ 2 = c, \tag{10.12}$$

where c is constant for each site.

To yield a physical state, one applies the projection operator P_{ij}'s to the virtual state $|\psi\rangle_v$ together with the physical vacuum state $|\Omega\rangle_p$ and then takes the vacuum expectation value on the virtual space as all the virtual modes must be annihilated and only physical modes are left,

$$\begin{aligned} |\psi\rangle_p &= {}_v\langle\Omega| \prod_{i,j} P_{ij} |\psi\rangle_v |\Omega\rangle_p \\ &= {}_v\langle\Omega| \prod_{i,j} P_{ij} \prod_{i,j,k} B_{i,1} H_{ij}^k V_{ij}^k |\Omega\rangle_v |\Omega\rangle_p \end{aligned} \tag{10.13}$$

This form of many-body fermion state is the starting point for a more general construction of fermionic resource states for MBQC.

Information flow in fPEPS

In the following, we show how the information stored in the left boundaries $B_{i,1}$ gets transmitted to the right by local measurements on an fPEPS. For simplicity, from now on, we assume $k = 1$, as shown in Fig. 10-5. The measurements are performed site by site from top to bottom and then from left to right starting from site $(1, 1)$ in column 1.

To illustrate the flow of information, we first look at the measurement on site $(1, 1)$. Suppose site $(1, 1)$ is measured in $|\phi_{11}\rangle = \mathcal{O}_{11} |\Omega_{11}\rangle_p$. To see what the state becomes after the measurement, we first rearrange $|\psi\rangle_p$ in Eq. 10.13 and commute the terms containing

modes on site $(1,1)$ together. We get:

$$|\psi\rangle_p = \sum_a {}_v\langle\Omega| \prod_{(i,j)\neq(1,1)} P_{ij} Q^a_{1,1} B^a_{i,1} H_{ij} V_{ij} |\Omega\rangle_v |\Omega\rangle_p$$
$$Q^a_{1,1} = \sum_a {}_v\langle\Omega_{11}| P_{11} B^a_{1,1} H_{11} V_{11} |\Omega_{11}\rangle_v |\Omega_{11}\rangle_p \tag{10.14}$$

where a denotes different terms in $B_{1,1}$ if input modes on site $(1,1)$ is entangled with other modes of $B_{i,1}$, which could possibly happen in a generic state as long as the total parity is fixed. Note that no extra signs are produced in this procedure as we are free to move the entangled pairs and the projections because they have fixed parities.

Using Eq. 10.13 and Eq. 10.14, it is obvious to see that after the measurement, the state becomes

$$|\phi_{11}\rangle \langle\phi_{11}|\psi\rangle_p = |\phi_{11}\rangle \sum_a {}_v\langle\Omega| \prod_{(i,j)\neq(1,1)} P_{ij} R^a_{1,1} B^a_{i,1} H_{ij} V_{ij} |\Omega\rangle_v |\Omega\rangle_p , \tag{10.15}$$

with

$$R^a_{1,1} = {}_p\langle\Omega_{11}| {}_v\langle\Omega_{11}| \mathcal{O}_{11} P_{11} B^a_{1,1} H_{11} V_{11} |\Omega_{11}\rangle_v |\Omega_{11}\rangle_p . \tag{10.16}$$

$R^a_{1,1}$ is an operator on the α virtual mode of site $(1,2)$ and the δ virtual mode of site $(2,1)$. We can hence interpret the effect of measuring site $(1,1)$ as information flow in the virtual space from site $(1,1)$ to site $(1,2)$ and $(2,1)$ as shown in Fig. 10-6. The encoded state changes from $B_{1,1}$ to $R_{1,1}$ and correspondingly certain operation is implemented. This is similar to the picture we had with spin MBQC where measurements on physical sites correspond to operations implemented on the information flow in the virtual space.

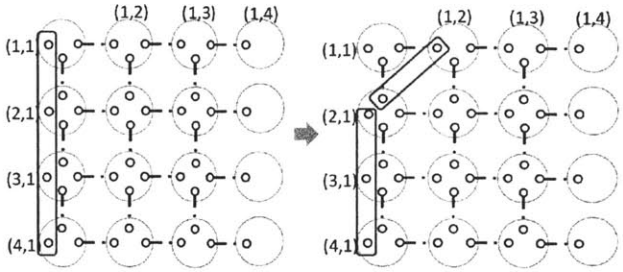

Figure 10-6: Illustration of boundary changes after measurement on site $(1,1)$. The boundary originally on site $(1,1)$ moves to site $(1,2)$ and site $(2,1)$. The new boundaries are $B_{i,1}(i \neq 1)$ and R_{11}.

This formalism provides a general framework to study MBQC based on many-body fermionic state. The simple example we studied before falls into this framework with $k = 2$ and trivial projection $P_{ij} = I$. Based on the general formulation, it is possible to find physically more feasible fPEPS resource state for MBQC. Extra care needs to be taken when dealing with measurement randomness on a general fPEPS and we discuss briefly possible difficulties in the next section.

Dealing with measurement randomness for general fPEPS

In dealing with measurement randomness for the simple model, we classified the by-products into two categories depending on whether the output contains the same parity as the input. Yet, we showed that the by-products are local and locally correctable as all the mode pairs ($\alpha\alpha'$, $\beta\beta'$, etc) have a fixed parity. However, in a general fPEPS state with possibly an odd number of bonds per direction ($k = 2n+1), n \in N$) and a more general encoding scheme, non-local by-products could occur and special attention is needed when designing MBQC schemes based on such states. As we show in the following, the non-locality of such by-products can be properly taken care of with careful design and is not a fundamental difficulty in using fPEPS states as MBQC resource states.

We use the $k = 1$ model to illustrate the basic idea. Assume that we are measuring the sites in a column-wise order, i.e. we first measure the first column from first row to last row and then second column from first row to last row, etc. Let us look more closely at the measurements on column 1, starting from site $(1,1)$, and moving downward. Suppose that the boundary modes are always ordered from up to down. So after measurement on site $(1,1)$, they are ordered from site $(1,2)$ to site $(2,1)$ to site $(3,1)$ etc. The parity constraint with a general encoding scheme is that the whole boundary chain has a fixed total parity, but each boundary mode may not. In particular, the boundary mode on site $(1,2)$ might not have a fixed parity. This leads to extra sign effect when site $(2,1)$ is measured. In particular, if site $(2,1)$ is measured in an odd basis which corresponds to an odd operation on the boundary, it applies a non-trivial sign factor $(-1)^{n_{\alpha_{1,2}}}$ to the boundary mode on site $(1,2)$. Similarly, measuring site $(i,1)$ in an odd basis causes a non-trivial sign factor on sites $(i',2)$ for $i' < i$. Therefore, the by-product induced is indeed non-local.

In general, after finishing measurements on the j'th column, the overall sign $S_{(i,j+1)}$ accumulated on site $(i,j+1)$ in column $j+1$ is determined by the number of odd measurement bases below site (i,j) in column j and the occupation number operator $n_{\alpha(i,j+1)}$ of α mode on site $(i,j+1)$. Define

$$N_{(i,j+1)} = \sum_{i',i'>i} f_{i'j}, \tag{10.17}$$

where f_{ij} is the parity of the measurement basis on site (i,j). Then, we obtain

$$S_{(i,j+1)} = (-1)^{n_{\alpha(i,j+1)} N_{(i,j+1)}} \tag{10.18}$$

Even though the by-products are non-local, they can be dealt with in a local way. Note that as long as one keeps track of all the measurement results, the total by-products that happen to the boundary modes can be determined after one finishes the measurements of one column. Moreover, the by-products factorize into a product form, of individual operators on each boundary mode separately, for example as given in Eq. 10.18. Such by-products can be incorporated into the operation to be implemented when measuring the column $j+1$ and can be corrected locally just like correcting Z by-product in spin systems.

To sum up, in a general fMBQC scheme based on fPEPS, non-local by-products do occur. But as they factorizes into a product form, they can be corrected locally.

10.3 Conclusion

In this chapter we generalized the measurement-based quantum computation scheme from spin systems to fermion systems. We gave a simple example of many-body fermion states

and demonstrated how it could be used as a universal resource state for MBQC. More generally, we provided a framework for constructing fermionic resource states for MBQC based on the fPEPS representation of fermion states and discussed ways to deal with the non-local by-products that might come up in the general scheme.

This framework provides a general starting point for the construction of new MBQC schemes. The ultimate goal is to find resource states that are easy to realize experimentally, for example in a free fermion system where particles move around but do not interact with each other. Unlike spin systems, which factorize into total product states and lose all computational power without interaction, the hopping of fermions in the lattice and their non-trivial mutual statistics can generate entanglement among different sites in space, which can subsequently provide the basis for the power of quantum computation.

Part V

Conclusion

Chapter 11

Summary and outlook

11.1 What we have learned about many-body entanglement

To summarize, in this thesis we aimed at a more systematic understanding of many-body entanglement in gapped quantum systems. Our theoretical study of this subject addressed not only the analytical and numerical aspects of the issue but also its experimental realization. Our results are mostly concerned with the representation, the classification and the application of many-body entangled states in gapped quantum systems. In particular,

1. In Part II, based on the tensor network representation of many-body entangled states, which was reviewed in Chapter 2 and 3, we first addressed the issue of how to extract the universal properties and hence determine which phase a many-body entangled state belongs to from its representative tensors. To achieve this, we presented a renormalization algorithm for tensor product states in Chapter 3 which flows the tensors to a fixed point form and allows the phase information to be easily extracted. Chapter 4 focused then on the tensor product representation of topologically ordered states and pointed out, interestingly, that small variations in the tensors do not always correspond to small perturbations in the physical systems. Therefore, for the tensor representation to be faithful to physical reality, certain variation directions are 'illegal' and should be carefully avoided. For topologically ordered systems with gauge symmetry, it was shown that only variations satisfying certain symmetry are allowed in the tensor.

2. Part III was devoted to the classification of many-body entangled states in gapped quantum systems with respect to their universal properties at large length scales, which can be measured macroscopically. As we are not interested in short distance structures of the states induced by local interactions of nearby particles, we need to set up an equivalence condition between many-body entangled states which allows smooth local deformations on the states. This was done carefully in Chapter 5 which provided the basis for the classification of gapped many-body states, hence zero-temperature gapped quantum phases, in the following chapters. In Chapter 6, we classified symmetry protected topological phases in one-dimensional systems. Actually, in one-dimension, the complete zero temperature gapped phase diagram can be understood, which we presented in [CGW11b]. Moreover, we studied the case of D_{2h} symmetry in spin chains and proposed how to experimentally distinguish different symmetry protected topological phases in [LCW11]. We moved on to two and higher

dimensions in Chapter 7, where we presented a systematic construction of symmetry protected topological phases in strongly interacting bosonic systems. Generalization of this approach to fermionic systems has led to new understanding of fermionic SPT phases as well [GW12].

3. In Part IV, we used our understanding of many-body entanglement structures in gapped quantum states to design applications of these states in quantum computation protocols. We focused on the measurement-based quantum computation model (reviewed in Chapter 8) which starts with a suitable many-body entangled states and employs only single body measurements to achieve the full power of quantum computation. The key to the realization of this model is to find an appropriate resource state which is easy to realize in the lab and stable against decoherence. We took one step towards this goal in Chapter 9 by finding a resource state as the gapped ground state of two-body interactions between spin 5/2 particles on a hexagonal lattice based on the tensor network representation of the state. More recently, resource states with physically more realistic forms of two-body interactions and smaller spin sizes (spin 3/2) have been proposed[Miy11, WAR11, CMDB10]. With our proof that spin 1/2 two-body frustration free Hamiltonians cannot have unique many-body entangled ground states[CCD$^+$11], such construction is approaching the optimum. Moreover, the connection between the measurement-based quantum computation and the tensor network representation enables us to have a more systematic understanding of the computational power of many-body entangled states. We showed in [CDJZ10] that almost all resource states that we know so far are equivalent to each other in computation power and can be converted through local measurements. Also using the fermionic version of tensor network representation, we generalized the measurement-based quantum computation model to fermionic systems in Chapter 10 which could lead to physically more feasible resource states.

11.2 Future directions

With these results, we gave our answer to the big question: is many-body entanglement really useful? After all we have so many powerful tools to deal with quantum many-body systems. By reducing quantum many-body systems to either classical systems or single-body systems, they provide great insight and perfect explanation for physical properties of quantum many-body systems in a broad class of situations. One might say, it is true that many-body entanglement does exist in principle, but by thinking of it do we learn anything new? Our answer to this question is Yes. With our systematic understanding of symmetry protected topological phases, construction of new topological models in strongly interacting systems and discovery of experimentally more feasible resource states for quantum computation, we give evidence that the many-body entanglement point of view could lead to new understanding that has never been achieved before in quantum many-body physics.

The theory of many-body entanglement is just at its beginning. By dealing directly with both the quantum and the many-body character of the system, it takes on the complexity of the problem and also opens up the door to more exciting discoveries. Here are a few directions which we think are going to be interesting:

1. In our work we focused on gapped many-body entangled states with only short range entanglement. For long range entangled states, many interesting examples are known

with exotic properties like fractional charge and fractional statistics and exciting applications like fault-tolerant quantum computation. However, a systematic understanding of such long range entangled states is still missing, especially for topologically ordered systems with chiral edge states. Among such chiral topological states is the quantum Hall state, whose experimental discovery led to the whole theory of topological order. However we have a limited understanding of its entanglement structure and many questions are open. For example, can we have a simple fixed point picture of its entanglement structure which captures all the universal features of the system? More specifically, can we describe its ground state using tensor network representation? If such a representation exist, we would have a variational approach to study quantum Hall systems and a better idea of in what kind of systems can such exotic quantum orders be realized. This would provide helpful information for the experimental realization of such phases.

2. While many interesting things can happen in gapped systems, the more exciting case is gapless systems, which are more responsive to external probes through their low energy excitations. Understanding of gapless systems is pretty complete in one dimension, thanks to conformal invariance, but in higher dimensions much less is known. Much has been understood about the entanglement structure in the ground state of gapless systems, as we reviewed in Chapter 1. But the key question is, how powerful is entanglement in the understanding of gapless systems? After all in gapless systems, the ground state is not the only state that exists at low temperature. There is a continuum of low energy excitations in the system above ground state even at very low temperatures and they decide many of the properties of the system under external perturbations. How much information then is contained in the entanglement structure of the ground state? In particular, can we determine the form of low energy excitations from just ground state entanglement? Recently, there has been proposal relating the entanglement structure of gapless states to the geometry of the holographic dual of the system[Swi09, EV11]. Such a connection suggests that many-body entanglement structure in certain gapless states encodes much of the universal information of the systems and could thereby lead to a more systematic understanding of gapless phases and phase transitions in two and higher dimensions.

3. Besides a qualitative understanding of quantum phase and phase transitions, many-body entanglement is likely to be the key to a more generic and powerful quantitative numerical simulation algorithm for quantum many-body systems. After all, a generic many-body quantum system is entangled. If we try to reduce the problem to a classical one, we run into the sign problem as with Quantum Monte Carlo. On the other hard, a brute force treatment of many-body entanglement leads to exponential complexity and the algorithm is restricted to extremely small system size, like in exact diagonalization. Incorporating the right amount of many-body entanglement in the simulation algorithm is the key to a successful numerical study of quantum many-body systems, as with the Density Matrix Renormalization Group (DMRG) method in one dimension. With the realization that matrix product representation in one dimension underlies the success of DMRG, algorithm based on two and higher dimensional tensor networks are extending this approach to systems beyond one dimension. For a more comprehensive review see [VMC08, Vid07]. A great deal of progress has been made, although the algorithms are not fully mature yet. In some cases it still

falls behind traditional methods (when they can be applied), and in other cases it has entered the competition[EV10]. A better understanding of the many-body entanglement structures will lead to a better identification of the important parameters in the simulation algorithm and hence a more efficient and powerful numerical approach to strongly correlated quantum many-body systems.

Finally, we would like to end with a comment that, like many other exciting developments in science nowadays, the theory of many-body entanglement thrives on interdisciplinary interaction. Growing out of the clash of ideas from two seeming very different subjects – quantum information and condensed matter physics – many-body entanglement provides a new point of view on quantum many-body physics, prompts new questions and proposes new approaches. With the fast development in both quantum information theory and condensed matter physics separately, we expect the theory of many-body entanglement to lead to a new era and become an essential part of our thinking, both qualitatively and quantitatively, about quantum many-body systems.

Bibliography

[AFF04] Eddy Ardonne, Paul Fendley, and Eduardo Fradkin. Topological order and conformal quantum critical points. *Annals of Physics*, **310**(2), 493 – 551, 2004. http://dx.doi.org/10.1016/j.aop.2004.01.004

[AFOV08] Luigi Amico, Rosario Fazio, Andreas Osterloh, and Vlatko Vedral. Entanglement in many-body systems. *Rev. Mod. Phys.*, **80**, 517–576, May 2008. http://link.aps.org/doi/10.1103/RevModPhys.80.517

[AKLT87] Ian Affleck, Tom Kennedy, Elliott H. Lieb, and Hal Tasaki. Rigorous results on valence-bond ground states in antiferromagnets. *Phys. Rev. Lett.*, **59**, 799–802, Aug 1987. http://link.aps.org/doi/10.1103/PhysRevLett.59.799

[AR07] Fabrizio Anfuso and Achim Rosch. String order and adiabatic continuity of haldane chains and band insulators. *Phys. Rev. B*, **75**, 144420, Apr 2007. http://link.aps.org/doi/10.1103/PhysRevB.75.144420

[AS06] Alexander Altland and Ben Simons. *Condensed Matter Field Theory*. Cambridge University Press, June 2006. http://dx.doi.org/10.1017/CBO9780511789984

[ASW84] Daniel Arovas, John R. Schrieffer, and Frank Wilczek. Fractional statistics and the quantum hall effect. *Phys. Rev. Lett.*, **53**, 722–723, Aug 1984. http://link.aps.org/doi/10.1103/PhysRevLett.53.722

[BAV09] Oliver Buerschaper, Miguel Aguado, and Guifré Vidal. Explicit tensor network representation for the ground states of string-net models. *Phys. Rev. B*, **79**, 085119, Feb 2009. http://link.aps.org/doi/10.1103/PhysRevB.79.085119

[BBC+93] Charles H. Bennett, Gilles Brassard, Claude Crépeau, Richard Jozsa, Asher Peres, and William K. Wootters. Teleporting an unknown quantum state via dual classical and einstein-podolsky-rosen channels. *Phys. Rev. Lett.*, **70**, 1895–1899, Mar 1993. http://link.aps.org/doi/10.1103/PhysRevLett.70.1895

[BD06] Tim P. Bodiya and Lu-Ming Duan. Scalable generation of graph-state entanglement through realistic linear optics. *Phys. Rev. Lett.*, **97**, 143601, Oct 2006. http://link.aps.org/doi/10.1103/PhysRevLett.97.143601

[BDTGA08] Erez Berg, Emanuele G. Dalla Torre, Thierry Giamarchi, and Ehud Altman. Rise and fall of hidden string order of lattice bosons. *Phys. Rev. B*, **77**, 245119, Jun 2008. http://link.aps.org/doi/10.1103/PhysRevB.77.245119

[BDZ08] Immanuel Bloch, Jean Dalibard, and Wilhelm Zwerger. Many-body physics with ultracold gases. *Rev. Mod. Phys.*, **80**, 885–964, Jul 2008. http://link.aps.org/doi/10.1103/RevModPhys.80.885

[BHM10] Sergey Bravyi, Matthew B. Hastings, and Spyridon Michalakis. Topological quantum order: Stability under local perturbations. *Journal of Mathematical Physics*, **51**(9), 093512, 2010. http://dx.doi.org/10.1063/1.3490195

[BHV06] Sergey Bravyi, Matthew B. Hastings, and Frank Verstraete. Lieb-robinson bounds and the generation of correlations and topological quantum order. *Phys. Rev. Lett.*, **97**, 050401, Jul 2006. http://link.aps.org/doi/10.1103/PhysRevLett.97.050401

[BK02] Sergey B. Bravyi and Alexei Y. Kitaev. Fermionic quantum computation. *Annals of Physics*, **298**(1), 210 – 226, 2002. http://dx.doi.org/10.1006/aphy.2002.6254

[BKRB08] Jan Benhelm, Gerhard Kirchmair, Christian F. Roos, and Rainer Blatt. Towards fault-tolerant quantum computing with trapped ions. *Nature Physics*, **4**(6), 463–466, April 2008. http://dx.doi.org/10.1038/nphys961

[BM08] Gavin K. Brennen and Akimasa Miyake. Measurement-based quantum computer in the gapped ground state of a two-body hamiltonian. *Phys. Rev. Lett.*, **101**, 010502, Jul 2008. http://link.aps.org/doi/10.1103/PhysRevLett.101.010502

[BMW09] Michael J. Bremner, Caterina Mora, and Andreas Winter. Are random pure states useful for quantum computation? *Phys. Rev. Lett.*, **102**, 190502, May 2009. http://link.aps.org/doi/10.1103/PhysRevLett.102.190502

[BR06] Stephen D. Bartlett and Terry Rudolph. Simple nearest-neighbor two-body hamiltonian system for which the ground state is a universal resource for quantum computation. *Phys. Rev. A*, **74**, 040302, Oct 2006. http://link.aps.org/doi/10.1103/PhysRevA.74.040302

[Bra06] Sergey Bravyi. Universal quantum computation with the $\nu = 5/2$ fractional quantum hall state. *Phys. Rev. A*, **73**, 042313, Apr 2006. http://link.aps.org/doi/10.1103/PhysRevA.73.042313

[BW90] B. Blok and Xiao-Gang Wen. Effective theories of the fractional quantum hall effect: Hierarchy construction. *Phys. Rev. B*, **42**, 8145–8156, Nov 1990. http://link.aps.org/doi/10.1103/PhysRevB.42.8145

[BZ06] B. Andrei Bernevig and Shou-Cheng Zhang. Quantum spin hall effect. *Phys. Rev. Lett.*, **96**, 106802, Mar 2006. http://link.aps.org/doi/10.1103/PhysRevLett.96.106802

[Car11] John Cardy. Measuring entanglement using quantum quenches. *Phys. Rev. Lett.*, **106**, 150404, Apr 2011. http://link.aps.org/doi/10.1103/PhysRevLett.106.150404

[CC08] Claudio Castelnovo and Claudio Chamon. Quantum topological phase transition at the microscopic level. *Phys. Rev. B*, **77**, 054433, Feb 2008. http://link.aps.org/doi/10.1103/PhysRevB.77.054433

[CC09] Pasquale Calabrese and John Cardy. Entanglement entropy and conformal field theory. *Journal of Physics A: Mathematical and Theoretical*, **42**(50), 504005, 2009. http://dx.doi.org/10.1088/1751-8113/42/50/504005

[CCD+11] Jianxin Chen, Xie Chen, Runyao Duan, Zhengfeng Ji, and Bei Zeng. No-go theorem for one-way quantum computing on naturally occurring two-level systems. *Phys. Rev. A*, **83**, 050301, May 2011. http://link.aps.org/doi/10.1103/PhysRevA.83.050301

[CCMP05] Claudio Castelnovo, Claudio Chamon, Christopher Mudry, and Pierre Pujol. From quantum mechanics to classical statistical physics: Generalized rokhsarkivelson hamiltonians and the stochastic matrix form decomposition. *Annals of Physics*, **318**(2), 316 – 344, 2005. http://dx.doi.org/10.1016/j.aop.2005.01.006

[CDJZ10] Xie Chen, Runyao Duan, Zhengfeng Ji, and Bei Zeng. Quantum state reduction for universal measurement based computation. *Phys. Rev. Lett.*, **105**, 020502, Jul 2010. http://link.aps.org/doi/10.1103/PhysRevLett.105.020502

[CGLW11] Xie Chen, Zheng-Cheng Gu, Zheng-Xin Liu, and Xiao-Gang Wen. Symmetry protected topological orders and the group cohomology of their symmetry group. *ArXiv e-prints*, June 2011. http://arxiv.org/abs/1106.4772

[CGW10] Xie Chen, Zheng-Cheng Gu, and Xiao-Gang Wen. Local unitary transformation, long-range quantum entanglement, wave function renormalization, and topological order. *Phys. Rev. B*, **82**(15), 155138, Oct 2010. http://dx.doi.org/10.1103/PhysRevB.82.155138

[CGW11a] Xie Chen, Zheng-Cheng Gu, and Xiao-Gang Wen. Classification of gapped symmetric phases in one-dimensional spin systems. *Phys. Rev. B*, **83**(3), 035107, Jan 2011. http://dx.doi.org/10.1103/PhysRevB.83.035107

[CGW11b] Xie Chen, Zheng-Cheng Gu, and Xiao-Gang Wen. Complete classification of one-dimensional gapped quantum phases in interacting spin systems. *Phys. Rev. B*, **84**, 235128, Dec 2011. http://link.aps.org/doi/10.1103/PhysRevB.84.235128

[CLW11] Xie Chen, Zheng-Xin Liu, and Xiao-Gang Wen. Two-dimensional symmetry-protected topological orders and their protected gapless edge excitations. *Phys. Rev. B*, **84**, 235141, Dec 2011. http://link.aps.org/doi/10.1103/PhysRevB.84.235141

[CMDB10] Jianming Cai, Akimasa Miyake, Wolfgang Dür, and Hans J. Briegel. Universal quantum computer from a quantum magnet. *Phys. Rev. A*, **82**, 052309, Nov 2010. http://link.aps.org/doi/10.1103/PhysRevA.82.052309

[CZG+09] Xie Chen, Bei Zeng, Zheng-Cheng Gu, Beni Yoshida, and Isaac L. Chuang. Gapped two-body hamiltonian whose unique ground state is universal for one-way quantum computation. *Phys. Rev. Lett.*, **102**, 220501, Jun 2009. http://link.aps.org/doi/10.1103/PhysRevLett.102.220501

[CZG+10] Xie Chen, Bei Zeng, Zheng-Cheng Gu, Isaac L. Chuang, and Xiao-Gang Wen. Tensor product representation of a topological ordered phase: Necessary symmetry conditions. *Phys. Rev. B*, **82**(16), 165119, Oct 2010. http://dx.doi.org/10.1103/PhysRevB.82.165119

[DGJO11] Jean Dalibard, Fabrice Gerbier, Gediminas Juzeliunas, and Patrik Öhberg. *Colloquium*: Artificial gauge potentials for neutral atoms. *Rev. Mod. Phys.*, **83**, 1523–1543, Nov 2011. http://link.aps.org/doi/10.1103/RevModPhys.83.1523

[dNR89] Marcel den Nijs and Koos Rommelse. Preroughening transitions in crystal surfaces and valence-bond phases in quantum spin chains. *Phys. Rev. B*, **40**, 4709–4734, Sep 1989. http://link.aps.org/doi/10.1103/PhysRevB.40.4709

[DVC00] Wolfgang Dür, Guifré Vidal, and J. Ignacio Cirac. Three qubits can be entangled in two inequivalent ways. *Phys. Rev. A*, **62**, 062314, Nov 2000. http://link.aps.org/doi/10.1103/PhysRevA.62.062314

[ECP10] Jens Eisert, Marcus Cramer, and Martin B. Plenio. *Colloquium* : Area laws for the entanglement entropy. *Rev. Mod. Phys.*, **82**, 277–306, Feb 2010. http://link.aps.org/doi/10.1103/RevModPhys.82.277

[EHK78] David E. Evans and Raphael Hegh-Krohn. Spectral properties of positive maps on c*-algebras. *Journal of the London Mathematical Society*, **s2-17**(2), 345–355, 1978. http://dx.doi.org/10.1112/jlms/s2-17.2.345

[EPR35] Albert Einstein, Boris Podolsky, and Nathan Rosen. Can Quantum-Mechanical description of physical reality be considered complete? *Physical Review Online Archive (Prola)*, **47**(10), 777–780, May 1935. http://dx.doi.org/10.1103/PhysRev.47.777

[EV10] Glen Evenbly and Guifré Vidal. Frustrated antiferromagnets with entanglement renormalization: Ground state of the spin-$\frac{1}{2}$ heisenberg model on a kagome lattice. *Phys. Rev. Lett.*, **104**, 187203, May 2010. http://link.aps.org/doi/10.1103/PhysRevLett.104.187203

[EV11] Glen Evenbly and Guifré Vidal. Tensor network states and geometry. *Journal of Statistical Physics*, **145**, 891–918, 2011. http://dx.doi.org/10.1007/s10955-011-0237-4

[Fey82] Richard Feynman. Simulating physics with computers. *International Journal of Theoretical Physics*, **21**, 467–488, 1982. http://dx.doi.org/10.1007/BF02650179

[FHHW09] Steven T. Flammia, Alioscia Hamma, Taylor L. Hughes, and Xiao-Gang Wen. Topological entanglement rényi entropy and reduced density matrix structure. *Phys. Rev. Lett.*, **103**, 261601, Dec 2009. http://link.aps.org/doi/10.1103/PhysRevLett.103.261601

[Fis94] Daniel S. Fisher. Random antiferromagnetic quantum spin chains. *Phys. Rev. B*, **50**, 3799–3821, Aug 1994. http://link.aps.org/doi/10.1103/PhysRevB.50.3799

[FK91] Juerg Froehlich and Thomas Kerler. Universality in quantum hall systems. *Nuclear Physics B*, **354**(2-3), 369 – 417, 1991. http://dx.doi.org/10.1016/0550-3213(91)90360-A

[FK10] Lukasz Fidkowski and Alexei Kitaev. Effects of interactions on the topological classification of free fermion systems. *Phys. Rev. B*, **81**(13), 134509, Apr 2010. http://dx.doi.org/10.1103/PhysRevB.81.134509

[FK11] Lukasz Fidkowski and Alexei Kitaev. Topological phases of fermions in one dimension. *Phys. Rev. B*, **83**(7), 075103, Feb 2011. http://dx.doi.org/10.1103/PhysRevB.83.075103

[FKM07] Liang Fu, Charles L. Kane, and Eugene J. Mele. Topological insulators in three dimensions. *Phys. Rev. Lett.*, **98**, 106803, 2007. http://link.aps.org/doi/10.1103/PhysRevLett.98.106803

[FNW92a] Mark Fannes, Bruno Nachtergaele, and Reinhard F. Werner. Abundance of translation invariant pure states on quantum spin chains. *Letters in Mathematical Physics*, **25**, 249–258, 1992. http://dx.doi.org/10.1007/BF00406552

[FNW92b] Mark Fannes, Bruno Nachtergaele, and Reinhard F. Werner. Finitely correlated states on quantum spin chains. *Communications in Mathematical Physics*, **144**, 443–490, 1992. http://dx.doi.org/10.1007/BF02099178

[FNW94] Mark Fannes, Bruno Nachtergaele, and Reinhard F. Werner. Finitely correlated pure states. *Journal of Functional Analysis*, **120**(2), 511 – 534, 1994. http://dx.doi.org/10.1006/jfan.1994.1041

[GC99] Daniel Gottesman and Isaac L. Chuang. Demonstrating the viability of universal quantum computation using teleportation and single-qubit operations. *Nature*, **402**(6760), 390–393, November 1999. http://dx.doi.org/10.1038/46503

[GE07] David Gross and Jens Eisert. Novel schemes for measurement-based quantum computation. *Phys. Rev. Lett.*, **98**, 220503, May 2007. http://link.aps.org/doi/10.1103/PhysRevLett.98.220503

[GE10] David Gross and Jens Eisert. Quantum computational webs. *Phys. Rev. A*, **82**, 040303, Oct 2010. http://link.aps.org/doi/10.1103/PhysRevA.82.040303

[GESPG07] Daivd Gross, Jens Eisert, Norbert Schuch, and David Pérez-García. Measurement-based quantum computation beyond the one-way model. *Phys. Rev. A*, **76**, 052315, Nov 2007. http://link.aps.org/doi/10.1103/PhysRevA.76.052315

[GFE09] David Gross, Steve T. Flammia, and Jens Eisert. Most quantum states are too entangled to be useful as computational resources. *Phys. Rev. Lett.*, **102**, 190501, May 2009. http://link.aps.org/doi/10.1103/PhysRevLett.102.190501

[GGL+91] Sivert H. Glarum, Stanley Geschwind, K. M. Lee, M. L. Kaplan, and J. Michel. Observation of fractional spin S =1/2 on open ends of S =1 linear antiferromagnetic chains: Nonmagnetic doping. *Phys. Rev. Lett.*, **67**, 1614–1617, Sep 1991. http://link.aps.org/doi/10.1103/PhysRevLett.67.1614

[GL50] Vitaly L. Ginzburg and Lev D. Landau. On the theory of superconductivity. *Zh. Ekaper. Teoret. Fiz.*, **20**, 1064–1082, 1950. http://dx.doi.org/10.1007/BF02731579

[GLSW09] Zheng-Cheng Gu, Michael Levin, Brian Swingle, and Xiao-Gang Wen. Tensor-product representations for string-net condensed states. *Phys. Rev. B*, **79**, 085118, Feb 2009. http://link.aps.org/doi/10.1103/PhysRevB.79.085118

[GME+02] Markus Greiner, Olaf Mandel, Tilman Esslinger, Theodor W. Hansch, and Immanuel Bloch. Quantum phase transition from a superfluid to a mott insulator in a gas of ultracold atoms. *Nature*, **415**(6867), 39–44, January 2002. http://dx.doi.org/10.1038/415039a

[GPS08] Stefano Giorgini, Lev P. Pitaevskii, and Sandro Stringari. Theory of ultracold atomic fermi gases. *Rev. Mod. Phys.*, **80**, 1215–1274, Oct 2008. http://link.aps.org/doi/10.1103/RevModPhys.80.1215

[GVW10] Zheng-Cheng Gu, Frank Verstraete, and Xiao-Gang Wen. Grassmann tensor network states and its renormalization for strongly correlated fermionic and bosonic states. *ArXiv e-prints*, April 2010. http://arxiv.org/abs/1004.2563

[GW09] Zheng-Cheng Gu and Xiao-Gang Wen. Tensor-entanglement-filtering renormalization approach and symmetry-protected topological order. *Phys. Rev. B*, **80**(15), 155131, Oct 2009. http://dx.doi.org/10.1103/PhysRevB.80.155131

[GW12] Zheng-Cheng Gu and Xiao-Gang Wen. Symmetry-protected topological orders for interacting fermions – fermionic topological non-linear sigma-models and a group super-cohomology theory. *ArXiv e-prints*, January 2012. http://arxiv.org/abs/1201.2648

[GWW10] Zheng-Cheng Gu, Zhenghan Wang, and Xiao-Gang Wen. A classification of 2D fermionic and bosonic topological orders. *ArXiv e-prints*, October 2010. http://arxiv.org/abs/1010.1517

[Hal83a] F. Duncan M. Haldane. Continuum dynamics of the 1-D heisenberg antiferromagnet: Identification with the O(3) nonlinear sigma model. *Physics Letters A*, **93**, 464, 1983. http://dx.doi.org/10.1016/0375-9601(83)90631-X

[Hal83b] F. Duncan M. Haldane. Nonlinear field theory of large-spin heisenberg antiferromagnets: Semiclassically quantized solitons of the one-dimensional easy-axis néel state. *Phys. Rev. Lett.*, **50**, 1153–1156, Apr 1983. http://link.aps.org/doi/10.1103/PhysRevLett.50.1153

[Has04] Matthew B. Hastings. Locality in quantum and markov dynamics on lattices and networks. *Phys. Rev. Lett.*, **93**, 140402, Sep 2004. http://link.aps.org/doi/10.1103/PhysRevLett.93.140402

[Has07] Matthew B. Hastings. An area law for one-dimensional quantum systems. *Journal of Statistical Mechanics: Theory and Experiment*, **2007**(08), P08024, 2007. http://dx.doi.org/10.1088/1742-5468/2007/08/P08024

[Has09] Matthew B. Hastings. Quantum adiabatic computation with a constant gap is not useful in one dimension. *Phys. Rev. Lett.*, **103**, 050502, Jul 2009. http://link.aps.org/doi/10.1103/PhysRevLett.103.050502

[HBP08] Michael J. Hartmann, Fernando G.S.L. Brando, and Martin B. Plenio. Quantum many-body phenomena in coupled cavity arrays. *Laser and Photonics Reviews*, **2**(6), 527–556, 2008. http://dx.doi.org/10.1002/lpor.200810046

[Hen04] Christopher L. Henley. From classical to quantum dynamics at rokhsarkivelson points. *Journal of Physics: Condensed Matter*, **16**(11), S891, 2004. http://dx.doi.org/10.1088/0953-8984/16/11/045

[HGF09] Benjamin Hsu, Eytan Grosfeld, and Eduardo Fradkin. Quantum noise and entanglement generated by a local quantum quench. *Phys. Rev. B*, **80**, 235412, Dec 2009. http://link.aps.org/doi/10.1103/PhysRevB.80.235412

[HHHH09] Ryszard Horodecki, Paweł Horodecki, Michał Horodecki, and Karol Horodecki. Quantum entanglement. *Rev. Mod. Phys.*, **81**, 865–942, Jun 2009. http://link.aps.org/doi/10.1103/RevModPhys.81.865

[HK05] Matthew B. Hastings and Tohru Koma. Spectral gap and exponential decay of correlations. *Communications in Mathematical Physics*, **265**(3), 23, 2005. http://arxiv.org/abs/math-ph/0507008

[HKA+90] Masayuki Hagiwara, Koichi Katsumata, Ian Affleck, Bertrand I. Halperin, and J. P. Renard. Observation of S =1/2 degrees of freedom in an S =1 linear-chain heisenberg antiferromagnet. *Phys. Rev. Lett.*, **65**, 3181–3184, Dec 1990. http://link.aps.org/doi/10.1103/PhysRevLett.65.3181

[HKC+06] Zoran Hadzibabic, Peter Kruger, Marc Cheneau, Baptiste Battelier, and Jean Dalibard. BerezinskiiKosterlitzThouless crossover in a trapped atomic gas. *Nature*, **441**(7097), 1118–1121, June 2006. http://dx.doi.org/10.1038/nature04851

[HLW94] Christoph Holzhey, Finn Larsen, and Frank Wilczek. Geometric and renormalized entropy in conformal field theory. *Nuclear Physics B*, **424**(3), 443 – 467, 1994. http://dx.doi.org/10.1016/0550-3213(94)90402-2

[HW05] Matthew B. Hastings and Xiao-Gang Wen. Quasiadiabatic continuation of quantum states: The stability of topological ground-state degeneracy and emergent gauge invariance. *Phys. Rev. B*, **72**, 045141, Jul 2005. http://link.aps.org/doi/10.1103/PhysRevB.72.045141

[HY97] Ross A. Hyman and Kun Yang. Impurity driven phase transition in the antiferromagnetic spin-1 chain. *Phys. Rev. Lett.*, **78**, 1783–1786, Mar 1997. http://link.aps.org/doi/10.1103/PhysRevLett.78.1783

[HZHL08] Aliocia Hamma, Wen Zhang, Stephan Haas, and Daniel A. Lidar. Entanglement, fidelity, and topological entropy in a quantum phase transition to topological order. *Phys. Rev. B*, **77**, 155111, Apr 2008. http://link.aps.org/doi/10.1103/PhysRevB.77.155111

[JL03] Richard Jozsa and Noah Linden. On the role of entanglement in quantum-computational speed-up. *Proceedings of the Royal Society of London. Series A: Mathematical, Physical and Engineering Sciences*, **459**(2036), 2011–2032, 2003. http://dx.doi.org/10.1098/rspa.2002.1097

[JVW09] Michael Johanning, Andrs F Varn, and Christof Wunderlich. Quantum simulations with cold trapped ions. *Journal of Physics B: Atomic, Molecular and Optical Physics*, **42**(15), 154009, 2009. http://dx.doi.org/10.1088/0953-4075/42/15/154009

[JZ05] Dieter Jaksch and Peter Zoller. The cold atom hubbard toolbox. *Annals of Physics*, **315**(1), 52 – 79, 2005. http://dx.doi.org/10.1016/j.aop.2004.09.010

[Kit01] Alexei Yu Kitaev. Unpaired majorana fermions in quantum wires. *PhysicsUspekhi*, **44**(10S), 131–136, 2001. http://dx.doi.org/10.1070/1063-7869/44/10S/S29

[Kit03] Alexei Yu Kitaev. Fault-tolerant quantum computation by anyons. *Annals of Physics*, **303**(1), 2 – 30, 2003. http://dx.doi.org/10.1016/S0003-4916(02)00018-0

[Kit06] Alexei Yu Kitaev. Anyons in an exactly solved model and beyond. *Annals of Physics*, **321**(1), 2 – 111, 2006. http://dx.doi.org/10.1016/j.aop.2005.10.005

[Kit09] Alexei Yu Kitaev. Periodic table for topological insulators and superconductors. *AIP Conference Proceedings*, **1134**(1), 22–30, 2009. http://dx.doi.org/10.1063/1.3149495

[KL87] Vadim Kalmeyer and Robert B. Laughlin. Equivalence of the resonating-valence-bond and fractional quantum hall states. *Phys. Rev. Lett.*, **59**, 2095–2098, 1987. http://link.aps.org/doi/10.1103/PhysRevLett.59.2095

[KL09] Israel Klich and Leonid Levitov. Quantum noise as an entanglement meter. *Phys. Rev. Lett.*, **102**, 100502, Mar 2009. http://link.aps.org/doi/10.1103/PhysRevLett.102.100502

[KLW08] Su-Peng Kou, Michael Levin, and Xiao-Gang Wen. Mutual chern-simons theory for z_2 topological order. *Phys. Rev. B*, **78**(15), 155134, Oct 2008. http://dx.doi.org/10.1103/PhysRevB.78.155134

[KLW09] Wing-Ho Ko, Patrick A. Lee, and Xiao-Gang Wen. Doped kagome system as exotic superconductor. *Phys. Rev. B*, **79**(21), 214502, Jun 2009. http://dx.doi.org/10.1103/PhysRevB.79.214502

[KM05a] Charles L. Kane and Eugene J. Mele. Quantum spin hall effect in graphene. *Phys. Rev. Lett.*, **95**, 226801, Nov 2005. http://link.aps.org/doi/10.1103/PhysRevLett.95.226801

[KM05b] Charles L. Kane and Eugene J. Mele. Z_2 topological order and the quantum spin hall effect. *Phys. Rev. Lett.*, **95**, 146802, Sep 2005. http://link.aps.org/doi/10.1103/PhysRevLett.95.146802

[KMS+05] Michael Köhl, Henning Moritz, Thilo Stöferle, Kenneth Günter, and Tilman Esslinger. Fermionic atoms in a three dimensional optical lattice: Observing fermi surfaces, dynamics, and interactions. *Phys. Rev. Lett.*, **94**, 080403, Mar 2005. http://link.aps.org/doi/10.1103/PhysRevLett.94.080403

[KP06] Alexei Kitaev and John Preskill. Topological entanglement entropy. *Phys. Rev. Lett.*, **96**(11), 110404, Mar 2006. http://dx.doi.org/10.1103/PhysRevLett.96.110404

[KRS06] Israel Klich, Gil Refael, and Alessandro Silva. Measuring entanglement entropies in many-body systems. *Phys. Rev. A*, **74**, 032306, Sep 2006. http://link.aps.org/doi/10.1103/PhysRevA.74.032306

[KSVC10] Christina V. Kraus, Norbert Schuch, Frank Verstraete, and J. Ignacio Cirac. Fermionic projected entangled pair states. *Phys. Rev. A*, **81**, 052338, May 2010. http://link.aps.org/doi/10.1103/PhysRevA.81.052338

[KT92] Tom Kennedy and Hal Tasaki. Hidden z2*z2 symmetry breaking in haldane-gap antiferromagnets. *Phys. Rev. B*, **45**, 304–307, Jan 1992. http://link.aps.org/doi/10.1103/PhysRevB.45.304

[KW09] Su-Peng Kou and Xiao-Gang Wen. Translation-symmetry-protected topological orders in quantum spin systems. *Phys. Rev. B*, **80**(22), 224406, Dec 2009. http://dx.doi.org/10.1103/PhysRevB.80.224406

[KWW04] Toshiya Kinoshita, Trevor Wenger, and David S. Weiss. Observation of a one-dimensional tonks-girardeau gas. *Science*, **305**(5687), 1125–1128, 2004. http://dx.doi.org/10.1126/science.1100700

[KZ08] Wolfgang Ketterle and Martin W. Zwierlein. Making, probing and understanding ultracold Fermi gases. *Nuovo Cimento Rivista Serie*, **31**, 247–422, May 2008. http://dx.doi.org/10.1393/ncr/i2008-10033-1

[Lan37] Lev D. Landau. Theory of phase transformations. *Phys. Z. Sowjetunion*, **11**, 26, 1937. http://dx.doi.org/10.1038/138840a0

[LBKJS11] Michael Levin, F. J. Burnell, Maciej Koch-Janusz, and Ady Stern. Exactly soluble models for fractional topological insulators in two and three dimensions. *Phys. Rev. B*, **84**, 235145, Dec 2011. http://link.aps.org/doi/10.1103/PhysRevB.84.235145

[LCW11] Zheng-Xin Liu, Xie Chen, and Xiao-Gang Wen. Symmetry-protected topological orders of one-dimensional spin systems with $D_2 + t$ symmetry. *Phys. Rev. B*, **84**, 195145, Nov 2011. http://link.aps.org/doi/10.1103/PhysRevB.84.195145

[LG12] Michael Levin and Zheng-Cheng Gu. Braiding statistics approach to symmetry-protected topological phases. *ArXiv e-prints*, February 2012. http://arxiv.org/abs/1202.3120

[LH08] Hui Li and F. Duncan M. Haldane. Entanglement spectrum as a generalization of entanglement entropy: Identification of topological order in non-abelian fractional quantum hall effect states. *Phys. Rev. Lett.*, **101**, 010504, Jul 2008. http://link.aps.org/doi/10.1103/PhysRevLett.101.010504

[LL58] Lev D. Landau and Evgeny M. Lifschitz. *Statistical Physics - Course of Theoretical Physics Vol 5.* Pergamon, London, 1958. http://www.amazon.com/Statistical-Physics-Third-Edition-Part/dp/0750633727

[Llo96] Seth Lloyd. Universal quantum simulators. *Science*, **273**(5278), 1073–1078, 1996. http://dx.doi.org/10.1126/science.273.5278.1073

[LN07] Michael Levin and Cody P. Nave. Tensor renormalization group approach to two-dimensional classical lattice models. *Phys. Rev. Lett.*, **99**, 120601, Sep 2007. http://link.aps.org/doi/10.1103/PhysRevLett.99.120601

[LR72] Elliott H. Lieb and Derek W. Robinson. The finite group velocity of quantum spin systems. *Communications in Mathematical Physics*, **28**, 251–257, 1972. http://dx.doi.org/10.1007/BF01645779

[LS09] Michael Levin and Ady Stern. Fractional topological insulators. *Phys. Rev. Lett.*, **103**, 196803, Nov 2009. http://link.aps.org/doi/10.1103/PhysRevLett.103.196803

[LSM61] Elliott Lieb, Theodore Schultz, and Daniel Mattis. Two soluble models of an antiferromagnetic chain. *Annals of Physics*, **16**, 407–466, December 1961. http://dx.doi.org/10.1016/0003-4916(61)90115-4

[LW05] Michael A. Levin and Xiao-Gang Wen. String-net condensation: A physical mechanism for topological phases. *Phys. Rev. B*, **71**(4), 045110, Jan 2005. http://dx.doi.org/10.1103/PhysRevB.71.045110

[LW06] Michael Levin and Xiao-Gang Wen. Detecting topological order in a ground state wave function. *Phys. Rev. Lett.*, **96**(11), 110405, Mar 2006. http://dx.doi.org/10.1103/PhysRevLett.96.110405

[LZG+07] Chao-Yang Lu, Xiao-Qi Zhou, Otfried Guhne, Wei-Bo Gao, Jin Zhang, Zhen-Sheng Yuan, Alexander Goebel, Tao Yang, and Jian-Wei Pan. Experimental entanglement of six photons in graph states. *Nature Physics*, **3**(2), 91–95, January 2007. http://dx.doi.org/10.1038/nphys507

[Mat01] Taku Matsui. The split property and the symmetry breakingof the quantum spin chain. *Communications in Mathematical Physics*, **218**, 393–416, 2001. http://dx.doi.org/10.1007/s002200100413

[MB07] Joel E. Moore and Leon Balents. Topological invariants of time-reversal-invariant band structures. *Phys. Rev. B*, **75**, 121306, Mar 2007. http://link.aps.org/doi/10.1103/PhysRevB.75.121306

[MDH79] Shang-keng Ma, Chandan Dasgupta, and Chin-kun Hu. Random antiferromagnetic chain. *Phys. Rev. Lett.*, **43**, 1434–1437, Nov 1979. http://link.aps.org/doi/10.1103/PhysRevLett.43.1434

[Miy11] Akimasa Miyake. Quantum computational capability of a 2d valence bond solid phase. *Annals of Physics*, **326**(7), 1656 – 1671, 2011. http://dx.doi.org/10.1016/j.aop.2011.03.006

[MQKZ10] Joseph Maciejko, Xiao-Liang Qi, Andreas Karch, and Shou-Cheng Zhang. Fractional topological insulators in three dimensions. *Phys. Rev. Lett.*, **105**, 246809, Dec 2010. http://link.aps.org/doi/10.1103/PhysRevLett.105.246809

[MRZ08] Omri Morgenshtern, Benni Reznik, and Idan Zalzberg. Quantum information with single fermions: teleportation and fermion-boson entanglement conversion. *ArXiv e-prints*, July 2008. http://arxiv.org/abs/0807.0850

[MS01] Roderich Moessner and Shivaji L. Sondhi. Resonating valence bond phase in the triangular lattice quantum dimer model. *Phys. Rev. Lett.*, **86**, 1881–1884, Feb 2001. http://link.aps.org/doi/10.1103/PhysRevLett.86.1881

[NC00] Michael A. Nielsen and Isaac L. Chuang. *Quantum Computation and Quantum Information*. Cambridge University Press, 1 edition, October 2000. http://www.amazon.com/exec/obidos/redirect?tag=citeulike07-20&path=ASIN/0521635039

[NCA+12] Sylvain Nascimbène, Yu-Ao Chen, Macros Atala, Monika Aidelsburger, Stefan Trotzky, Belén Paredes, and Immanuel Bloch. Experimental realization of plaquette resonating valence bond states with ultracold atoms in optical superlattices. *ArXiv e-prints*, February 2012. http://arxiv.org/abs/1202.6361

[Ng94] Tai-Kai Ng. Edge states in antiferromagnetic quantum spin chains. *Phys. Rev. B*, **50**, 555–558, Jul 1994. http://link.aps.org/doi/10.1103/PhysRevB.50.555

[Nie06] Michael A. Nielsen. Cluster-state quantum computation. *Reports on Mathematical Physics*, **57**(1), 147 – 161, 2006. http://dx.doi.org/10.1016/S0034-4877(06)80014-5

[OT08] Roberto Oliveira and Barbara M. Terhal. The complexity of quantum spin systems on a two-dimensional square lattice. *Quantum Info. Comput.*, **8**(10), 900–924, November 2008. http://dl.acm.org/citation.cfm?id=2016985.2016987

[PB08] Belén Paredes and Immanuel Bloch. Minimum instances of topological matter in an optical plaquette. *Phys. Rev. A*, **77**, 023603, Feb 2008. http://link.aps.org/doi/10.1103/PhysRevA.77.023603

[PB10] Dmytro Pesin and Leon Balents. Mott physics and band topology in materials with strong spin-orbit interaction. *Nature Phys*, **6**(5), 376–381, May 2010. http://dx.doi.org/10.1038/nphys1606

[PBTO12] Frank Pollmann, Erez Berg, Ari M. Turner, and Masaki Oshikawa. Symmetry protection of topological phases in one-dimensional quantum spin systems. *Phys. Rev. B*, **85**, 075125, Feb 2012. http://link.aps.org/doi/10.1103/PhysRevB.85.075125

[PGVCW08] David Pérez-García, Frank Verstraete, J. Ignacio Cirac, and Michael M. Wolf. Peps as unique ground states of local hamiltonians. *Quant.Inf.Comp.*, **8**, 0650, 2008. http://www.citebase.org/abstract?id=oai:arXiv.org:0707.2260

[PGVWC07] David Pérez-García, Frank Verstraete, Michael M. Wolf, and J. Ignacio Cirac. Matrix Product State Representations. *Quant. Inf. Comput.*, **7**, 401, May 2007. http://arxiv.org/abs/quant-ph/0608197

[PGWS+08] David Pérez-García, Michael M. Wolf, Mikel Sanz, Frank Verstraete, and J. Ignacio Cirac. String order and symmetries in quantum spin lattices. *Phys. Rev. Lett.*, **100**(16), 167202, Apr 2008. http://dx.doi.org/10.1103/PhysRevLett.100.167202

[PMCV10] Bogdan Pirvu, Valentin Murg, J Ignacio Cirac, and Frank Verstraete. Matrix product operator representations. *New Journal of Physics*, **12**(2), 025012, 2010. http://dx.doi.org/10.1088/1367-2630/12/2/025012

[PRF07] Stefanos Papanikolaou, Kumar S. Raman, and Eduardo Fradkin. Topological phases and topological entropy of two-dimensional systems with finite correlation length. *Phys. Rev. B*, **76**, 224421, Dec 2007. http://link.aps.org/doi/10.1103/PhysRevB.76.224421

[PTBO10] Frank Pollmann, Ari M. Turner, Erez Berg, and Masaki Oshikawa. Entanglement spectrum of a topological phase in one dimension. *Phys. Rev. B*, **81**, 064439, Feb 2010. http://link.aps.org/doi/10.1103/PhysRevB.81.064439

[PV06] Martin B. Plenio and Shashank Virmani. An introduction to entanglement measures. *ArXiv e-prints*, June 2006. http://arxiv.org/abs/quant-ph/0504163

[PWM+04] Belen Paredes, Artur Widera, Valentin Murg, Olaf Mandel, Simon Folling, Ignacio Cirac, Gora V. Shlyapnikov, Theodor W. Hansch, and Immanuel

Bloch. Tonks-Girardeau gas of ultracold atoms in an optical lattice. *Nature*, **429**(6989), 277–281, May 2004. http://dx.doi.org/10.1038/nature02530

[QHRZ09] Xiao-Liang Qi, Taylor L. Hughes, S. Raghu, and Shou-Cheng Zhang. Time-reversal-invariant topological superconductors and superfluids in two and three dimensions. *Phys. Rev. Lett.*, **102**, 187001, May 2009. http://link.aps.org/doi/10.1103/PhysRevLett.102.187001

[QHZ08] Xiao-Liang Qi, Taylor L. Hughes, and Shou-Cheng Zhang. Topological field theory of time-reversal invariant insulators. *Phys. Rev. B*, **78**(19), 195424, Nov 2008. http://dx.doi.org/10.1103/PhysRevB.78.195424

[RB01] Robert Raussendorf and Hans J. Briegel. A one-way quantum computer. *Phys. Rev. Lett.*, **86**, 5188–5191, May 2001. http://link.aps.org/doi/10.1103/PhysRevLett.86.5188

[RBB02] Robert Raussendorf, Daniel E. Browne, and Hans J. Briegel. The one-way quantum computer - a non-network model of quantum computation. *Journal of Modern Optics*, **49**, 1299, 2002. http://dx.doi.org/10.1080/09500340110107487

[RBB03] Robert Raussendorf, Daniel E. Browne, and Hans J. Briegel. Measurement-based quantum computation on cluster states. *Phys. Rev. A*, **68**, 022312, Aug 2003. http://link.aps.org/doi/10.1103/PhysRevA.68.022312

[Rea90] Nicholas Read. Excitation structure of the hierarchy scheme in the fractional quantum hall effect. *Phys. Rev. Lett.*, **65**, 1502–1505, Sep 1990. http://link.aps.org/doi/10.1103/PhysRevLett.65.1502

[RG00] Nicholas Read and Dmitry Green. Paired states of fermions in two dimensions with breaking of parity and time-reversal symmetries and the fractional quantum hall effect. *Phys. Rev. B*, **61**, 10267–10297, Apr 2000. http://link.aps.org/doi/10.1103/PhysRevB.61.10267

[RHG05] Robert Raussendorf, Jim Harrington, and Kovid Goyal. A fault-tolerant one-way quantum computer. *Annals of Physics*, **321**(9), 26, 2005. http://arxiv.org/abs/quant-ph/0510135

[Roy06] Rahul Roy. Topological invariants of time reversal invariant superconductors. *ArXiv e-prints*, August 2006. http://arxiv.org/abs/cond-mat/0608064

[RQHZ08] Sri Raghu, Xiao-Liang Qi, Carsten Honerkamp, and Shou-Cheng Zhang. Topological mott insulators. *Phys. Rev. Lett.*, **100**, 156401, Apr 2008. http://link.aps.org/doi/10.1103/PhysRevLett.100.156401

[RS91] Nicholas Read and Subir Sachdev. Large- N expansion for frustrated quantum antiferromagnets. *Phys. Rev. Lett.*, **66**, 1773–1776, Apr 1991. http://link.aps.org/doi/10.1103/PhysRevLett.66.1773

[RSFL10] Shinsei Ryu, Andreas P Schnyder, Akira Furusaki, and Andreas W W Ludwig. Topological insulators and superconductors: tenfold way and dimensional hierarchy. *New Journal of Physics*, **12**(6), 065010, 2010. http://dx.doi.org/10.1088/1367-2630/12/6/065010

[Sac01] Subir Sachdev. *Quantum Phase Transitions*. Cambridge University Press, new edition edition, April 2001. http://www.amazon.com/exec/obidos/redirect?tag=citeulike07-20&path=ASIN/0521004543

[SBMS11] Brian Swingle, Maissam Barkeshli, John McGreevy, and Todadri Senthil. Correlated topological insulators and the fractional magnetoelectric effect. *Phys. Rev. B*, **83**(19), 195139–+, May 2011. http://dx.doi.org/10.1103/PhysRevB.83.195139

[SCPG10] Norbert Schuch, J. Ignacio Cirac, and David Pérez-García. Peps as ground states: Degeneracy and topology. *Annals of Physics*, **325**(10), 2153 – 2192, 2010. http://dx.doi.org/10.1016/j.aop.2010.05.008

[SF09] Masatoshi Sato and Satoshi Fujimoto. Topological phases of noncentrosymmetric superconductors: Edge states, majorana fermions, and non-abelian statistics. *Phys. Rev. B*, **79**, 094504, Mar 2009. http://link.aps.org/doi/10.1103/PhysRevB.79.094504

[SFR+11] H. Francis Song, Christian Flindt, Stephan Rachel, Israel Klich, and Karyn Le Hur. Entanglement entropy from charge statistics: Exact relations for noninteracting many-body systems. *Phys. Rev. B*, **83**, 161408, Apr 2011. http://link.aps.org/doi/10.1103/PhysRevB.83.161408

[Sho97] Peter W. Shor. Polynomial-time algorithms for prime factorization and discrete logarithms on a quantum computer. *SIAM Journal on Computing*, **26**(5), 1484–1509, 1997. http://dx.doi.org/10.1137/S0097539795293172

[SMF99] Todadri Senthil, J. B. Marston, and Matthew P. A. Fisher. Spin quantum hall effect in unconventional superconductors. *Phys. Rev. B*, **60**, 4245–4254, Aug 1999. http://link.aps.org/doi/10.1103/PhysRevB.60.4245

[SPGC11] Norbert Schuch, David Pérez-García, and Ignacio Cirac. Classifying quantum phases using matrix product states and projected entangled pair states. *Phys. Rev. B*, **84**, 165139, Oct 2011. http://link.aps.org/doi/10.1103/PhysRevB.84.165139

[SRFL08] Andreas P. Schnyder, Shinsei Ryu, Akira Furusaki, and Andreas W. W. Ludwig. Classification of topological insulators and superconductors in three spatial dimensions. *Phys. Rev. B*, **78**(19), 195125, Nov 2008. http://dx.doi.org/10.1103/PhysRevB.78.195125

[SW10] Brian Swingle and Xiao-Gang Wen. Topological Properties of Tensor Network States From Their Local Gauge and Local Symmetry Structures. *ArXiv e-prints*, January 2010. http://arxiv.org/abs/1001.4517

[Swi09] Brian Swingle. Entanglement renormalization and holography. *ArXiv e-prints*, May 2009. http://arxiv.org/abs/0905.1317

[SWVC07] Norbert Schuch, Michael M. Wolf, Frank Verstraete, and J. Ignacio Cirac. Computational complexity of projected entangled pair states. *Phys. Rev. Lett.*, **98**, 140506, Apr 2007. http://link.aps.org/doi/10.1103/PhysRevLett.98.140506

[SWVC08] Norbert Schuch, Michael M. Wolf, Frank Verstraete, and J. Ignacio Cirac. Entropy scaling and simulability by matrix product states. *Phys. Rev. Lett.*, **100**(3), 030504, Jan 2008. http://dx.doi.org/10.1103/PhysRevLett.100.030504

[TF10] Andrea Tomadin and Rosario Fazio. Many-body phenomena in qed-cavity arrays. *J. Opt. Soc. Am. B*, **27**(6), A130–A136, Jun 2010. http://dx.doi.org/10.1364/JOSAB.27.00A130

[THZ+09] Dimitris I. Tsomokos, Alioscia Hamma, Wen Zhang, Stephan Haas, and Rosario Fazio. Topological order following a quantum quench. *Phys. Rev. A*, **80**, 060302, Dec 2009. http://link.aps.org/doi/10.1103/PhysRevA.80.060302

[TPB11] Ari M. Turner, Frank Pollmann, and Erez Berg. Topological phases of one-dimensional fermions: An entanglement point of view. *Phys. Rev. B*, **83**(7), 075102, Feb 2011. http://dx.doi.org/10.1103/PhysRevB.83.075102

[TSG82] Daniel C. Tsui, Horst L. Stormer, and Arthur C. Gossard. Two-dimensional magnetotransport in the extreme quantum limit. *Phys. Rev. Lett.*, **48**(22), 1559–1562, May 1982. http://dx.doi.org/10.1103/PhysRevLett.48.1559

[Val02] Leslie G. Valiant. Quantum circuits that can be simulated classically in polynomial time. *SIAM Journal on Computing*, **31**(4), 1229–1254, 2002. http://dx.doi.org/10.1137/S0097539700377025

[VC04] Frank Verstraete and J. Ignacio Cirac. Valence-bond states for quantum computation. *Phys. Rev. A*, **70**, 060302, Dec 2004. http://link.aps.org/doi/10.1103/PhysRevA.70.060302

[VC10] Frank Verstraete and J. Ignacio Cirac. Continuous matrix product states for quantum fields. *Phys. Rev. Lett.*, **104**, 190405, May 2010. http://link.aps.org/doi/10.1103/PhysRevLett.104.190405

[VCL+05] Frank Verstraete, J. Ignacio Cirac, José I. Latorre, Enrique Rico, and Michael M. Wolf. Renormalization-group transformations on quantum states. *Phys. Rev. Lett.*, **94**, 140601, Apr 2005. http://link.aps.org/doi/10.1103/PhysRevLett.94.140601

[VDDMV02] Frank Verstraete, J. Dehaene, B. De Moor, and H. Verschelde. Four qubits can be entangled in nine different ways. *Phys. Rev. A*, **65**, 052112, Apr 2002. http://link.aps.org/doi/10.1103/PhysRevA.65.052112

[VdNLDB08] Maarten Van den Nest, Kris Luttmer, Wolfgang Dür, and Hans J. Briegel. Graph states as ground states of many-body spin-1/2 hamiltonians. *Phys. Rev. A*, **77**, 012301, Jan 2008. http://link.aps.org/doi/10.1103/PhysRevA.77.012301

[VdNMDB06] Maarten Van den Nest, Akimasa Miyake, Wolfgang Dür, and Hans J. Briegel. Universal resources for measurement-based quantum computation. *Phys. Rev. Lett.*, **97**, 150504, Oct 2006. http://link.aps.org/doi/10.1103/PhysRevLett.97.150504

[Vid03] Guifré Vidal. Efficient classical simulation of slightly entangled quantum computations. *Phys. Rev. Lett.*, **91**, 147902, Oct 2003. http://link.aps.org/doi/10.1103/PhysRevLett.91.147902

[Vid07] Guifré Vidal. Entanglement renormalization. *Phys. Rev. Lett.*, **99**, 220405, Nov 2007. http://link.aps.org/doi/10.1103/PhysRevLett.99.220405

[VLRK03] Guifré Vidal, José I. Latorre, E. Rico, and A. Kitaev. Entanglement in quantum critical phenomena. *Phys. Rev. Lett.*, **90**, 227902, Jun 2003. http://link.aps.org/doi/10.1103/PhysRevLett.90.227902

[VMC08] Frank Verstraete, Valentin Murg, and J.Ignacio Cirac. Matrix product states, projected entangled pair states, and variational renormalization group methods for quantum spin systems. *Advances in Physics*, **57**(2), 143–224, 2008. http://dx.doi.org/10.1080/14789940801912366

[VWPGC06] Frank Verstraete, Michael M. Wolf, David Pérez-García, and J. Ignacio Cirac. Criticality, the area law, and the computational power of projected entangled pair states. *Phys. Rev. Lett.*, **96**, 220601, Jun 2006. http://link.aps.org/doi/10.1103/PhysRevLett.96.220601

[WAR11] Tzu-Chieh Wei, Ian Affleck, and Robert Raussendorf. Affleck-kennedy-lieb-tasaki state on a honeycomb lattice is a universal quantum computational resource. *Phys. Rev. Lett.*, **106**, 070501, Feb 2011. http://link.aps.org/doi/10.1103/PhysRevLett.106.070501

[Wen89] Xiao-Gang Wen. Vacuum degeneracy of chiral spin states in compactified space. *Phys. Rev. B*, **40**(10), 7387–7390, Oct 1989. http://dx.doi.org/10.1103/PhysRevB.40.7387

[Wen90] Xiao-Gang Wen. Topological orders in rigid states. *International Journal of Modern Physics B*, **4**(2), 239, 1990. http://dx.doi.org/10.1142/S0217979290000139

[Wen91] Xiao-Gang Wen. Mean-field theory of spin-liquid states with finite energy gap and topological orders. *Phys. Rev. B*, **44**(6), 2664–2672, Aug 1991. http://dx.doi.org/10.1103/PhysRevB.44.2664

[Wen02] Xiao-Gang Wen. Quantum orders and symmetric spin liquids. *Phys. Rev. B*, **65**(16), 165113, Apr 2002. http://dx.doi.org/10.1103/PhysRevB.65.165113

[Whi92] Steven R. White. Density matrix formulation for quantum renormalization groups. *Phys. Rev. Lett.*, **69**, 2863–2866, Nov 1992. http://link.aps.org/doi/10.1103/PhysRevLett.69.2863

[Wit83] Edward Witten. Global aspects of current algebra. *Nuclear Physics B*, **223**(2), 422 – 432, 1983. http://dx.doi.org/10.1016/0550-3213(83)90063-9

[WN90] Xiao-Gang Wen and Qian Niu. Ground-state degeneracy of the fractional quantum hall states in the presence of a random potential and on high-genus riemann surfaces. *Phys. Rev. B*, **41**(13), 9377–9396, May 1990. http://dx.doi.org/10.1103/PhysRevB.41.9377

[WWZ89] Xiao-Gang Wen, Frank Wilczek, and Anthony Zee. Chiral spin states and superconductivity. *Phys. Rev. B*, **39**(16), 11413–11423, Jun 1989. http://dx.doi.org/10.1103/PhysRevB.39.11413

[WZ71] Julius Wess and Bruno Zumino. Consequences of anomalous ward identities. *Physics Letters B*, **37**(1), 95 – 97, 1971. http://dx.doi.org/10.1016/0370-2693(71)90582-X

[WZ92] Xiao-Gang Wen and Anthony Zee. Classification of abelian quantum hall states and matrix formulation of topological fluids. *Phys. Rev. B*, **46**, 2290–2301, Jul 1992. http://link.aps.org/doi/10.1103/PhysRevB.46.2290

[Xu12] Cenke Xu. Unconventional quantum critical points. *ArXiv e-prints*, February 2012. http://arxiv.org/abs/1202.6065

[YK10] Bohm-Jung Yang and Yong Baek Kim. Topological insulators and metal-insulator transition in the pyrochlore iridates. *Phys. Rev. B*, **82**, 085111, Aug 2010. http://link.aps.org/doi/10.1103/PhysRevB.82.085111

[Yos11] Beni Yoshida. Classification of quantum phases and topology of logical operators in an exactly solved model of quantum codes. *Annals of Physics*, **326**(1), 15 – 95, 2011. http://dx.doi.org/10.1016/j.aop.2010.10.009

[ZRV09] Yi Zhang, Ying Ran, and Ashvin Vishwanath. Topological insulators in three dimensions from spontaneous symmetry breaking. *Phys. Rev. B*, **79**, 245331, Jun 2009. http://link.aps.org/doi/10.1103/PhysRevB.79.245331